INVESTIGATIONS ON THE DEVELOPMENT OF A NEW MAGNETORHEOLOGICAL GRINDING TOOL FOR FINISHING OF CYLINDRICAL BLIND HOLES SURFACE

A thesis submitted in fulfilment of the requirement for the award of the degree of

DOCTOR OF PHILOSOPHY

IN

MECHANICAL ENGINEERING

Submitted by

ANKIT AGGARWAL

Roll No. 901608007

Under the supervision of

Dr. ANANT KUMAR SINGH

Associate Professor, MED

Department of Mechanical Engineering,

Thapar Institute of Engineering and Technology, Patiala-147004, India

(Deemed to be University)

April, 2022

CONTENTS

CERTIFICATE

I, Ankit Aggarwal, Roll No. 901608007, hereby declared that the thesis entitled **"Investigations on the Development of a New Magnetorheological Grinding Tool for Finishing of Cylindrical Blind Holes Surface"** submitted to the Department of Mechanical Engineering at Thapar Institute of Engineering and Technology, Patiala, Punjab (India) is an authenticated record of my own research work for the award of the degree "Doctor of Philosophy" under the supervision of **Dr. Anant Kumar Singh.** This report has not been submitted to any other institute for the award of any other degree.

Ankit Aggarwal

Place: Patiala

Ankit Aggarwal

Dated: 21-04-2022

Roll No. 901608007

This is to certify that above declaration made by the student is correct to the best of my knowledge.

Verified By:

21/04/2022

Dr. Anant Kumar Singh
(Supervisor)
Associate Professor
Department of Mechanical Engineering
Thapar Institute of Engineering and Technology, Patiala- 147001 (Punjab)
India

ACKNOWLEDGEMENT

First and the foremost, I wish to thank my supervisor **Dr. Anant Kumar Singh** for his valuable support and guidance. I am sincerely gratitude to him for judging my potential and providing me an interesting topic according to my capability. I am thankful for his positive suggestions, and meticulous guidance that helped me to improve my talent to write scientific research papers and carry out the new research. His patience and motivation enhanced me up to achieve my goal. I feel really honoured to have worked under his mentorship throughout my entire Ph.D. work.

I thank the doctoral committee members **Dr. T.K. Bera** (Chairman, Board of Studies), **Dr. Dheeraj Gupta**, **Dr. Satish Kumar Sharma** and **Dr. R.K. Gupta** for the feedback and reviews that were given on my research proposal and progress monitoring presentations. Their guidance was beneficial for me to improve my research work. I am also thankful to **Dr. Tarun Nanda** and **Dr. Anu Mittal**, our Ph.D. coordinators for their approachability and keeping me informed with all the relevant communication through E-mails.

I am thankful to my parents who has always supported and consistently motivated me. I am thankful to my younger sisters Dr. Anchal Aggarwal (MD, medicine) for her motivational and emotional support throughout my entire research work. I am thankful to my mentor Dr. Harry Garg (Sr. Principal Scientist, CSIR-CSIO, Chandigarh) for always motivating me throughout my entire research work. I was also encouraged by my research team members Dr. Manpreet Singh, Dr. Sunil Kumar Paswan, Mr. Kunal Arora, Mr. Anirudh Chana, and Mr. Ravi Dutt Yadav. I am also thankful to my friends Mr. Gagandeep Singh, Mr. Prakhar Jain and Dr. Vipin Kumar Sharma who motivated me throughout this research. From the core of my heart, I thank to my entire family members for their never-ending love, encouragement, and support.

I thank to "**Almighty God**" for giving me the strength and patience for successfully completing my goal.

Ankit Aggarwal

Ankit Aggarwal

Abstract

Fine finishing of the inner surfaces of cylindrical blind hole (CBH) components is currently in high demand in the manufacturing industry as a means of reducing friction and improving functional efficiency. The industries like automobile, medical, and mould manufacturing are currently looking for fine finished CBH-type components with increased functional performance. Fine finished CBH-type industrial components like moulds are used to make plastic parts such as drosophila vials, bottle caps, light covers, etc. This increases the service life of finished products while also improving their aesthetic appearance and dimensional precision. The other CBH-type components like femoral head-neck taper junction and brake master cylinder also require fine finishing for increasing their functional performance. For the finishing of such CBH-type workpieces in industries, the most common method is to use a traditional handheld grinding technique. In this process, the bonded abrasive wheel is utilized for finishing the CBH workpiece surfaces which result in tensile residual stresses, heat-affected zones, microcracks, and many other defects. Surface fatigue, contact stiffness, and corrosion can all increase if these faults are not removed. Beyond that, there is no control over the finishing forces that act on the workpiece surface during the traditional finishing process.

To achieve efficient and defect-free finished surfaces, a permanent magnet-based technique with two tools was recently developed for the MR finishing of longitudinal and bottom flat surfaces of the CBH type workpieces. The use of permanent magnets restricts the in-process control over the finishing forces. Also, this process can be utilized for the finishing of workpieces having a particular diameter size. Therefore, a tool is required for fine finishing of straight or tapered longitudinal and flat end surfaces of the CBH-type workpieces of variable sizes. This is possible only by keeping the tool eccentric from the central axis of the workpiece. Further, in-process control is required for fine finishing of the CBH-type workpiece made up of different materials. To address these issues, a magnetorheological polishing fluid-based technique with a new electromagnetically controlled single tool has been designed and developed for fine finishing both the longitudinal and flat end surfaces of CBH-type workpieces in a manner similar to internal cylindrical grinding.

For the design and development of the magnetorheological grinding (MRG) tool, magnetostatic finite element analysis (FEA) is performed. The FEA result reveals that the initially proposed single MRG tool without grooves can be used to finish both the surfaces of the CBH-type workpieces. Also, the best dimensions of the MRG tool are obtained using FEA. Further, FEA is performed to achieve a higher and uniform magnetic flux density (MFD) over the MRG tool with grooves. After the FEA, the MRG tool with grooves is found more effective in fine finishing both the surfaces of the CBH-type workpieces. The MFD is also analyzed experimentally. It is found that the MRG tool with grooves provides higher and uniform MFD over its longitudinal and flat end finishing surfaces.

Further, theoretical analysis is performed to understand the mechanism during finishing of the straight or tapered longitudinal and flat end surfaces of the cylindrical blind hole type workpiece

using the newly developed MRG tool. The influence of the MFD, path followed and the number of active abrasive particles have been explored in-depth using theoretical analysis. Also, in the theoretical analysis, a surface roughness model is developed to predict finishing with the present MRG tool. From the theoretical model, the surface roughness achieved over the longitudinal surface is 99 nm and on the flat end surface is 56 nm using the present developed MRG tool. Further, these values of the theoretical surface roughness values are compared with the experimentally obtained values. On comparing, the experimentally obtained values with the theoretically calculated value, the percentage error is found in the range of 4.67 to 10.33 on the longitudinal surface and 5 to 12 on the flat end surface of the CBH type workpiece. Thus, from the results of the theoretical analysis, it is found that the MRG tool is capable of fine finishing the tapered longitudinal as well as flat end surfaces of the CBH-type workpiece.

After the efficacy through the theoretical analysis, the performance of the developed MRG tool is validated for the finishing of tapered longitudinal as well as flat end surfaces of the CBH type workpieces, the detailed experimentation is performed. For finishing over the tapered longitudinal surface, a swivel rotating vise is used. This rotating vise provides a uniform working gap between the longitudinal MRG tool surface and the tapered longitudinal CBH-type workpiece surface. First, the magnetorheological finishing is performed over the typical EN31 CBH type mould cavity utilized for the manufacturing of spray bottle cap hoods. To perform the fine finishing, the composition of the magnetorheological polishing (MRP) fluid and optimum process parameters is predicted using the response surface methodology technique. After fine finishing using the predicted optimum process parameters, the reduction in surface roughness value is found as 80 nm from 350 nm over the tapered longitudinal surface and 50 nm from 320 nm over the flat end surface of the typical EN31 CBH type workpiece.

In addition, a performance analysis of the current MRG tool for the finishing of the typical H13 CBH type mould cavity is carried out. After utilizing the predicted optimum process parameters for the finishing over the typical H13 CBH type mould cavity surfaces, the performance of the MRG tool is analysed. The results of the roughness value over tapered longitudinal surface reduces to 70 nm from 450 nm and 60 nm on flat end surface from 320 nm validates the performance capability of the present developed MRG tool. The surface characteristics like scanning electron microscope micrographs, optical microscope, and mirror images are improved significantly along with the reduction in waviness on both surfaces. Thus, the present process can help to achieve fine finished CBH type mould cavity surfaces for making clear polycarbonate light covers. The overall results reveal that the present MRG tool-based process is capable of fine finishing the tapered longitudinal and flat end surfaces of the CBH type mould cavities used in different industries.

Keywords: Electromagnetically controlled grinding wheel type tool, blind hole type workpieces, magnetic flux density, magnetorheological (MR) polishing fluid, surface roughness, fine finishing.

LIST OF FIGURES

LIST OF TABLES

LIST OF ABBREVIATIONS

AAPs	Active abrasive particles
ANOVA	Analysis of variance
BEMRF	Ball end magnetorheological finishing
BHBC	Blind hole type ball cup
BTU	Ball transfer unit
CBH	Cylindrical blind hole
CCD	Central composite design
CIPs	Carbonyl iron particles
DOE	Design of experiments
EIPs	Electrolytic iron particles
FEA	Finite element analysis
HMI	Human-machine interface
MFD	Magnetic flux density
MFS	Magnetic field strength
MN	Magnetic normal
MR	Magnetorheological
MRF	Magnetorheological finishing
MRAFF	Magnetorheological abrasive flow finishing
MRG	Magnetorheological grinding
MRP	Magnetorheological polishing fluid
MRH	Magnetorheological honing
MRHF	Magnetorheological hemispherical finishing
MRR	Material removal rate
PLC	Programable logic controller
RSM	Response surface methodology
R-MRH	Rotational magnetorheological honing
S/N	Signal-to-noise ratio
SEM	Scanning electron microscopy
SR	Surface roughness
TS	Tangential shear
WG	Working gap

LIST OF NOMENCLATURES

A_0 Vertical cross-sectional area of the MRG tool across the measured point Q (m^2)

C Percentage concentration of abrasive particles

A_c Tool core's cross-sectional area around point M (m^2)

A_f Cross-section area of indentation portion generated due to the indented abrasive particle on the flat end surface (m^2)

A_{ft} Projected area of MRP fluid on the flat end surface of the cylindrical blind hole type workpiece (m^2)

A_l Cross-section area of indentation portion generated due to the indented abrasive particle on tapered longitudinal surface (m^2)

A_t The total surface area of the end product in contact with the mould cavity (mm^2)

A_{tl} Projected area of MRP fluid on the tapered longitudinal surface of the cylindrical blind hole workpiece (m^2)

B Magnetic flux density, MFD (T)

B_o MFD at any point Q (X, Y, Z) over the longitudinal and flat end MRG tool surfaces (T)

$B_f(g_f)$ Magnetic field in the WG incorporating the magnetic effect of the MRP fluid and the CBH work part (Wb/m^2) over flat end surface (T)

$B_l(g_l)$ Magnetic field in the WG incorporating the magnetic effect of the MRP fluid and the CBH work part (Wb/m^2) over the tapered longitudinal surface (T)

B_s Magnetic flux density on point M over the finishing surfaces of the MRG tool (T)

B_{Total} Total magnetic flux density (T)

C_s % volume concentration of silicon carbide abrasive particle

d_{cl} Pitch of the helical path (m)

D_{idf} Indentation depth of the abrasive into the flat end surface (m)

D_{idl} Indentation depth of the abrasive into the tapered longitudinal surface (m)

D_{if} AAP's indented diameter on the flat end surface (m)

D_{il} AAP's indented diameter on the longitudinal surface (m)

d_{sc} Diameter of the single abrasive particle (m)

E Percentage concentration of EIPs

F_{af} Axial force over flat end surface (N)

F_{al} Axial force over the longitudinal surface (N)

F_{cs} The resultant of the axial and net TS force that is acting on the longitudinal, and flat end surfaces of the CBH type workpiece (N)

F_{cf} Total shear force over flat end surface (N)

F_{cl} Total shear force over the longitudinal surface (N)

F_{Ej} Ejection force (N)

F_{fr} Frictional force (N)

F_{nmf} Magnetic normal force for the flat end surface (N)

F_{nml} Magnetic normal force for the longitudinal surface (N)

F_{ntf} Net tangential shear force over the flat end surface (N)

F_{ntl} Tangential shear force over the longitudinal surface (N)

F_{rt} Reaction force that occurs due to surface roughness of the mould (N)

g_f Thickness of the MRP fluid in WG over the flat end MRG tool surface (m)

g_l Thickness of the MRP fluid in working gap (WG) over longitudinal MRG tool surface (m)

H Magnetic field strength (A/m).

H_{avg} Average of total MFS produced at point M (A/m)

H_{BHN} Brinell hardness number (BHN) of the cylindrical blind hole type workpiece

H_m Resultant of the total MFS produced along X, Y, and Z-axis (A/m)

H_x Component of the MFS along X-axis (A/m)

H_y Component of the MFS along with Y-axis (A/m)

H_z Component of the MFS along Z-axis (A/m)

I Magnetizing direct current (A)

$I_{l,f}$ Current uses to finish the tapered longitudinal and flat end surfaces of the cylindrical blind hole (CBH) type mould cavity

l_1 Length of the longitudinal finishing MRG tool surface (mm)

l_2 Distance of the starting point of the longitudinal surface of the MRG tool from the electromagnetic coil (mm)

l_3 Length of the electromagnetic coil (mm)

L_{ft} Length of the spiral path covered by single AAP over the flat end CBH work part surface (m)

L_{lg} Helical path length covered by single AAP (m)

L_n The normal load (N)

L_w Length covered on the tapered longitudinal surface of the CBH type mould cavity along with the reciprocation motion of the MRG tool (mm)

m_a Mass an electrolytic iron particle (kg)

M_{Cr} MRG tool core's magnetization (A-m^2/Kg)

M_{cw} CBH work part's magnetization (A-m^2/Kg)

M_{EI} Magnetization of the electrolytic iron particles (A-m^2/Kg)

m_{sc} Single SiC abrasive particle's mass (Kg)

n Finishing set number

n_1 Number of turns in the electromagnetic coil

N_f Total number of AAPs in MRP fluid during finishing of the flat end CBH work part surface

N_{lg} Total number of AAPs in the MRP fluid during finishing of the tapered longitudinal CBH work part surface

N_{tf} Rotational MRG tool speed for finishing the flat end CBH work part surface (rpm)

N_{tl} Rotational MRG tool speed for finishing the longitudinal CBH work part surface (rpm)

N_{wf} Rotational CBH work part speed for finishing the flat end CBH work part surface (rpm)

N_{wl} Rotational speed of the CBH workpiece for finishing its longitudinal surface (rpm)

$R_{l,f}$ The tool reciprocation finish the tapered longitudinal and flat end surfaces of the cylindrical blind hole workpiece (rpm)

R_t The distance that varies with the AAP location from the center axis of the MRG tool (m).

Rw The distance that varies with the active abrasive particle location from the center axis of the work part (m).

$R_{1,2}$ Tool reciprocation of the MRG tool without and with grooves over longitudinal CBH workpiece (cm/min).

$R_{3,4}$ Tool reciprocation of the MRG tool without and with grooves over flat CBH workpiece (cm/min).

R Radius of the electromagnetic coil (mm)

Rw Rotation of the blind hole type ball cup (rpm)

r' Magnitude of the vector r'

r Variable inner radius of the tapered CBH type workpiece surface (m)

Ra_f^n Final surface roughness after MR finishing over flat end surface of CBH workpiece (nm) in nth finishing time

Ra_f^{n-1} Initial surface roughness before MR finishing is complete over flat end surface of CBH workpiece (nm) in n^{th} finishing time

Ra_i The initial average roughness value of the surface (nm)

Ra_f The final average roughness value of surface (nm)

Ra_l^n Final surface roughness after MR finishing set is complete over the longitudinal surface of CBH workpiece (nm) in n^{th} finishing set

Ra_l^{n-1} Initial surface roughness before MR finishing is complete over the longitudinal surface of CBH workpiece (nm) in n^{th} finishing set

$\%\Delta Ra_{c,l,f}$ The percentage reduction in SR while finding the percentage of MRP fluid components for finishing the tapered longitudinal or flat end CBH type mould workpiece

$\%\Delta Ra$ The percentage reduction in average surface roughness

r_t Radius of the MRG tool (mm)

r_w Internal CBH work part radius on its open end (mm)

r_{w1} Internal CBH work part radius towards its flat end (mm)

Tr Rotation of the magnetorheological hemispherical finishing (MRHF) tool (rpm)

$T_{l,f}$ The tool rotation to finish the tapered longitudinal and flat end surfaces of the cylindrical blind hole workpiece (rpm)

$T_{1,2}$ Tool rotation of the MRG tool without and with grooves over longitudinal CBH workpiece (rpm)

$T_{3,4}$ Tool rotation of the MRG tool without and with grooves over flat CBH workpiece (rpm).

T_f Time period to complete half of the cycle during finishing with the MRG tool over the flat end CBH type workpiece surface (min)

T_l Time period to complete half of the cycle during finishing with the MRG tool over the tapered longitudinal CBH type workpiece surface (min)

ΔT Temperature difference between the temperature molten plastic and solidified end product temperature (^oC).

$W_{l,f}$ The tapered longitudinal and flat end surfaces of the cylindrical blind hole workpiece rotation (rpm)

$W_{1,2}$ Longitudinal end workpiece rotation along with without and with grooves MRG tool (rpm)

$W_{3,4}$ Flat end workpiece rotation along with without and with grooves MRG tool (rpm)

W_s The specific wear (mm^3/ N-mm).

u_l Tangential relative velocity of the AAPs over the longitudinal MRG tool surface (cm/min)

u_f Tangential relative velocity of the AAPs over the flat end MRG tool surface (cm/min)

v_l MRG tool's reciprocation speed over longitudinal CBH type workpiece surface (cm/min)

v_f Reciprocation speed of the MRG tool over the flat end CBH type workpiece surface (cm/min)

V_{mf} Theoretical volume of material removed on the flat end surface (m^3)

V_{ml} Theoretical volume of material removed on the tapered longitudinal surface (m^3)

V_{sc} Vol. of single SiC particle (m^3)

α_s Linear thermal expansion coefficient of the end product (mm/^oC)

γ Angle between section AOD (rad)

θ Helix angle (rad) at any point say S over the helical path

θ' Net helix angle (rad) of the helical path over the tapered longitudinal surface

θ_1 Angular position of the AAP on the spiral path (rad)

τ_o MRP fluid's dynamic yield stress under magnetic field (N/m^2)

τ_f Shear stress exerted by the AAP owing to rotation of CBH workpiece during finishing its flat end surface (N/m^2)

τ_l Shear stress exerted by the AAP owing to rotation of CBH workpiece during finishing its tapered longitudinal surface (N/m^2)

$\varnothing$ Angle among the magnetic field vector and normal to the surface (magnitude B) (deg)

μ Viscosity of the MRP fluid under dynamic yield shear stress (m^2/s)

μ_o Magnetic permeability of air (N/A^2)

μ_{rc} Relative permeability of MRG tool core

μ_{rw} Relative permeability of CBH work part

μ_{mrp} Relative permeability of MRP fluid

ω_w Angular speed of the CBH type workpiece surface (rad/min)

ω_t Angular speed of the tool surface (rad/min)

ω_{af} Angular speed of AAP over the flat end surface (rad/min)

ω_{al} Angular speed of AAP over the tapered longitudinal surface (rad/min)

φ Angle among the resultant of MFD component and electric current segment length, *Idl* (rad)

χ Magnetic mass susceptibility (m^3/Kg)

CHAPTER 1

INTRODUCTION

1.1 Introduction

The surface roughness is found to be critical for a number of fundamental issues, including friction, contact deformation, contact joint tightness, and positional accuracy (Gadelmawla *et* al., 2002). So, to overcome these issues, surface finishing is required in industries for the components to improve their operational functionality, reliability, consistent performance, and service life (Jain, 2008, Alauddin *et* al., 1996). In addition, the finely finished surfaces of industrial components contribute a variety of important attributes to the parts such as dimensional precision, reduced power loss, increased corrosion and wear resistance, and so on (Das *et* al., 2012; Jain *et* al., 2007). Hence, fine surface finishing plays an important role in industries. In modern industries, the demand for a finely finished surface of the cylindrical blind hole type components has increased in order to reduce friction and improve functionality. Moulds for the manufacturing of plastic parts like drosophila vials, bottle caps, etc., and femoral head taper junction are examples of cylindrical blind hole (CBH) type industrial components which require fine finished surfaces (Sirwal and Singh, 2018). To improve the service life, aesthetic appearance, and precise dimensional accuracy of end products, fine finishing the surfaces of such CBH type components is necessary (Maan *et* al., 2017; Cheng *et* al., 2008). The performance of the finishing processes is improved to save time and expenses (Okada *et* al., 2008). Finishing processes are to be employed to overcome friction-related issues, but achieving precision and minimizing surface defects is also necessary (Bedi and Singh, 2016; Taufik and Jain, 2017). The selection of an appropriate finishing process is crucial to finish a particular component to meet the functional requirement. So, in this chapter, the traditional and advanced finishing processes that can be used for finishing the internal cylindrical surfaces, flat surfaces, or cylindrical blind hole type workpiece surfaces are studied.

1.2 Traditional finishing processes to finish the workpieces having flat or internal cylindrical surface

In traditional finishing processes, owing to direct contact of the sharp-edged multipoint cutting tool with the workpiece surface, the material is removed. The tightly bonded abrasives behave like the multipoint cutting edges. Finishing the cylindrical surface or flat end surface of the workpieces

with the traditional finishing processes can produce uncontrolled finishing forces. Owing to this, several surface defects such as micro-cracks, pitting etc., appear on the finished surface of the workpieces (Singh and Singh, 2019a). Finishing a component with exceptional material properties (high tensile strength, high heat resistance, high hardness, and so on), complex-shaped components, and microscopic details is a time-consuming process (Sankar *et* al., 2009). The cylindrical-shaped workpieces with the fine internal finishing surface are utilized in a variety of industries and individual machinery equipment. Various traditional finishing processes are used to finish the inside surface of cylindrical workpieces. Some of the most important traditional finishing processes are discussed below.

1.2.1 Grinding

The grinding process is the oldest and most widely used finishing method in the industry. Some of the different grinding processes used are surface grinding, cylindrical grinding, centerless grinding, belt grinding, and internal grinding process. For flat and cylindrical surfaces, the surface grinder and cylindrical grinder are the most common grinding processes. In these grinding processes, a grinding wheel is used as a tool with many cutting edges (Linke *et* al., 2017). The abrasive particles are used with the multiple cutting edges (Linke *et* al., 2013). The material is removed in the form of microchips by the abrasive particles bonded to the grinding wheel (Nadolny *et* al., 2016). A uniform distribution of grinding abrasive particles is an important characteristic in the grinding process (Linke and Dornfeld., 2012). One of the types of grinding process is the internal cylindrical grinding process. In this process, a wheel with bonded abrasives removes material from the internal surface of the workpiece during the finishing process as shown in Fig. 1.1 (Tawakoli *et* al., 2006).

The diameter of cylindrical grinding wheel is always smaller than the diameter of the holes being ground. A cylindrical workpiece is mounted in a chuck and turned in the opposite direction with the revolving and reciprocating cylindrical wheel of the grinder for internal grinding. The grinding wheel having bonded abrasives perform finishing as it comes in contact with the cylindrical workpiece surface. The internal cylindrical grinding is performed on the bearing ring (Nadolny and Kieraś, 2020). The cylindrical grinding plays a vital role in finishing the mechanical components such as brake master cylinder, engine valve, governor bushes, linkage lever governor, etc. The grinding characteristic of the workpiece surface is influenced by the non-uniformity of

the abrasive particles in the grinding wheel. Also, the process has some limitations like no control over finishing forces. As a result, the workpiece experiences lower dimensional accuracy and subsurface defects (Jackson and Hitchiner, 2012).

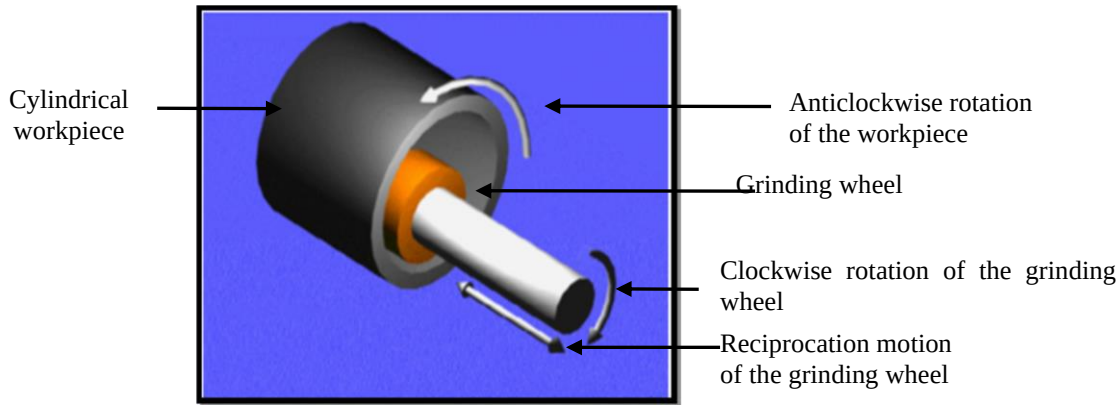

Fig. 1.1 Principle of internal cylindrical grinding (Tawakoli *et* al., 2006).

1.2.2 Honing

Honing is a surface finishing process that can be used on ferrous and non-ferrous cylindrical workpieces. In the honing process (Cabanettes *et* al., 2015), the tool rotates and reciprocates simultaneously inside the cylindrical workpieces as shown in Fig. 1.2.

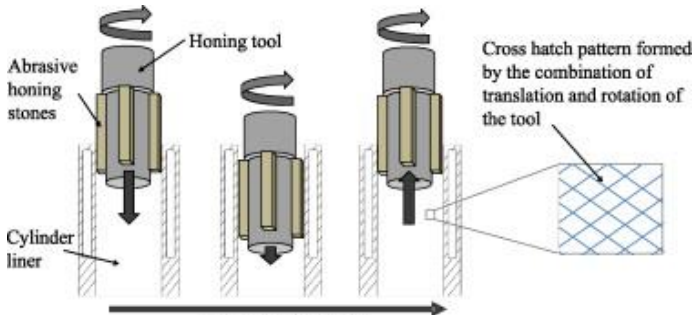

Fig. 1.2 Finishing the internal cylinder liner using the abrasive honing stones (Cabanettes *et* al., 2015).

Owing to these tool motions, the cross-hatched lay pattern is generated, and these are utilised to retain oil on the honed surface. During the honing process, the inside cylindrical workpiece is honed with a honing stone to achieve a finely finished surface. The honing stone in this tool is composed of cemented abrasive grains. The honing stone is similar to a grinding wheel, but it has more fine particles, allowing it to adapt to the shape of the workpiece surface during abrasion (Tilger *et* al., 2017). A honing stone is made of cubic boron nitride (CBN), silicon carbide (SiC), alumina, and diamond (Sabri *et* al., 2010). In the honing process, a higher contact area is offered

by the honing stone than in the grinding process. Because of this higher contact area, the heat generation takes place during finishing which is dissipated simultaneously (Hashimoto *et* al., 2016). As a result, low-temperature rise causes less thermal damage. For honing on the interior cylindrical surface, the speed of rotation, reciprocating, length of the honing stone, stroke, stroke position, and pressure on the honing stone are the characteristics to consider. In honing, the speed of the honing tool is slower than the grinding wheel rotational speed (Sabri *et* al., 2011) whereas the material removal rate is higher than in grinding. The honing process eliminates up to 0.3 mm of the material thickness (Grabon *et* al., 2010). The honing process can be used for the finishing of engine cylinder walls, compressor bodies, valve bodies, bearings, and hydraulic cylinders. Finishing the non-symmetrical and non-cylindrical workpiece surfaces is the primary limitation of the honing process. Also, the traditional honing can provide surface finishing to a limited level of surface finishing owing to the rigid hard bonded abrasives (Jain, 2009; Bedi and Singh, 2018a).

1.3 Advanced finishing processes for the internal cylindrical surface and external surface of the workpieces

The necessity for nano-level surface finishing with outstanding surface properties has raised the continual advancements in material science and its use in various industries. It is proven to be a challenging effort to meet these standards using the traditional finishing process (Jain, 2008). Achieving nanoscale surface finishing along with high accuracy over the applications made up of newly developed materials is a tedious task by utilizing the traditional finishing processes. Traditional finishing processes are also found ineffective to finish the products with various shapes and sizes (Singh *et* al., 2011). As a result, several types of advanced finishing processes have been developed to achieve high precision, high accuracy, improve the interchangeability of parts, improve superb quality, and increase fatigue life (Jha and Jain, 2006a). The advanced finishing processes can be sub-categorized as without and with external control over the finishing forces. The abrasive flow machining (AFM) (Loveless *et* al., 1994), rotational abrasive flow finishing (R-AFF) (Sankar *et* al., 2016) are the advanced finishing processes for the internal cylindrical workpiece surface without external control over finishing force. Further, the magnetic abrasive finishing (MAF) process (Heng *et* al., 2017; Mulik and Pandey, 2013), magnetorheological abrasive flow finishing (MRAFF) process (Jha and Jain, 2004), and rotational magnetorheological abrasive flow finishing (R-MRAFF) process (Das *et* al., 2010) are the advanced finishing processes with external control over the finishing forces that are mostly utilized to finishing the external or

the internal cylindrical surface workpieces which are non-ferromagnetic. Further, for the finishing of the internal cylindrical surface of both ferromagnetic and non-ferromagnetic workpieces, the magnetorheological honing process (Bedi and Singh, 2018a; Grover and Singh, 2018a) is used. In this process, the magnetic field is generated over the finishing surface of the tool either using an electromagnet or permanent magnet. In a further development, the permanent magnet-based rotational magnetorheological honing (Paswan and Singh, 2019) process is used for enhancing the finishing rate of the existing magnetorheological honing process.

1.3.1 Abrasive flow machining (AFM)

AFM is an interior cylindrical surface finishing process that utilizes an abrasive-laden viscoelastic polymer fluid. The AFM process is used to finish edges, complex surfaces and deburring the surfaces (Rhoades, 1991).

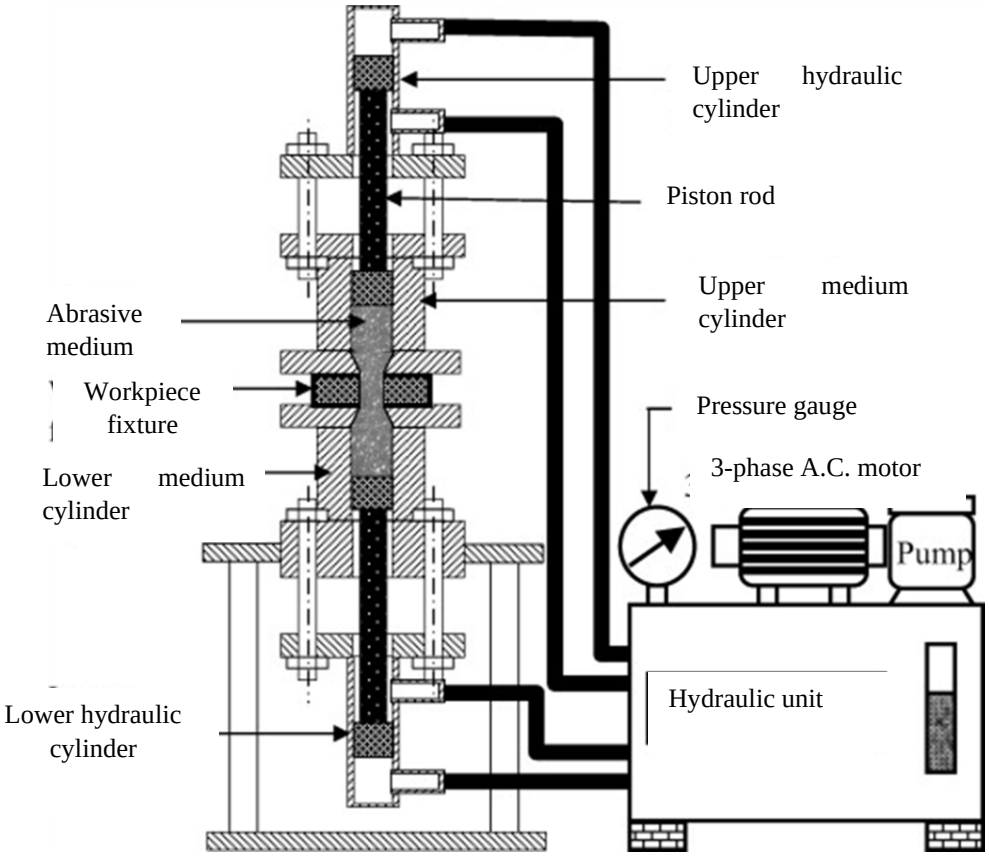

Fig. 1.3 Schematic diagram of abrasive flow finishing experimental set-up (Sankar *et* al., 2009).

In this process as shown in Fig. 1.3, two pistons on either side extrude a semi-solid media (viscoplastic polymer media packed with abrasives) back and forth via an obscure passage of the workpiece. The abrasives interact in this process when the passage is restricted and material removal occurs. In comparison to traditional internal cylindrical surface finishing processes, the machining action in the AFM process is uniform and minimum surface defects (Loveless *et* al., 1994; Sankar *et* al., 2009). This is because in AFM process, high peaks that are formed during machining are removed uniformly after finishing. From critical aerospace and medical industrial components to greater production rates, the AFM process offers finishing over a wide range of applications (Ibrahim *et* al., 2014, Mali and Manna, 2009). Surface roughness (*Ra*) was measured using AFM and found as 0.18 µm after a five-minute cycle from an initial roughness value of 1.9 µm on a multi-port aluminium extrusion die (Rhoades, 1991). The limitation of AFM is that it can be used for finishing the obscure passage of a cylindrical workpiece but is not suitable for flat surfaces and open curved surfaces (Jain, 2008). The uncontrolled finishing force applied by abrasive particles in this process cause many surface defects on the internal workpiece surface such as pits, grooves, and erosion marks (Jha, *et* al., 2007).

1.3.2 Rotational abrasive flow finishing (R-AFF)

The R-AFF process was carried out to achieve a superior surface quality, increased material removal rate (MRR), and close tolerances as compared to the abrasive flow finishing (AFF). The cylindrical workpiece is provided with rotational motion simultaneously with the reciprocating motion of the abrasive laden finishing medium using hydraulic actuators in this process (Sankar *et* al., 2010) as shown in Fig. 1.4. When the finishing medium is reciprocated along with the rotational motion of the workpiece, the active abrasive particles perform a finishing action over the cylindrical workpiece surface (Sankar *et* al., 2010). Thus, enhancing the relative motion of active abrasive particles in R-AFF process by combining the rotating motion of the workpiece cylinder into the previously developed abrasive flow finishing (AFF) process. This process is used in the same way as abrasive flow finishing (AFF). However, due to the added rotating motion of the workpiece in this operation, the material removal rate has increased by 80 %. The improvement in the percentage change in roughness value is 44 % in the R-AFF process (Sankar *et* al., 2010).

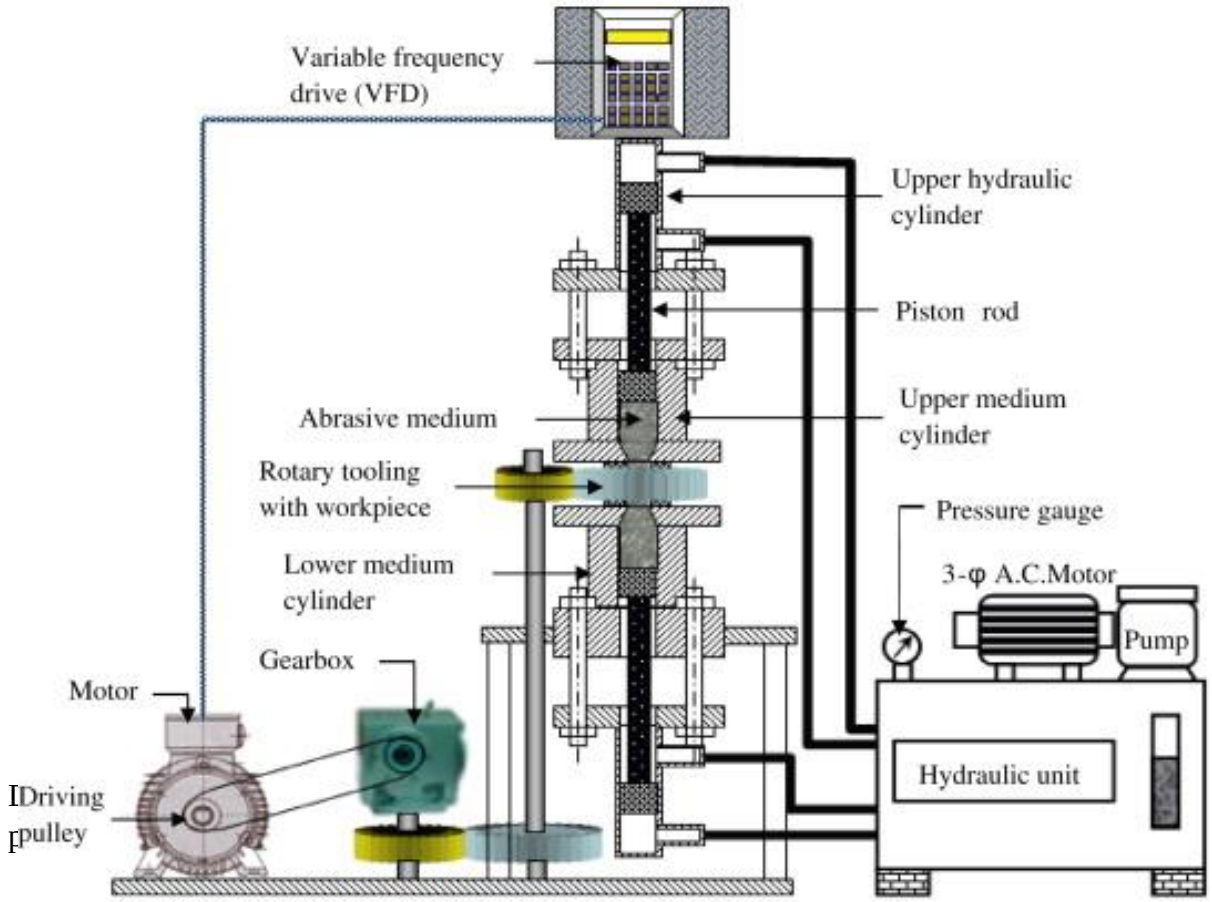

Fig. 1.4 Schematic diagram of rotational abrasive flow finishing (R-AFF) experimental set-up (Sankar *et* al., 2010).

1.3.3 Fluid jet polishing (FJP)

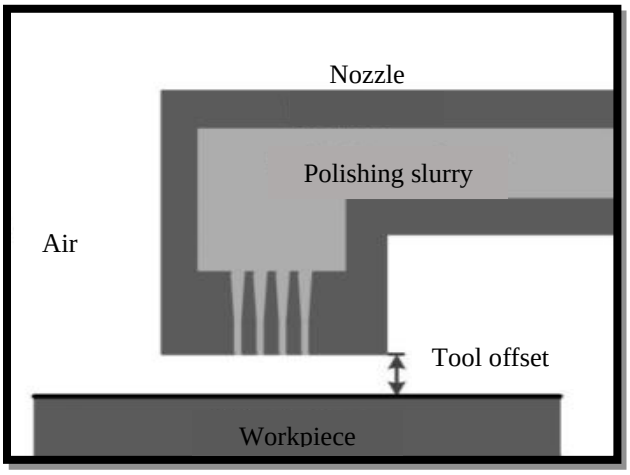

Fig. 1.5 Schematic diagram of the fluid multi-jet polishing (Wang *et al.*, 2017).

In this process, the orifices for the abrasive slurry jets have been designed for the precise finishing of the inner cylindrical surface. The abrasive slurry is allowed to flow through the orifices which impinge on the internal workpiece surface with high pressure. As the abrasive particles are present in these high-pressure jets, so these abrasives collide with the asperities present on the internal cylindrical workpiece surface. To obtained fine finishing on the entire cylindrical workpiece surface, the workpiece is allowed to rotate at a requisite speed. Thus, the material is removed from the entire internal cylindrical workpiece surface. The surface roughness obtained with this process was around 20 nm (Wang *et al.*, 2017). The schematic diagram of the fluid multi-jet polishing is shown in Fig. 1.5. The fluid jet polishing plays a vital role in finishing the components such as molds and optical glass, etc. The limitation of this fluid jet polishing process is the tool erosion owing to which the working gap doesn't remain constant leading to non-uniform finishing.

1.3.4 Magnetic abrasive finishing (MAF)

MAF process utilizes the magnetic field to perform surface finishing on the workpiece surface. This process is used to finish the flat external and internal cylindrical shapes with different sizes of surfaces. This process helps to improve the wear resistance and mechanical properties of the workpieces (Kurore *et* al., 1983). The MAF process is used for the finishing of flat workpiece surface (Kadhum *et* at. 2015). The MAF setup used for the finishing flat workpiece surface is shown in Fig. 1.6. In this process, the electromagnetic core magnetizes the magnetic iron particles utilized to hold the abrasive particles. As the MAF device is provided by rotary motion so finishing is performed over the flat workpiece surface. Thus, the finishing is performed over the flat workpiece surface. The MAF process plays a vital role of finishing in industries such as medical, optical, electrical etc. Further, the MAF process is used for interior surface finishing of the tube-shaped workpiece so it is known as the internal MAF process (Yamaguchi and Shinmura, 1999; Li *et* al., 2018). The internal MAF process is depicted schematically in Fig. 1.7, with the stationary external magnetic poles. Inside the tubular workpiece, a mixed powder of magnetic and abrasive particles is used.

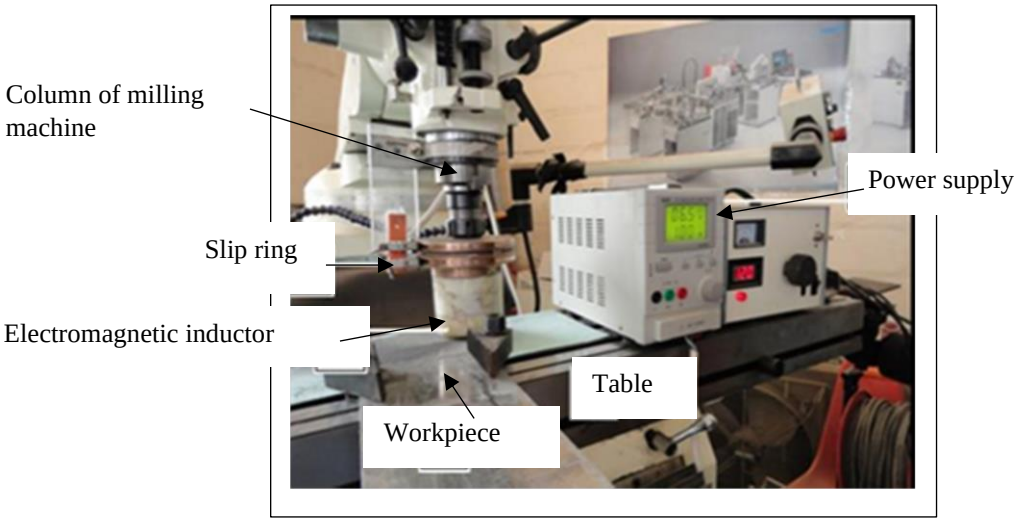

Fig. 1.6 Magnetic abrasive finishing setup for the flat workpiece surface (Kadhum *et* at. 2015).

This mixed powder owing to the magnetic flux density accumulates at the finishing area, and provides the finishing force on the inside surface of the cylindrical workpiece. An electromagnetic coil or a permanent magnet can be used to generate a magnetic field (Wang and Hu, 2005; Verma *et* al., 2017). The relative motion of magnetic abrasive particles on the internal surface of the workpiece cylinder abrades the material, resulting in the internal surface finishing of the workpiece cylinder, as the workpiece rotates at a high rotational speed. Using a permanent magnet or electromagnetic field, this process was primarily employed to finish the internal cylindrical surface of hard materials such as silicon nitride (Wang and Hu, 2005). Although this process uses powdered magnetic and abrasive particles, the presence of a magnetic flux density generated by the magnets results in the formation of a flexible magnetic abrasive brush (FMAB).

Using this flexible magnetic abrasive brush, the MAF process was employed to effectively finish the internal surface of a non-ferromagnetic (SUS304) cylindrical tube (Yamaguchi *et* al., 2007). The source of the magnetic field is kept outside of the cylindrical workpieces, as it is in most of the literature on the MAF process. During the finishing process, the FMAB generated by dry magnetic iron powder and abrasive particles under the influence of a magnetic field can cause scratches on the finished surface of soft workpiece materials (Heng *et* al., 2017). Also, due to the surface finishing with the dryness of the powder, a substantial temperature rise may cause thermal damage to the finishing surface of soft materials.

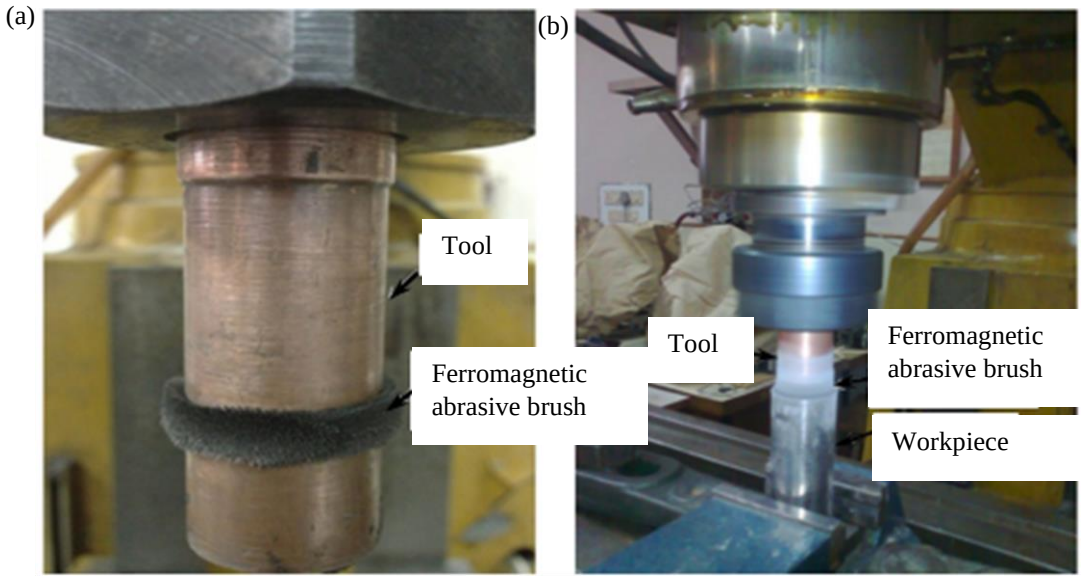

Fig. 1.7 Experimental setup of magnetic abrasive finishing (a) tool with abrasive brush (b) setup during experimentation (Verma *et* al., 2017).

1.4 Magnetorheological polishing (MRP) fluid

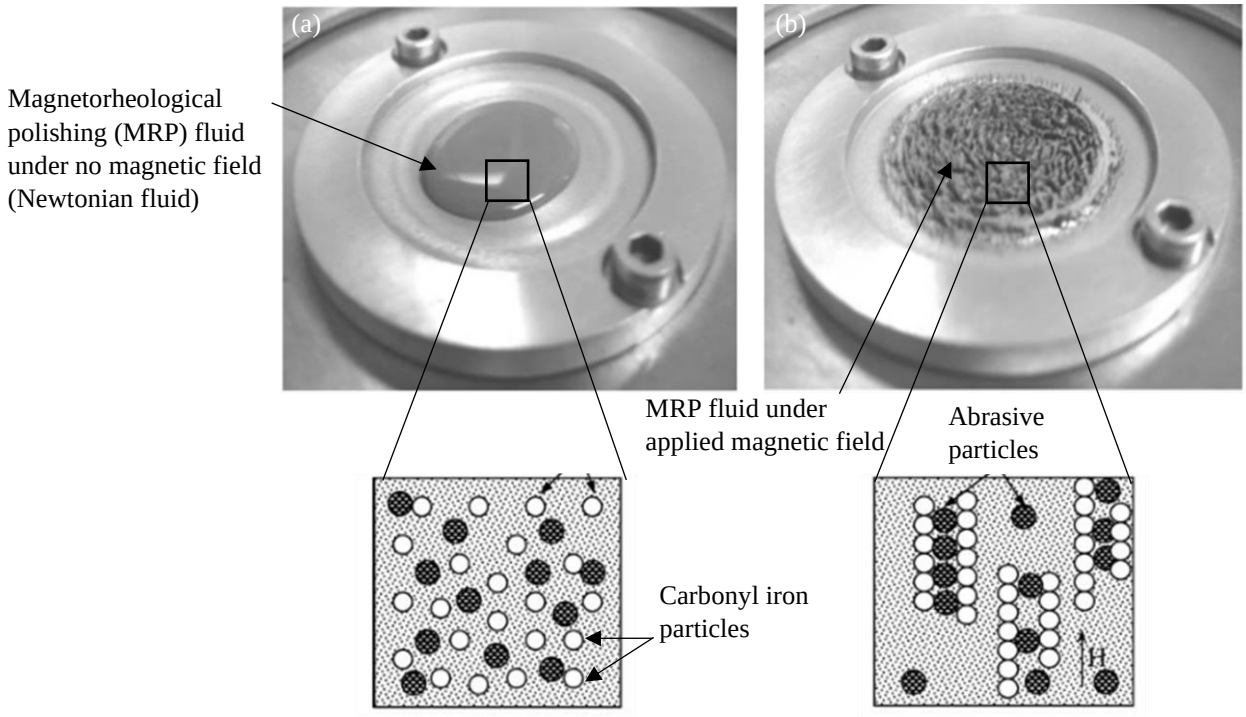

Fig. 1.8 Magnetorheological polishing fluid (a) in the absence of the magnetic field, and (b) under the action of applied magnetic field (Sidpara *et* al., 2009; Jha *et* al., 2007).

Magnetorheological polishing (MRP) fluid acts as a smart fluid under the action of magnetic field (Khatri *et* al., 2018) which can be observed in Figs. 1.8 (a) and (b). The MRP fluid is made by homogeneously mixing magnetic iron and abrasive particles in a base fluid that contains a carrier medium such as vegetable oil, mineral oil, paraffin oil, and some surfactants or stabilisers such as grease, glycerol, or oleic acid (Jha and Jain, 2004). The MRP fluid behaves like a Newtonian fluid in the absence of a magnetic field. In the presence of a magnetic field, however, this fluid behaves like a non-Newtonian fluid (Sidpara *et* al., 2009).

As per the Bingham plastic model, when stress is applied to the stiffened MRP fluid in the presence of a magnetic field, it acts like a semi-solid. The magnetic particles of the MR polishing fluid form dipoles when an external magnetic field is applied to them. The particles with different poles are attracted and form chain structures of the magnetic iron particles. The MRP fluid has a very fast response time under the influence of the external magnetic field, with responses time in milliseconds (Sidpara *et* al., 2009). The characteristics of MRP fluids are as follows.

- Under the applied magnetic field, its viscosity increases.
- The base fluid used in MRP fluid is oil, which makes it corrosive-resistant.
- MRP fluid is extremely responsive to magnetic fields.
- Under the influence of the magnetic field, the MRP fluid has a high yield strength.

1.4.1 Composition of the magnetorheological polishing fluid

The magnetorheological polishing (MRP) fluid play a vital role in the MR finishing process when the magnetic field is applied. The MRP fluid comprises of the magnetic iron particles, abrasives suspended in a base fluid or carrier medium, such as oil or distilled water along with the surfactants or additives like wax or AP3 grease (Niranjan and Jha, 2014). To make the MRP fluid, different formulations of iron particles and abrasives are suspended and blended homogeneously in the base fluid (Chen *et* al., 2016). The temperature change and chemical composition of the MRP fluid alter its rheological character (Sidpara *et* al., 2009). The rheological properties of the MRP fluid vary depending on the iron particle, abrasive particle, and base fluid compositions used, as well as the magnitude of the magnetic field. A detailed study about each constituent of the MRP fluid can be obtained as follows.

1.4.1.1 Magnetic iron particles

The magnetorheological polishing fluid's magnetic iron particles are the most important components. These particles are the solitary in the polishing fluid that are responsible for forming chain structures and grabbing abrasive particles under the influence of a magnetic field. The finishing process is carried out by the gripped abrasive particles. This is owing to the magnetorheological polishing (MRP) fluid's rheological properties. The iron particles in the polishing fluid produce dipoles as a result of the magnetic field applied in the MRP fluid. Under the influence of an external magnetic field, each magnetic iron particle is attracted to the opposite pole of a nearby particle. A columnar or chain structure is generated as a result of the action performed by each magnetic iron particle of the MRP fluid under the influence of the magnetic field. The strength of the magnetic field determines the strength of the poles generated in magnetic iron particles. As the distance of the MRP fluid from the magnetic field increases, the strength of the iron particle chain structure becomes weak (Jha and Jain, 2006) which affects the finishing performance. The magnetic particles as carbonyl iron particles (CIPs) and electrolytic iron particles (EIPs) are the most widely used. The CIPs are made of pure iron and pentacarbonyl. The CIPs are observed to be spherical in shape. The EIPs are made by electrolytically depositing metal from an aqueous solution, which produces a suitable electrolytic iron.

1.4.1.2 Abrasive particles

The non-magnetic hard particles in the MRP fluid are grasped into the chain structure of the magnetic iron particles when the magnetic field is present. These abrasives remove material during the finishing process due to their hardness and the fact that they are bound into the rigid chains of magnetic particles. Abrasive particles come in contact with the workpiece surface during the finishing process. The abrasive particles must abrade the peaks of the surface roughness while finishing, the properties of the abrasives are critical for the finishing process. Shape, size, and hardness are three abrasive properties that influence finishing performance (Torrance, 2002). Silicon carbide (SiC), carbon boron nitride (CBN), and alumina (Al_2O_3) abrasive particles are commonly utilized.

1.4.1.3 Carrier fluid

The carrier fluid in the MR polishing fluid is used to suspend the magnetic and abrasive particles. For optimal performance of the MRP fluid, the carrier fluid must have the characteristics such as high boiling point, corrosion resistance, low freezing point, and the ability to impart rheological behaviour to the MR polishing fluid. The most common carrier fluids are used as oil-based or water-based. Because of its high viscosity, the oil-based carrier fluid is proven to be more efficient against sedimentation (Sidpara *et* al., 2009). The examples of carrier fluid are vegetable oil, paraffin oil, water, mineral oil etc.

1.4.1.4 Stabilizers/additives

The stabilisers are added to the carrier fluid to adequately scatter the abrasive particles and magnetic iron particles for creating the MR polishing fluid (Sidpara *et* al., 2009). The AP3 grease or thixotropic additives are added to the MRP fluid to improve stability of particle. In addition, to prevent the oxidation of suspended magnetic iron particles in the MR polishing solution, various additives are added. Glycerol is added to the MRP fluid as a stabiliser to improve the suspension of magnetic and abrasive particles in the polishing fluid (Sidpara and Jain, 2012).

1.5 Magnetorheological polishing (MRP) fluid-based finishing processes for internal cylindrical surface and external flat surface of the workpieces

The magnetically controlled advanced finishing processes that use the MRP fluid as a finishing medium are known as magnetorheological polishing fluid-based finishing processes. By adjusting the external magnetic field, the rheological behaviour of the MRP fluid can be changed as needed. Because of this quality of the MRP fluid, MR fluid-based finishing processes can finish a wide range of workpieces, from hard to soft materials, and from simple to sophisticated intricate geometric designs. As a result, finishing processes for the flat surface or inside surface of cylindrical workpieces have been developed. The ball end magnetorheological finishing process is used for the finishing of flat workpiece surface (Alam and Jha, 2017). On the other hand, the MR fluid-based finishing processes like MRAFF and R-MRAFF processes are developed for effective internal finishing of non-ferromagnetic cylindrical workpieces (Jha and Jain, 2004; Das *et* al. 2010), whereas others are suitable for internal finishing of both non-ferromagnetic and

ferromagnetic cylindrical workpieces (Bedi and Singh, 2018a; Grover and Singh, 2018a). Further, the advantages of using MRP fluid-based finishing processes are as follows.

- Capability to finish the workpiece surface single nanometer-scale close to the centerline in the surface roughness profile.
- Capability to finish a wide range of flat to intricated workpiece surfaces, including soft and hard materials, ferromagnetic and non-magnetic materials.
- The base fluid in MRP fluid functions as a cooler during the finishing process. Thus, there is a low risk of damage from heat generation, grain deformation, and residual stress.
- Capablility of precise process control which results in fine finishing.
- Controlling the magnetic field during the finishing process applies controlled finishing forces to the workpieces' finishing surfaces.
- Because of the utilization of the MRP fluid in the finishing process, no wear of cutting tool occurs.

1.5.1 Magnetorheological abrasive flow finishing (MRAFF)

An abrasive-laden MRP fluid based MRAFF is established to maintain the flexibility of the abrasive flow machining (AFM) process while having the determinism and controllability of the magnetorheological finishing (MRF) process (Jha and Jain, 2004). The external magnetic field controls the rheological property of magnetorheological polishing (MRP) fluid, which is employed as a finishing medium in the MRAFF (Saraswathamma *et* al., 2015). As a result, the performance of the MRAFF process is influenced by the externally applied magnetic field, hydraulic cylinder extrusion pressure, and the number of finishing cycles. MRP fluid is supplied from both sides of the opposing cylinder in this hydraulically powered system. As shown in Fig. 1.9, the magnet's north and south poles are placed outside of the cylinder.

The carbonyl iron powder (CIP) particles are magnetised and the MR polishing fluid is stiffened by the magnetic lines formed by the electromagnetic poles. The MRP fluid is made up of CIPs and silicon carbide (SiC) abrasives that are suspended in a grease and mineral oil mixture. Material removal from the workpiece's finishing surface is a result of the extrusion pressure acting on the MRP fluid. As a result, the internal surface of the cylinder is finished. In the MRAFF process, the optimum surface finish was achieved as 0.09 μm average surface roughness after 200 finishing

cycles from 0.32 µm initial average surface roughness (Jha and Jain, 2006b). In this process, the MRP fluid was used with the CIPs of a diameter of 18 µm and silicon carbide (SiC) particles of a diameter of 19 µm. The magnetic field of 0.531 T was utilized during the finishing operation (Jha and Jain, 2006b).

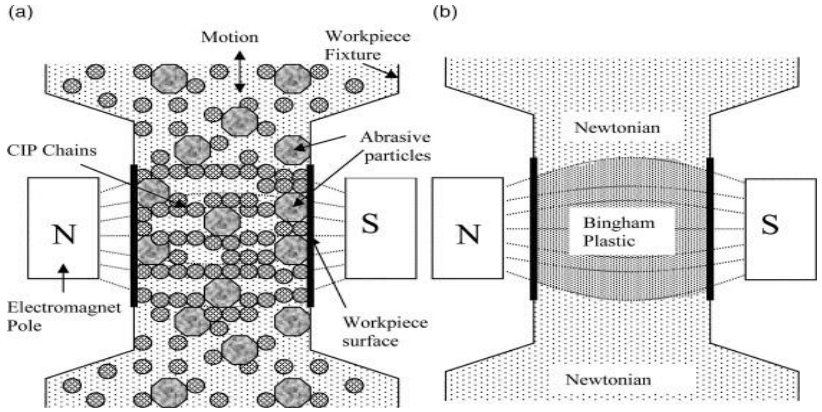

Fig. 1.9 Magnetorheological abrasive flow finishing process (a) mechanism and (b) change in rheological behaviour of MR polishing fluid during finishing (Jha and Jain, 2004).

1.5.2 Rotational magnetorheological abrasive flow finishing (R-MRAFF) process

The R-MRAFF (Das *et* al., 2010) is the enhancement in the existing magnetorheological abrasive flow finishing (MRAFF) (Jha and Jain, 2004) process which is utilized to finish the internal surface of non-magnetic cylindrical workpieces.

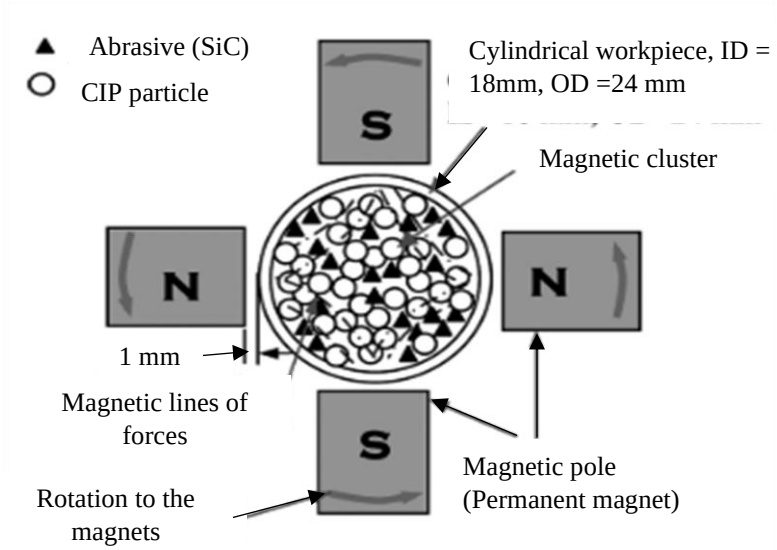

Fig. 1.10 Schematic diagram of rotational magnetorheological abrasive flow finishing (R-MRAFF) process for internal finishing of stainless-steel tube (Das *et* al., 2010).

The magnetic poles are retained externally to the cylindrical workpiece in this process, but they are made to rotate while magnetorheological polishing fluid is reciprocated inside the workpiece (Das *et* al., 2011). To achieve the appropriate surface finish, the motion of the magnetorheological polishing (MRP) fluid is regulated by the hydraulic unit associated with the setup (Fig. 1.10).

The MRP fluid is extruded through the internal cylindrical workpiece surface and reciprocated along the tube's axis by two opposing pistons in the workpiece cylinder by a hydraulic unit in this operation (Das *et* al., 2010). External rotational motion is also applied to the magnetic poles at the same time. The permanent magnetic poles that surround the cylindrical workpiece rotate along with the MRP fluid medium. During finishing the inner surface of the cylindrical stainless-steel workpiece, this process produces a surface finish of 16 nm from 490 nm after 1200 finishing cycles (Das *et* al., 2010). This process on the other hand, is found to be more successful for finishing the interior surface of non-ferromagnetic cylindrical workpieces madeup of steel, high-speed steel and marine-grade steel but least effective for ferromagnetic cylindrical workpieces. This is because the source of magnetic field was placed outside the cylindrical workpiece. As a result, the magnetic field at the internal surface of the ferromagnetic workpiece cylinder is stronger than the magnetic field in the MRP fluid. When a ferromagnetic workpiece cylinder is finished, the magnetization effects cause the MRP fluid's magnetic particles to stick to the finishing surface. As a result, abrasive particles find it difficult to move relative to the ferromagnetic cylindrical workpiece surface, resulting in inefficient finishing.

1.5.3 Ball end magnetorheological finishing (BEMRF) process

The BEMRF process (Singh *et* al., 2011) designed and developed tool for the finishing of the flat or 3D external workpieces. There is in-process control to regulate the finishing forces. This is owing the use of electromagnet which magnetizes the tool core as can be observed in Figs. 1.11 (a) and (b). The finishing medium used is the magnetorheological polishing (MRP) fluid. This MRP fluid is pressurised through the hollow tool core towards the workpiece surface. This MRP fluid on reaching the tool’s finishing surface forms a stiffened ball end of MRP fluid under the action of applied magnetic field. This stiffened ball end of MRP fluid owing to the tool’s rotation and reciprocation performs finishing on the flat workpiece surface (Singh *et* al., 2012). After finishing the flat workpiece surface using the BEMRF process, the surface roughness value

achieved was 19.7 nm from 142.9 nm in 120 min. The limitation of the BEMRF process is that it can be used for the finishing of only the external surface of the workpieces.

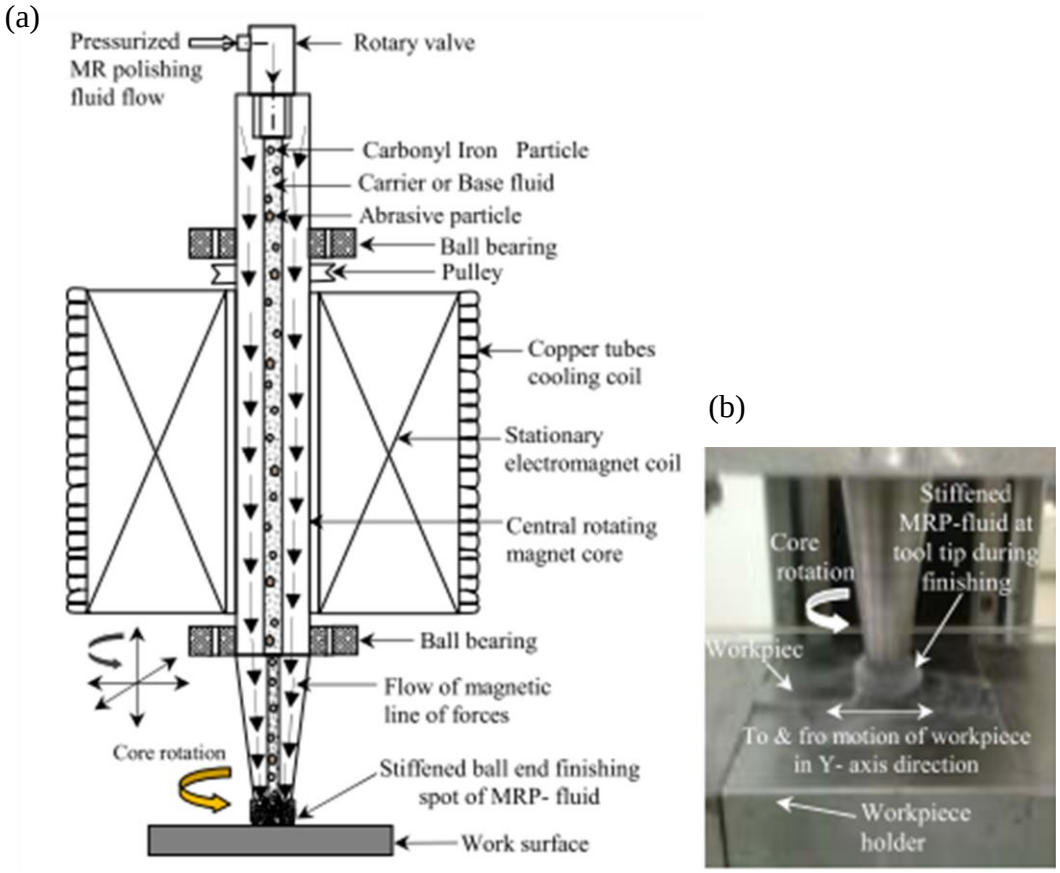

Fig. 1.11 (a) Schematic of mechanism of ball end MR finishing process and (b) the motions involved during finishing process (Singh *et* al., 2012).

1.5.4 Magnetorheological honing (MRH) process

The fluid-based MR polishing process was developed to finish the inside surface of cylindrical workpieces. The MRH experimental setup is depicted in Fig. 1.12(a). However, in the existing MRAFF (Jha and Jain, 2006b) and R-MRAFF (Das *et* al., 2010) processes, the MRP fluid was kept over the internal surface of the cylinder and the magnetic poles are placed over the outer side surface of the cylindrical workpiece. The iron particles in the MRP fluid get magnetised and form a chain structure when exposed to a magnetic field. The chain structure's stiffness depends upon their distance from the electromagnet. The stiffness of the chain structure decreases as the distance from the magnetic field source increases (Jha and Jain, 2006b). As a result, in the case of a cylindrical workpiece, the MRP fluid becomes stuck on the finishing surface and resists the relative

motion of active abrasives over the interior surface. To overcome the problems related to this process, a MRH process has been developed (Bedi and Singh, 2018a) as shown in the Fig. 1.12 (a). In this MRH process, the internal cylindrical workpiece surface is finished by rotating and reciprocating an electromagnetic tool.

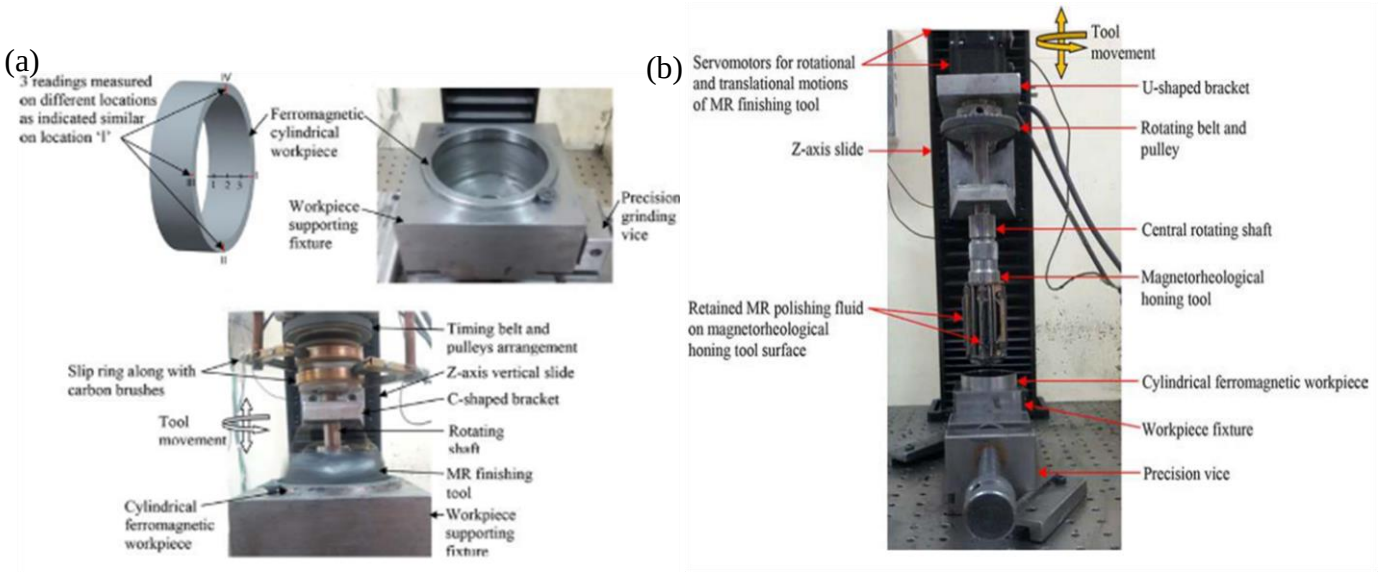

Fig. 1.12 Photograph of the (a) electromagnetic based magnetorheological honing (MRH) process (Bedi and Singh, 2018a), and (b) permanent based MRH process for finishing of the internal surface of the the ferromagnetic cylindrical workpiece (Grover and Singh, 2018a).

As the electromagnetic tool rotates in the vicinity of the internal cylindrical workpiece surface, the strength of magnetic field is higher on tool's surface and found capable to finish ferromagnetic internal cylindrical surface. The surface roughness value achieved on the internal mild steel cylindrical workpiece surface is 83 nm in 90 min from 420 nm (Bedi and Singh, 2018a). Further, a permanent magnet based MRH process (Fig. 1.12(b)) is designed and developed for finishing the variable diametric ferromagnetic internal cylindrical workpiece surface (Grover and Singh, 2018a). In this process, permanent magnets are used as the source to generate magnetic field. Also, the diameter of the tool can be adjusted according to the internal cylindrical workpiece surface diameter. This provision for variation in tool diameter allows fine finishing various cylindrical workpieces with variable diameter. The surface roughness obtained over the internal cylindrical workpiece surface is 88 nm in 60 min from 371 nm (Grover and Singh, 2018a). However, to increase the productivity of the MRH process, the R-MRH process is employed.

1.5.5 Rotational magnetorheological honing (R-MRH) process

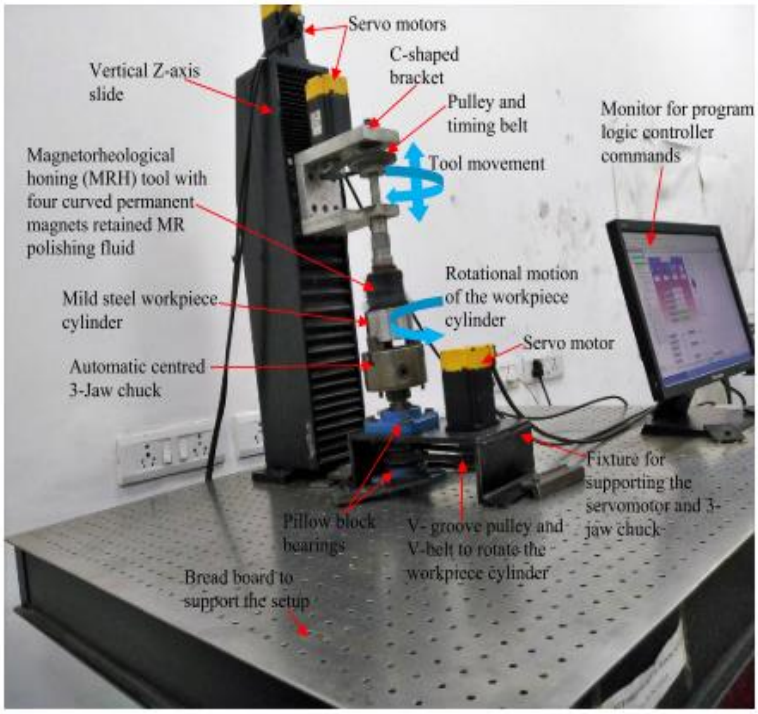

Fig. 1.13 Photograph of the experimental setup used for rotational magnetorheological honing process (Paswan and Singh, 2019).

After developing the MRH process, a rotational magnetorheological honing (R-MRH) tool (Paswan and Singh, 2019) was developed for the finishing of internal ferromagnetic cylindrical workpiece surface which can be observed from Fig. 1.13. In this R-MRH process, productivity of the process is improved by providing the rotational motion to the cylindrical workpiece. This rotational motion to the workpiece is provided using the fixture for supporting the 3-jaw chuck. The rotational motion provided to the cylindrical workpiece is in opposite direction to the rotating R-MRH tool. This also helps to provide shuffling of the abrasive particles with the fresh edged abrasive particles during finishing of the internal cylindrical workpieces. The surface roughness value obtained over the internal cylindrical workpiece surface is 60 nm which is reduced from 330 nm after 60 min of the finishing time.

1.6 Magnetorheological finishing the internal surfaces of the cylindrical blind hole (CBH) type workpieces

Further for finishing the longitudinal as well as flat end surfaces of the cylindrical blind hole (CBH) type workpieces, a new magnetorheological finishing process was developed (Bedi and Singh, 2018b). In this process, two tools are used made up of aluminium which holds the permanent magnetic strips as can be observed from Fig. 1.14 (a) and (b). In Fig. 1.14.(a), the tool can be utilized for the finishing of longitudinal surface of the CBH type workpiece. After finishing the longitudinal surface of the CBH type workpiece, the flat end surface of the CBH type workpiece is finished using the second tool as can be seen in Fig. 1.14(b).

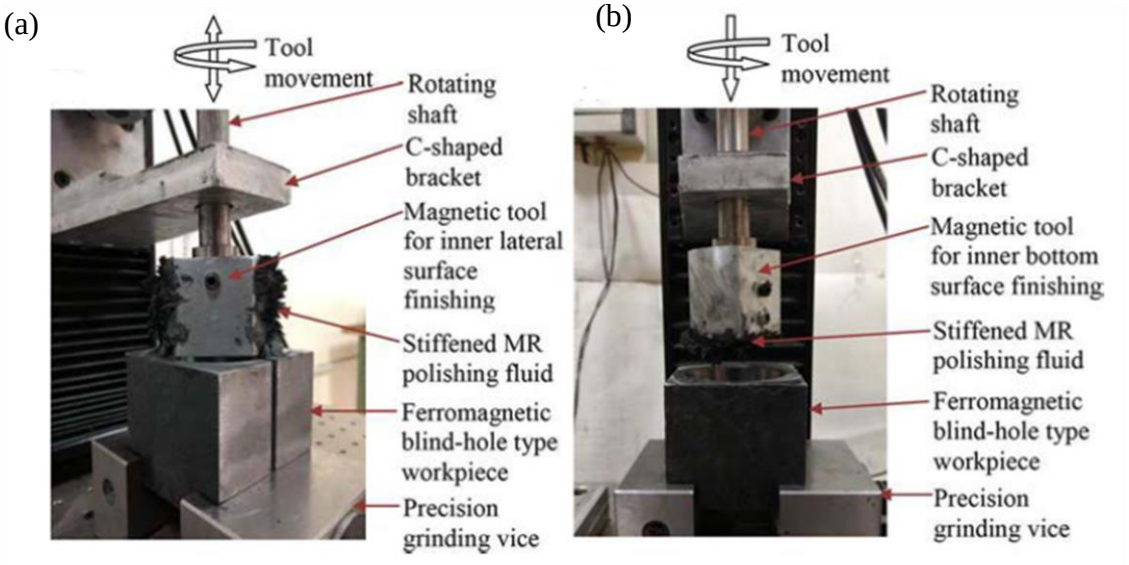

Fig. 1.14 (a) MR lateral finishing tool surface and (b) MR bottom finishing tool surface for the finishing of cylindrical blind hole type workpiece (Bedi and Singh, 2018b).

After performing the MR finishing using this process, the surface roughness value achieved over the longitudinal surface of the CBH type workpiece is 152 nm from 471 nm while on the flat end surface of the CBH type workpiece is 145 nm which is reduced from 476 nm. The finishing on the both the surface were done for 90 min. However, in this process two different tools are used for finishing the tapered longitudinal and flat end surfaces of the workpiece. Owing to which the processing time increases. Therefore, a single MR finishing tool is required for the finishing of longitudinal and flat end surfaces of the CBH type workpieces.

1.7 Applications of various internal cylindrical blind hole type parts utilized in various industries

The fine finished internal cylindrical blind hole type components which are free from defects are required in various industries. Some of the industries which require such fine finished components are as follows.

- In medical industries, the spray bottle cap hood and drosophila vials are manufactured using mould cavities. These fine finished mould cavities may enhance the efficacy of the injection moulding process and the surface quality of the end products.
- In aviation industry, the cover of various lights is manufactured using mould cavities. These fine finished mould cavities may enhance the efficacy of the injection moulding process and the surface quality of the end products.
- In medical industries, the femoral head neck taper junction requires fine finishing. Fine finishing may improve the wear resistance and service life of the hip joint.
- Automobile industries also need fine finished blind hole type cylindrical components (brake master cylinder). Fine finishing of such components may improve their functional performance, service life and reduces the power loss by reducing friction on the internal surfaces of such components.

CHAPTER 2

LITERATURE REVIEW

Cylindrical blind hole (CBH) type components with uniform and high integrity of the fine finished internal surfaces are critical aspects for enhancing operational functionality in industries like automobile and mould manufacturing (Yamaguchi and Shinmura, 1999). Dimensional accuracy, close fit, tolerance, decreased wear, increased tool service life, and minimal losses due to decrease in friction are some of the benefits of nano-finishing in components (Jha and Jain, 2009, Singh and Singh, 2019a). Achieving higher accuracy and nano-scale internal surface finishing is a time-consuming and labour-intensive task (Gorana *et* al., 2004). The flat or interior cylindrical surfaces are often finished using traditional finishing processes such as internal cylindrical grinding, and honing (Tawakoli *et* al., 2007; Sabri and Mansori, 2010). Grinding wheel with strongly bonded abrasives are used in grinding process. For finishing the external flat or internal cylindrical surfaces of the workpiece, the grinding wheel is provided with rotational as well as reciprocation motion. During the finishing of the internal cylindrical workpiece surface, rotation is also provided to the workpiece (Tawakoli *et* al., 2007). The material is abraded and finishing is performed as a result of the rubbing action of the hard abrasive particles on the workpiece surface.

Further in honing process, the tool structure holds the honing stones for finishing the internal cylindrical workpiece surface. Honing stones have strongly bonded abrasives that finish the inside cylindrical surface. In this process, depending on the requirement of the inner diameter of the workpiece cylinder to be finished, the diameter of the tool with honing stones can be adjusted radially inward and outward. Due to these traditional finishing processes, uncontrollable finishing forces act over the workpiece surface. These uncontrolled finishing forces generate surface defects such as deep grooves, surface irregularity, cavities, residual stress, heat-affected zone, torn and folded metals, and ploughed materials retained over the final surface (Gupte *et* al., 2008; Jain, 2009). So, to overcome the issues related to the traditional finishing processes, several advanced finishing processes have been developed. This chapter contains the literature on traditional and advanced finishing processes. Further, it includes the problems related to the traditional finishing processes in attaining a fine-finished flat or internal cylindrical surface of the component. Also, the development of numerous advanced finishing processes, their material removal mechanism,

and the theoretical analysis for finishing the flat or internal cylindrical surfaces of the workpiece are discussed in this chapter.

2.1 Literature related to the traditional finishing processes for finishing the flat or internal cylindrical workpiece surface

The detailed literature review regarding traditional processes for the finishing of the internal cylindrical and flat surfaces are discussed as follows.

Jaworski and Trzepieciński (2016) investigated the surface layer characteristics over the cuboid workpiece surface of low alloy high speed steel using the disk type surface grinder. The disk type surface grinding wheel used is 95A24K. The influence of grinding parameters like grinding depth and lengthwise feed is analysed for surface roughness, micro-hardness and grinding efficiency. For increasing the efficiency of the grinding process by varying its parameters, it's better to increase the lengthwise feed than the grinding depth. Also, to avoid burn and crack generation during the sharpening of the tools made up of low alloy high speed steel, the grinding temperature should be maintained as low as possible.

Tawakoli *et* al. (2007) developed a prototype of the machine having an internal cylindrical grinding tool. Two transmissible grinding wheels were mounted on a spindle in this machine, with their axes of rotation perpendicular to the workpiece rotating axis. In this process, a 7 KW electric motor as the spindle driver, a flat belt for power transfer, and two grinding wheels for the left and right sides of the unit were used to design and construct an internal cylindrical grinding unit. The grinding wheel's abrasive granules were made of natural or synthetic cubic boron nitride (CBN) with grain sizes of B126 and B252. For the experiment, the workpiece material used was steel with a grade of 90MnCrV8. This material has a Vickers hardness of 750. Surface roughness was improved upto 0.1 µm and 0.2 µm using this newly developed setup by adjusting the infeed per grinding from 0.15 to 0.3 mm, respectively. Despite these benefits of this internal cylindrical workpiece, it was only applicable for a cylindrical bore of a large diameter such as 100- 110 mm.

Jeevanantham *et* al. (2017) studied and investigated the influence of machining parameters on the material removal rate and surface roughness in the internal grinding process. Experiments were carried out over the EN8 and EN31 steel materials. Cutting force, cutting speed, and depth of cut

are the machining parameters that were monitored in this study to examine their effect on material removal rate (MRR) and surface roughness. The workpiece was positioned in the chuck of the lathe machine and the grinding wheel was held in the tailstock for testing purposes. Both the workpiece and the grinding wheel were made to rotate in the opposite direction of each other, with the tool reciprocating at the same time. From the results in the form of the relation between input parameters and output parameters, the surface roughness of an EN8 steel cylindrical workpiece increases from 0.661 to 0.694 μm with an increase in depth of cut and cutting force from 0.13 to 0.2 mm and 44.33 to 114.1 N, respectively. The surface roughness of EN31 steel workpiece material increases from 0.628 to 0.682 μm when the same variation of the depth of cut and cutting force are used. As a result, it was determined that to achieve a high-surface finish on EN8 and EN31 steel, the depth of cut and cutting forces must be kept as low as possible during the finishing process.

Lee and Malkin (1993) presented the investigation into the mechanics of bore honing. An experimental setup was developed for this study which included honing machine with spindle speed measuring sensors, expansion pressure, honing head displacement, and a computer interface. The data is collected and analysis is performed using the computer-based interface of the setup. The electric motor utilized to drive the honing machine has a configuration of 3 to 6V with 2.25 KW power. A hydraulic pump was utilised to reciprocate the honing head during the internal bore, which was operated by a 2.25 KW electric motor. In this process, the relationship between surface roughness and material removal rate as a function of the grit sizes of honing stones supplied were analysed. Result shows that the stones with a coarser grit produce a rough surface. The surface roughness requirement after utilizing the honing process restricts the grit size which further affects the removal rate.

Buj-Corral *et* al. (2014) investigated the influence of process parameters on the surface roughness value after honing over the internal surface of the steel cylinder. The parameters considered for finishing the internal cylindrical workpiece are grain size, the density of abrasive, tangential speed of the cylinder, the linear speed of the honing head, and pressure. The abrasives of the honing stone used in the finishing process are made up of cubic boron nitride. for the analysis, the central composite design was utilized. After the analysis, the optimum results are obtained as density as 75 g/cm^3, grain size as 89.6 FEPA, linear speed as 32 cm/min, tangential speed as 25 cm/min and

pressure as 300 N/cm^2. Grain size with medium value needs to be considered and the pressure close to a higher value is considered for the finishing of the internal cylindrical workpiece surface. Further, in this process, most significant variables for material removal rate were found as grain size and pressure, followed by tangential speed and density.

2.2 Literature related to advanced finishing processes for the internal cylindrical or flat surfaces of the workpieces without rheological behavior in the finishing medium

Kim *et* al. (1997) utilized a magnetic abrasive jet machining (MAJM) process for the finishing of a circular tube. In this process, the working fluid (air) mixed with magnetic abrasive particles are jetted into the cylindrical tube made up of SUS 304 grade material. The magnetic abrasives used in this process are the combination of alumina (Al_2O_3) and iron particles which are mixed through a chemical reaction. On the other hand, the magnetic pole is provided on the external surface of this cylindrical tube. As the jet of fluid with magnetic abrasive particles flows into the tube and the external magnetic field is applied. The magnetic abrasive particles are attracted towards the internal surface of the tube. As these particles interact with the internal surface of the tube, the finishing action is performed. Further, the machining conditions like jet velocity, the angle of impingement of the jet, size of the abrasive particles were used for experimentation. The optimum results were found as jet velocity as 40 m/s, angle of impingement of the jet 25º-30º and size of the abrasive particles as 300-400 µm. The roughness value over the workpiece surface was reduced from 0.5 to 0.15 µm. The significant improvement in the surface finish is obtained up to 10 min and thereafter become constant.

Barletta and Tagliaferri (2006) developed fluidized bed-assisted abrasive jet machining for the finishing of stainless steel 316 L cylindrical workpiece. The setup used for finishing the stainless steel 316 L workpiece comprises of the compressor, venturi pipes, 2 fluidized beds, a nozzle, three-way valves, a couple of abrasive tanks, measuring and control instruments. In this process, the compressed air sucks the abrasives and feed them to the nozzle. This nozzle helps to jet the abrasives towards the workpiece surface. As these abrasives flow over the workpiece, the impinging of these abrasives causes material removal from the workpiece surface. The parameters considered in this process are abrasive size, jet velocity, and machining cycle. The material removal rate was linear to jet velocity and the significant response of the surface roughness was seen upto the first two cycles. The smaller the abrasive size, the surface roughness value is

considerably low. The surface roughness changes from an initial surface value of 1.5 to 0.015 mm in 4 machining cycles with a mesh size of 220 and jet speed of 10 m/s. Further, these findings demonstrate that fluidized bed hydrodynamic enhances the properties of the jet fluid, and therefore the abrasive design and dispersion throughout the workpiece, resulting in improved overall finishing outcomes.

Walia *et* al. (2006) proposed a centrifugal force-assisted abrasive flow machining process for the finishing of extruded brass rod with the central bore. In this process, a special nylon fixture is used to hold the workpiece. The media used in this process comprises of polymer, gel, and abrasives. The attachment is specially designed which surrounds the workpiece. During the finishing process, the media flows through the workpiece cavity. As the media flows over the workpiece surface, the centrifugal force acts over the abrasive particles. This force is owing to the centrifugal force-generating (CFG) rod. Due to this centrifugal force acting over the abrasive particles, the finishing action takes place. The parameters that were considered for the process are abrasive concentration as 1:2, polymer to gel ratio as 4:3, and temperature as 32ºC. The surface finish after 3 cycles was reduced to 0.068 µm from the initial value of 0.95 µm at the rotational speed of CFG rod at 70 rpm, extrusion pressure as 34 bar, and grit size as 250 µm.

Sankar *et* al., (2009) developed an abrasive flow finishing (AFF) process for the finishing of cylindrical workpieces made up of aluminum (Al) alloy, Al alloy/SiC metal composite with 10% SiC and Al with SiC 15% volume fraction. A cylindrical workpiece is placed between a workpiece holder. In the present work styrene butadiene rubber (SBR) is used as polymer carrier, hydraulic oil as processing oil and SiC of mesh size 220 as abrasive particles. After finishing is performed over the cylindrical workpiece surface, it is observed that as the extrusion pressure increases upto 6 MPa, there is an increase in roughness. But on further increment in extrusion pressure, a decrease in trend can be observed. It is found that the better change in surface roughness value was obtained on aluminum with 10 percent of SiC concentration. The initial surface roughness of the workpiece was reduced from 0.6 µm to 0.25 µm in 200 cycles. This is due to the high yield strength and elastic modulus of the Al alloy/SiC metal matrix composite which is not possible in aluminum alloy as it deforms plastically.

Sankar *et* al. (2010) developed the rotational-AFF process. In this process, rotation is provided to the cylindrical workpiece to enhance the performance of the process. Further, the finishing medium is reciprocated using the hydraulic actuators on either side of the workpiece. As the workpiece rotates along with the abrasives, a net relative speed acting over the abrasive particle's upsurges. As the abrasive particles flow over the workpiece surface shearing takes place due to the net relative speed. Owing to this, there is an improvement in surface finishing and material removal rate. In this rotational- AFF process, 75% of butadiene and 25% styrene mixture is used as a finishing medium. The theoretical study is carried out for the active abrasive motions and shear forces acting over the workpiece surface. The workpieces were made up of aluminium alloy and its metal matrix composite. Also, a comparative study is carried out in this work to validate the enhancement in the rotational-AFF process. After the comparison, it is found that the rotational-AFF process presents surface roughness of 44% and material removal rate of 80%, which is higher than the AFF process.

Wang and Hu (2005) proposed a magnetic abrasive finishing (MAF) process for the internal cylinder workpiece surface. In this process, the magnetic abrasive particles placed inside the cylinder tube under the action of the applied magnetic field form the flexible magnetic brush. This magnetic field attracts the magnetic abrasive particles toward the internal surface of the workpiece. As the magnetic poles rotate and vibrate, the shear forces are applied to remove the material from the workpiece surface. The workpiece used in this process is Ly12 aluminium alloy, 316L stainless steel, and H62 brass. To analyse the finishing capability and maximum material removal by the MAF process, there were four different experiments performed over the 316L workpiece material. The initial surface roughness value was kept between 0.8 to 1.5 μm for performing the experimentation. The surface roughness value achieved after the finish for 4 min is 0.1 μm. On further finishing over the workpiece surface for 4 min, no change in surface roughness is observed over the internal cylindrical workpiece surface. The heating of the finishing surface is a constraint of this process, and it is most appropriate for hard materials. It can produce a variety of concerns with finishing operations on soft materials, such as thermal damage, scratch marks, and less effective finishing.

Kang *et* al. (2012a) developed a new high-speed machine for magnetic abrasive finishing (MAF) of capillary tubes made up of stainless steel. In this process, the magnetic abrasive particles are introduced into the hollow stainless steel capillary tube and the magnetic source is placed at various

places outside the tube. As the spindle rotates, the workpiece rotates at 30000 min^{-1}. The finishing mixture comprises of iron particles 80% by weight and 20% by weight of magnetic abrasives. The other parameters used for the finishing of the capillary tube workpiece are feed as 0.59 mm/s and feed length as 12.7 mm. The results from the previous MAF process (Kang and Yamaguchi, 2012) reveal that it can finish a 72 mm long tube with surface roughness reducing from 2-3 µm to ~0.2 µm in 180 min of finishing time. But with the present high-speed MAF, the 50.8 m long tube can be finished in 10 min upto 0.1 µm.

Singh *et* al. (2020) performed finishing on the internal Inconel 625 tube using the chemically assisted MAF (CMAF) process. Hard alloys like Inconel are finished using the CMAF process. In this process, the finishing is performed by chemical reaction using etchants. As the etchant makes the workpiece surface soft. Then the magnetic abrasive finishing is performed over the workpiece tube surface of Ø 25 mm × 150 mm × 2 mm. The enhancement in the roundness of the workpiece was analysed. This etched workpiece is held by the lathe machine chuck and the magnets are attached using the aluminium fixture. The process parameters were taken as workpiece rotational speed, the weight percentage of the abrasive particles, and chemical composition as 300 rpm, 30 %, and 60 gm/lt. After 75 min of finishing time, the maximum percentage enhancement in inner roundness was achieved upto 32. The enhancement in the internal surface quality after applying the CMAF process was analysed through the improved texture in the scanning electron microscopy image.

2.3 Literature related to advanced finishing processes for the internal cylindrical or flat surfaces of the workpieces with magnetorheological behaviour in the finishing medium

Several advanced finishing processes based on the abrasive fluid finishing medium have been developed to provide good surface qualities over the internal cylindrical or flat surface of the various industrial components. The literature review about the advanced finishing processes with magnetorheological behaviour are discussed below.

Jha and Jain (2004) proposed the magnetorheological abrasive flow finishing (MRAFF) process for the finishing stainless steel cylindrical samples. The magnetorheological polishing (MRP) fluid used in this process comprises of 20% of carbonyl iron powder (CIP- grade CS from BASF, avg. particle size 18 µm), 20% volume of silicon carbide (SiC) abrasive powder of mesh size 400 along

with carrier fluid 60% (80% of paraffin oil and 20% of grease). The magnetic field is placed externally across the stainless-steel workpiece. As the magnetic source is placed outside the workpiece, so the iron particles move towards the internal surface of the cylindrical workpiece. As the MRP fluid is pushed back and forth by the pistons through the passage formed in the workpiece and the fixture, so the abrasives abrade the roughness from the stainless-steel workpiece surface and the finishing process is performed. In the case of ferromagnetic workpiece also the magnetic field is applied from outside of the workpiece. Thus, resistance is experienced by the relative motion of the active abrasive particles while finishing. Thus, the finishing on the ferromagnetic internal cylindrical workpiece surface can be found less effective. So, this MRAFF process is limited to finish the non-ferromagnetic internal cylindrical workpieces surface. In this process, as the MRP fluid's rheological viscous properties depend upon the magnetic field strength, so its effect on surface roughness is graphically reported in Fig. 2.1.

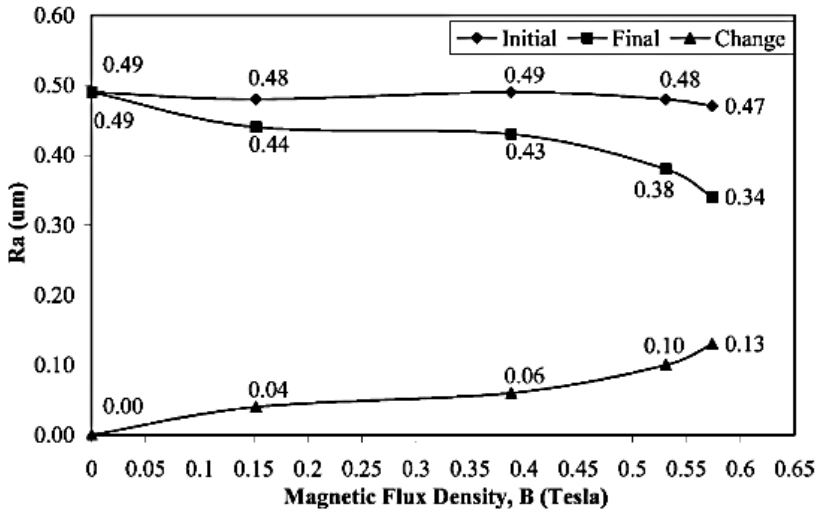

Fig. 2.1 Effect of magnetic field strength on Ra value over the internal cylindrical stainless steel workpiece surface (Jha and Jain 2004).

Das *et* al., (2010) developed the rotational-MRAFF process setup by providing the rotational motion to the permanent magnet. In this process, the MRP fluid is prepared by homogeneously mixing 26.6% volume concentration of electrolytic iron powder, SiC abrasive particles as 13.4% with base fluid (paraffin as 48% and AP3 grease as 12%). Similar to the MRAFF process, the MRP fluid is extruded through the stainless-steel tube. The trials were carried out by managing the reciprocation motion of the magnetorheological polishing (MRP) fluid as a finishing medium, with the rotational motion of the magnets. The mirror-like surface finish might be attained in the

nanoscale with such controlled motions. The finishing process parameters were taken as extrusion pressure of 40 bar, the rotational speed of magnet of 149 rpm, and abrasive mesh size of 153. After 1200 finishing cycles the surface roughness is reduced to 16 nm from ~490 nm.

Singh *et* al. (2012) proposed a new ball end magnetorheological finishing process to finish the ferromagnetic flat workpiece surface. The composition of the MRP fluid is carbonyl iron particles of CS grade as 20%, SiC abrasive powder as 20%, and carrier fluid (paraffin oil and AP3 grease) as 60%. In this process, the pressurized MRP fluid is passed through the electromagnetic tool. Under the action of the applied magnetic field, the supplied MRP fluid forms stiffened ball end finishing spot of MRP fluid. This stiffened ball end MRP fluid due to rotational tool core and reciprocation perform finishing over the flat workpiece surface. The finishing process parameters are central rotating tool core speed, working gap, current, and feed rate of to and fro motion of the workpiece are 500 rpm, 0.66 mm, 4 A, and 50 mm/min, respectively. After 120 min of MR finishing, the surface roughness is reduced from 142.9 nm to 19.7 nm as reported in Fig. 2.2. This process can only be utilized for the finishing of external workpiece surfaces.

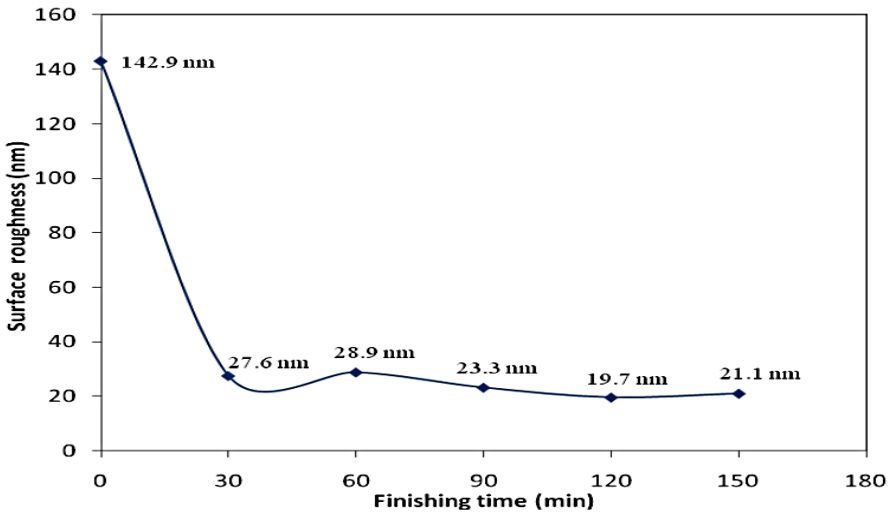

Fig. 2.2 Effect of finishing time on surface roughness value of ferromagnetic workpiece (Singh *et* al., 2012).

Wang *et* al. (2015) developed a magnetorheological finishing process for the finishing of internal cubical surface made up of tool steel of Cr12. Permanent magnets are used over the tool surface for the finishing of the workpiece. The MR polishing fluid used for the finishing of the Cr12 die cavity is iron powder, SiC, water, and polyethylene glycol. The volume ratio of solid to the liquid

used in this MRP fluid-based finishing process is 1:1. The finishing process parameters are considered as a stroke of reciprocation movement, reciprocating cycle and polishing gap as 40 mm, 12000, and 0.5 mm, respectively. The surface roughness value achieved after MR finishing is 0.134 µm on the plain surface and 0.278 µm on the corner from the initial surface roughness value of 0.303 µm. The results show that the with the increase in the corner radius of the die cavity, the magnetic flux density between the tool and the workpiece upsurges. The workpiece used in this magnetorheological finishing process is having a cubical internal surface. The tool in this process comprises a permanent magnetic tool. As the finishing is performed with the tool in this process over the workpiece surface, the corners cannot be significantly finished. This is due to the relatively more working gap where magnetic flux density is not sufficient for the required level of stiffens in the magnetorheological polishing fluid. After the corner radius is increased, a relative decrease in the working gap results in an increase in magnetic flux density and correspondingly an increase in stiffness of the magnetorheological polishing fluid. Further, with the increase in magnetic flux density, there is an improvement in surface finishing.

Bedi and Singh (2018c) developed an electromagnetic magnetorheological finishing process that can be utilized for the finishing of ferromagnetic and non-ferromagnetic internal cylindrical workpiece surfaces. In the existing processes like MRAFF and R-MRAFF, the magnetic source was kept outside of the workpiece where a higher magnetic field can be experienced and reduced towards the inner workpiece surface as can be observed from Fig. 2.3(a). This may result in the resistance to the relative motion of the MRP fluid over the ferromagnetic workpiece surface. So, this process (Bedi and Singh, 2018c) is developed with an electromagnetically magnetized tool core which is placed towards the internal surface of the ferromagnetic cylindrical workpiece. A higher gradient of magnetic flux density (Fig. 2.3(b)) in the working gap permits easy movement of the abrasive particle's away from the finishing tool surface and towards the internal workpiece surface. After 90 min of finishing time, the final surface roughness value is 83 nm which is reduced from the initial value of 368 nm. The diameter of this electromagnetic tool is made with 70 mm, so it cannot finish different workpieces with small and variable diameters.

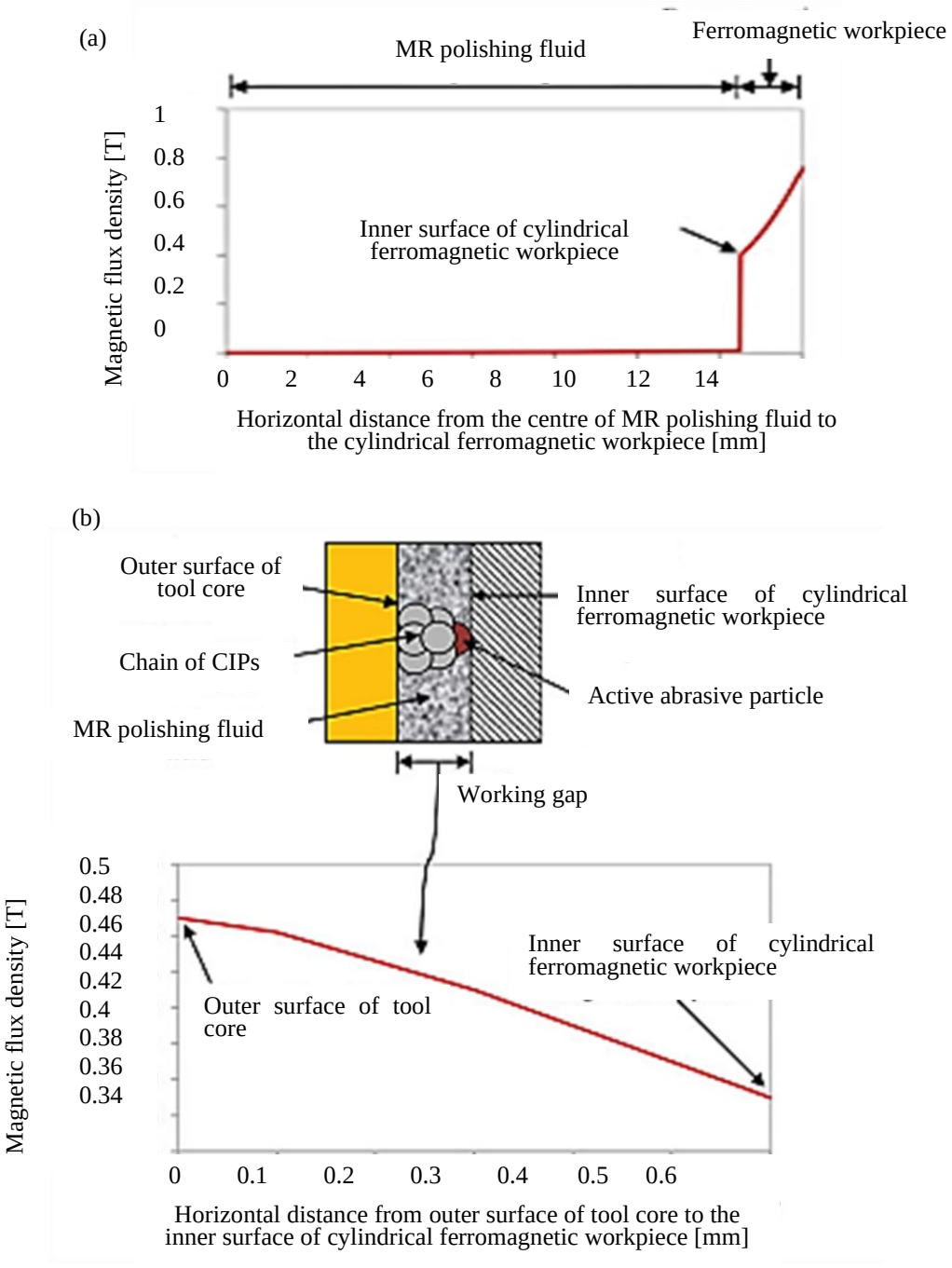

Fig. 2.3 2D plot of magnetic flux density distribution using magnetostatic finite element analysis (a) between the MRP fluid and the cylindrical ferromagnetic workpiece surface, and (b) between the MRP fluid and cylindrical ferromagnetic workpiece surface (Bedi and Singh, 2018c).

Grover and Singh (2017a) developed an electromagnetic MRH tool for the finishing of an internal cylindrical mild steel workpiece. In this process, the magnetic flux density of the I and rectangular shape of the tool core is compared.

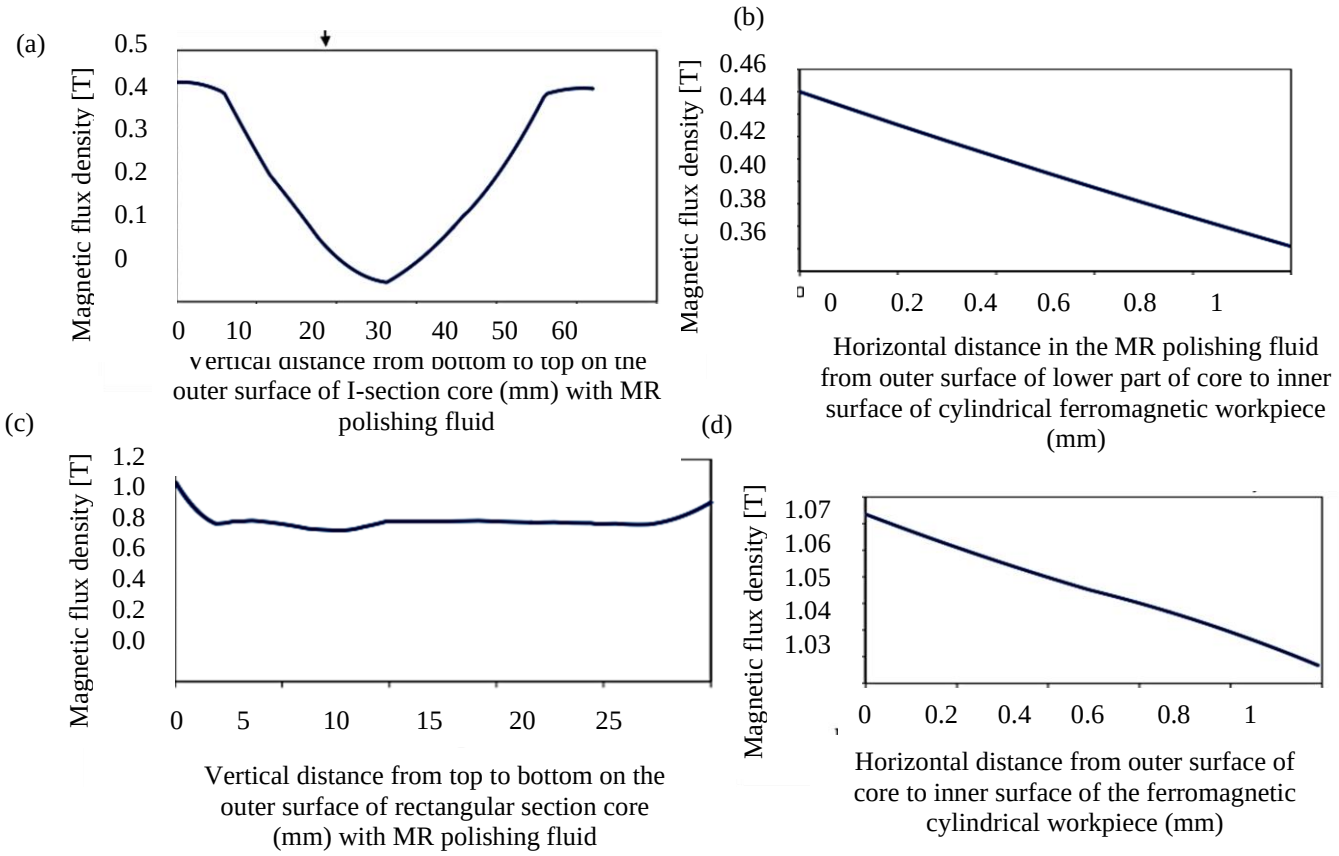

Fig. 2.4 2D plots of magnetic flux density (a) over the outer I-shaped tool surface, (b) within the working gap, (c) over the outer rectangular shaped tool surface, and (d) within the working gap (Grover and Singh, 2017a).

The magnetic flux density on the I-shaped tool core in Fig. 2.4 (a) and (b) is uniform and higher as compared to the rectangular tool core which can be observed from Fig. 2.4 (c) and (d). This enhancement in the process with the developed rectangular-shaped tool core is validated through experimentation. Thus, the MRP fluid used for experimentation is composed of 20% volume concentration of CIP, 20% volume concentration of SiC, and 60% volume concentration of base fluid. The process parameters used for finishing are current, working gap, MRH tool rotational and reciprocation speed as 2 A, 1 mm, 500 rpm, and 55 cm/min, respectively. After finishing for 100

min over the internal cylindrical workpiece surface, the surface roughness is reduced to 97 nm from the initial value of 518 nm using the MRH tool with the rectangular-shaped core. On the other hand, the I-shaped MRH tool can finish upto 224 nm from the initial surface roughness value of 510 nm. These results present that the rectangular-shaped MRH tool is effective to finish the internal cylindrical workpiece surface.

Grover and Singh (2017b) developed an improved magnetorheological honing (MRH) process which can fine finish the internal cylindrical workpieces with variable diameters. The MRH process uses permanent magnetic strips to hold the magnetorheological polishing (MRP) fluid. The mechanism utilized in this process permits the radial adjustment of the magnetic strips for their easy inward and outward movement. The tool diameter varies from 32 to 60 mm as per the requirement.

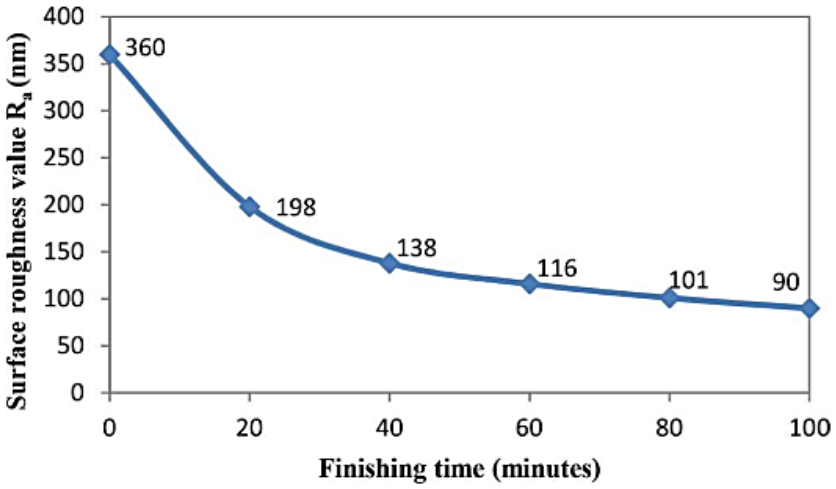

Fig. 2.5 Reduction in surface roughness value (Ra) during the finishing of the internal surface of the cylindrical ferromagnetic workpiece by using the present magnetorheological honing process in 100 min of finishing time (Grover and Singh, 2017b).

The MRP fluid utilized in this process comprises of 20 % of SiC abrasive particles with mesh size as 19 µm, 20 % vol. of carbonyl iron particles with mesh size 18 µm, and base fluid as 60 % (80 % paraffin oil and 20 % AP3 grease by weight). A mild steel ferromagnetic internal cylindrical workpiece surface is fine finished using this process. The process parameters utilized during finishing with the MRH process are tool rotation, tool reciprocation, and working gap as 400 rpm, 70 cm/min, and 0.6 mm, respectively. The surface roughness value after 100 min of finishing time is reduced to 90 nm from the initial value of 360 nm as can be observed in Fig. 2.5. Also, in this

study, only the rotational and reciprocation motion of the MRH tool is studied on the fixed cylindrical workpiece surface. Further, the role of tangential and axial shear forces in the finishing mechanism was not examined due to the rotation of the cylindrical workpiece in this work.

Alam and Jha (2017) developed a model for the theoretical analysis of the surface roughness and mechanism associated with the ferromagnetic workpiece using the ball end magnetorheological finishing tool. In this process, first the model of the variation in magnetic flux density in the working gap is developed. Then, the theoretical models of the normal indentation and shear forces are developed to perceive the material removal mechanism. The Brinell hardness model was used to calculate the indenting force. From the model, finally the surface roughness value is calculated. CIPs of 19 μm and SiC of 18 μm with average particle diameter form a BCC unit cell structure was proposed in this work. Considering the parameters like current, working gap, tool rotation as 3 A, 1 mm and 200 rpm, the surface roughness value is reduced to 78 nm in 10 min of finishing time. On comparing the theoretical and experimental data, the percentage errors was found to be in the range of 7.23 to 31.19.

Paswan and Singh (2019) proposed a model to enhance the finishing performance of the existing magnetorheological honing (MRH) tool by adding rotational motion to the cylindrical workpiece. Owing to the addition of the cylindrical workpiece rotation, the relative motion of the active abrasive particle is increased. This increase in relative motion has reduced the gap between the pitch formed by the single active abrasive particle, thus the magnetorheological honing tool is able to finish the internal cylindrical workpiece surface at a higher finishing rate. The path length of the rotational MRH tool is calculated and compared with the existing MRH tool. Also, the theoretical model is developed to calculated the surface roughness value for the developed rotational MRH process. For the experimentation, the workpiece rotation, working gap, tool rotation and reciprocation are taken as 40 rpm, 1.7 mm, 400 rpm and 70 cm/min, respectively. After, the experimentation the surface roughness value is reduced from 330 nm to 60 nm in 60 min of finishing time. The percentage error between the theoretically calculated and experimentally obtained surface roughness value is in the range of 3.33 to 5.92.

2.4 Literature related to advanced finishing processes for finishing both the surfaces of cylindrical blind hole type workpieces using magnetorheological polishing fluid as finishing medium

Bedi and Singh (2018b) proposed two magnetorheological finishing tools that are utilized for finishing the surfaces of the cylindrical blind hole type workpieces. The EN31 CBH type workpiece with an inner diameter of 50 mm and bore length of 48 mm is finished using this process. First, the lateral tool surface with permanent magnetic strips is used for the finishing of the lateral surface of the CBH type workpiece. The finishing process parameters used for the finishing of the lateral surface of the CBH type workpiece are rotational tool speed as 800 rpm, translational tool speed as 10 cm/min, working gap as 2 mm. After finishing the lateral CBH type workpiece surface for 90 min, the surface roughness value is reduced to 152 nm from 471 nm (Fig. 2.6). Further, another tool with a permanent magnet towards the bottom surface is used for the finishing of the inner bottom CBH type workpiece surface. The finishing process parameters used for the finishing of the inner bottom CBH type workpiece surface is rotational tool speed of 800 rpm, and working gap as 2 mm..

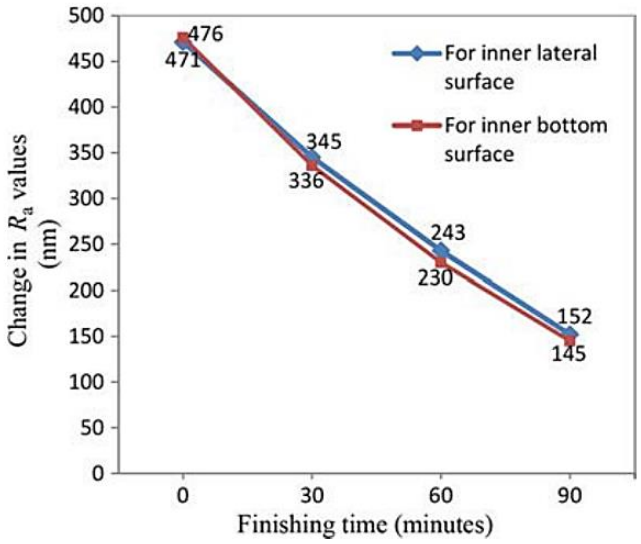

Fig. 2.6 Change in Ra values with respect to finishing time over the inner lateral and bottom surfaces of the CBH EN-31 type workpiece (Bedi and Singh, 2018b).

After performing the finishing process, the surface roughness is reduced to 145 nm from 476 nm in 90 min of finishing time (Fig. 2.6). However, the tool replacement time for finishing the lateral and bottom surfaces of the CBH type workpiece increases the total processing time of the final

product. Also, this process utilizes permanent magnets which provide hindrance in-process control while finishing is performed over the internal surfaces of the CBH type workpieces.

2.5 Research gaps

After studying the literature review, it has been seen that many finishing processes are evolved as per the need to the finishing of different types of materials, shapes and sizes of the workpieces, level of finishing etc. In this way various traditional and advanced finishing processes have been developed. As the traditional finishing process utilizes the direct contact of the bonded abrasive particles with the workpiece surface, the surface defects such as micro or macro cracks, thermal damage, change in microstructures, and residual stresses may occur (Gupte *et* al., 2008). Owing to these defects, a nano-level finishing cannot be achieved over the surface of the workpiece with excellent surface characteristics (Bedi and Singh, 2018a). The grinding processes are used for the finishing of the internal and flat workpiece surfaces (Jaworski and Trzepieciński, 2016; Tawakoli *et* al., 2007). Also, the honing process is used for the finishing of the internal cylindrical surfaces (Lee and Malkin, 1993). These traditional finishing processes don't have much control over finishing forces. Also, difficulties can be found in finishing complex shapes using the traditional finishing processes.

So, the advanced finishing processes came into existence, which can finish the parts better than the traditional finishing processes. The advanced finishing processes like abrasive flow finishing (AFF) and rotational abrasive flow finishing (R-AFF) are capable of finishing the complex geometries and inaccessible areas over the workpiece surface. In this finishing process, the internal cylindrical workpiece surface is finished using the abrasive medium which is accelerated and allowed to flow through the restricted passage (Jain, 2008). Therefore, the prediction of the results becomes tough and found inefficient for the intended function. Further, the magnetorheological abrasive flow finishing (MRAFF) (Jha and Jain, 2004) and R-MRAFF (Das *et* al., 2010) processes are used for finishing the internal cylindrical workpiece surface made up of non-ferromagnetic material. But these processes are not found effective for the finishing of the ferromagnetic workpiece (Bedi and Singh, 2018). Next, the magnetic abrasive finishing is capable to finish the flat or internal cylindrical workpiece surface. But this process is only applicable for the finishing of hard and non-ferromagnetic workpieces. This is owing to the use of a source for magnetization towards the external surface of the workpiece (magnets outside the workpiece surface). Also, the

heat may generate owing to the dry abrasives and magnetic iron particles. A new ball end magnetorheological finishing process is used for the finishing of the flat and 3D external workpiece surfaces (Singh *et* al., 2012). The magnetorheological honing process is developed to finish the internal cylindrical surface of both the ferromagnetic and non-ferromagnetic workpieces (Bedi and Singh, 2018a). But the limitation is that they cannot be used for the finishing of the variable diameters of the internal cylindrical surface (Grover and Singh, 2017a). So, the improvement was made in the magnetorheological honing process in which a tool with the strip of permanent magnets as similar to the conventional honing tool was used for the finishing of the cylindrical workpieces with different internal diameters. The tool was capable of finishing both types of cylindrical workpieces (ferromagnetic and non-ferromagnetic) and was suitable for workpieces with different diameters. This process is capable to finish the internal cylindrical workpiece surface upto a particular range (34 to 60 mm diameter) only (Grover and Singh, 2017b). Further, a new rotational-MRH process is used to enhance the performance of the pre-existing MRH process. Also, the tool of the rotational-MRH process is kept same as 34 to 60 mm in diameter, so it cannot be used for finishing the workpiece with a smaller diameter. Further, two tools were used for the finishing of cylindrical blind hole (CBH) type workpiece surfaces (Bedi and Singh, 2018b). The replacement time of the tool may increase the processing time of the finishing.

From the literature, it is found that two permanent magnetic tools are used for the finishing of longitudinal and flat end surfaces of the CBH type workpiece. The range of the MRH tool to finishing diameter is found to vary upto a certain limit (34 to 60 mm diameter). Also, there is no in-process control over the finishing forces owing to the use of permanent magnets when different workpieces with different materials need to be finished. So, from the above discussions, the important literature gaps are reported as follows.

- The existing MR finishing processes (Bedi and Singh, 2018b) are capable to finish only a single diameter internal cylindrical surface or limited to a particular range of diameter. Beyond the range whether below or above, these MR honing processes are not capable to perform finishing.

- Using two separate permanent magnet-based tools for finishing the internal longitudinal and flat end surfaces of the cylindrical blind hole type workpiece (Bedi and Singh, 2018b), may increase processing time and reduces the productivity of the process.
- There is likely, no such magnetorheological finishing process which is designed and developed to finish both the internal cylindrical as well as the flat end surfaces of the cylindrical blind hole type workpieces with a single tool.
- The theoretical analysis for the magnetic flux density and surface roughness is required for the single electromagnetic magnetorheological finishing tool to understand the finishing mechanism performed over the CBH type workpiece surfaces.
- An electromagnetic MR finishing process is required to fine finish the cylindrical blind hole type workpiece having different diameters. This can be achieved by the eccentric movement of the MR finishing tool as a similar mechanism to the traditional internal cylindrical grinding process.
- There is likely, no such magnetorheological finishing processes which can finish the internal cylindrical tapered surface of the CBH type workpiece.

On considering the above-mentioned literature gaps, there is a requirement for fine finishing the internal longitudinal and flat end surfaces of the cylindrical blind hole type components that are utilized in various industries. So, to fine finish the longitudinal and flat end surfaces of the CBH type workpiece, a new single magnetorheological polishing fluid-based electromagnetically controlled tool is required to be designed and developed. This tool can perform the finishing operation similarly in mechanism to the grinding wheel of the traditional internal cylindrical grinding process. Thus, it is named as a magnetorheological grinding tool. To validate the magnetorheological grinding tool for the finishing of longitudinal and flat end surfaces of the CBH type workpiece, preliminary experiments need to be performed. Further, the theoretical analysis for surface roughness is experimentally validated for the longitudinal and flat end surfaces of the CBH type workpiece. Later, the performance of the developed magnetorheological grinding tool is required to be experimentally examined for finishing the cylindrical tapered internal mould cavities made up of EN31 and H13 materials. During the experimental analysis over tapered internal mould cavities, the optimum process parameters are to be predicted for finishing the

longitudinal and flat end CBH type workpiece surfaces using the developed magnetorheological grinding tool. Later, an investigation is to be performed using surface roughness profile and surface characteristics over the MR finished CBH type workpiece surfaces to check the performance of the developed magnetorheological grinding tool. Based on the research gaps as identified through the literature, the research objectives are mentioned below.

2.6 Research objectives

- Design and development of the magnetorheological grinding tool for the finishing of cylindrical blind holes surface.
- Theoretical study of the finishing mechanism with the developed magnetorheological grinding tool for change in surface roughness.
- Experimentally examine the performance of the developed magnetorheological grinding tool to finish the industrial components such as cylindrical tapered internal mould cavities used for the manufacturing of various cylindrical tapered type end products.
- Analyse the effects of input process parameters such as abrasive particles, iron particles, magnetizing current, working gap, the rotational speed of the cylindrical blind hole type workpiece, rotational and reciprocation speed of the tool on the process response like surface finish improvement using response surface methodology in order to optimize the process performance with the developed magnetorheological grinding tool.
- Investigate surface characteristics and roughness profiles of the finished blind hole surfaces with the developed magnetorheological grinding tool with the help of the roughness tester and scanning electron microscopy.

2.7 Organization of the thesis chapters

The thesis is organized into the following chapters including the references.

Chapter 1 introduces the applicability of the various traditional and advanced finishing processes utilized for the finishing of cylindrical longitudinal or flat surfaces of the workpieces. This chapter also describes the advantages of utilizing the advanced finishing process over the traditional finishing process.

Chapter 2 contains the discussion about the existing literature review about the traditional and advanced finishing processes utilized for the finishing of the cylindrical longitudinal surface or flat surface of the workpieces. From this literature work, the requirement of present work for the effective, uniform, and fine finishing of longitudinal and flat end surfaces of the cylindrical blind hole (CBH) type workpieces are reported. The research objectives of the present work are reported at the end of this chapter.

Chapter 3 describes the design and development of the magnetorheological grinding (MRG) tool to fine finish the longitudinal and flat end surfaces of the CBH type workpiece.

Chapter 4 reports the theoretical analysis for the change in surface roughness value in the developed MRG tool-based process for fine finishing the longitudinal and flat end surfaces of the CBH type workpieces.

Chapter 5 discusses the preliminary experiments to validate the performance of the presently designed single electromagnetic based MRG tool for fine finishing over the longitudinal and flat end surfaces of the CBH type mould cavity.

Chapter 6 reports the effects of finishing process parameters on the $\%\Delta Ra$ utilizing response surface methodology to predict the optimum parameters for better finishing of interior longitudinal and flat end surfaces of CBH type mould cavity made up of EN31 and H13 materials. Further, the improvement in the surface is investigated using a roughness profile. Also, surface quality enhancement is investigated using the surface characteristics such as scanning electron microscopy and circularity.

Chapter 7 provides the conclusions and significant outcomes from the present research work and also define the scope for future work.

CHAPTER 3

DESIGN AND DEVELOPMENT OF THE MAGNETORHEOLOGICAL GRINDING TOOL FOR THE FINISHING OF CYLINDRICAL BLIND HOLES SURFACE

As stated under the research gaps (chapter 2), the existing MR finishing processes are used either to finish the flat, 3D external, or internal cylindrical through-hole surface of the workpieces. Also, two permanent magnet-based magnetorheological finishing tools are used to achieve finishing over the longitudinal and flat end surfaces of the cylindrical blind hole (CBH) type workpiece (Bedi and Singh, 2018). The tool replacement for each surface of the CBH type workpiece can be time-consuming, and overall finishing time gets increased. Further, this MR finishing process with two separately permanent magnet-based tools (Sirwal and Singh, 2018; Bedi and Singh, 2018; Sirwal and Singh, 2020) can find difficulty in fine finishing the longitudinal and flat end surfaces of the CBH type workpieces with a diameter of less than 50 mm. This restriction is because of the coaxial rotation of the CBH type workpiece and the tool. Therefore, a single magnetic tool is required to fine finish the CBH type workpieces with different diameters. This is only possible when the smaller rotating tool operates eccentrically from the center of the CBH type workpiece with an operating mechanism similar to the internal centerless grinding process. Also, the permanent magnet-based tools can find difficulty in controlling the magnetic force for different workpiece materials due to the constant magnetic flux density. This results in difficulty for in-process control in the permanent magnet-based magnetorheological finishing (MRF) processes. So, there is a need to develop an electromagnetic-based tool with eccentric rotation to overcome the issues related to the permanent magnet-based MRF processes. So, an electromagnetic-based magnetorheological grinding (MRG) tool with eccentric rotation is designed and developed in the present work.

3.1 Design and development of magnetorheological grinding tool for the finishing of cylindrical blind holes surface

To fulfill the requirement to fine finish the longitudinal and flat end surfaces of the cylindrical blind hole type workpiece, a new electromagnetic magnetorheological grinding (MRG) tool is designed which can operate eccentrically from the center of the workpiece as similar to the centreless grinding process as shown in Figs. 3.1(a) and (b). Further, the flat end surface of the

CBH type workpiece is finished using the flat MRG tool surface. During finishing, the setup used to magnetize and hold the MRG tool core is shown in Fig. 3.2.

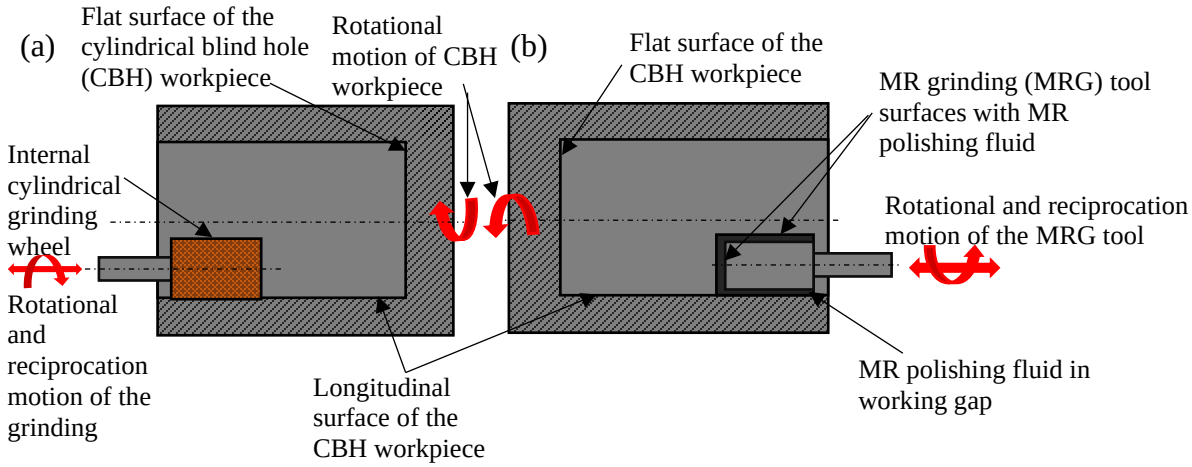

Fig. 3.1 Schematic diagram with working principle of the (a) traditional internal cylindrical grinding process and (b) the proposed process with the MR grinding (MRG) tool used to finish the longitudinal as well as flat end surfaces of the cylindrical blind hole (CBH) workpiece.

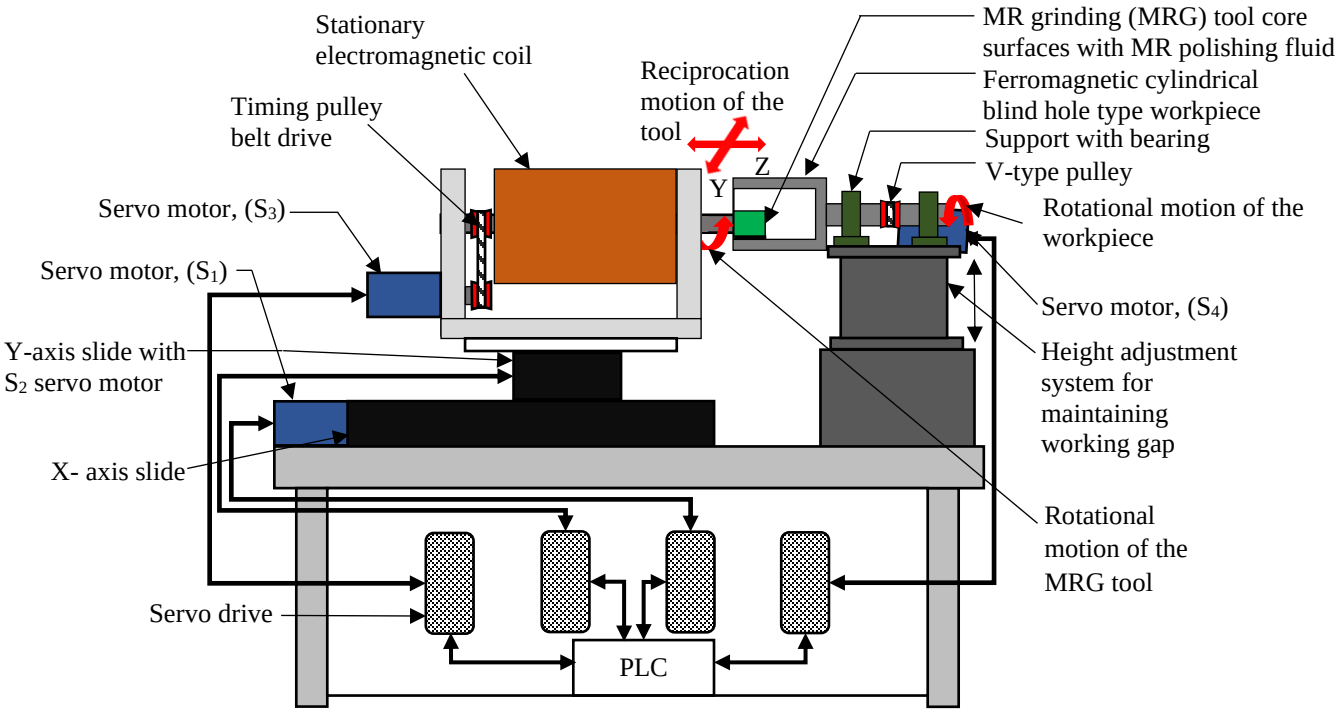

Fig. 3.2 Schematic diagram of the magnetorheological grinding (MRG) tool while finishing the internal surfaces of the blind hole workpiece with the different controlled motions.

In the present work, the longitudinal and flat end surfaces of the cylindrical blind hole (CBH) type workpiece is finished using the magnetic longitudinal and flat end surfaces of the

magnetorheological grinding (MRG) tool (Fig. 3.2). For maintaining the uniform working gap between the longitudinal surface of the CBH type workpiece and the longitudinal MRG tool surface, the height adjustment system is used. Thus, an electromagnetically controlled single MR grinding tool can perform finishing on both the surfaces of the CBH type workpiece with different controlled motions as shown in Fig. 3.2. Also, the presently proposed tool must ensure a higher and uniform concentration of magnetic flux (B) which is to be acquired on the finishing surfaces of the MRG tool. This results in strongly retaining the magnetorheological polishing (MRP) fluid on the finishing surfaces of the MRG tool.

To design the MRG tool, the magnetostatic finite element (FE) analysis is performed for obtaining the maximum possible value of magnetic flux density on the finishing surfaces of the MRG tool. The magnetic flux density (B) plays a significant role in magnetorheological finishing processes in providing strength to the MRP fluid which performs finishing on the workpiece surface. The dimensions of the finishing surfaces of the MRG tool are selected based on different trials performed in the magnetostatic FE analysis for obtaining the maximum value of B. The Ansoft Maxwell V13 is used for the FE analysis. The computer-aided design (CAD) models of the initially proposed MRG tool without any grooves on its finishing surfaces is depicted in Figs. 3.3(a) and (b).

The CAD model of the magnetorheological grinding (MRG) tool comprises of the electromagnetic tool core, a copper coil wound around the tool core, a layer of magnetorheological polishing (MRP) fluid placed over the surfaces of the MRG tool in the working gap and the ferromagnetic cylindrical blind hole (CBH) type workpiece. The thickness of magnetorheological polishing (MRP) fluid is kept as 0.6 mm in the working gap amid the MRG tool and the CBH type workpiece surfaces. The material with their properties has been allotted to each part of the electromagnetic model based on the literature (Bedi and Singh, 2018c; Grover and Singh, 2018b). The coil of copper with relative permeability as 1, turns of copper wire (diameter of wire as 0.8 mm) as 2600 and current as 2A, the finishing media is MRP fluid with relative permeability as 5, the tool core and the ferromagnetic CBH type workpiece of mild steel with relative permeability as 600 are assigned. After the parameters are assigned to the model, the sectioning of the coil is done, and then the sectioned portions are separated from each other. Further, one of the separated portions of the coil is provided with an excitation (current) value. After assigning all these values, the environment is given to the electromagnetic setup, and the finite element (FE) analysis is executed.

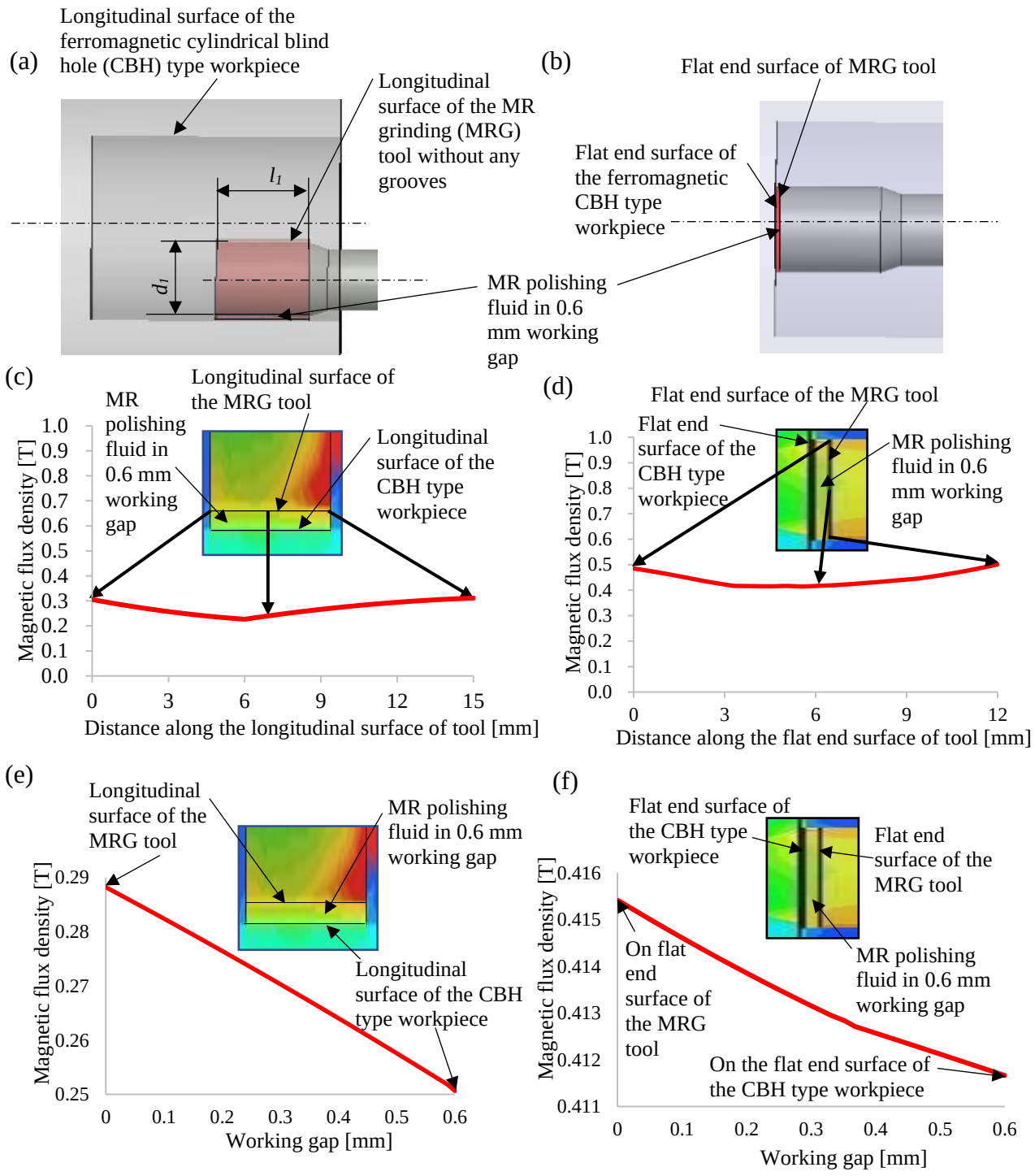

Fig. 3.3 CAD model with (a) longitudinal surface and (b) flat end surface of the MR grinding (MRG) tool without any grooves, 2D plot of the FE analysis of magnetic flux density distribution on the (c) longitudinal surface, and (d) flat end surface of the MRG tool without any grooves, in working gap with (e) longitudinal surface and (f) flat end surface of the tool and ferromagnetic cylindrical blind hole (CBH) type workpiece surfaces.

After the FE analysis with different trials for obtaining maximum flux density, the length of the longitudinal finishing surface of the MRG tool is found as 15 mm (l_1) and diameter of the flat end surface of the MRG tool is found as 12 mm (d_1), which is depicted in Fig. 3.3(a). The value of magnetic flux density is obtained as 0.2875 T on the longitudinal surface and 0.4153 T on the flat end surface of the initially designed MRG tool, which is depicted in Figs. 3.3(c) and (d). The magnetic flux is obtained more on the finishing surfaces of the MRG tool and reduces towards the surfaces of the CBH type workpiece, which can be observed from the 2D plot of the magnetic flux gradient as depicted in Figs. 3.3(e) and (f). This helps the MRG tool to retain the MRP fluid on its surfaces during the finishing process. Thus, from the results of the FE analysis, it is analysed that the initially proposed single MRG tool can be used to finish both the surfaces of the CBH type workpiece. The final dimensions of the initially proposed MRH tool core after different trials of the FE analysis for obtaining maximum magnetic flux density on its finishing surfaces (Fig. 3.3 c and d) is shown in Fig. 3.4 (a-d). The 2D drawing of the projected front view, projected side view, 3D CAD view and fabricated magnetorheological grinding tool is shown in Fig. 3.4 (a-d).

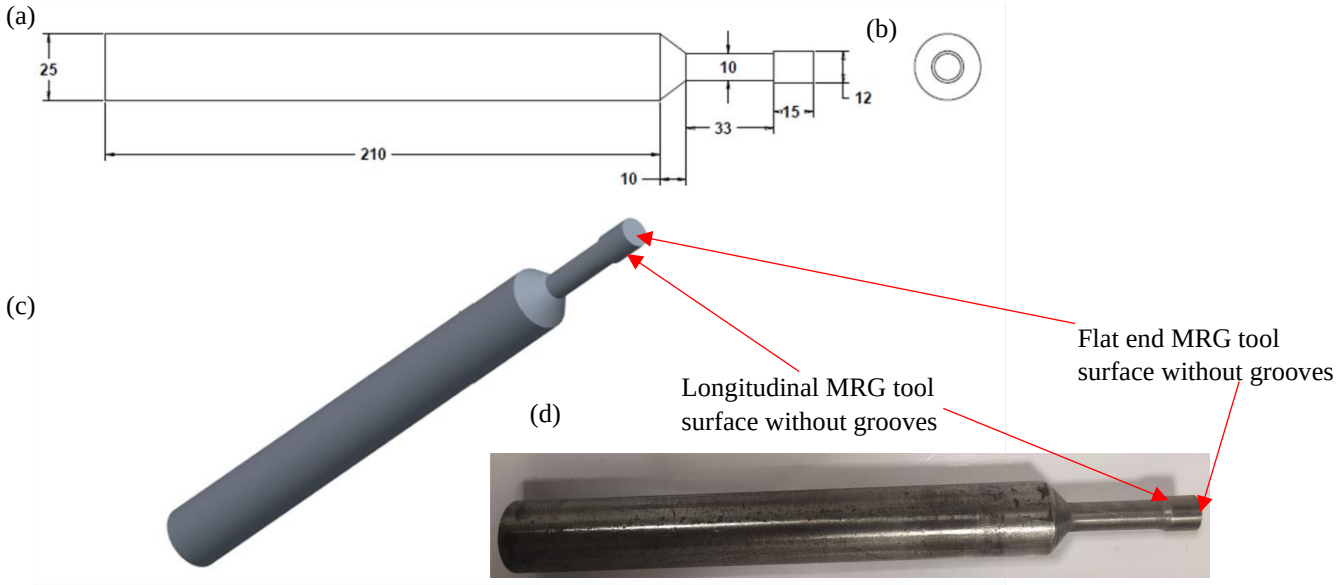

Fig. 3.4 2D drawing of the (a) projected front view, (b) projected side view, (c) 3D CAD model, and (d) fabricated magnetorheological grinding tool without grooves.

After different trials of the FE analysis for inducing maximum magnetic flux density on the finishing surfaces of the MRG tool (Fig. 3.3 c and d), the number of turns of copper wire (diameter 0.8 mm) on the electromagnetic coil is obtained as 2600 with the dimensions as shown in Fig. 3.5.

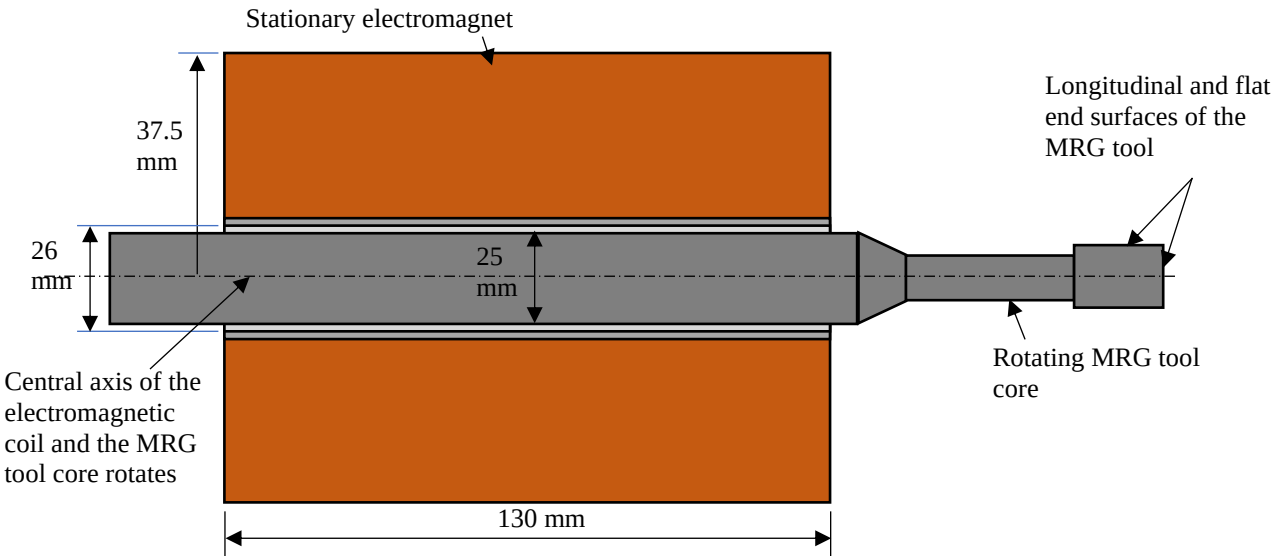

Fig. 3.5 Dimensions of the electromagnetic tool coil along with the initial proposed MRG tool core without grooves on its finishing surfaces.

Further the FE analysis has been performed to achieve higher flux density on the finishing surfaces of the magnetorheological grinding (MRG) tool with the edge effect phenomenon. The edge effect phenomenon is dependent on the geometrical shape of the MRG tool surfaces. In this phenomenon, the flow of magnetic field lines is localized at the sharp edges, which enhances the magnitude of the magnetic flux density (Singh and Singh, 2019b). So, grooves are made on the finishing surfaces of the proposed MRG tool. Next, to check the effect of the grooves on the finishing surfaces of the MRG tool for a higher concentration of magnetic flux density, finite element (FE) analysis has been performed. Initially, the trials were performed on different shapes of the grooves, such as rectangular, square, and V-shaped. Later on, the trials on variation in the dimensions of the grooves were performed on the MRG tool. The design of the MRG tool was found best with V-shaped grooves, as depicted in Figs. 3.6 (a)−(f). This is because there is more sharpness on the edges of the V-shaped grooves as compared to the rectangular and square-shaped grooves. This leads to the localization of the magnetic field lines on the V-shaped grooves of the finishing surfaces of the MRG tool (Singh and Singh, 2019b). Two grooves are made on the longitudinal surface and two grooves on the flat end surface of the MRG tool as depicted in Figs. 3.6 (a) and (b). The width of each groove is found to be 2 mm with a depth of 0.5 mm, where the maximum magnetic field is achieved. After the finite element (FE) analysis, the 2D magnetic flux density plot along the length of the longitudinal and flat end surfaces of the MRG tool with V-grooves are obtained as depicted

in Figs. 3.6 (c) and (d). It can be seen from the 2D plots that the value of the magnetic flux density (B) is high along the longitudinal and flat end surfaces of the improved MRG tool with V-grooves.

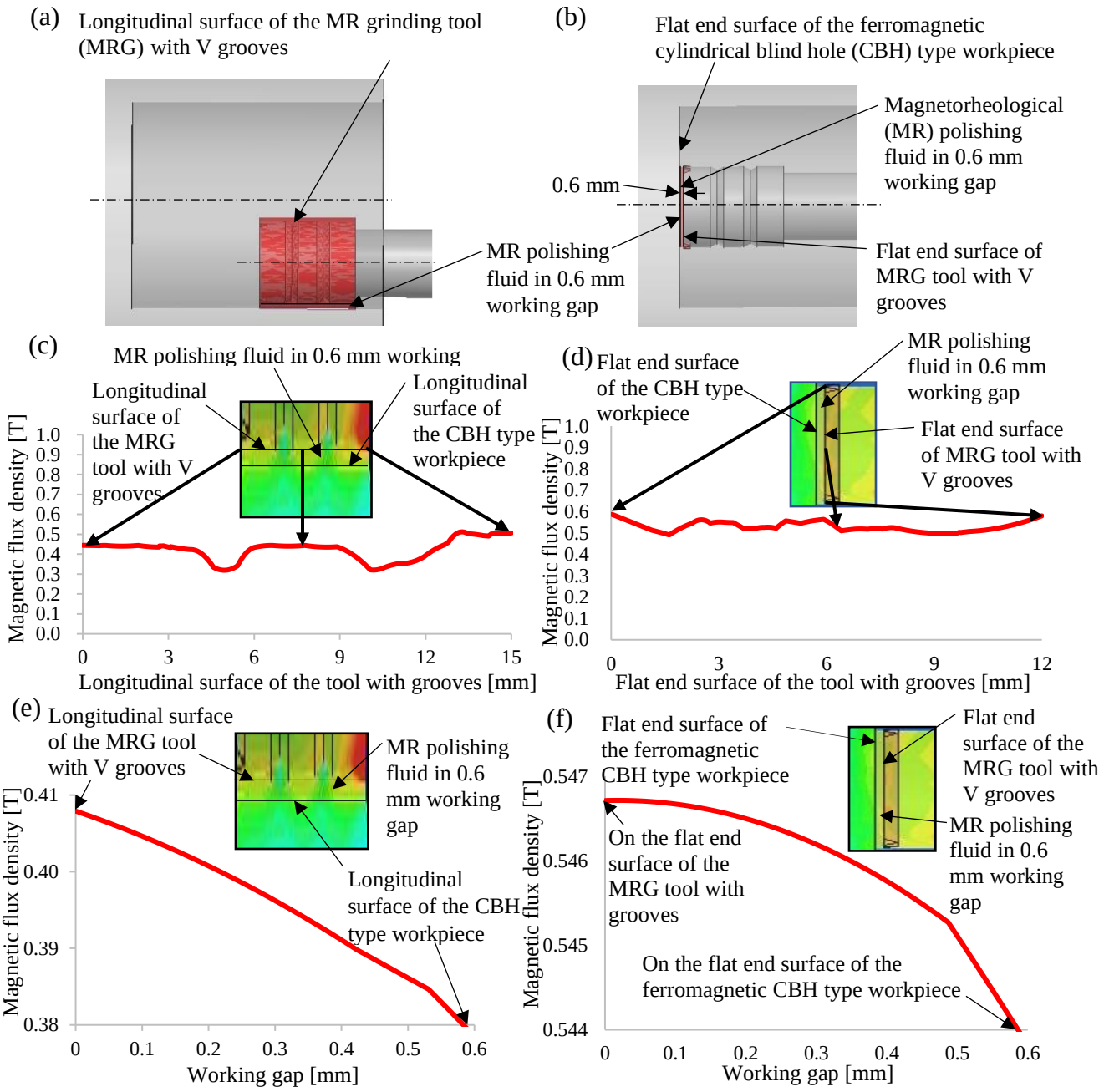

Fig. 3.6 CAD model with (a) longitudinal surface and (b) flat end surface of the MR grinding (MRG) tool having V-grooves, 2D plot of the FE analysis of magnetic flux density distribution on the (c) longitudinal surface and (d) flat end surface of the MRG tool having V-grooves, in working gap with (e) longitudinal surface and (f) flat end surface of the tool and ferromagnetic cylindrical blind hole (CBH) type workpiece surface.

The grooves made on the longitudinal and flat end surfaces of the MRG tool helps to attain the edge effect due to which there is an increment in the concentration of magnetic flux density (Fig. 3.6) as compared to the MRG tool without grooves (Fig. 3.4). This increases the concentration of magnetic flux density over the MRG tool with grooves which can help to retain the iron particles chains of MRP fluid more strongly and uniformly on the finishing surfaces of the tool. This further provides uniform strength to the active abrasive particles (AAPs) for removing the surface asperities during finishing.

The FE analysis results show that the value of magnetic flux density achieved on the longitudinal surface of the MRG tool with grooves is 0.4076 T (Fig. 3.6c) as compared to the MRG tool without grooves (0.2876 T) (Fig. 3.4c) to finish the longitudinal surface of the CBH type workpiece. The concentration of magnetic flux density starts decreasing towards the longitudinal surface of the CBH type workpiece and reduces to 0.3797 T as seen in the graph between magnetic flux density vs. working gap in Fig. 3.6(e). Also, magnetic flux density (B) as compared to the MRG tool without grooves (Fig. 3.4d) on the flat end surface of the MRG tool with grooves get increased from 0.4153 T to 0.5467 T due to the grooves as depicted in Fig. 3.6(d). Further, the value of magnetic flux density is more towards the finishing surfaces of the MRG tool and less on the surfaces of the cylindrical blind hole (CBH) type workpiece (Figs. 3.6e, f or Figs. 3.4e, f) which forms a magnetic flux gradient. This trend in the flux gradient helps in moving the iron particles of the MRP fluid towards the finishing surfaces of the MRG tool and active abrasives towards the longitudinal and flat end surfaces of the CBH type workpiece to perform finishing. It can be observed that the results in the case of the magnetorheological grinding (MRG) tool with grooves have a higher value of magnetic flux density as compared to that obtained on the tool surfaces without grooves.

This represents that the edge effects phenomenon occurs, which enhances the value of B on the longitudinal and flat end surfaces of the MRG tool. Also, the grooves made on the finishing surfaces of the MRG tool can retain the MRP fluid more strongly (Alam *et* al., 2019). Thus, enhanced magnetic flux density on the MRH tool surfaces having V-grooves can provide comparatively better finishing on the longitudinal and flat end surfaces of the CBH type workpieces. The 2D drawing of the projected front view, projected side view, 3D CAD view and fabricated magnetorheological grinding tool with grooves is shown in Fig. 3.7 (a-d). Also, the final

design of the MRG tool core having V-grooves along with the electromagnetic system is shown in Fig. 3.8.

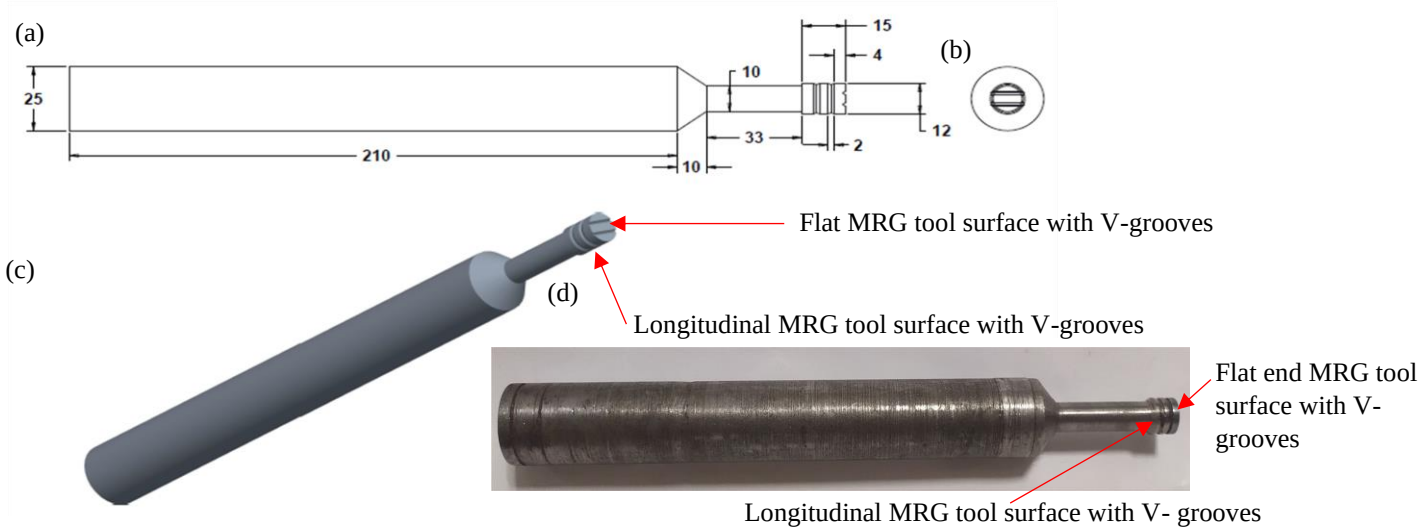

Fig. 3.7 2D drawing of the (a) projected front view, (b) projected side view, (c) 3D CAD model, and (d) fabricated magnetorheological grinding tool with V-grooves.

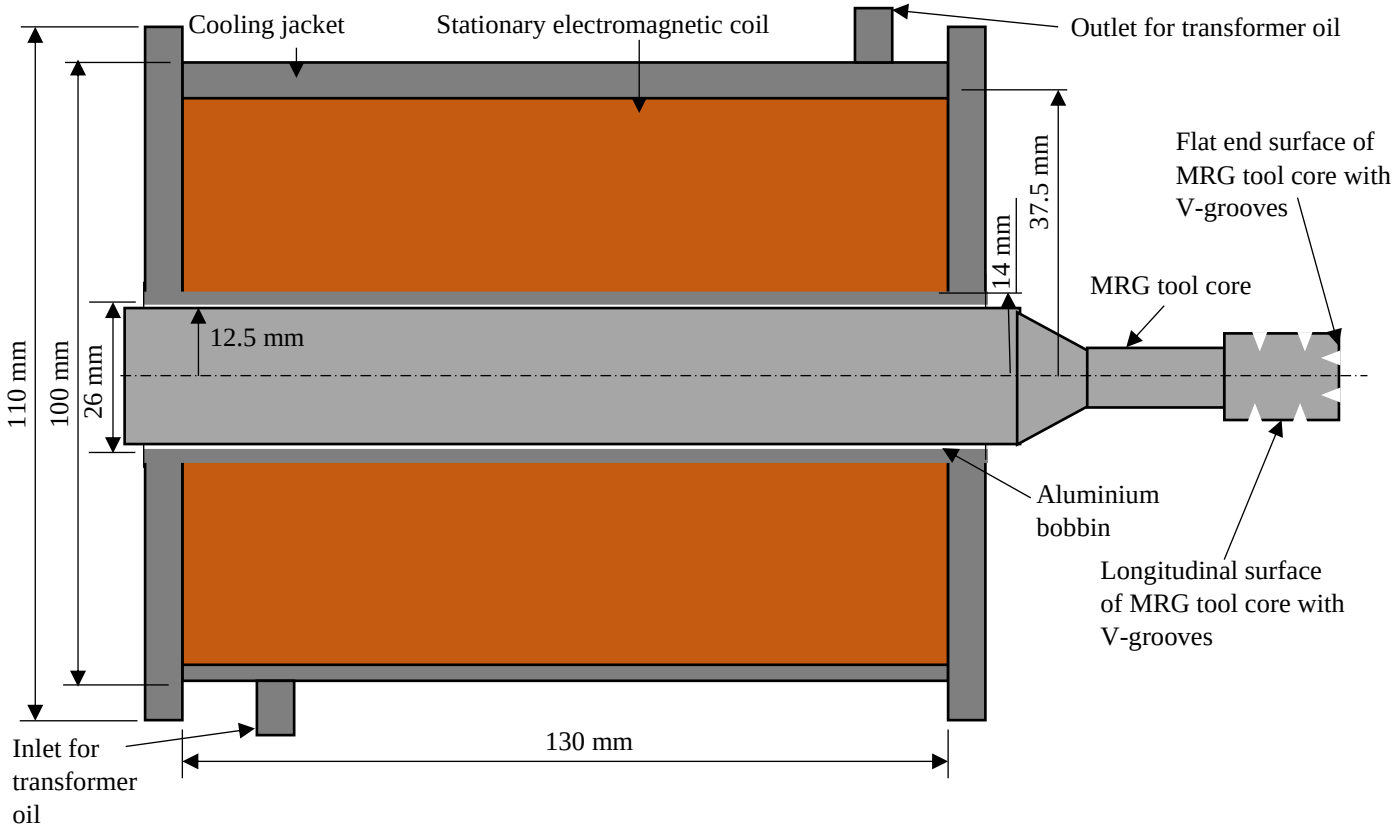

Fig. 3.8 Final geometrical dimensions of the electromagnetic coil over the aluminium bobbin along with the rotating MRG tool core having V-grooves on its finishing surfaces.

3.1.1 Final design of the electromagnet coil along with MRG tool core having V-grooves

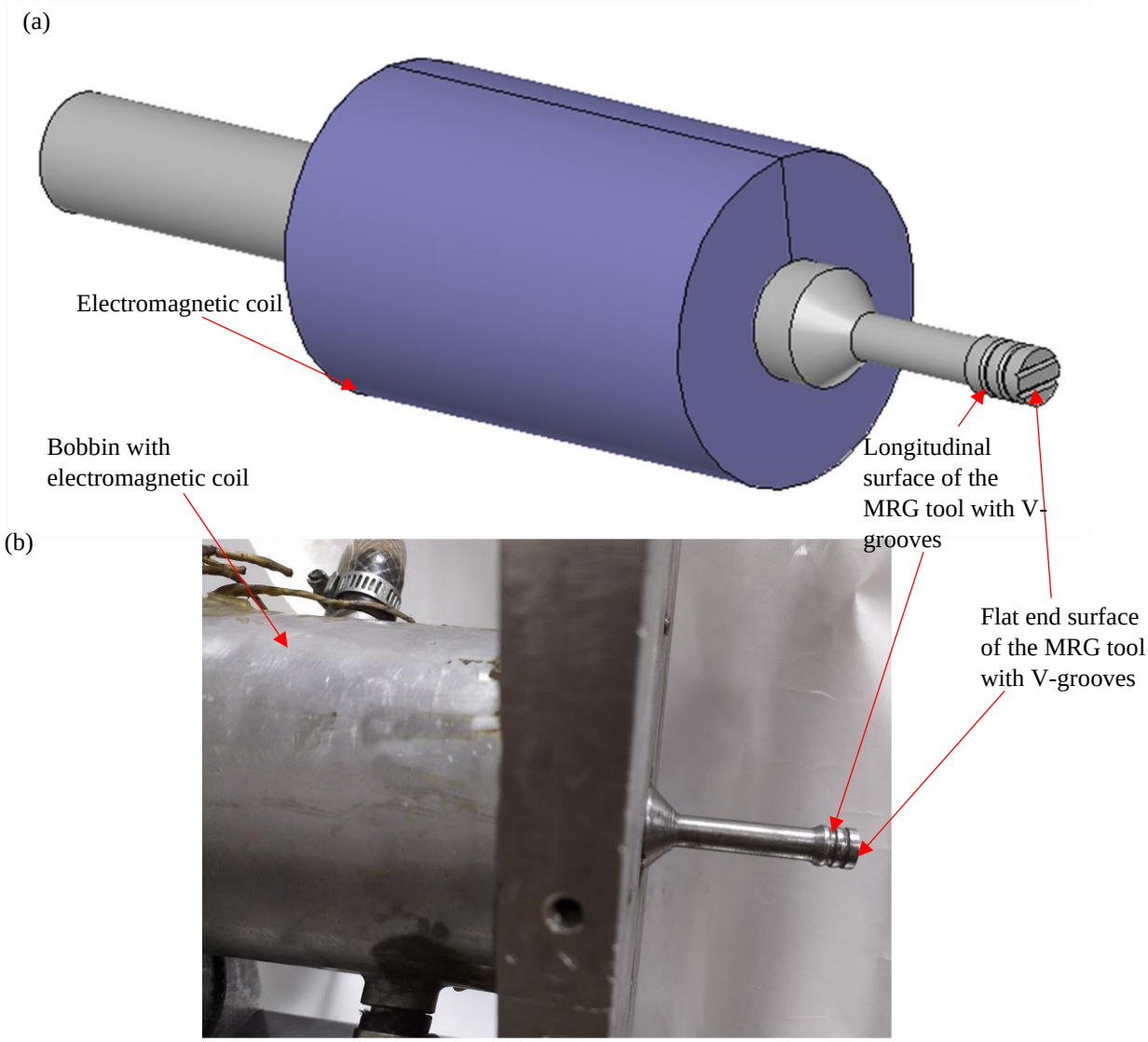

Fig. 3.9 (a) 3D CAD model of the electromagnetic coil with the final designed magnetorheological grinding (MRG) tool core and (b) its fabricated photograph.

The copper coil is used to magnetized the electromagnetic tool, which generates a magnetic field owing to the supply of direct current. The DC current is supplied using the regulating DC power supply. The copper wire size, supply current, radius of the wounded electromagnet coiling, and the number of turns of the copper coiling are the factors that effect of magnetic flux density at the tool core tip surface. Before selecting the electromagnet coil's final parameters, a magnetostatic finite element analysis was used to compare these dependent parameters. The 20-gauge copper wire (0.8 mm in diameter) with 2600 turns at 2 A current produced the highest flux density at the

tool core tip surface. The bobbin is an internal component of the electromagnetic tool. As the tool core is to be rotated inside the aluminium bobbin and the copper wire would be coiled over the bobbin, the dimensions of the aluminium bobbin were determined by the tool core and copper coil dimensions. The bobbin's internal diameter is determined by the least gap through which the tool core may rotate, as well as minimal magnetic flux losses.

The magnetic coil is enclosed by an aluminium cover that works as a cooling jacket. The detailed dimensions of the aluminium cover are shown in Fig. 3.8. The cooling jackets for the copper coil winding are provided by this cover. Due to the continuous DC current supply to the electromagnet coil during the MR finishing, the coil heats up. The loss of magnetic field at the tool core tip surface increases as the coil heats up. The electromagnetic coil is equipped with a cooling jacket to reduce magnetic field loss owing to temperature increases. During MR finishing, coolant is supplied in the cooling jacket to lower the temperature of the electromagnetic coil. The electromagnetic coil with the cooling jacket is mounted on a C-shaped bracket that keeps the copper coil stationary. Thus, the final 3D CAD model of the electromagnetic coil along with the magnetorheological grinding tool is designed and fabricated as shown in Fig. 3.9 (a) and (b). This MRG tool is utilized for the finishing of the longitudinal and flat end surfaces of the CBH type workpieces.

3.1.2 Experimentally measurement of the magnetic flux density on the designed magnetorheological grinding (MRG) tool core surface

After assembling the setup for the MRG tool, the final design of the MRG tool with and without the V-shaped grooves was fabricated. After fabrication of the electromagnetic MRG tool cores, the value of magnetic flux density was also measured experimentally on the finishing surfaces of the MRG tool in the vicinity of the ferromagnetic cylindrical blind hole (CBH) type workpiece surface using the digital gauge meter as presented in Fig. 3.10. The value of magnetic flux density was measured at five different points marked with red dots over the longitudinal and flat end surfaces of the MRG tool core without and with grooves as espied in Figs. 3.10(a) and (b). In Figure 3.10(a), the concentration of magnetic flux is measured along the longitudinal surface and flat end surface of the CBH type workpiece using the MRG tool without grooves. Similarly, in Fig. 3.10(b), the concentration of magnetic flux is measured along the longitudinal and flat end surfaces of the CBH type workpiece using the MRG tool with V-grooves. The concentration of magnetic flux density graphs is compared for the longitudinal and flat end surfaces of the MRG tool without and with grooves.

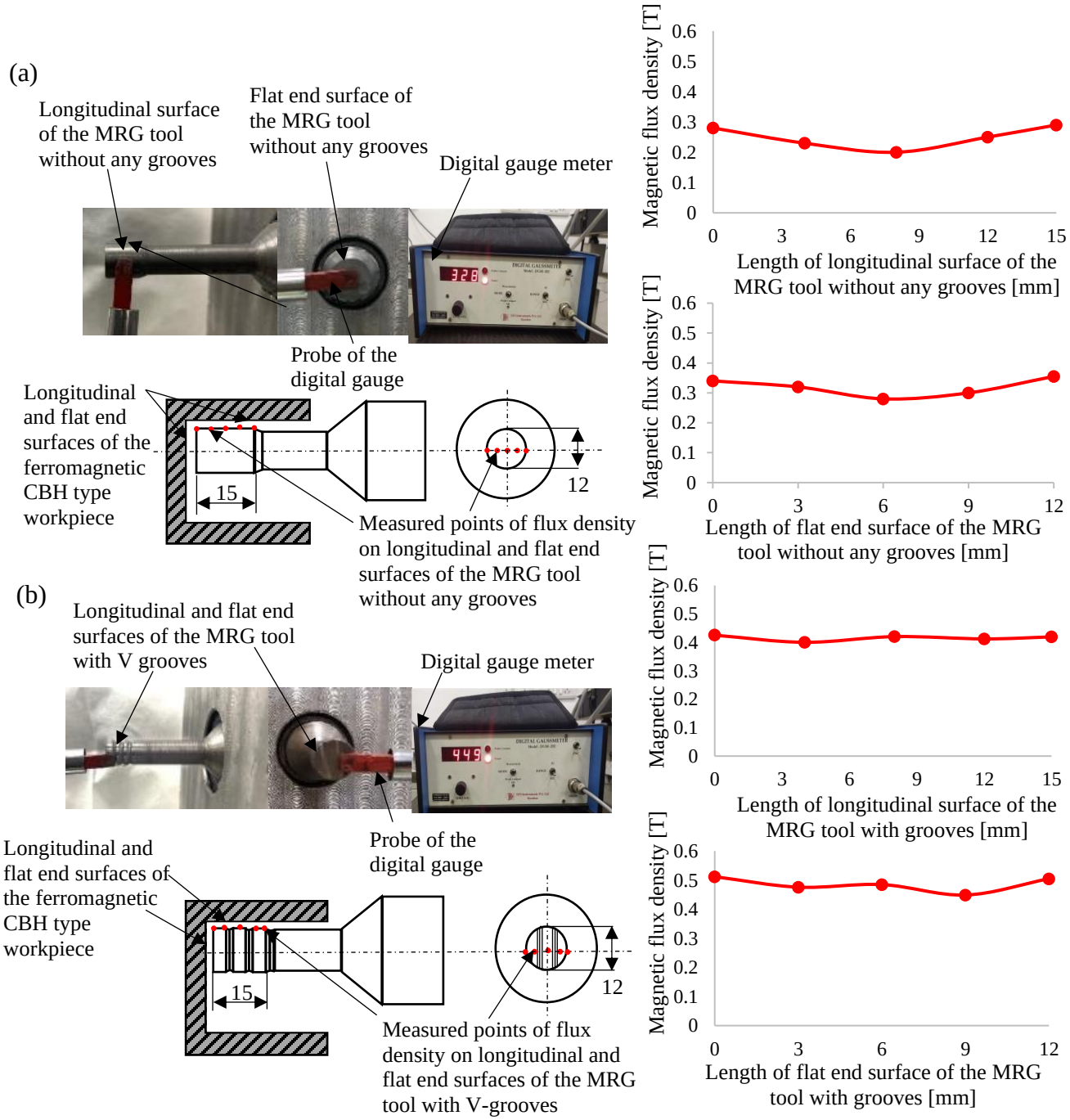

Fig. 3.10 Experimentally measured magnetic flux density on the longitudinal and flat end finishing surfaces of the fabricated MR grinding (MRG) tool (a) without grooves and (b) with grooves in the vicinity of the ferromagnetic cylindrical blind hole (CBH) workpiece using digital gauge meter.

Thus, it can be analyzed experimentally also from Fig. 3.10(b) that the MRG tool with V-shaped grooves is an appropriate design to incite a higher concentration of magnetic flux density over the finishing surfaces of the tool in comparison with the MRG tool without grooves (Fig. 3.10a). The

strength of the magnetic flux density over the finishing surfaces of the tool is the governing factor for the magnetorheological (MR) finishing rate. The higher value of magnetic flux density upsurges the bonding strength of iron particle (IP) chains on the MRG tool surfaces having V-shaped grooves. Due to this increase in the bonding strength of the IP chains, the finishing on the surfaces of the CBH type workpiece gets enhanced. The value of magnetic flux density on the electromagnetic tool core surfaces is accountable for the stiffness of the IP chains present in MR polishing (MRP) fluid. When the MRP fluid gets stiffened under a higher concentration of magnetic flux density over the MRG tool surfaces having V-shaped grooves, the active abrasive particles (AAPs) are held rigidly by the IP chains, which further leads to the more effective removal of surface asperities from the CBH type workpieces. Therefore, the presently designed MRG tool with V-shaped grooves is used for effectively MR finishing of the interior surfaces of the CBH type workpieces.

3.2 Design of height adjustment system for maintaining a uniform working gap

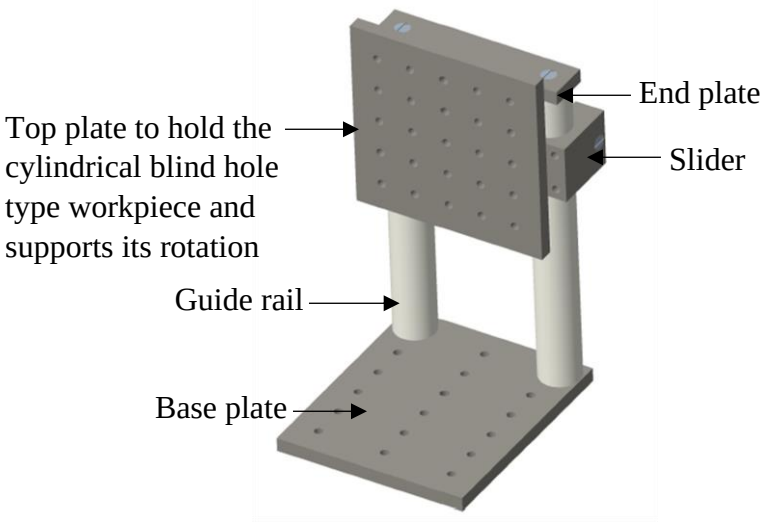

Fig. 3.11 Three-dimensional CAD model of the height adjustment system for maintaining uniform working gap during finishing of longitudinal surface of the cylindrical blind hole type workpiece.

Based on the eccentric operation of the magnetorheological grinding tool's operational requirement, a structure is required to maintain a uniform gap between the longitudinal surface of the cylindrical blind hole type workpiece surface and the finishing surface of the magnetorheological grinding tool. So, a height adjustment system is designed and fabricated as shown in Fig. 3.11.

3.2.1 Base plate of the height adjustment system

The base plate is used for fixing the height adjustment system to the rest of the system. The material selected for the base plate is aluminium, thus reducing the weight of the height adjustment system as compared with that made from mild steel material. The dimensions of the base plate can be observed from the front view, side view, and top view in Fig. 3.12(a−c). The projected side view in 3-D CAD model of the base plate can be observed from Fig. 3.12 (d). The thickness of the base plate is taken as 10 mm. An array of M6 holes is made for rigidly fixing the height adjustment system to the rest of the experimental setup.

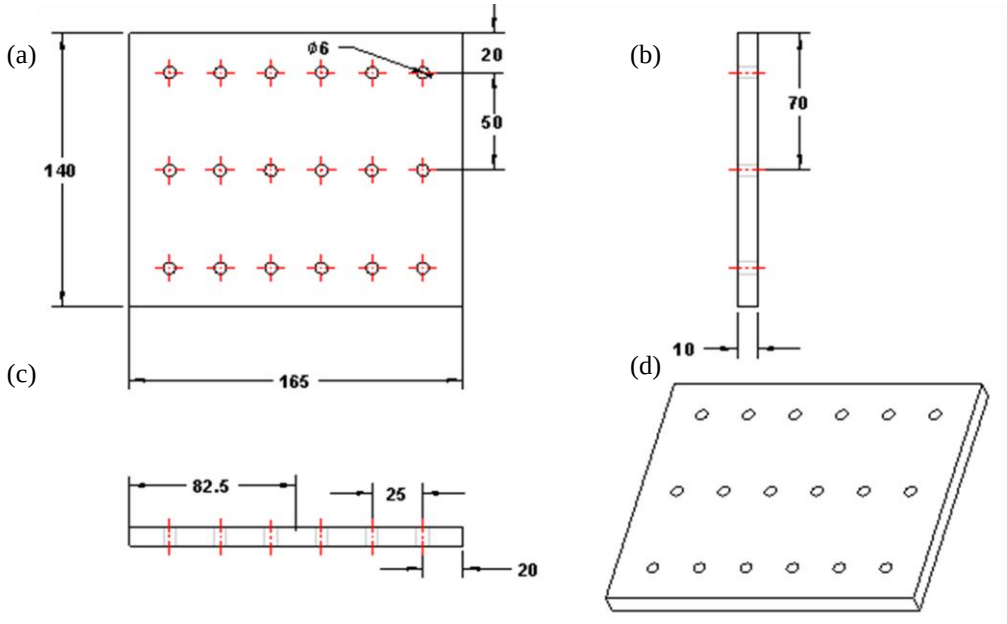

Fig. 3.12 2D drawing of the (a) projected front view, (b) projected side view, (c) projected top view, and (d) three-dimensional CAD model of the base plate to mount the height adjustment system (all dimensions in mm).

3.2.2 Guide rail of the height adjustment system

The guide rails of the height adjustment system guide to move along these guides with support to the upper system The dimensions of the guide plate can be observed from the front view, side view, and top view in Fig. 3.13(a−c). The projected side view in 3-D CAD model of the guide rail can be observed from Fig. 3.13 (d). Two guide rails are used which are fixed on either side of the bottom plate. The guides are made up of steel material with a smooth surface and corrosion-

resistant properties. These guides are made with the 240 mm in length which is long enough to adjust a uniform gap between the longitudinal magnetorheological tool surface and the internal longitudinal CBH type workpiece surface at any position in the given height range.

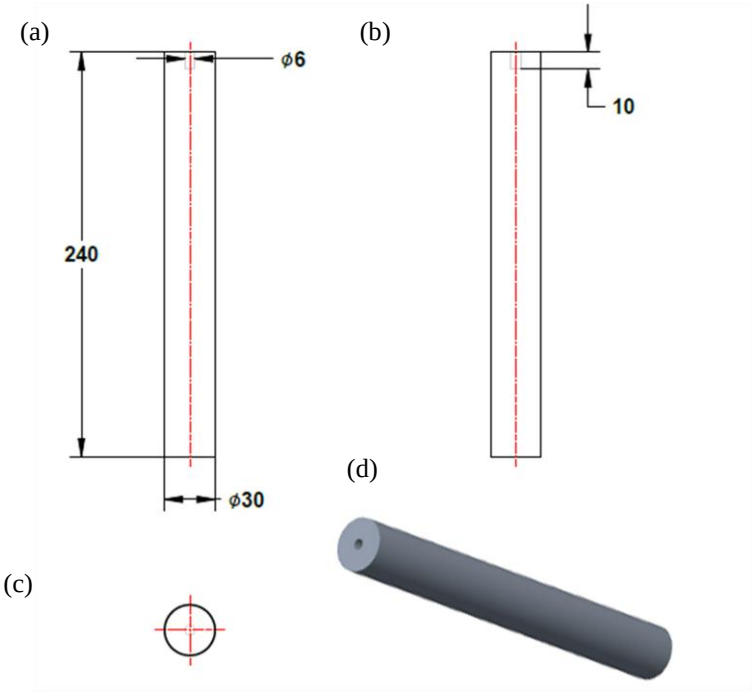

Fig. 3.13 2D drawing of the (a) projected front view, (b) projected side view, (c) projected top view, and (d) three-dimensional CAD model of the guide rail for the height adjustment system (all dimensions in mm).

3.2.3 Slider of the height adjustment system

The slider of the height adjustment system helps to maintain height and fix the position of the workpiece. The nut and bolt along with the washer obtained from the market are used for fixing the position of the slider at a particular position. The slider is made up of aluminium material to reduce the weight of the height adjustment system. The dimensions of the slider can be observed from the front view, side view, and top view in Fig. 3.14(a−c). The projected side view in 3-D CAD model of the slider can be observed from Fig. 3.14 (d). A slider is used for each guide rail.

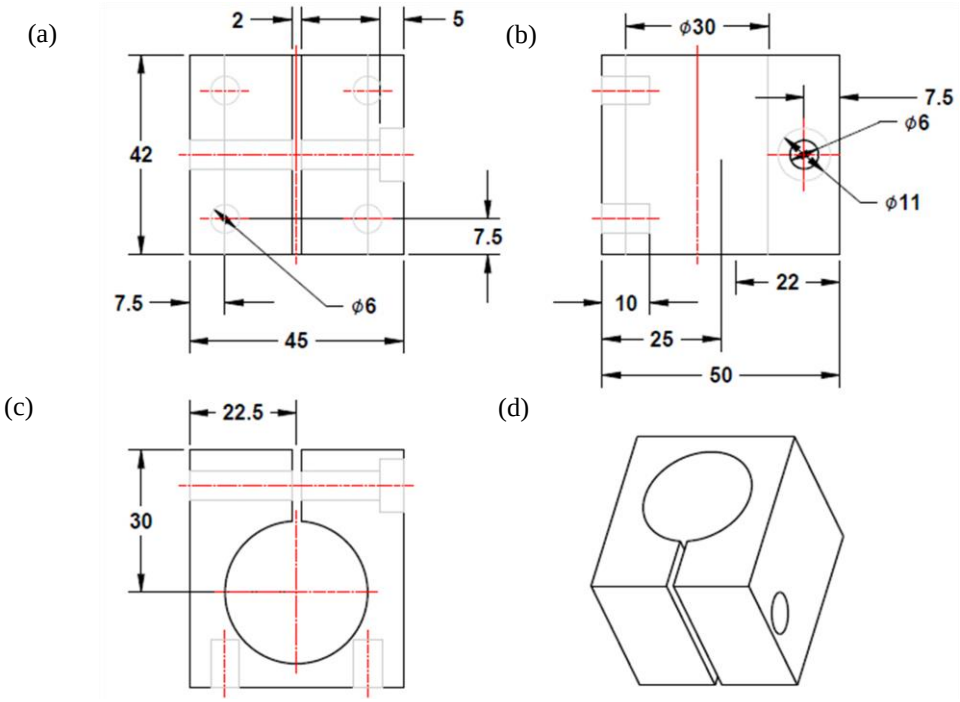

Fig. 3.14 2D drawing of the (a) projected front view, (b) projected side view, (c) projected top view, and (d) three-dimensional CAD model of the slider for the height adjustment system (all dimensions in mm).

3.2.4 End plate of the height adjustment system

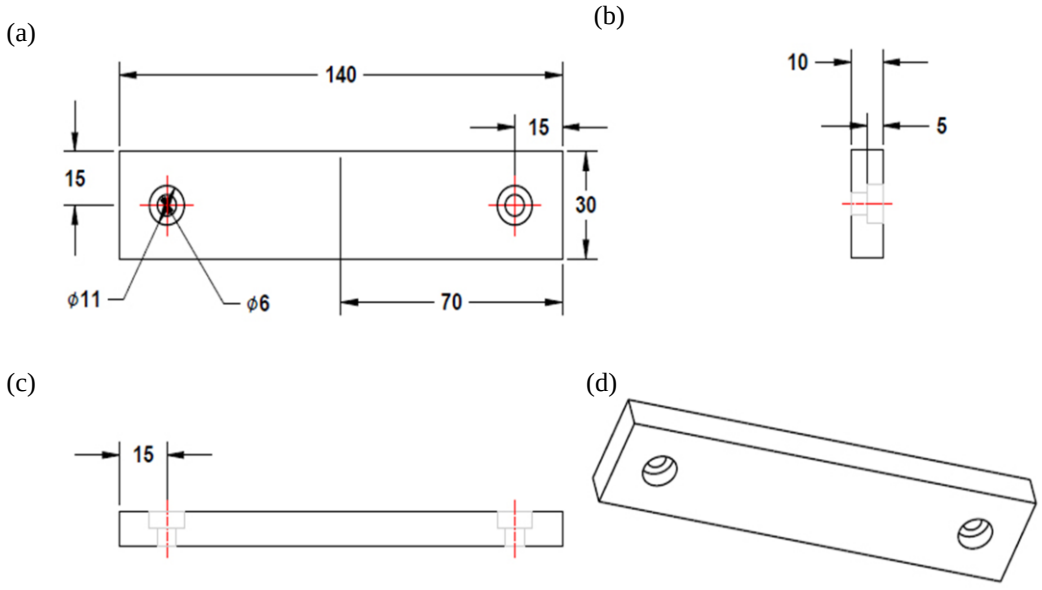

Fig. 3.15 (a) Projected front view, (b) projected side view, (c) projected top view, and (d) three-dimensional CAD model of the end plate of the height adjustment system (all dimensions in mm).

The end plate used in the height adjustment system helps to limit the motion of the slide table up to the maximum height of the guide rail. The material used for making the end plate is aluminium. The dimensions of the end plate can be observed from the front view, side view, and top view in Fig. 3.15(a−c). The projected side view in 3-D CAD model of the end plate can be observed from Fig. 3.15 (d).

3.2.5 Top plate of the height adjustment system

The top plate used in the height adjustment system helps to hold the pummer blocks using the M6 Allen bolt. The material used for making the top plate is aluminium. The dimensions of the top plate can be observed from the front view, side view, and top view in Fig. 3.16(a−c). The projected side view in 3-D CAD model of the top plate can be observed from Fig. 3.16 (d). The top plate is also fixed to the slider table using the bolt. This plate holds the rotating cylindrical blind hole type workpiece on its position while the finishing process is performed.

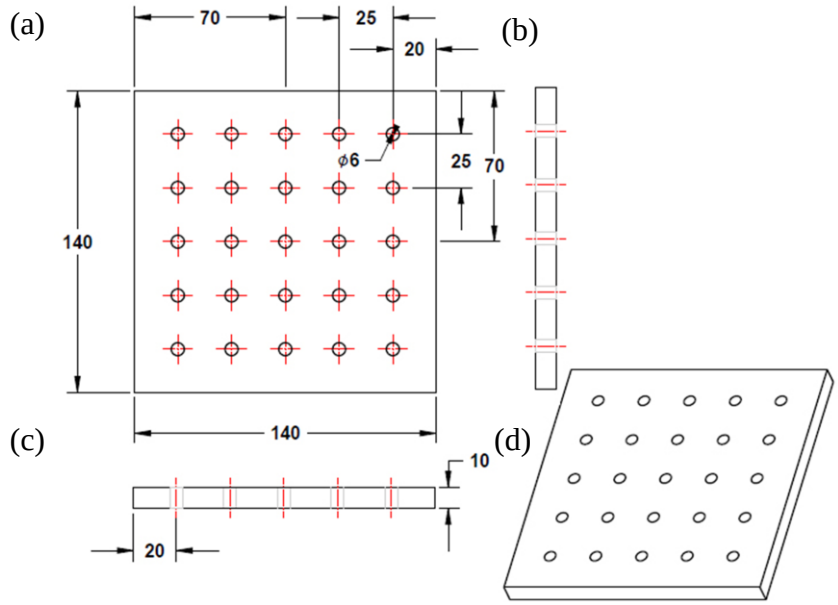

Fig. 3.16 2D drawing of the (a) projected front view, (b) projected side view, (c) projected top view, and (d) three-dimensional CAD model of the top plate for the height adjustment system (all dimensions in mm).

3.3 Design of fixture for holding the cylindrical blind hole type workpiece

To hold the cylindrical blind hole type workpieces, the workpiece fixture is required. This workpiece fixture must be made in such a way that the rotation can be provided to the workpiece during finishing. So, the workpiece fixture comprises of cylindrical blind hole type workpiece holder and a shaft. The detailed 3-dimensional CAD model of the components used for making the fixture for holding cylindrical blind hole type workpiece.

3.3.1 Design of the cylindrical blind hole type workpiece holder

The cylindrical blind hole type workpieces were held using the workpiece holder. The workpiece holder is made up of mild steel because of its wear resistance and strength. The dimensions of the workpiece holder can be observed from the front view, side view, and top view in Fig. 3.17(a−c). The projected side view in 3-D CAD model of the workpiece holder can be observed from Fig. 3.17 (d). The holes in the workpiece holder as presented in Fig. 3.17(b) are used for rigidly holding the inserted workpiece to avoid any play. This workpiece holder is screwed to the shaft which is inserted into the plummer blocks.

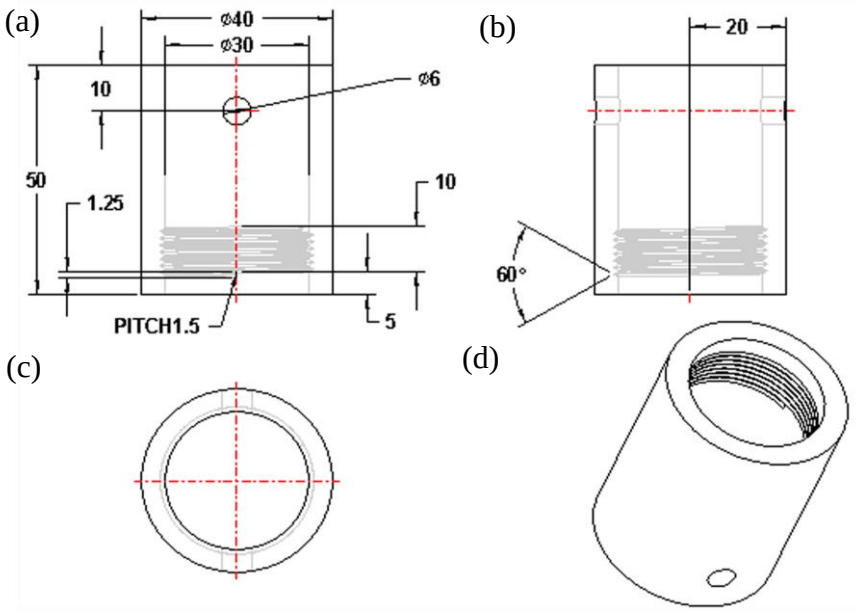

Fig. 3.17 2D drawing of the (a) projected front view, (b) projected side view, (c) projected top view, and (d) three-dimensional CAD model of the CBH type workpiece holder (all dimensions in mm).

3.3.2 Design of the shaft used to rotate the cylindrical blind hole type workpiece along with the fixture

The shaft is used for holding the workpiece holder and allow its rotation. A seat of 40 mm and 5 mm thick is made to avoid the wobbling of the workpiece holder during rotation.This wobbling may occur due to the tolerance within the threads. The diameter of the shaft is considered to 20 mm due to the bore of the adjustable plummer blocks available in the market. The dimensions of the shaft for the workpiece holder can be observed from the front view, side view, and top view in Fig. 3.18(a) and (b). The projected side view in 3-D CAD model of the shaft for the workpiece holder can be observed from Fig. 3.18 (c).

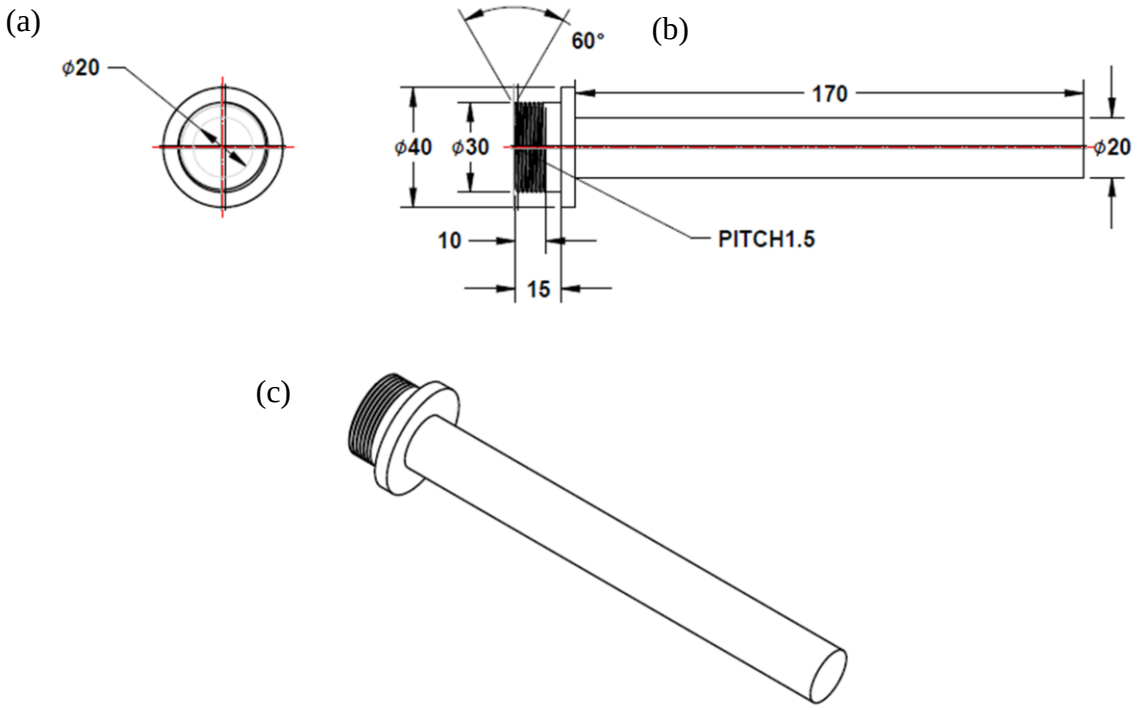

Fig. 3.18 2D drawing of the (a) projected front view, (b) projected side view and (c) three-dimensional CAD model of the shaft for workpiece holder (all dimensions in mm).

The actual assembled photograph of the cylindrical blind hole type workpiece fixture can be observed in Fig. 3.19. The tolerance is referred to the space between the crest and trough of the screws. This causes wobbling of the workpiece. As the wobbling occurs, a uniform working gap can't be achieved between the CBH type workpiece surface and the MRG tool surface. To avoid the chances of wobbling in the workpiece, a workpiece holder seat is introduced as shown in Fig. 3.19.

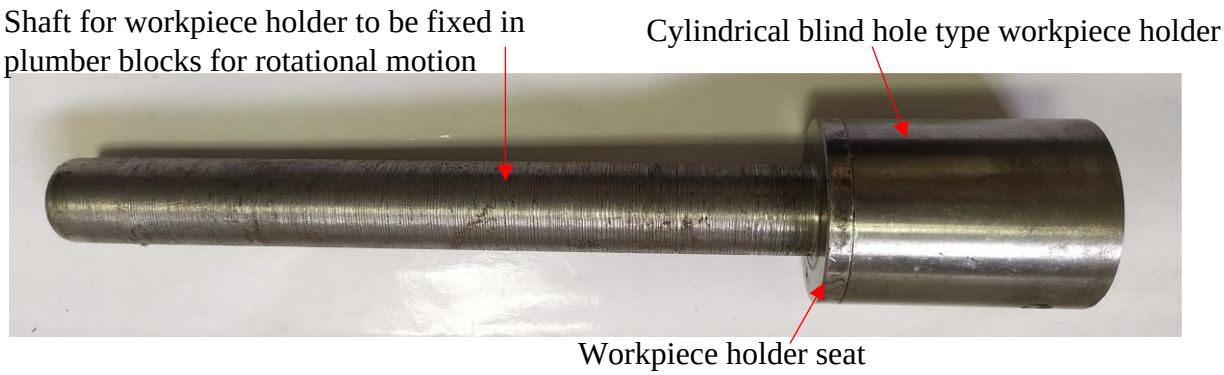

Fig. 3.19 Photograph of the assembled cylindrical blind hole type workpiece fixture.

3.4 Selection of linear slides

For delivering controlled movements to the tool core and cylindrical workpiece, the newly developed magnetorheological grinding (MRG) tool requires a precise motion control system. The horizontal Z-axis and Y-axis slides are used to provide accurate and precise controlled motion. The motion control system is designed to determine how much distance travel is necessary by the electromagnetic tool and cylindrical workpiece fixture to perform MR finishing on any industrial cylindrical blind hole type workpieces. Maintaining the working gap and performing MR finishing on the entire surface of the cylindrical blind hole type workpiece necessitates the MRG tool's and the cylindrical workpiece fixture's linear motions. The precision motion-controlled horizontal Z-axis and Y-axis linear slides fulfill this needs. The Z-axis is fastened to the sliding plate of the horizontal Y-axis slider, which allows it to reciprocate along the Y-axis. The magnetorheological grinding tool is mounted over the Z-axis slide.

The horizontal Z-axis slide and Y-axis slide were selected based on the loading condition and the moveable distance needed. The linear guideways have a state load rating that resists the static permitted moment. When a linear guideway is subjected to an extremely heavy force or an impact load while at rest or in motion, localised permanent deformation can occur between the guideways surface and the blocks. When the quantity of permanent deformation reaches a specific threshold, it becomes a hindrance to the linear guideway's smooth operation. The linear guideways have basic dynamic and static load values of 14.7 kN and 23.47 kN, respectively. These are selected for the maximum loading conditions that the linear guideways can withstand while working.

The linear slides' sizes are determined by the working area and the required movement in both slides. This owing to the ease of replacing the internal cylindrical blind hole type workpieces that

the horizontal Y-axis slide requires more length than the Z-axis slide. The length of the slide is determined by the length of cylindrical workpieces to be finished. The horizontal Z-axis slide with a length of 600 mm, the width of 120 mm, and height of 80 mm was selected based on the application length range. The horizontal Z-axis linear slide is made up of four aluminium plates, two side plates, and two corner plates that are connected by threaded screws slots. The bearing seats in the corner retain the bearings that keep the screw spindle in a straight line, allowing the screw nut to function smoothly on the screw spindle. The linear guideways are held in place by bolt assemblies on the side plates. The tool must reciprocate, which necessitates the use of linear guideways with square blocks. Total 8 square blocks (4 for horizontal Z-axis and 4 for Y-axis) with 4 accurate guideways are utilized in the horizontal Z-axis and Y-axis slides. With the assistance of a bearing set, the assembly of the precise screw spindles (1 mm pitch) with accurate ball screws is fastened to the aluminium plates frame. The aluminium frame of the Y-axis slide is 270 mm long, 120 mm wide, and 50 mm high, and it holds the accurate guideways and screw spindle assembly that provides reciprocation to the Z-axis.

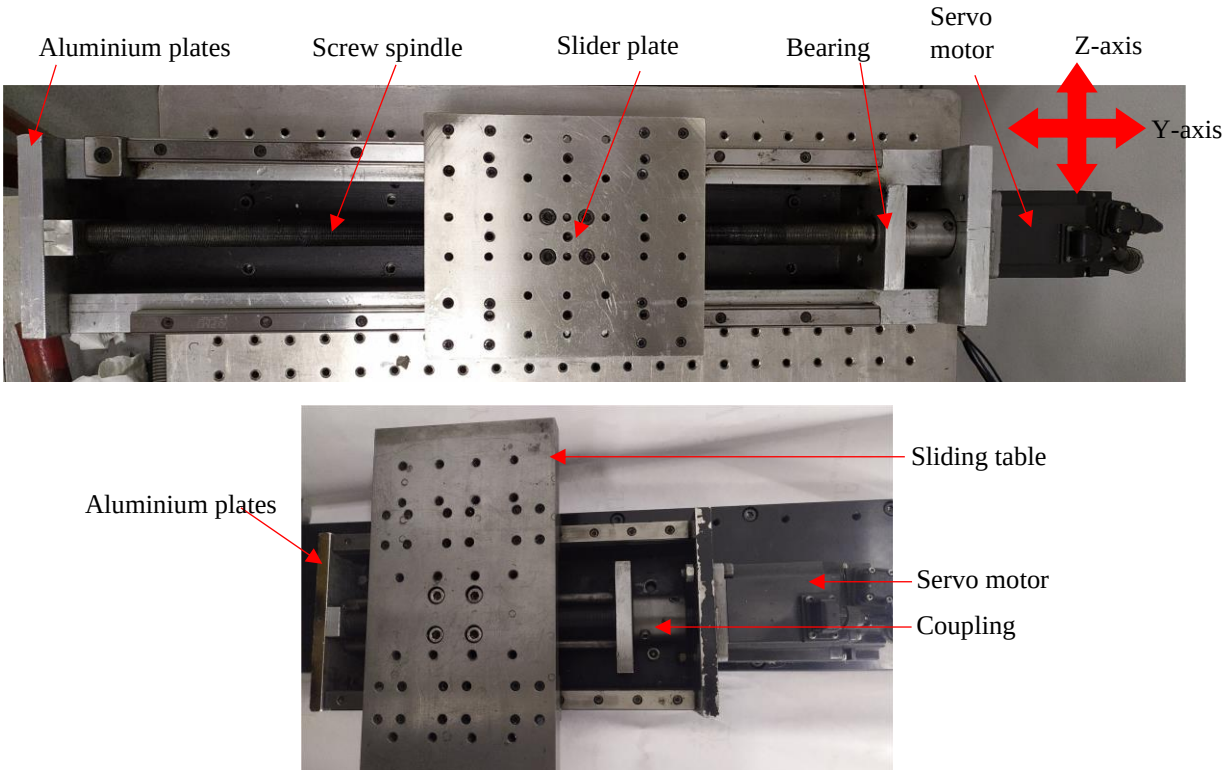

Fig. 3.20 (a) Horizontal Y-axis linear slide which holds the Z-axis slide and (b) Z-axis slide with slider plate to hold the newly developed magnetorheological grinding tool.

Servo drives offer reciprocation and rotating motion to the tool and workpiece fixture using programmable logic-controlled servo motors. These servo motors enable precise and accurate motion control. The programmable logic controller (PLC) controls the requisite rotating and reciprocation motions of the electromagnetic tool and cylindrical blind hole type workpiece. Servo drives receive instruction from the PLC output and rotate the servo motors to perform the various motions. As shown in Fig. 3.1, four servo drives are linked to the PLC to control the four servo motors with servo drives for varied necessary motions to execute MR finishing on the internal surfaces of cylindrical blind hole type workpieces. PLC provides instructions to servo drives, which connect with servo motors and rotate according to programmed input parameters.

3.5 Selection of servo motors

The applications which require high rotational speeds utilize the timing belt driven linear systems. Servo motor as shown in Fig. 3.21 is used in linear systems because of their ability to precisely control position, speed, and torque.

Fig. 3.21 Programmable controlled servo motor to provide motion to slides and cylindrical blind hole type workpiece.

The constant and intermittent drive torques are necessary for the application which must be determined before sizing and selecting the servo motor. So, for controlling the different motions of the present developed MR grinding tool, the MITSUBISHI HG-KR43 model was chosen. The 400 W servo motor has a rated torque of 1.3 Nm and a maximum torque of 3.8 Nm. The servo motor torque rating is selected based on its higher rating than the torque rating required by the magnetic tool during finishing. The servo motor's rated speed is 3000 rpm, with a maximum speed of 5000 rpm, which is sufficient for experimental use in setup for the MRG tool. The servo motor

weighs 1.4 kg and may be readily handled and clamped. The total of four servo motors are used in the system.

3.6 Selection of swivel vise

The swivel vise as shown in Fig. 3.22 is a key component when finishing is performed over the different tapered longitudinal cylindrical blind hole type workpiece surfaces. The secondary purpose of the swivel vise is to add height to the setup for the cylindrical blind hole type workpiece. The swivel vise dimensions are chosen based on the applications of internal tapered cylindrical blind hole type workpieces.

Fig. 3.22 Swivel vise for maintaining uniform working gap during finishing of the internal tapered longitudinal surface using the magnetorheological grinding tool.

With the use of this swivel vise fixture, tapered cylindrical mould cavities used for the manufacturing of spray bottle cap hoods and light covers can be uniformly finished by the present MR grinding tool while maintaining the uniform working gap. The dimensions of the swivel vise were chosen based on the applications for the present setup. A regular swivel vise is also purchased. The dimensions of the swivel vise base is used as 300 mm in length, 100 mm in breadth, and 110 mm in height. The M6 holes are bored at the top surface of the swivel vise to attach the height adjustment system that is utilized to maintain height and provide support to the internal cylindrical blind hole type workpiece. With the use of a nut-bolt arrangement, this vise includes a rotating base that can be turned at a 360-degree angle and set to any angle as needed.

3.7 Assembly of complete setup to perform finishing over the internal longitudinal and flat end surfaces of the cylindrical blind hole type workpieces using the newly developed single magnetorheological grinding tool (MRG) tool

After the fabrication and assembly of all the parts, the setup of the MR grinding (MRG) tool is developed for performing the experimentation. The experimental setup with the MRG tool to finish the interior surfaces of the cylindrical blind-hole (CBH) work parts can be seen in Fig. 3.23. The present setup consists of a stationary electromagnetic coil, programmable logic controller (PLC), and a height adjustment system for maintaining the working gap. The PLC system controls the motions of the MRG tool and CBH type workpiece during the finishing operation in the proposed process. In the present setup, four servo motors (S_1, S_2, S_3, and S_4) are used in the process of getting different types of motions. The motion to the Y-axis slide is provided using a servo motor (S_1), which is used for the tool's reciprocation motion along the Y-axis to achieve the MR finishing along the flat end surface of the CBH type workpieces. The Z-axis slide is fixed over the Y-axis slide using bolts. The tool structure is bolted on the Z-axis slide. The Z-axis slide is driven by a S_2 servo motor to provide reciprocation to the MRG tool along Z-axis. The reciprocation motion of the tool along the Y-axis performs finishing over the inner flat end surface of the CBH type workpieces. The tool structure comprises a C-type clamp that holds the ball bearing, MRG tool core, bobbin, timing pulley belt drive, and servo motor (S_3) in its position. The ball bearings are installed in the tool structure to hold and provide frictionless MRG tool core rotation. The timing pulley belt drive system helps in the smooth transmission of the rotational motion from the servo motor (S_3) to the developed MRG tool core. Further, the structure of the workpiece holder has been designed in such a way that the CBH type workpiece can be kept in a horizontal position as shown in Fig. 3.23. The structure of the workpiece holder is fabricated so that its height can be easily adjusted, and a required gap can be maintained between the internal longitudinal surface of the CBH type workpieces and the longitudinal end of the grinding wheel type MR finishing (MRG) tool. The CBH type workpiece rotates in a direction contrary to the MRG tool core rotation. Owing to this, the relative motion between the MRP fluid along with the MRG tool and the interior surfaces of the CBH type workpiece gets increased (Paswan and Singh, 2020). This leads to an increase in more shearing off surface asperities from the CBH type workpiece. The rotational motion to the CBH type workpiece is provided using a servo motor (S_4) with the assistance of the V-type pulley belt drive. For finishing the inner surfaces of the CBH type workpiece, the tool core is magnetized with the help of an electromagnetic coil that is wound over the stationary aluminum

bobbin. The MRG tool core passes through this aluminum bobbin and rotates concentrically. During its operation, when the current is allowed to pass through the stationary electromagnetic coil, the heat is produced. So, to avoid overheating to the coil and also to avoid the change in viscosity of MRP fluid due to the temperature rise, the coolant is passed through the aluminium cooling jacket over the electromagnetic coil.

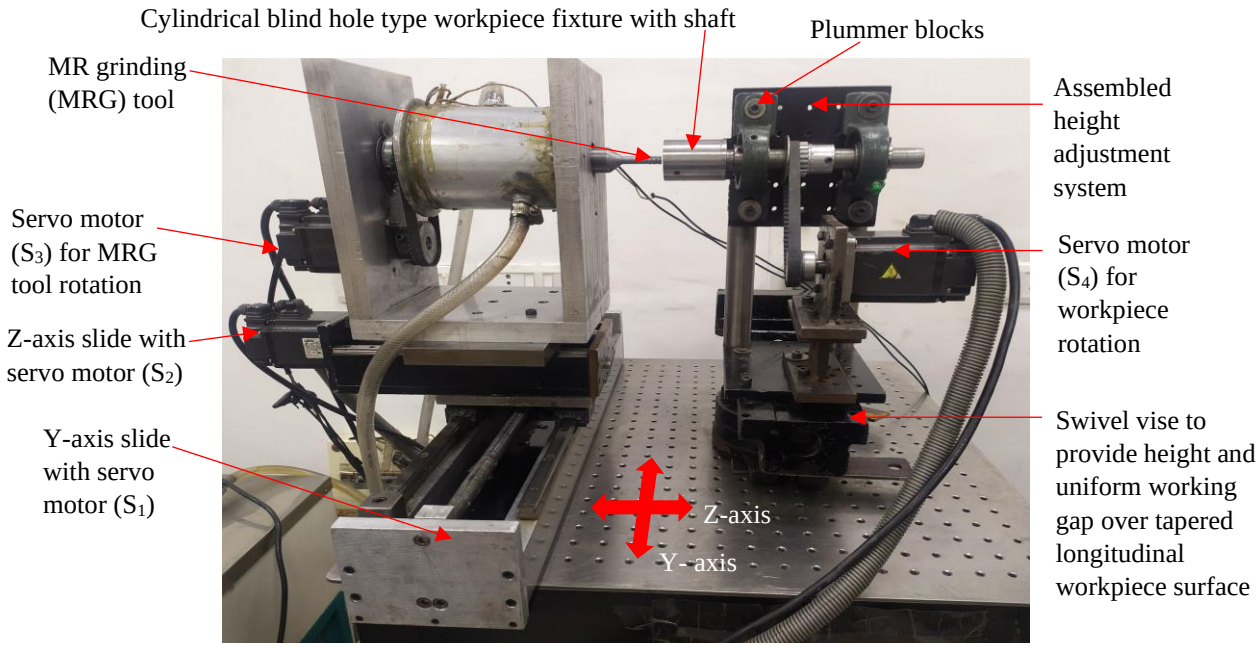

Fig. 3.23 Complete assembly of the experimental setup for the magnetorheological grinding tool used in finishing the cylindrical blind hole type workpiece surfaces.

Owing to the induced concentration of magnetic flux density, the MRP fluid becomes stiff and is capable enough to shear off the surface asperities due to which improvement in the surfaces of the cylindrical blind-hole (CBH) type workpiece is obtained. The finishing action, which is performed on the inner longitudinal surface of the rotational CBH type workpiece, has been achieved through rotational and reciprocation motions of the MRG tool and rotation of the CBH workpiece. When the process of finishing is performed on the longitudinal surface of the CBH type workpiece, the tool's reciprocation motion is transmitted by the Z-axis slide, and the rotational motion to the MRG tool core is provided with a timing pulley belt drive. Next, the finishing action is performed on the internal flat end surface of the CBH type workpiece. Here, the process is the same as in the case of a longitudinal surface, but the difference is that the reciprocation motion in the Y-direction is provided for MR finishing of the entire flat end surface of the CBH type workpieces. In this

process, the eccentric rotation of the single MRG tool helps to finishing the different CBH type workpieces with variable diameters. This eccentric rotation of the single MRG tool helps to fine finish the longitudinal and flat end surfaces of the CBH type workpieces. Thus, the present developed process with the single MRG tool can provide MR finishing on both internal surfaces (longitudinal and flat) of the CBH type workpieces.

3.8 Mechanism of finishing over longitudinal and flat end surfaces of the cylindrical blind hole type workpiece with the presently designed magnetorheological grinding (MRG) tool

During the MR finishing (MRF) process using the newly developed MRG tool, the normal magnetic, tangential shear (TS), and axial forces act on the longitudinal and flat end surfaces of the CBH type workpiece as revealed in Figs. 3.24(a) and (b). The magnetizing current generates a magnetic field that produces a normal magnetic force. The TS force acts owing to the rotation of the MRG tool and the CBH type workpiece. The force acting due to the reciprocation motion of the MRG tool over the longitudinal and flat end surfaces of the CBH type workpiece is the axial force. These forces act in different directions on both the surfaces of the CBH type workpiece due to the effect of the magnetic field and involvement of the various motions of the MRG tool as well as the CBH type workpiece as shown in Fig. 3.24. When the finishing is performed over the longitudinal and flat end surfaces of the CBH type work part, the force that acts normal to the surfaces of the CBH type workpiece is the normal magnetic force ($F_{nml,nmf}$). This force is produced owing to the magnetic field on the finishing surfaces of the MRG tool. The normal magnetic force attracts the iron particles towards the finishing surfaces of the MRG tool. Thus, it causes the levitation effect that brings the non-magnetic abrasive particles forward in contiguity with the surfaces of the CBH type workpiece as revealed in Figs. 3.24(a) and (b). These active abrasive particles (AAPs) that are responsible for finishing are bonded by IPs present in the MRP fluid. Due to this, the AAPs indent on the surfaces of the CBH type workpiece for shearing the asperities due to applied motions of the MRG tool and the CBH work part. The normal magnetic force ($F_{nml,nmf}$) can be calculated using Eq. (3.1) which is acting on the longitudinal and flat end surfaces of the CBH work part, respectively through an active abrasive particle (Sidpara and Jain, 2012).

$$F_{nml,nmf} = \{m_a \mu_o \chi_m H \Delta H\} \quad (3.1)$$

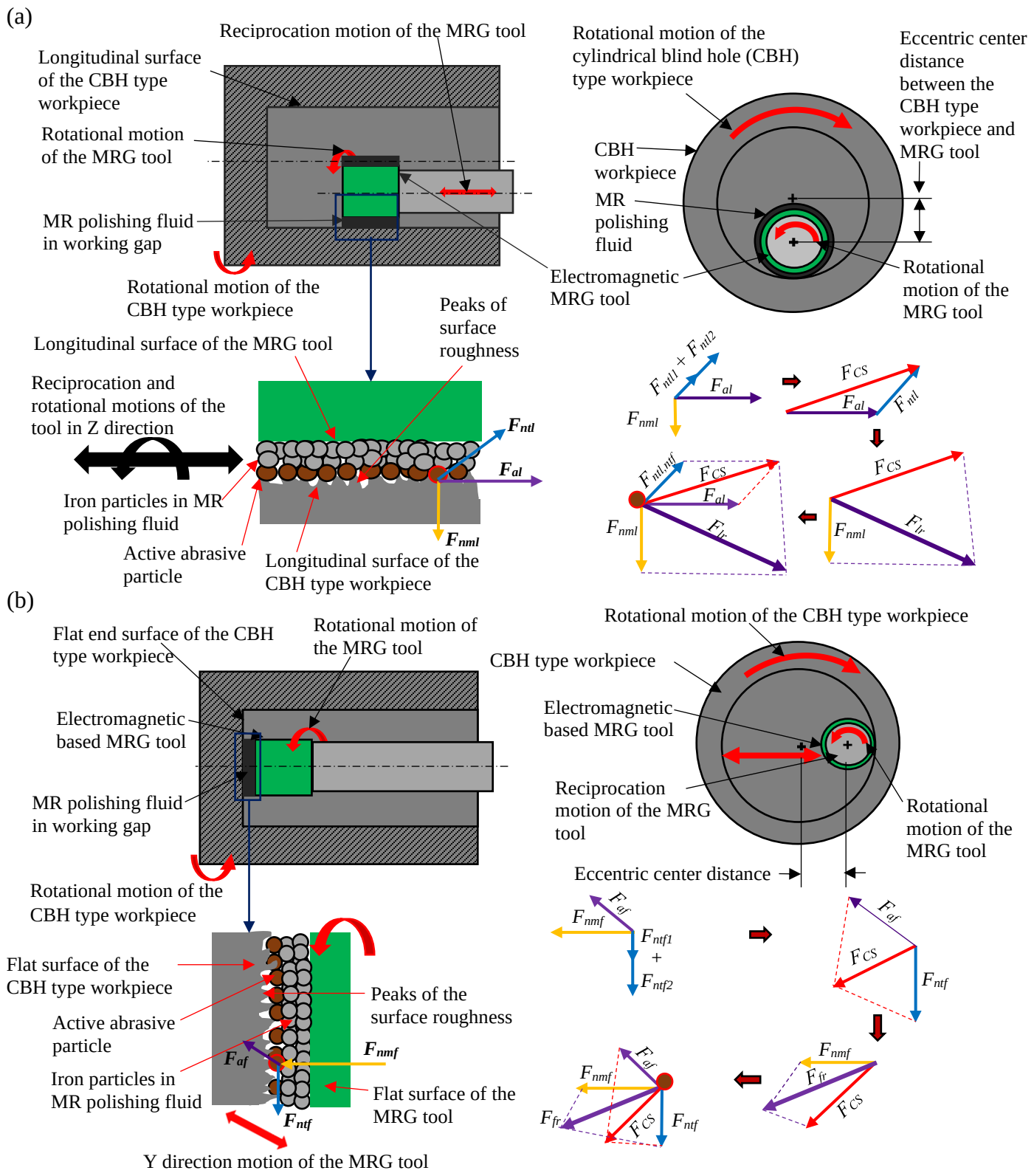

Fig. 3.24 Schematic diagram of finishing mechanism of (a) longitudinal surface and (b) flat end surface of the cylindrical blind hole (CBH) type workpiece with the newly designed MR grinding (MRG) tool.

where $F_{nml,nmf}$ is the normal magnetic force acting on the longitudinal and flat end surfaces of the CBH work part, m_a is the mass in kg of the single iron particles (IP), μ_o is the free space magnetic permeability in H/m, χ_m magnetic susceptibility in m^3/kg of the iron particles, H is the magnetic field strength in A/m.

The force owing to the simultaneous rotation of the MRG tool and the workpiece is the tangential shear (TS) force which has an essential role in the finishing mechanism. After the indention of the AAPs due to normal magnetic force, the TS force removes the asperities from the surface of the CBH work part.

The CBH type workpiece is provided with the rotation in the opposite direction to the rotation of the MRG tool. This enhances the TS force applied by the AAPs on the surfaces of the CBH type workpiece due to an increase in relative motion in this process (Paswan and Singh, 2019). Thus, the net TS force ($F_{ntl,ntf}$) is the sum of the TS force owing to the MRG tool rotation ($F_{ntl1,ntf1}$) and the CBH type workpiece rotation ($F_{ntl2,ntf2}$), which is expressed in Eqs. (3.2) and (3.3).

$$F_{ntl,ntf} = F_{ntl1,ntf1} + F_{ntl2,ntf2} \tag{3.2}$$

$$F_{ntl,ntf} = m_{sc}\omega_t^2 R_t + m_{sc}\omega_w^2 R_w \tag{3.3}$$

where $m_a\omega_w{}^2R_w$ is a TS force (F_{ntl1}) owing to CBH type workpiece rotation, $m_a\omega_t{}^2R_t$ is the TS force (F_{ntl2}) owing to the MRG tool rotation. m_{sc} is the mass of an AAP, ω_t is the angular speed of the MRG tool surface, R_t is the distance that varies with the AAP location from the center axis of the MRG tool, ω_w is the angular speed of the CBH type workpiece surface, and R_w is the distance that varies with the active abrasive particle location from the center axis of the work part.

Further, the force acting due to the MRG tool reciprocation motion is the axial force ($F_{al,af}$). As the MRG tool reciprocates over the workpiece surfaces, the surface asperities are sheared off from the entire surface axially. The axial force acting on the AAP can be calculated using Eq. (3.4).

$$F_{al,af} = \tau_a A_a \tag{3.4}$$

where τ_a is the MRP fluid yield stress, and A_a is the active abrasive particle's projected area on the CBH type workpiece surfaces. Further, the axial force (F_{al}) imposed by the reciprocation feed of the tool on the longitudinal surface of the CBH type workpiece is presented in Fig. 3.24(a). The axial force act in the Z-axis direction when finishing the longitudinal surface of the CBH type workpiece. But when the flat end surface of the inner cylindrical blind hole (CBH) type workpiece

is finished, the axial force (F_{af}) acts in the Y-axis direction for the reciprocation motion of the MRG tool as presented in Fig. 3.24(b). A tangential shear force acting due to rotation of the MRG tool and the workpiece along with the axial force generates the cutting shear force (F_{CS}) for both the surfaces of the cylindrical blind hole (CBH) type workpiece which can be observed in Figs. 3.24(a) and (b). This force helps to net shearing off the asperities from the surfaces of the CBH type workpiece in the form micro-chips (Mehra *et* al., 2018). Thus, the cutting shear (CS) force (F_{CS}) can be calculated from Eq. (3.5).

$$F_{CS} = F_{ntl,ntf} + F_{al,af} \tag{3.5}$$

The CS force (F_{CS}) is the resultant of the axial and net TS force that is acting on the longitudinal, and flat end surfaces of the CBH type workpiece, which is expressed in Eq. (3.5). Finally, the total net force (F_{lr} or F_{fr}) is obtained, which is the resultant of the CS force (F_{CS}) and the normal force ($F_{nml,nmf}$), as presented in Figs. 3.24(a) and (b). The total net force helps in removing the surface asperities from the internal surfaces of the CBH type workpiece. Here, the surface asperities in the case of longitudinal surface are perpendicular to the reciprocation motion of the magnetorheological grinding (MRG) tool. Whereas, in the case of the flat end surface, the asperities are pointing towards the flat end surface of the MRG tool along the Y-axis direction. To shear off these asperities from both the surfaces of the CBH type workpiece, the cutting shear force (F_{CS}) is acting in a different direction as per the position of the longitudinal and flat end surfaces of the CBH type workpiece which can be observed in Figs. 3.24(a) and (b). Thus, both the surfaces of the CBH type workpiece get finished with a single newly designed MRG tool in the present work.

3.9 Design and development of an additional magnetorheological hemispherical finishing tool for the finishing of blind hole type ball cup surface of ball transfer unit

In the manufacturing and aerospace industries, positioning equipment is utilized to load/unload, orient, feed or control the cargo within a workplace for handling, storing, and transportation (Saputro and Erdebilli, 2016; Rajeev, 2018). The major type of position equipment are used as the ball transfer units (BTUs), turntables, manipulators, industrial robots, etc. The BTUs are used as integral parts of the feed devices, aircraft cargo bay, cargo ships, conveyor systems, and vehicles that hold cargo (Brewer, 2016).

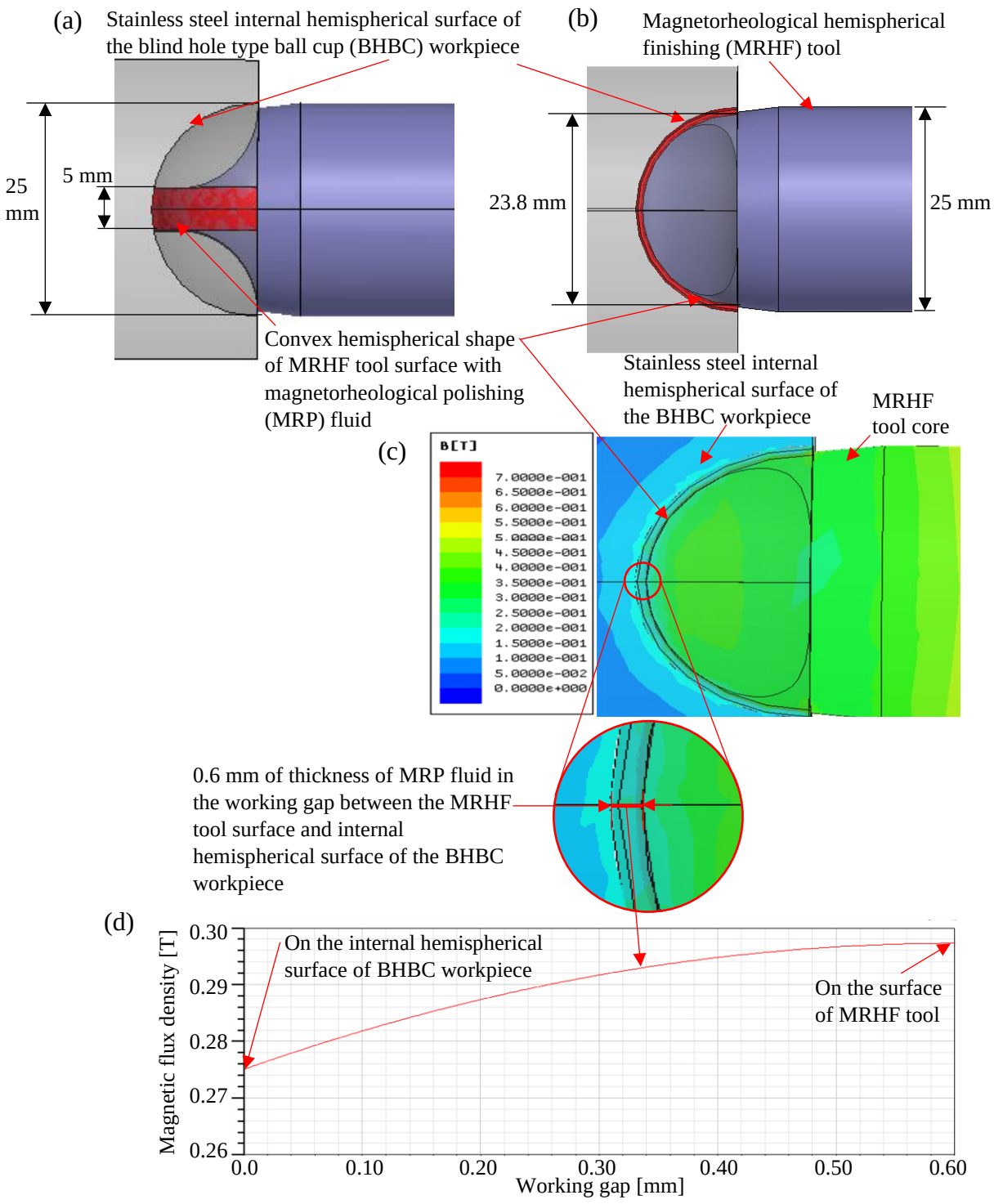

Fig. 3.25 Model of the magnetorheological hemispherical finishing (MRHF) tool along with MRP fluid and the internal hemispherical surface of blind hole type ball cup (BHBC) workpiece of the ball transfer unit (a) when viewing from a side, (b) after 90º rotation, (c) distribution of magnetic flux density and (d) the 2D plot of the flux density in 0.6 mm working gap between the convex surface of the MRHF tool and the internal surface of the BHBC workpiece through magnetostatics finite element analysis.

The BTU is comprised of parts such as the main body with a hemispherical-shaped ball cup, a load ball, the supporting balls, and a cover installed over the main body (Masciarelli, 1987). In the ball transfer unit (BTU), the finely finished ball cup surface along with its dimensional accuracy is highly required to resist corrosion, noise, and vibration (Mapelli and Barella, 2007; Turnbull *et* al., 2020). This also helps in reducing the resistance produced between the small balls and the ball cup surface due to a reduction in friction (Stegmiller, 2016). Further, it can enhance functional performance and service life by reducing wear and total frictional torque. Also, the power consumed to transport the load over the BTU can reduce.

So, to fulfill the requirement to fine finish the blind hole type ball cup (BHBC) surface of the ball transfer unit (BTU), a new electromagnetic magnetorheological hemispherical finishing (MRHF) tool is designed. To attain a fine finished internal BHBC work part surface, the MRHF tool must ensure a higher and uniform magnetic flux density (MFD) over its finishing surface. This helps to maintain the magnetorheological polishing (MRP) fluid over the MRHF tool's end surface uniformly with higher shear strength. The MFD, therefore, plays a lead role to hold the MRP fluid over the end surface of the MRHF tool. So, to fulfill this requirement, the magnetostatic finite element analysis (MFEA) is executed to achieve a uniform and higher MFD over the electromagnetic MRHF tool surface.

For the MFEA, the CAD (computer-aided design) model of the present finishing system is made using PTC creo software as espied in Figs. 3.25(a) and (b). The CAD model consists of the MRHF tool, electromagnetic coil, MRP fluid in the 0.6 mm working gap (WG), and BHBC workpiece of stainless-steel material. The WG amid the MRHF tool surface and the internal BHBC work part surface is filled by MRP fluid. For the study of MFD, this CAD model is exported into the Ansys Maxwell V13 software. Each part of the CAD model is assigned with the respective material and the relative permeability (μ_r). The material of the electromagnetic coil is assigned as copper with its μ_r of 1, mild steel of the MRHF tool with its μ_r of 600, MRP fluid in the WG with its μ_r of 5 (Grover and Singh, 2017b) and stainless steel of the BHBC workpiece with μ_r of 1 (Bedi and Singh, 2018b). After assigning the value of μ_r to all the parts of the present finishing system, the electromagnetic coil with 2600 turns is sectioned and split into two. Further, one of the sections with the electromagnetic coil is assigned with the current excitation value of 2 A. After all these values are assigned, the environment is given to the present finishing setup. The environment is

the insulation given to the electromagnetic setup during the simulation for magnetic flux density. This restricts the leakage of magnetic flux outside of the environment. Next, the solution to the setup is added in the magneto-static model which is later validated for the MFEA results. Based on the MFEA for the higher and uniform MFD on the tool surface, the final MRHF tool dimensions are shown in Figs. 3.25(a) and (b), respectively. These dimensions are selected on the basis of different trials in the MFEA by varying the width of the convex surface in order to obtain the higher MFD. Here, the MRHF tool surface with 23.8 mm diameter is restricted based on the application for the ball cup surface of the ball transfer unit.

After the MFEA, the MRHF tool with converging shape and width of its finishing convex surface as 5 mm can be seen in Fig. 3.25 (b). The side view and the view after 90º rotation of the MRHF tool is presented in Figs. 3.25 (a) and (b). The MFD distribution and the 2D plot in 0.6 mm WG amid the convex MRHF tool surface and the interior BHBC surface can be observed in Figs. 3.25 (c) and (d). In Fig. 3.25 (c), it can be observed that the MFD along the circumference finishing surface of the MRHF tool is uniform which is represented by cyan colour. This can provide uniform magnetic force over the entire BHBC workpiece surface which further may help in uniform fine finishing. Next, the variation in the trend of the magnetic field within the WG can be observed from Fig. 3.25 (d). The negative slope change in the magnetic field reveals the relative motion between the MRP fluid and the workpiece surface and the finishing take place. After the finite element analysis, the MRHF tool is fabricated which is shown in Fig. 3.26.

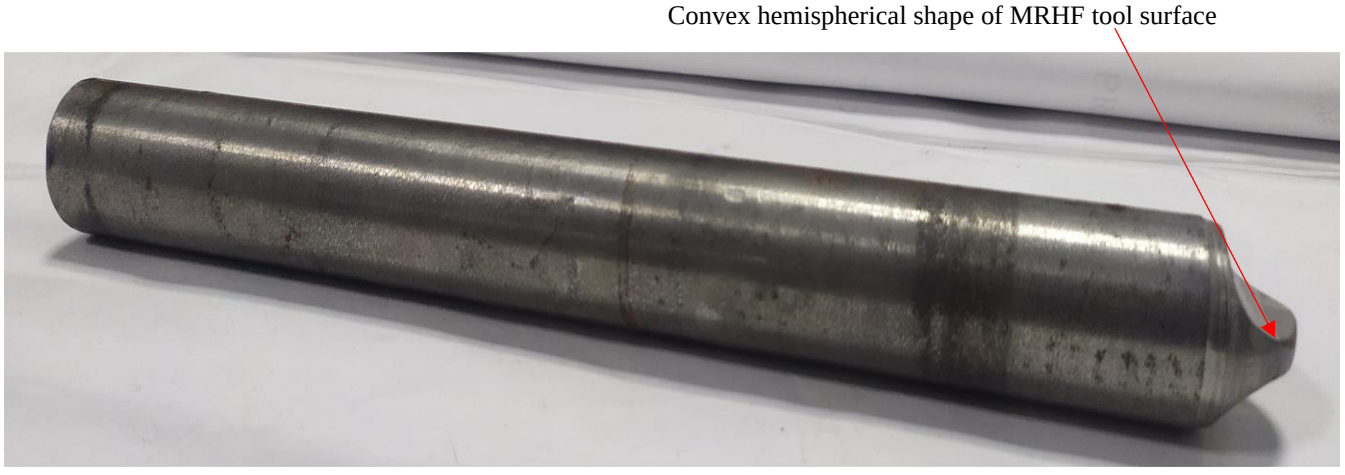

Fig. 3.26 Fabricated magnetorheological hemispherical finishing tool core for finishing the blind hole type ball cup workpiece surface.

(a)

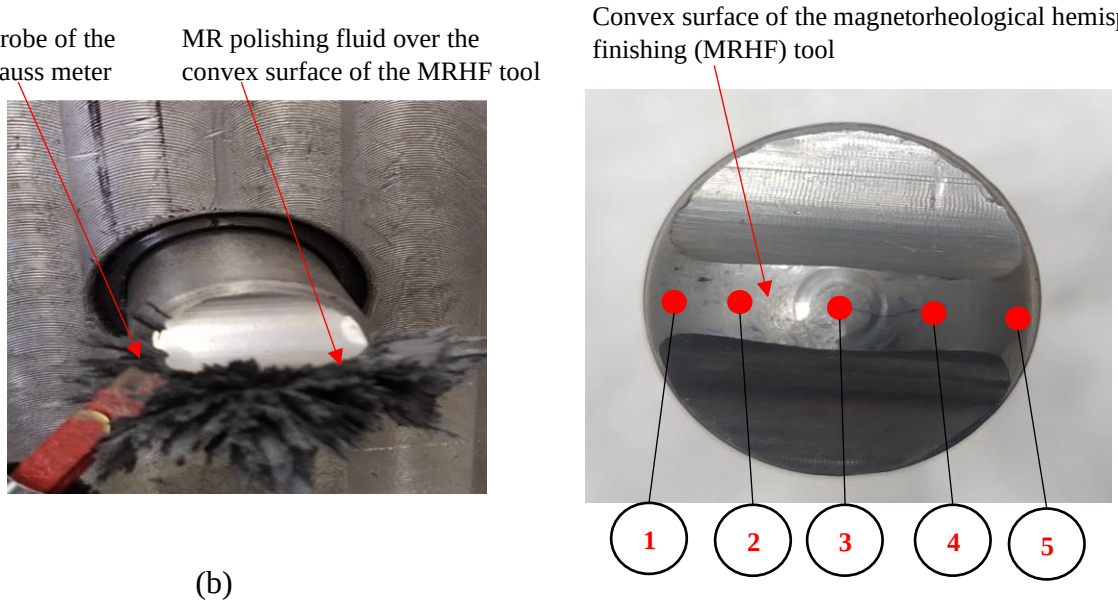

(b)

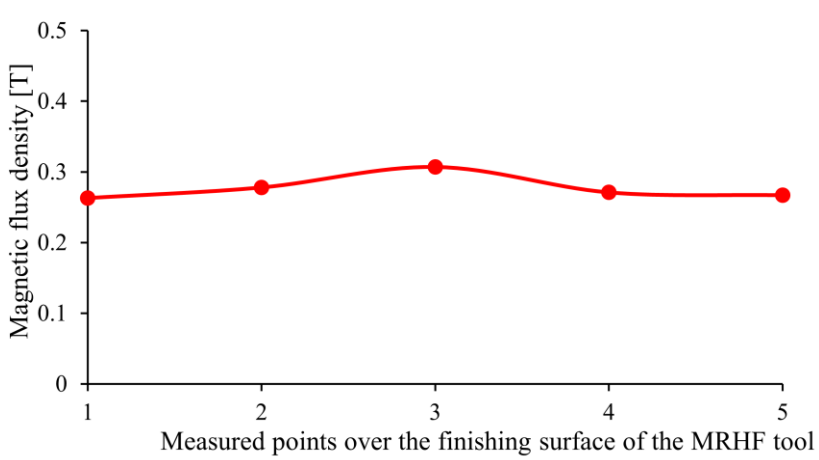

Fig. 3.27 Experimental measured magnetic flux density (MFD) (a) using probe of the gauss meter at five different points, and (b) graph of MFD at five different points over the convex finishing surface of the MRHF tool covered with magnetorheological (MR) polishing fluid.

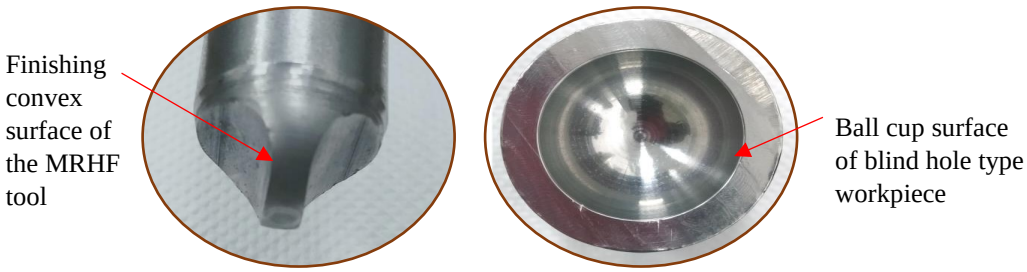

Fig. 3.28 Final fabricated magnetorheological hemispherical finishing (MRHF) tool for finishing the internal hemispherical blind hole type ball cup (BHBC) surface of ball transfer unit.

This further helps to hold the MRP fluid over the new MRHF tool surface during the fine finishing of BHBC workpiece surface as can be observed in Fig. 3.27 (a) and (b). Thus, the final fabricated MRHF tool core used for the finishing of BHBC workpiece can be observed from the Fig. 3.28.

3.10 Conclusions

The following conclusions have been made from the design and development of a new single electromagnetic magnetorheological grinding (MRG) tool for finishing the longitudinal and flat end surfaces of cylindrical blind hole type workpieces.

- The design of a new single electromagnetic MRG tool successfully demonstrates the magnetization of its both surfaces which is used to achieve finishing over the longitudinal and flat end surfaces of the cylindrical blind hole type workpiece surfaces.
- The results of the finite element analysis show that the MRG tool with V-shaped grooves has a more uniform and higher magnetic flux density distribution on the finishing surfaces than the MRG tool without grooves. This could be due to the edge effect of the V-shaped grooves on the MRG tool's finishing surfaces, which help in concentrating higher magnetic flux density.
- The MRG tool which has V-shaped grooves on its finishing surface, produces a stronger and more consistent magnetic field, which helps in fine-finishing the longitudinal and flat end surfaces of CBH work components at a faster rate. The magnetic field gradient further reveals that the MRP fluid remains stiffer on the longitudinal and flat end finishing surfaces of the MRG tool with V-grooves than on the internal surfaces of the CBH workpieces when finishing is done.
- The MRG tool performs finishing eccentrically over the longitudinal cylindrical blind hole type workpiece surface. Thus, this permits the use of the MRG tool for different workpieces with variable diameters.
- The MRG tool is capable to maintain a uniform working gap between the tapered longitudinal CBH type workpiece surface and the longitudinal surface of the MRG tool using the rotating swivel vise. This uniform working gap helps to provide uniform finishing over the entire tapered longitudinal CBH type workpiece surface.
- The overall results revealed that the present developed process which uses a single MR grinding tool with V-grooves is found more useful as compared to the MR grinding tool

without any grooves for fine finishing the inner longitudinal and flat end surfaces of various industrial cylindrical blind-hole type workpieces like mould cavities, automobile actuators, femoral head taper junction, etc.

- The magnetic flux density (MFD) in the 0.6 mm gap over the magnetorheological hemispherical finishing (MRHF) tool is found 0.297 T and that on the interior BHBC work part surface is 0.275 T. Thus, this gradient of MFD in the gap states that the MRP fluid remains stiffened on the MRHF tool surface. Also, the uniformity in MFD over the MRHF tool surface makes it feasible to perform uniform and fine finishing over the interior BHBC work part surface of the ball transfer unit (BTU).

CHAPTER 4

THEORETICAL STUDY OF THE FINISHING MECHANISM WITH THE DEVELOPED MAGNETORHEOLOGICAL GRINDING TOOL FOR CHANGE IN SURFACE ROUGHNESS

In this chapter, a theoretical model has been developed to predict the surface roughness (SR) value on the interior tapered longitudinal and flat end surfaces of the cylindrical blind (CBH) type workpieces while finishing with the single electromagnetic newly designed magnetorheological grinding (MRG) tool. To analyze the performance of the present process with the MRG tool, initially, the theoretical analysis of the magnetic flux density (MFD) amid the working gap (WG) is done. Further, the numerically calculated value of MFD is validated through experimentally measured values at the respective location using the probe of the gaussmeter over both the longitudinal and flat end surfaces of the MRG tool. The path length followed by the active abrasive particle (AAP) over the tapered longitudinal and flat end surfaces of the CBH type workpiece is analyzed. Later, the number of AAPs present in the magnetorheological polishing (MRP) fluid are calculated over the tapered longitudinal and flat end surfaces of the CBH type workpiece. Finally, by using the developed theoretical analysis for MFD along with the path length and number of AAPs, a theoretical SR model is developed while finishing the interior tapered longitudinal and flat end surfaces of the CBH type workpieces with the present MRG tool. Further for the validation of the developed theoretical SR model, the experiments were performed over both the surfaces of the CBH type work part made up of EN-31 material. This EN-31 material is utilized for the finishing process as it is used to make mould for the manufacturing of plastic parts. Later, the error is calculated between the experimental and theoretical SR value in the form of a percentage. Thus, the developed theoretical model can be utilized to predict the reduction in SR value over the interior tapered longitudinal and flat end surfaces of the CBH type workpieces while finishing with the single electromagnetic MRG tool. This theoretical SR model of the present process can find its usefulness for the prediction of SR value over the various industrial CBH type components in an application where precision is an important factor such as femoral head taper junction, actuators and moulds of plastic parts like drosophila vials, spray bottle hoods, etc.

4.1 Material removal mechanism

During finishing with the newly developed MRG tool-based process, the magnetorheological polishing (MRP) fluid utilized which contains electrolytic iron particles (EIPs) and abrasive particles. As the MRG tool is magnetized, the EIPs form chain-like structures under the action of the applied magnetic field. Owing to this, the active abrasive particles (AAPs) are rigidly gripped in the EIP chains. Thus, this imposes the magnetic normal (MN) force on the AAPs which are in contact with the CBH type work part surfaces as espied in Figs. 4.1 (a) and (b). This MN force helps in indenting the AAPs on the CBH type work part surface.

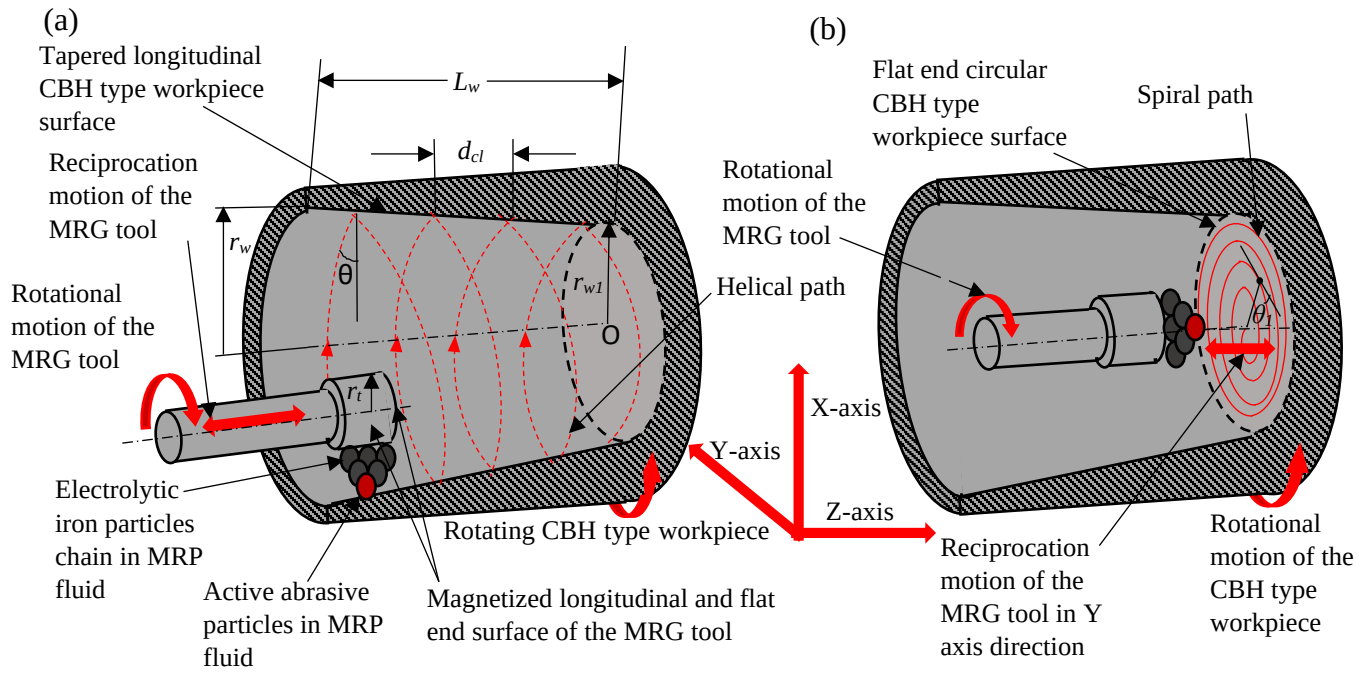

Fig. 4.1 Schematic diagram of the finishing mechanism in a (a) tapered longitudinal and (b) flat end surfaces of the cylindrical blind hole (CBH) type workpiece using the magnetorheological grinding (MRG) tool.

When abrading action takes place owing to the sliding of the AAPs over the tapered longitudinal and flat end CBH type work part surfaces, different paths are followed by AAPs. During finishing of the tapered longitudinal CBH type work part surface, the path followed is the helical path. This path is formed by the simultaneous motion of the rotating work part, and reciprocation of the rotating tool with radius r_t as espied in Fig. 4.1(a). The helical path travelled by the AAP starts from the open end of the tapered longitudinal CBH type workpiece surface with radius, r_w and

ends towards the flat end CBH type workpiece surface with radius, r_{w1}. While AAP travels along the helical path the rotational angle of the r_w from the X-axis is θ. Further, as AAP follows the helical path over the tapered longitudinal CBH type workpiece surface, the height of one complete turn forms the pitch (d_{cl}) while AAP travels along the length (L_w) of the workpiece. Owing to the simultaneous increment in the rotational speed of the CBH type work part and reciprocation speed of the MRG tool, there may be a decrease in the pitch (d_{cl}) when a single AAP follows the dedicated path on the tapered longitudinal CBH type work part surface.

Further, the same single electromagnetic MRG tool is utilized to perform finishing over the flat end surface of the same CBH type work part while following the spiral path formed by the motions of the rotating workpiece along with simultaneous rotating and reciprocating tool as shown in Fig. 4.1(b). In this spiral path, dr_t is the variable radial distance of the AAP due to the rotating MRG tool, θ_1 is the angle between the spiral and the tangent.

Further, the material in the vicinity of the penetrated abrasive particles is removed due to relative motion among the rotating CBH type work part and the MRG tool [Paswan and Singh, 2019a; Jain *et* al., 1999]. This ploughed material is removed as micro-chips. Thus, finishing can be achieved over the tapered longitudinal and flat end CBH type work part surfaces with the newly developed MRG tool in the direction of path followed by the AAPs. In the present work, the CBH type work part is provided with rotation in the opposite direction of the tool rotation to enhance the relative motion of the AAPs over the roughness peaks (Paswan and Singh, 2019a). Also, the rotation of the CBH type work part along with the rotating and reciprocation of the tool that helps to achieve finishing over its entire interior surfaces with the newly developed single electromagnetic MRG tool.

4.1.1 Analysis of shear forces acting over the tapered longitudinal CBH type work part surface during finishing with the MRG tool

Due to the rotational as well as reciprocation speed of the MRG tool over the rotating tapered longitudinal surface of the CBH type workpiece, the active abrasive particles (AAPs) experience the axial force (F_{al}) along with the tangential shear (TS) force (F_{ntl}). Figure 4.2(a) depicts the forces acting on the tapered longitudinal surface during finishing with the MRG tool. The finishing medium used is the MRP fluid which acts like a Bingham plastic fluid (Sidpara *et* al., 2009). As the longitudinal MRG tool surface experiences the magnetic field, the MRP fluid gets stiffend. This stiff MRP fluid with AAPs indent over the tapered longitudinal surface of the CBH type

workpiece owing to magnetic normal (MN) force. Further, the MRG tool is provided with rotational motion along the oppositely rotating CBH type workpiece. The TS force is experienced by the AAPs owing to the rotation of the MRG tool and the rotating CBH type workpiece. Thus, the tangential shear (TS) force can be calculated through TS stress acting over the AAPs of the MRP fluid on the workpiece surface. The TS stress (τ_l) is expressed in Eq. (4.1).

$$\tau_l = \tau_0 + \mu \frac{d(u_l)}{dg_l} \tag{4.1}$$

where τ_l is the shear stress of the MR polishing fluid (viscous fluid) or TS stress acting on the tapered longitudinal surface of the CBH type workpiece, τ_o is the dynamic yield stress of MRP fluid which is viscous under applied magnetic field, μ is the viscosity of the MRP fluid under dynamic yield stress, u_l is the tangential relative velocity of the AAPs in the MRP fluid, g_l is the working gap (WG) between the longitudinal MRG tool surface and the taper longitudinal CBH type work part surface and $\frac{d(u_l)}{dg_l}$ is the shear rate along the tangential direction. The tangential relative velocity (u_l) of the AAPs over the rotating interior tapered longitudinal surface of the CBH type workpiece is calculated from Eq. (4.2).

$$u_l = \frac{2\pi N_{tl} r_t}{60} + \frac{2\pi (N_{wl} \int_{r_{w1}}^{r_w} dr)}{60} \tag{4.2}$$

where N_{tl} is the rotational MRG tool speed, r_t is the radius of the MRG tool, N_{wl} is the rotational CBH type workpiece speed during finishing of its longitudinal surface, r_w is the radius towards the open end of the CBH type work part and r_{w1} is the radius towards the flat end surface of the CBH type workpiece. In Eq. 4.2, as the radius of the tapered longitudinal surface of the CBH workpiece starts decreasing from its open end towards the flat end surface, so the integration is applied to the radius (r_{w1} to r_w). Further, using Eqs. (4.1) and (4.2), the tangential shear stress acting over the interior tapered longitudinal surface of the CBH workpiece is given in Eq. (4.3).

$$\tau_l = \tau_0 + \frac{\pi \mu r_t}{30} \left(\frac{d(N_{tl})}{dg_l} \right) + \frac{\pi \mu (r_w - r_{w1})}{30} \left(\frac{d(N_{wl})}{dg_l} \right) \tag{4.3}$$

The TS force (F_{ntl}) acting over the tapered longitudinal CBH type work part surface utilizing the newly developed MRG tool is calculated using Eq. (4.3) and given in Eq. (4.4).

$$F_{ntl} = \frac{\pi}{4} D_{il}^2 \, \tau_l = \frac{\pi}{4} D_{il}^2 \left\{ \tau_0 + \frac{\pi \mu r_t}{30} \left(\frac{d(N_{tl})}{dg_l} \right) + \frac{\pi \mu (r_w - r_{w1})}{30} \left(\frac{d(N_{wl})}{dg_l} \right) \right\} \tag{4.4}$$

where D_{il} is the indentation diameter of the AAP's indented portion on the tapered longitudinal CBH type work part surface. As the TS force (F_{ntl}) acts owing to the relative motion between the rotating longitudinal MRG tool and rotational motion of the CBH type workpiece. So, the indented

AAPs experiencing TS force (F_{ntl}) collide with the asperities present circumferentially over the tapered longitudinal CBH type work part surface (Fig. 4.2(a)) and performs finishing.

Further, due to the reciprocating MRG tool, the axial shear force (F_{al}) is experienced by the AAPs. This force (F_{al}) is acting parallel to the reciprocation motion of the MRG tool and can be calculated from Eq. (4.5).

$$F_{al} = \frac{\pi}{4} D_{idl}^2 \left(\tau_0 + \mu \frac{d(v_l)}{dg_l}\right) \tag{4.5}$$

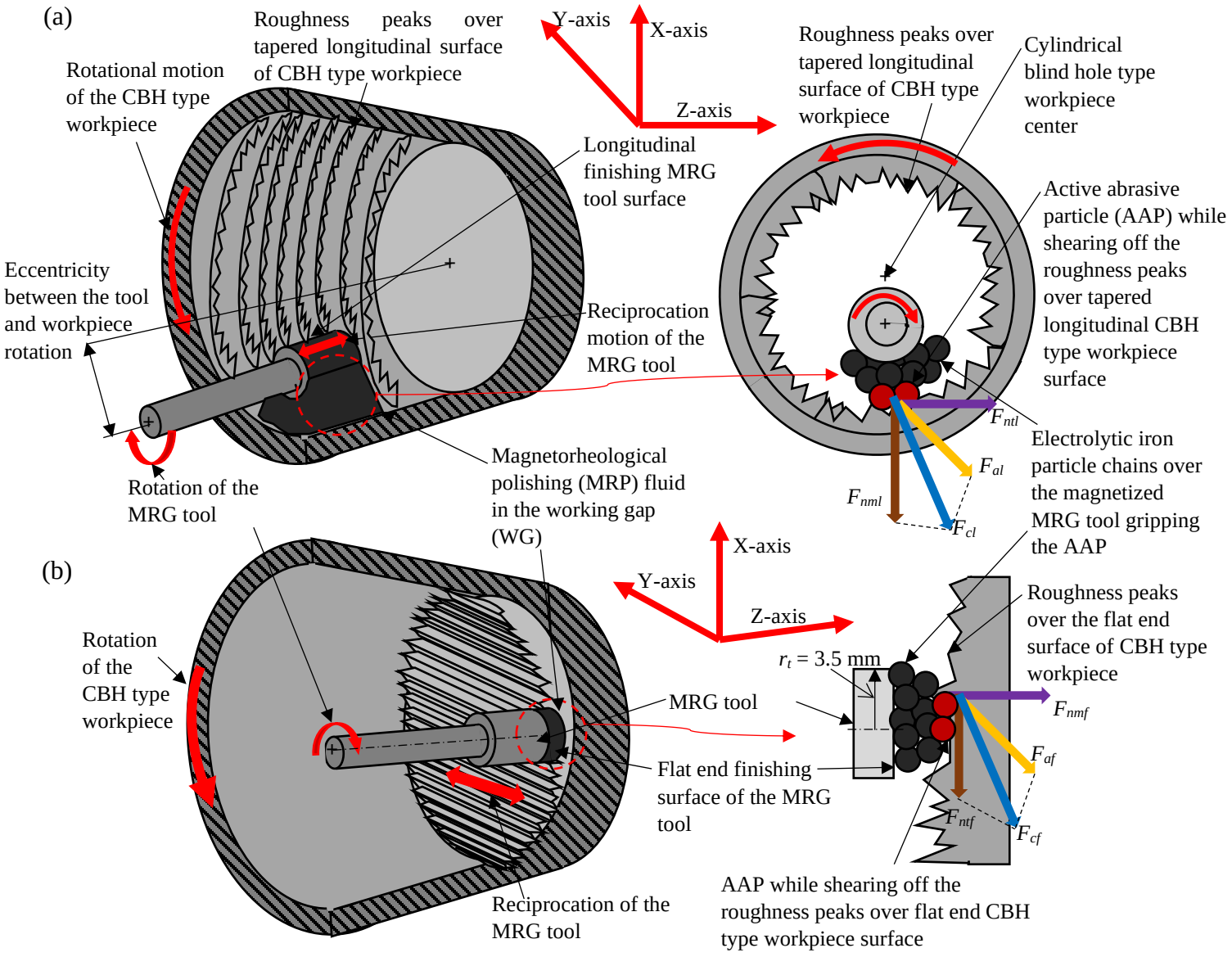

Fig. 4.2 Finishing mechanism in the magnetorheological grinding (MRG) process for the (a) tapered longitudinal, and (b) flat end cylindrical blind hole (CBH) type workpiece surfaces.

where the shear rate along the reciprocation motion of the MRG tool is denoted as $\frac{d(v_l)}{dg_l}$ for the longitudinal surface, v_l is the reciprocation speed of the MRG tool over the longitudinal CBH type workpiece surface. As this axial force (F_{al}) is experienced by the AAPs, the asperities present along the length of the CBH type workpiece are sheared off. Thus, the total shear force (F_{cl}) is taking place due to the resultant of the tangential and axial forces as mentioned in Eq. (4.6). This F_{cl} shear off the surface roughness (SR) peaks as shown in Fig. 4.2 (a).

$$F_{cl} = (F_{ntl}^2 + F_{al}^2)^{\frac{1}{2}} \tag{4.6}$$

This resultant F_{cl} helps in the removal of material from the entire interior tapered longitudinal CBH type work part surface during MR finishing with the present single electromagnetic MRG tool. Also, the rotational MRG tool motion and CBH type work part motion in opposite direction increases the AAP's relative velocity on the interior tapered longitudinal CBH type work part. Owing to this there is an increment in shearing rate which consecutively increases the resultant F_{cl}. This results in an improvement in finishing performance over the tapered longitudinal surface of the CBH type workpiece.

4.1.2 Analysis of shear forces acting over the flat end CBH type work part surface during finishing with the MRG tool

The shear force acting on the flat end rotating CBH type work part surface with the rotation and reciprocation of the flat end finishing surfaces of the same single electromagnetic MRG tool is espied in Fig. 4.2 (b). Thus, the AAPs experience tangential shear (TS) force (F_{ntf}), as well as the axial force (F_{af}), respectively. Figure 4.2(b) depicts the total shear force (F_{cf}) which acts tangentially to the rotational tool speed. Here, due to the rotating MRG tool, the active abrasive with the flat end tool surface is changing its position from 0 (minimum at the center of the tool) to r_t (maximum radius of radius of the tool i.e. r_t = 3.5 mm in present case) (Fig. 4.2). So, the value of F_{ntf} on the flat end surface of the CBH workpiece gets varied from minimum at the center position of the tool to maximum at outer edge of the tool (r_t = 3.5 mm). The TS stress acting over the AAPs present in MRP fluid is expressed in Eq. (4.7).

$$\tau_f = \tau_0 + \mu \frac{d(u_f)}{dg_f} \tag{4.7}$$

where τ_f is the shear stress of the MR polishing fluid (viscous fluid) (or) TS stress acting on the AAPs, u_f is the tangential relative velocity of the AAPs over the flat end surface of the CBH workpiece, $\frac{d(u_f)}{dg_f}$ is the shear rate along the tangential direction, and g_f is the WG amid the flat MRG tool surface and the flat end CBH type work part surface.

The AAP's tangential relative velocity (u_f) over rotating interior flat end surface of the CBH type workpiece is calculated from Eq. (4.8).

$$u_f = \frac{2\pi(N_{tf}\int_0^{r_t} dr_t)}{60} + \frac{2\pi(N_{wf}\, r_{w1})}{60} \tag{4.8}$$

where N_{tf} is the rotational MRG tool speed, dr_t is the radial distance of the AAP on the flat end surface of the MRG tool due to its rotation, N_{wf} is the rotational CBH type workpiece speed during finishing of its flat end surface, and r_{w1} is the radius of the flat end surface of the CBH type workpiece (Fig. 4.1). The total TS stress (τ_f) acting over the flat end CBH type work part surface can be calculated by Eq. (4.9) while incorporating Eq. (4.8) in Eq. (4.7).

$$\tau_f = \tau_0 + \frac{\pi\mu\int_0^{r_t} dr_t}{30}\left(\frac{d(N_{tf})}{dg_f}\right) + \frac{\pi\mu r_{w1}}{30}\left(\frac{d(N_{wf})}{dg_f}\right) \tag{4.9}$$

where τ_f is the TS stress of the MRP fluid (viscous fluid) acting during the finishing of flat end CBH type workpiece surface. Thus, the TS force (F_{ntf}) acting over the flat end surface of the CBH type work part utilizing the newly developed single electromagnetic MRG tool is calculated using Eq. (4.10).

$$F_{ntf} = \frac{\pi}{4}D_{if}^2 \times \tau_f = \frac{\pi}{4}D_{if}^2 \times \left\{\tau_0 + \frac{\pi\mu\int_0^{r_t} dr_t}{30}\left(\frac{d(N_{tf})}{dg_f}\right) + \frac{\pi\mu r_{w1}}{30}\left(\frac{d(N_{wf})}{dg_f}\right)\right\} \tag{4.10}$$

where D_{if} is the indentation diameter of the AAP's over the flat end CBH type work part surface. Further, as the MRG tool reciprocates, an axial force (F_{af}) is exerted over the inner flat end CBH type work part surface through the AAPs. This force (F_{af}) is acting parallel to the reciprocation motion of the MRG tool in Y-axis direction (Fig. 4.2b) and can be calculated from Eq. (4.11)

$$F_{af} = \left(\frac{\pi}{4}D_{if}^2\right) \times \left(\tau_0 + \mu\frac{d(v_f)}{dg_f}\right) \tag{4.11}$$

where the rate of shear along the reciprocation MRG tool speed is denoted as $\frac{d(v_f)}{dg_f}$ for the flat end CBH type work part surface, v_f is the reciprocation speed of the MRG tool over the flat end CBH

type workpiece surface in Y-axis direction. Further, the total shear force (F_{cf}) is taking place due to the resultant of the tangential and axial forces as given in Eq. (4.12) for the flat end CBH type work part surface. This F_{cf} clip off the SR peaks as shown in Fig. 4.2(b).

$$F_{cf} = \left(F_{ntf}^2 + F_{af}^2\right)^{\frac{1}{2}} \tag{4.12}$$

Thus, this F_{cf} is the resultant of the shear forces acting on the flat end CBH type work part surface. This force helps in material removal from the vicinity of the indented AAPs which performs finishing over the flat end rotating CBH type work part surface due to the relative motion of the rotating and reciprocating single electromagnetic MRG tool.

4.2 Theoretical investigation of roughness model over the CBH type workpiece surfaces during finishing with the present magnetorheological grinding (MRG) process

In the present study, an electromagnetic copper coil is used for the generation of a magnetic field over the finishing surfaces of the MRG tool. There are two surfaces (cylindrical longitudinal and flat end surfaces) of the present electromagnetic MRG tool which can perform finishing over both the surfaces of the CBH type work part (Fig. 4.1). When finishing is performed with the longitudinal surface of the present single electromagnetic MRG tool, the axis of the rotating and reciprocating tool is eccentric to the axis of rotation of the CBH type workpiece (Fig. 4.1a). But, during finishing using the flat end MRG tool surface, the axis of rotation (along Z-axis) and the reciprocation (along Y-axis) of the tool are perpendicular to each other (Fig. 4.1b). Thus, the calculation of the magnetic flux density (MFD) over a single electromagnetic MRG tool is applicable for both of its surfaces in this process. Further for analysing the finishing mechanism over the tapered longitudinal and flat end CBH type work part surfaces, a theoretical roughness model is developed. To develop the theoretical model of the surface roughness (SR) value in the present single electromagnetic MRG tool-based process for the CBH type work part surfaces, the assumptions which need to be considered are as follows.

- All the particles present in the MRP fluid are assumed to be spherical in shape to simplify the calculations involved in this study of the finishing mechanism (Jha and Jain *et* al., 2006; Singh *et* al., 2013).

- The abrasive particles size is considered as an average diameter of 15 µm and average electrolytic iron particles (EIPs) diameter as 18 µm. These SiC and EIP particles are considered to be uniformly suspended in the base fluid (Paswan and Singh, 2019).
- During practical use of the magnetic system, there might be some magnetic field losses and leakage in the finishing process. But these are neglected during force calculation in relation to the MFD.
- The magnetic flux lines are considered uniform along the length of the MRG tool.
- All the other forces (i.e. gravitational, centrifugal and coriolis force) with minor magnitude acting on the AAPs are neglected.
- During finishing of the tapered longitudinal surface, the curvature of the MRG tool surface is not concentric with the surface of the CBH type workpiece due to their different diameters. However, for simplifying the calculation, the gap remains constant in the working gap (WG). Thus, the projected area of the MRG tool surfaces is taken exactly same over the internal surfaces of the CBH type workpiece.

In the present work, the magnetized single electromagnetic MRG tool retains the MRP fluid on its surfaces. The magnetic EIPs in this fluid are aligned with the magnetic field line induced over the MRG tool surfaces. Because of this behaviour of the EIPs, the levitation phenomenon occurs among the non-magnetic SiC abrasive particles (APs) that are pushed towards the CBH type workpiece surfaces. Therefore, the magnetic normal ($F_{nml,nmf}$) force (Fig. 4.2) pushes the APs away from the finishing longitudinal and flat end surfaces of the magnetized single electromagnetic MRG tool. The longitudinal portion of the MRG tool generates the magnetic flux lines in the radially outward direction whereas the flat end of the same tool generates the magnetic flux lines parallel to the electromagnet. So, the magnetic normal ($F_{nml,nmf}$) force can be experienced in the constrained space between the MRG tool surfaces and the internal tapered longitudinal as well as flat end surfaces of the ferromagnetic CBH type work part. Thus, this force ($F_{nml,nmf}$) helps in the indentation of APs over the CBH type work part surfaces. The indented APs over the internal CBH type work part surfaces when under the action of resultant force (due to the tangential and axial forces) can help in finishing it.

4.2.1. Modeling of induced magnetic flux density (MFD) due to single electromagnetic MRG tool

In this study, the specifications of a single electromagnetic MRG tool are shown in Fig. 4.3(a). The shape of the finishing surfaces of the single electromagnetic MRG tool is cylindrical along the longitudinal surface and straight circular along the flat end surface. The radius (r_t) of the MRG tool is 3.5 mm, radius of the MRG tool core at point M (r_c) is 3 mm (Fig. 4.3(b)), and the length (l_1) along the longitudinal surface is 15 mm. The distance of the starting point of the longitudinal surface of the MRG tool from the starting of the coil (l_2) is 32 mm. The dimensions of the electromagnetic coil are 110 mm in length (l_3) and radius (R) as 35 mm. The calculation of the MFD has been performed on the longitudinal and flat end surfaces of the single electromagnetic MRG tool using Biot Savart law (Guo *et* al., 2008). The magnetic field strength (MFS) at an arbitrary point M (X, Y, Z) (Fig. 4.3(a)) at a certain distance from the electromagnetic coil within the MRG tool core is calculated using Eq. (4.13).

$$H(X,Y,Z) = \frac{n_1 I}{4\pi}\int_0^{2\pi}\frac{dlr\prime}{(r')^3}d\varphi \tag{4.13}$$

where the total number of turns for the excitation coil is denoted by n_1, I is the excitation current in A, dl is the vector along the path whose magnitude is the length of the differential element of the coil, r' is the distance from dl to point M and φ is the angular position of dl considered on the loop. The cross product of dl and r' can be calculated using Eq. (4.14) (Guo *et* al., 2008).

$$\overrightarrow{dl} \times \overrightarrow{r'} = zR\cos\varphi d\varphi \hat{\imath} + zR\sin\varphi d\varphi \hat{\jmath} + \{R^2 - R(x\cos\varphi + y\sin\varphi)\}\, d\varphi \hat{k} \tag{4.14}$$

The magnitude of the vector $\overrightarrow{r'}$ is obtained using Eq. (4.15). From Eq. (4.15), $r'^3$is obtained and expressed in Eq. (4.16).

$$r' = \sqrt{(x - R\cos\varphi)^2 + (y - R\sin\varphi)^2 + (z)^2} \tag{4.15}$$

$$r'^3 = \{x^2 + y^2 + z^2 + R^2 - 2R(x\cos\varphi + y\sin\varphi)\}^{3/2} \tag{4.16}$$

Equations (4.14) and (4.16) are substituted in Eq. (4.13) for Biot-savart law. Finally, these are utilized for calculating the MFS within the MRG tool core in X, Y, and Z directions. The generated MFS by the electromagnetic coil over point M (X, Y, Z) is expressed in Eqs. (4.17) – (4.19).

$$H_X = \frac{n_1 I}{4\pi}\int_0^{2\pi}\frac{Rz\sin\varphi}{\{x^2+y^2+z^2+R^2-2R(x\cos\varphi+y\sin\varphi)\}^{\frac{3}{2}}}d\varphi \tag{4.17}$$

$$H_Y = \frac{n_1 I}{4\pi}\int_0^{2\pi}\frac{Rz\cos\varphi}{\{x^2+y^2+z^2+R^2-2R(x\cos\varphi+y\sin\varphi)\}^{\frac{3}{2}}}d\varphi \tag{4.18}$$

$$H_Z = \frac{n_1 I}{4\pi}\int_0^{2\pi} \frac{R(R - x\cos\varphi - y\sin\varphi)}{\{x^2+y^2+z^2+R^2-2R(x\cos\varphi+y\sin\varphi)\}^{\frac{3}{2}}}\,d\varphi \qquad (4.19)$$

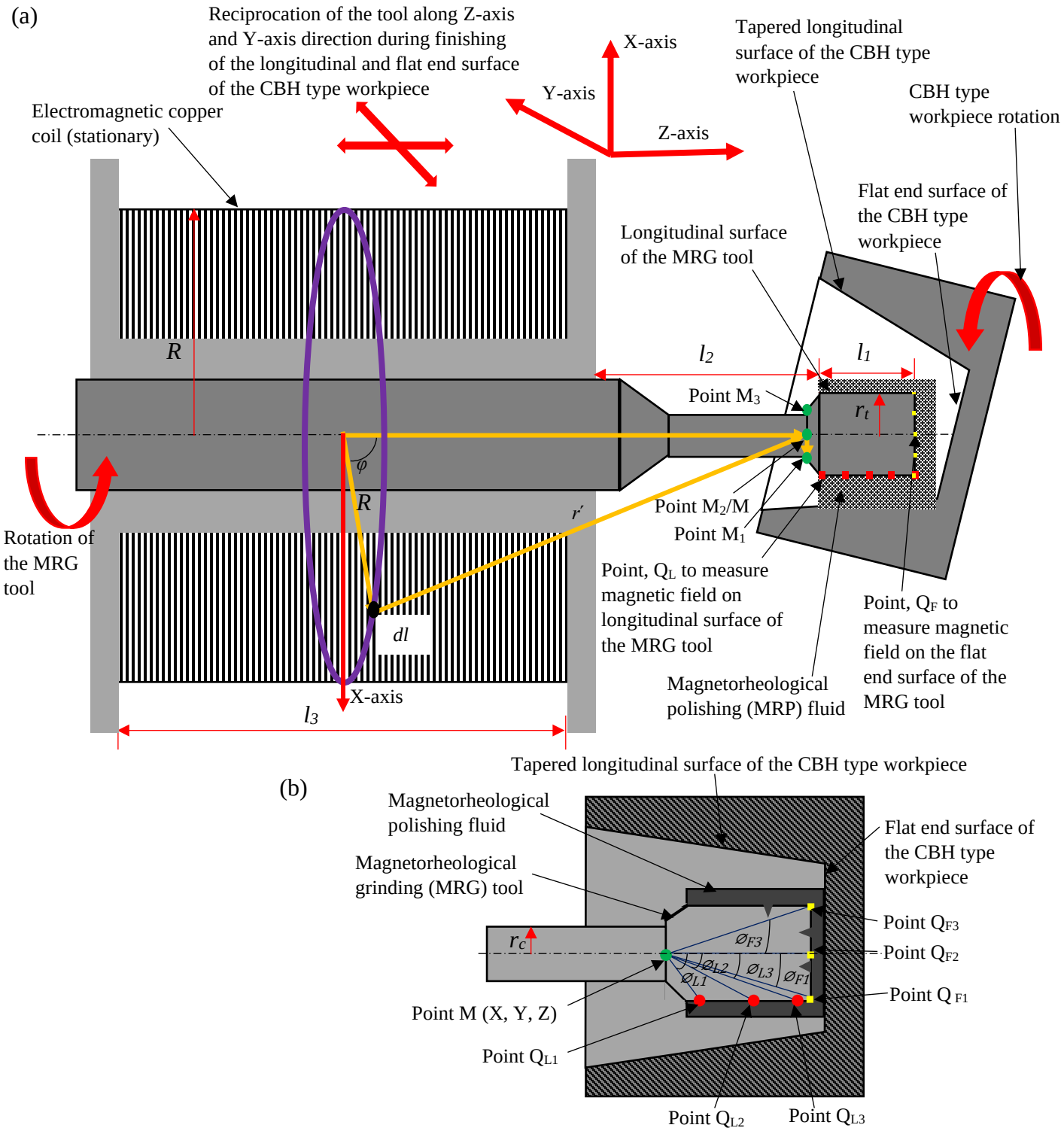

Fig. 4.3 (a) Schematic diagram of finishing mechanism of the tapered longitudinal and flat end cylindrical blind hole (CBH) type work part surfaces, and (b) the magnetic flux density at different points over the magnetorheological grinding (MRG) tool surfaces to be calculated.

Here, H_X, H_Y, and H_Z are the components of the MFS along the X, Y, and Z-axis. After utilizing Eqs. (4.17-4.19), the values of H_X, H_Y, H_Z components are calculated for point M (X, Y, Z). Further using the calculated values from Eqs. (4.17-4.19), the total MFS is calculated. The resultant of the total magnetic field strength (H_m) at a point M (X, Y, Z) on the MRG tool is calculated using Eq. (4.20).

$$H_m = (H_X^2 + H_Y^2 + H_Z^2)^{\frac{1}{2}} \quad (4.20)$$

The average of the MFS (H_{avg}) at three different positions (M_1, M_2, and M_3) in line with point M are considered. The average MFS at point M can be calculated from Eq. (4.21).

$$H_{avg} = \frac{H_{m1}+H_{m2}+H_{m3}}{3} \quad (4.21)$$

where H_{m1}, H_{m2}, and H_{m3} is the MFS at points M_1, M_2, and M_3 respectively on the MRG tool core surface (Fig. 4.3(a)).

Further, Eq. (4.22) is used to calculate MFD (B_s) at point M in free space from the source of MFS (H_{avg}) using Eq. (4.21).

$$B_s = \mu_o H_{avg} \quad (4.22)$$

where B_s is the magnetic flux density (MFD) at point M of the MRG tool core and μ_o is the magnetic permeability of air in free space, $4\pi \times 10^{-7}$ N/A^2.

Further, the value of MFD obtained from Eq. (4.22) at point M is utilized to calculate the MFD value at points $Q_{L,F}$ on the tool longitudinal and flat end surface (Fig. 4.3). As the magnetic field spread outwards through the longitudinal and flat end finishing surfaces of the MRG tool. So, different MFD values can be experienced over different points ($Q_{L,F}$ (X, Y, Z)) over the surfaces of the MRG tool as espied in Fig. 4.3(b). Thus, the MFD over points $Q_{L,F}$ (X, Y, Z) can be calculated using Eq. (4.23).

$$B_s A_c = B_o A_s \quad (4.23)$$

where A_c is the cross-section area of the tool core across point M (radius of this cross section area, r_c as shown in Fig. 4.3(b)), B_o is the MFD over the points $Q_{L,F}$ (X, Y, Z) calculated on the finishing surfaces of the MRG tool, the A_s is the inclined cross-sectional area (along M to $Q_{L,F}$) of the measured points ($Q_{L,F}$) on the MRG tool . From Fig.4.3(b), A_s is calculated through Eq. (4.24).

$$\cos \varnothing = \frac{A_o}{A_s} \quad (4.24)$$

$$A_s = \frac{A_o}{\cos \varnothing} \quad (4.25)$$

Using Eq. (4.25) in Eq. (4.23), MFD over points $Q_{L,F}$ can be calculated as Eq. (4.26).

$$B_s A_c \cos\varnothing = B_o A_o \quad (4.26)$$

where A_c is the cross-section area of the tool core across point M (radius of this cross section area, r_c as shown in Fig. 4.3(b)), B_o is the MFD over the points $Q_{L,F}$ (X, Y, Z) calculated on the finishing surfaces of the MRG tool, the A_o is the vertical cross-sectional area of the measured points ($Q_{L,F}$) on the MRG tool finishing surface, and $\varnothing$ is the angle between the center line of the MRG tool and resultant projected line (from M to $Q_{L,F}$) towards a point Q on the tool surface.

Further, the finishing surfaces of the MRG tool, the EIPs present in MRP fluid over the finishing surfaces of the MRG tool, and the surfaces of the ferromagnetic CBH type workpiece get magnetized by the magnetic field (B_o) in working gap (WG) due to the electromagnetic copper coil. Therefore, the magnitude of the total magnetic field (B_{Total}) in the WG between the MRG tool and the CBH type work part surfaces is evaluated from Eq. (4.27) or Eq. (4.28).

$$B_{Total} = B_o + \mu_o\mu_{rc}(M_{Cr}) + \mu_o\mu_{mrp}(M_{EI}) + \mu_o\mu_{rw}(M_{cw}) \quad (4.27)$$

$$B_{Total} = \frac{B_s A_c \cos\varnothing}{A_o} + \mu_o\mu_{rc}(M_{Cr}) + \mu_o\mu_{mrp}(M_{EI}) + \mu_o\mu_{rw}(M_{cw}) \quad (4.28)$$

where B_{Total} is the total MFD in the WG which is filled with the MRP fluid, μ_{rc} is the relative permeability (RP) of the MRG tool as 600, M_{Cr} is the magnetization of the material of the MRG tool (Fig. 4.4 (a)), μ_{mrp} is the MRP fluid's RP as 5 (Paswan *et* al., 2017), M_{EI} is the electrolytic iron particle's magnetization (Fig. 4.4 (b)), μ_{rw} is the RP of the CBH type work part material (ferromagnetic) as 300, and M_{cw} is the CBH type work part material's magnetization (EN-31 steel) from Fig. 4.4(c). The graphs between the M-B curve of mild steel MRG tool, electrolytic iron particles (EIPs), and EN-31 steel in Fig. 4.4 (a-c) are obtained using the vibrating-sample magnetometer instrument.

Table 4.1. Magnetic flux density (MFD) on the MRG tool surface included the magnetization effect of the interior cylindrical blind hole (CBH) type work part surfaces, EIPs in MRP fluid in working gap of 1 mm.

Type of surface of CBH type workpiece	Points on tool surface	Angle and coordinates of point Q with respect to point M (Fig. 4.3)	Theoretical magnetic flux density (T) in the working gap Eq. (4.28)	Experimental magnetic flux density (T)	Percentage error
Longitudinal surface	Q_{L1}	$\varnothing_{L1}$ = -49.40° (-3.5, 0, 3)	0.287	0.290	1.03
	Q_{L2}	$\varnothing_{L2}$ = -37.875° (-3.5, 0, 4.5)	0.338	0.335	0.89
	Q_{L3}	$\varnothing_{L3}$ = -17.65° (-3.5, 0, 11)	0.399	0.390	2.31
Flat end surface	Q_{F1}	$\varnothing_{F1}$ = -13.134° (-3.5, 0, 15)	0.409	0.398	2.76
	Q_{F2}	$\varnothing_{F2}$ = 0° (0, 0, 15)	0.413	0.408	1.22
	Q_{F3}	$\varnothing_{F3}$ = 13.134° (3.5, 0, 15)	0.409	0.401	1.99

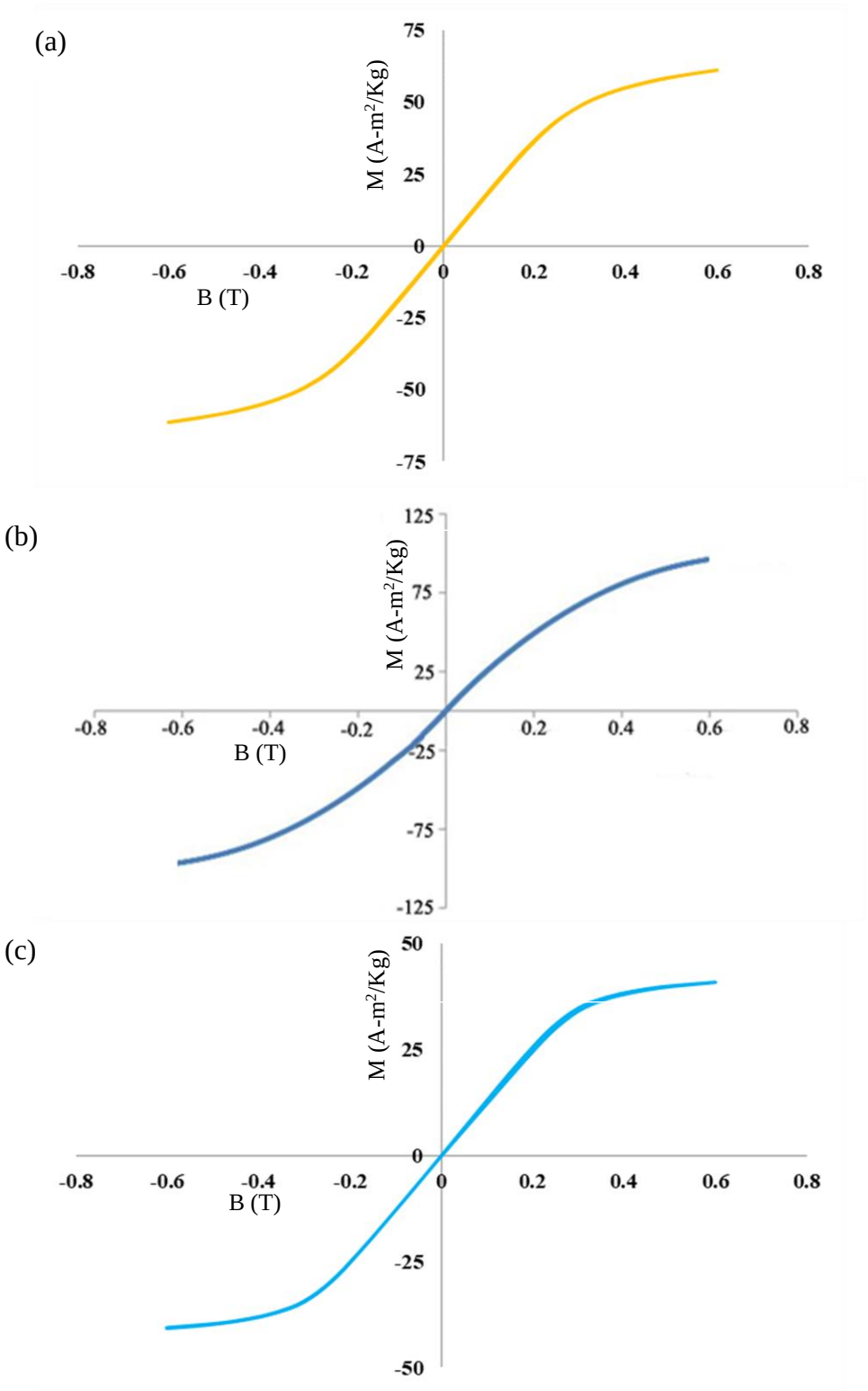

Fig. 4.4 M-B curve of (a) mild steel MRG tool, (b) electrolytic iron particles (EIPs), and (c) EN-31 steel.

Thus, the MFD is calculated from Eq. (4.28) at certain locations amid the WG over the longitudinal and flat end surfaces of the single electromagnetic MRG tool as stated in Table 4.1. Also, the theoretical results of the MFD are compared with the experimental results (measured with digital gauss meter) using Table 4.1. Hence, this validates the model of induced magnetic flux density (MFD) over the longitudinal and flat end surfaces of the single electromagnetic MRG tool. Also, the theoretically calculated and experimentally obtained MFD values in Tables 4.1 reveals the capability of the single electromagnetic MRG tool to generate the MFD on its finishing surfaces which is further used to retain the MRP fluid over its longitudinal and flat end surfaces. This results in MR finishing over the tapered longitudinal and flat end CBH type work part surfaces. Further, a linear function is obtained from Tables 4.2 and 4.3 which is expressed by Eqs. (4.29) and (4.30).

$$B_l(g_l) = -32.22g_l + 0.3332 \tag{4.29}$$

$$B_f(g_f) = -48.75g_f + 0.407 \tag{4.30}$$

where $B_l(g_l)$ and $B_f(g_f)$ is the MFD in the WG, g_l and g_f is the WG between the longitudinal and flat end surfaces of the MRG tool and the corresponding CBH type work part surfaces. Further, these Eqs. (4.29) and (4.30) are used for magnetic normal (MN) force calculation to analyse the indentation of the AAPs.

4.2.2 Calculation of magnetic normal (MN) force to indent abrasive particles over the work part surfaces during finishing with the magnetorheological grinding (MRG) process

In the present newly developed single electromagnetic MRG tool-based process to fine finish the cylindrical blind hole (CBH) type work part surfaces, the MN force acting to indent the abrasive particles over the work part surfaces in the working gap (WG) is expressed in Eqs. (4.31) and (4.32).

$$F_{nml} = \frac{m_a \chi B_l(g_l) \frac{dB_l(g_l)}{dg_1}}{\mu_o} \tag{4.31}$$

$$F_{nmf} = \frac{m_a \chi B_f(g_f) \frac{dB_f(g_f)}{dg_f}}{\mu_o} \tag{4.32}$$

where F_{nml} and F_{nmf} is the MN force which is helpful in the indentation of AAPs over the interior tapered longitudinal and flat end surfaces of the CBH type work part respectively, m_a is the mass of an electrolytic iron particle (EIP) in kg and its average diameter size considered as 15 µm, χ is the EIP's magnetic susceptibility. The term $B_l(g_l)$ and $B_f(g_f)$ are the variation of MFD in the working gap g_l and g_f w.r.t. the longitudinal and flat end surfaces of the single electromagnetic

MRG tool and the CBH type workpiece surfaces. $\frac{dB_l(g_l)}{dg_l}$ and $\frac{dB_f(g_f)}{dg_f}$ is the variation of magnetic flux density gradient in WG.

Therefore,$\frac{dB_l(g_l)}{dg_l}$ and $\frac{dB_f(g_f)}{dg_f}$ is calculated by differentiating the Eqs. (4.29) and (4.30) which is expresses as in Eqs. (4.33) and (4.34), respectively.

$$\frac{dB_l(g_l)}{dg_l} = -32.22 \tag{4.33}$$

$$\frac{dB_f(g_f)}{dg_f} = -48.75 \tag{4.34}$$

Further, to find the value of the MN force (F_{nml} or F_{nmf}), the EIP's magnetic susceptibility (χ) in the MRP fluid during MRF process is found from Eq. (4.35).

$$\chi = \frac{\mu_o M_{EI}}{B_l(g_l) \; or \; B_f(g_f)} \tag{4.35}$$

where μ_o is the magnetic permeability of air in free space, 4π x 10^{-7} N/A^2 and M_{EI} is the electrolytic iron particle's magnetization (Fig. 4.4 (b)).

Table 4.2 Magnetic normal force in the working gap (WG) amid the longitudinal MRG tool surface and tapered longitudinal cylindrical blind hole type work part surface.

Distance from the longitudinal MRG tool surface (m) upto tapered longitudinal CBH type workpiece surface (working gap, g_l)	Theoretical magnetic flux density, $B_l(g_l)$ (T) Eq. (4.28)	Mass susceptibility of the electrolytic iron particle (χ) (m^3/kg) Eq. (4.35)	Magnetic normal force (F_{nml}) in the working gap (N) from Eq. (4.31)
0.0001	0.330	2.20×10^{-4}	4.46×10^{-8}
0.0002	0.327	2.16×10^{-4}	4.35×10^{-8}
0. 0003	0.324	2.13×10^{-4}	4.24×10^{-8}
0. 0004	0.320	2.10×10^{-4}	4.14×10^{-8}
0. 0005	0.317	2.07×10^{-4}	4.04×10^{-8}
0. 0006	0.314	2.05×10^{-4}	3.95×10^{-8}
0. 0007	0.311	2.02×10^{-4}	3.86×10^{-8}
0. 0008	0.307	2.00×10^{-4}	3.78×10^{-8}
0. 0009	0.304	1.98×10^{-4}	3.70×10^{-8}
0. 0010	0.301	1.96×10^{-4}	3.63×10^{-8}

Table 4.3 Magnetic normal force in the working gap (WG) amid the flat end MRG tool surface and flat end cylindrical blind hole type work part surface.

Distance from the flat MRG tool surface (m) upto flat end CBH type workpiece surface (working gap, g_f)	Theoretical magnetic flux density, $B_f(g_f)$ (T) Eq. (4.28)	Electrolytic iron particle's mass susceptibility (χ) (m^3/kg) Eq. (4.35)	Magnetic normal force (F_{nmf}) in working gap (N) from Eq. (4.32)
0.0001	0.402	2.02×10^{-4}	7.56×10^{-8}
0.0002	0.397	2.04×10^{-4}	7.55×10^{-8}
0. 0003	0.392	2.06×10^{-4}	7.54×10^{-8}
0. 0004	0.388	2.09×10^{-4}	7.54×10^{-8}
0. 0005	0.383	2.11×10^{-4}	7.53×10^{-8}
0. 0006	0.378	2.14×10^{-4}	7.53×10^{-8}
0. 0007	0.373	2.17×10^{-4}	7.52×10^{-8}
0. 0008	0.368	2.19×10^{-4}	7.51×10^{-8}
0. 0009	0.363	2.22×10^{-4}	7.51×10^{-8}

After calculating the MFD, the magnetic normal (MN) force is calculated at different working gap (WG) among the MRG tool surfaces and CBH type work part surfaces as reported in Tables 4.2 and 4.3. Due to these forces, the surfaces of the CBH type work part can experience a force by the AAP through an overall effect of EIP in the WG. Thus, the average MN force values obtained from Tables 4.2 and 4.3 are considered for further calculations. Thus, the MN force over the tapered longitudinal surface (F_{nml}) and flat end surface (F_{nmf}) of the CBH type work part are calculated as 4.02×10^{-8} N and 7.53×10^{-8} N, respectively.

4.2.3 Calculation of number of active abrasive particles (AAPs) of the MRP fluid present in the working gap (WG) for finishing the cylindrical blind hole (CBH) type work part surfaces

The MRP fluid resides in the WG amid the finishing surfaces of the single electromagnetic MRG tool and the CBH type work part surface. In this work, the MRP fluid comprises of 19 % by volume concentration (vol. con.) of abrasive particles, 26 % by vol. con. of EIPs and 55 % by vol. con. of base fluid (80 % paraffin and 20 % AP3 grease). To develop the theoretical surface roughness (SR) model, initially the projected area of the MRG tool over the surfaces of the CBH type work part is analysed where AAPs get indented. In the present process, the longitudinal and flat end surfaces of the single electromagnetic MRG tool are used for finishing both the CBH type work part surfaces. For the analysis, the radius (r_t) of the MRG tool is 3.5 mm and 15 mm of length (l_1) as

shown in Fig. 4.3 (a). The diameter of the CBH type work part towards its open end ($2\times r_w$) is 21 mm and towards the flat end surface is 18 mm ($2\times r_{w1}$) (Fig. 4.1(a)). Further, for finding the no. of active abrasives, the variation in diameter between the MRG tool surface and the tapered CBH type workpiece longitudinal surface is neglected. Thus, the working gap (WG) is considered constant throughout the active finishing area of the longitudinal surface. So, the projected area of the MRG tool surface is taken over internal surfaces of the CBH type workpiece. Initially, the longitudinal MRG tool surface is considered for analysis of the projected area required for finding the AAPs as espied in Fig. 4.5. Here, as the MRG tool is performed finishing eccentrically to the center of cylindrical blind hole (CBH) type work part keeping a WG amid them as 1.0 mm in longitudinal surface and 0.9 mm in flat end surface.

For finding the effective active area of MRP fluid in contact with the tapered longitudinal CBH type work part surface, the value of angle γ is required as espied in Fig. 4.5(a). Here, γ is the angle between AO and OD. So, the value of γ is calculated in ΔOAW using Eq. (4.36).

$$sin\,\gamma = \frac{2AW}{(r_w + r_{w1})} \tag{4.36}$$

where AW is equal to the radius of the MRG tool (r_t), r_w and r_{w1} are the radius of the tapered CBH type work part. Using the value of γ *in* degrees, the value of arc length of ADC is calculated using Eq. (4.37).

$$Arc\ length\ (ADC) = \frac{(r_w + r_{w1})\pi\gamma}{180} \tag{4.37}$$

For finding the number of AAPs used to finish the tapered longitudinal CBH type work part surface, the area of the active abrasives region on workpiece longitudinal surface is calculated from Eq. (4.38).

$$Projected\ area\ of\ the\ active\ abrasives\ region\ on\ the\ tapered\ longitudinal\ surface\ of\ the\ CBH\ type\ workpiece,\ A_{tl} = Arc\ length,\ (ADC)l_1 \tag{4.38}$$

Thus, the projected area of the active abrasive region on the tapered longitudinal CBH type work part surface is calculated as 1.008×10^{-4} m^2.

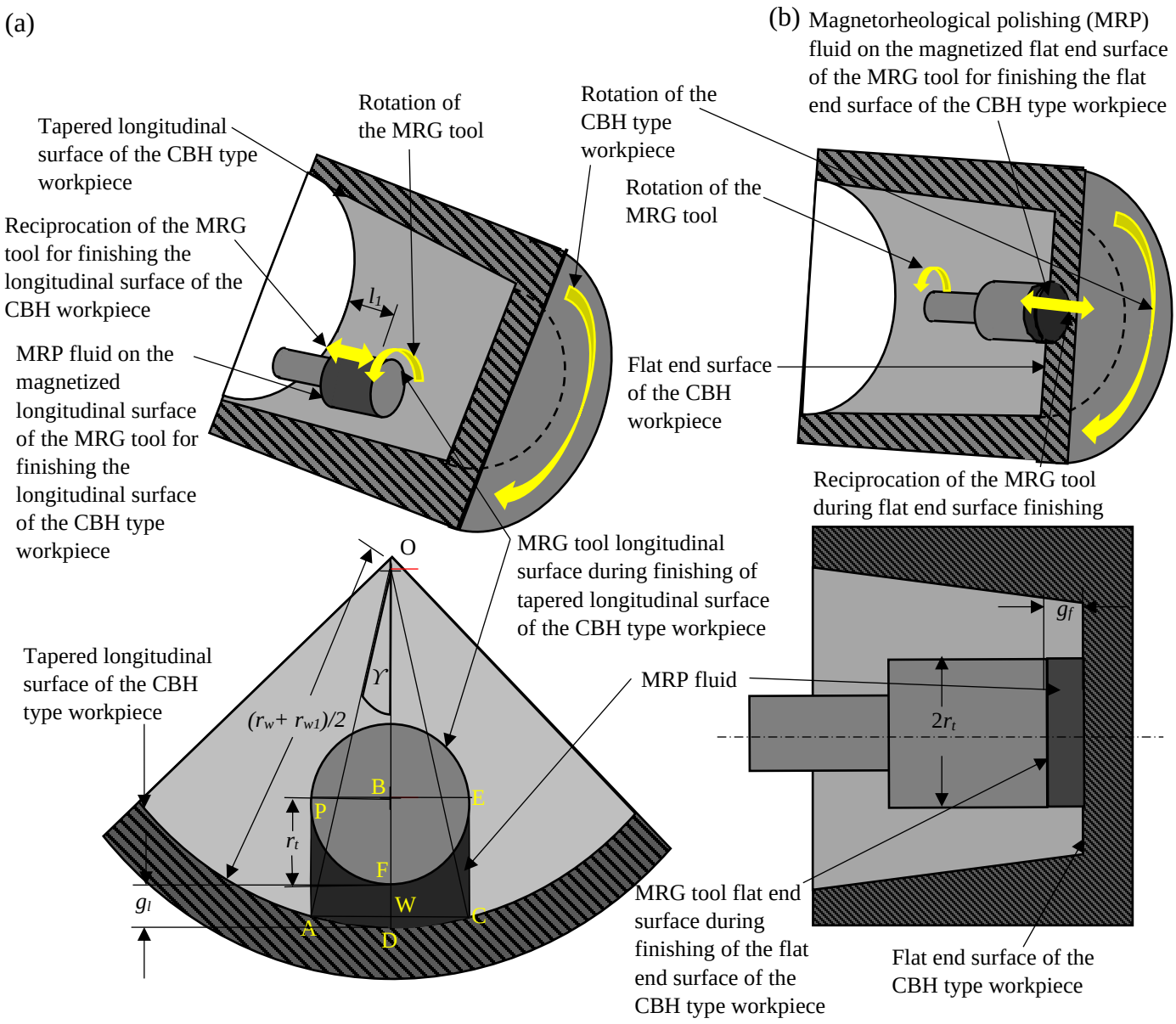

Fig. 4.5. Magnetorheological polishing (MRP) fluid retain on the (a) magnetized longitudinal surface, and (b) flat end surface of the magnetorheological grinding (MRG) tool during finishing the cylindrical blind hole (CBH) workpiece surfaces.

Further, using Eq. (4.38), the number of AAPs involved in finishing the tapered longitudinal CBH type work part surface can be calculated using Eq. (4.39).

$$No.of\ AAPs\ involved\ in\ finishing\ of\ the\ tapered\ longituidnal\ CBH\ type\ workpiece\ surface\ ,\ N_{lg} = \frac{C_s A_{tl} d_{sc}}{V_{sc}} \quad (4.39)$$

where C_s is the % vol. con. of abrasive particles within MRP fluid, d_{sc} is the diameter of the abrasive particle as 15 μm and V_{sc} is the volume of a single abrasive particle. Thus, the no. of AAPs (N_{lg}) present during finishing of the tapered longitudinal CBH type work part surface is found as 1,62,596.

Further, the number of AAPs involved in finishing the flat end CBH type work part surface is calculated. To calculate the no. of AAPs over the flat end CBH type work part surface, the AAPs projected area is calculated using Eq. (4.40).

Projected area of the AAP region on the flat end surface of the CBH type workpiece,

$$A_{ft} = \pi r_t^2 \tag{4.40}$$

where r_t is the radius of the MRG tool. Thus, using Eq. (4.40), the projected area of the AAP region on the flat end surface is calculated as 3.848×10^{-5} m^2. Hence, using Eq. (4.40), the number of AAPs involved in finish the flat end CBH type work part surface can be calculated using Eq. (4.41).

No. of AAPs involved in finishing the flat end surface of the CBH type workpiece,

$$N_f = \frac{C_s A_{ft} d_{sc}}{V_{sc}} \tag{4.41}$$

where C_s is the % vol. con. of abrasive particles in the MRP fluid, d_{sc} is the diameter of the abrasive particle as 15 μm and V_{sc} is the volume of a single abrasive particle in m^3. Thus, the no. of AAPs available in the MRP fluid during finishing of the flat end CBH type work part surface is calculated as 62,775.

4.2.4 Calculation of single AAP's path followed during finishing over the cylindrical blind hole (CBH) type work part surfaces

To examine the path being followed by the AAP over the internal tapered CBH type work part surfaces, Fig. 4.6 is utilized. First, the path length followed by the AAP while finishing the longitudinal rotating tapered CBH type work part surface owing to the simultaneous rotation and reciprocation MRG tool motion is considered. For calculating the path travelled by the AAP over the tapered longitudinal surface of the CBH type workpiece, the helix angle is required to be calculated. From Eq. (4.42), the helix angle (θ) can be calculated for the helical path formed by

the AAP at any point say *S* as presented in Fig. 4.6 (a) over the tapered longitudinal surface of the CBH type workpiece surface.

$$\tan\theta = \frac{v_l}{\omega_{al}} \tag{4.42}$$

$$\theta = \tan^{-1}\left\{\frac{30v_l}{\pi r(N_{wl}+N_{tl})}\right\} \tag{4.43}$$

where v_l is the reciprocation speed of the MRG tool, ω_{al} is the angular speed of AAP over the tapered longitudinal surface, sum of N_{tl} and N_{wl} is the net rotational speed of AAP on the tapered longitudinal CBH type workpiece surface, and r is the variable inner radius of the tapered CBH type workpiece surface. Thus, the net helix angle (θ') of the helical path formed over the internal tapered longitudinal CBH type workpiece surface is calculated using expression in Eq. (4.44).

$$\theta' = \tan^{-1}\left(\int_{r_w}^{r_{w1}}\left(\frac{30v_l}{\pi r(N_{wl}+N_{tl})}\right)dr\right) \tag{4.44}$$

From Eq. (4.44), the value of the net helix angle (θ') of the active abrasive particle is calculated as 2.168 radian when r_w is taken as 10.5 mm, r_{w1} as 9 mm, v_l as 16 cm/min, N_{tl} as 520 rpm and N_{wl} as 80 rpm. For calculating the length of the helical path, the time taken (T_l) to complete half cycle during finishing over the tapered longitudinal surface of the CBH type work part is calculated from Eq. (4.45). This is utilized to find path length over the tapered longitudinal CBH type work part surfaces.

$$T_l = \frac{L_w}{v_l} \tag{4.45}$$

where L_w is the taper length of the longitudinal CBH type work part surface along the reciprocating path (mm) (Fig. 4.1a). Thus, on substituting the values of Eqs. (4.44) and (4.45), the length of the helical path (L_{lg}) covered by the AAP over the tapered longitudinal surface of the CBH type workpiece can be calculated from the expression in Eq. (4.46).

$$L_{lg} = \frac{T_l v_l}{\sin\theta'} \tag{4.46}$$

So, this Eq. (4.46) is utilized to calculate the total path length travelled by a single AAP over the tapered longitudinal surface of the CBH type workpiece. After calculating the helical path length (L_{lg}) for the tapered longitudinal surface, the investigation is also performed for the path being followed by the AAPs during finishing operation for the flat end CBH type work part surface.

Further, the spiral path is produced by the AAP owing to the simultaneous motion of the MRG tool over the rotating flat end circular CBH type work part surface as espied in Figs. 4.1(b) and 4.6(b). For calculating the length of the spiral path (L_{ft}) followed by the AAP over the flat end CBH type work part surface, the spiral angle (θ_1) in Fig. 4.6(b) is calculated from Eq. (4.47).

$$\theta_1 = \tan^{-1}\left(\frac{v_f}{\omega_{al}}\right) = \tan^{-1}\left(\frac{30 v_f}{\pi r_{w1}(N_{wf}+N_{tf})}\right) \tag{4.47}$$

where v_f is the reciprocation speed of the MRG tool, ω_{af} is the angular speed of AAP over the flat end surface, sum of N_{tf} and N_{wf} is the net rotational speed of AAP on the flat end CBH type workpiece surface. The time taken (T_f) during finishing of half of the cycle completed during finishing over the flat end surface of the CBH type work part is calculated from Eq. (4.48). This is utilized to find path length over the flat end CBH type work part surfaces.

$$T_f = \frac{2\, r_{w1}}{v_f} \tag{4.48}$$

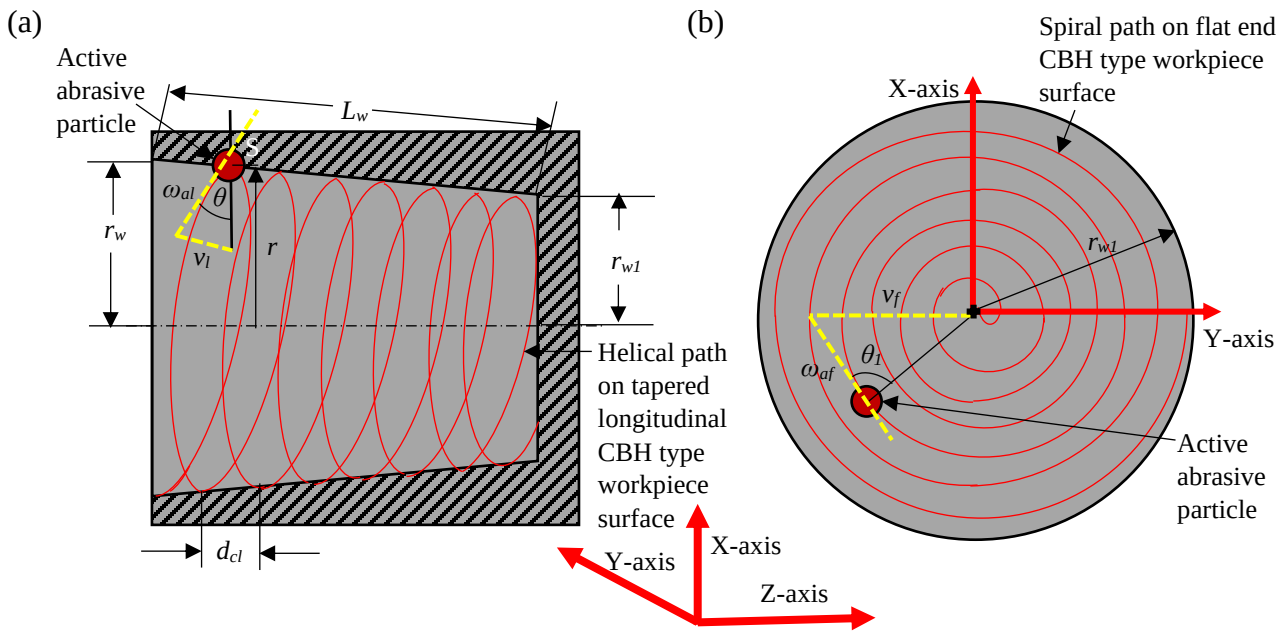

Fig. 4.6 (a) Helical path and (b) spiral path followed by the active abrasive particle (AAP) on the tapered longitudinal and flat end surfaces of the cylindrical blind hole (CBH) type workpiece.

Thus, on substituting the values of Eqs. (4.47) and (4.48), the length of the spiral path (L_{ft}) covered by AAP over the flat end surface of the CBH type workpiece can be calculated from the expression in Eq. (4.49).

$$L_{ft} = \frac{T_f\, v_f}{\sin\theta_1} \tag{4.49}$$

So, this Eq. (4.49) is utilized to calculate the spiral path length travelled by a single AAP over the flat end surface of the CBH type workpiece. As the spiral path is formed by the AAP over the flat end surface of the CBH type workpiece, so this helps to achieve finishing over the entire flat end surface of the CBH type workpiece using the present MRG tool-based process.

4.2.5 Model for volume of material removed and change in surface roughness (SR) value over the longitudinal and flat end CBH type work part surfaces with the MRG tool based process

The abrasive particles indent on the interior CBH type work part surfaces owing to the magnetic normal (MN) force as espied in Fig. 4.2. Also, the abrasive particles follow the helical path in between the radius r_w and r_{w1} over the tapered longitudinal surface of the CBH type workpiece due to simultaneous rotating and reciprocation of the MRG tool surface as espied in Figs. 4.1(a) and 4.6(a). Further, the abrasive particles follow the spiral path over the flat end surface of the rotating CBH type workpiece due to simultaneous rotation and reciprocation of the MRG tool surface as espied in Figs. 4.1(b) and 4.6(b). First, the material removal is evaluated over the tapered longitudinal CBH type work part surface, the area of the indented part of the AAP is perpendicular to the total spiral path length. The same is done for the flat end CBH type work part surface where the area of the indented AAP is multiplied with the total length of the spiral path. The indented portion of the AAP can be observed in Figs. 4.7 (a) and (b), where d_{sc} is AAP's diameter, $D_{il,if}$ are the AAP's indented diameters, and $D_{idl,idf}$ is the indented depth during finishing over the tapered longitudinal and flat end CBH type work part surfaces. Thus, the indented diameters ($D_{il,if}$) of the AAP during the finishing over the tapered longitudinal surface and flat end surface of the CBH type work part is calculated using Eqs. (4.50) and (4.51) (Singh and Singh, 2020).

$$D_{il} = \left(d_{sc}^2 - (d_{sc} - \frac{2\times10^{-6}F_{nml}}{9.8\pi H_{BHN} d_{sc}})^2\right)^{\frac{1}{2}} \tag{4.50}$$

$$D_{if} = \left(d_{sc}^2 - (d_{sc} - \frac{2\times10^{-6}F_{nmf}}{9.8\pi H_{BHN} d_{sc}})^2\right)^{\frac{1}{2}} \tag{4.51}$$

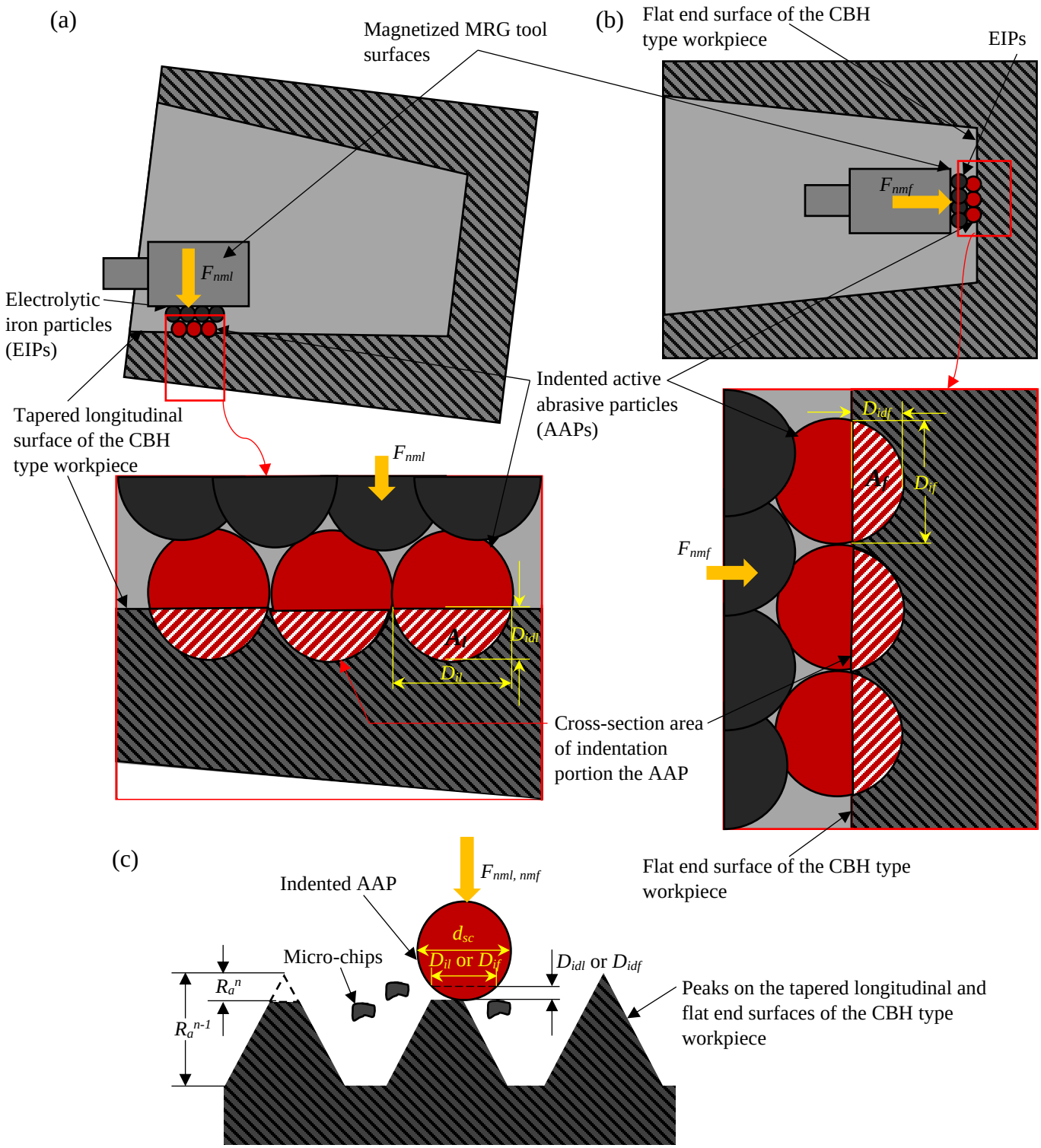

Fig. 4.7. Schematic representation of (a) an indented active abrasive particle (AAP) over the internal tapered longitudinal surface, (b) an indented AAP on the internal flat end surface of the CBH type workpiece and (c) roughness peak geometry while material cut out by the AAP while finishing with the magnetorheological grinding (MRG) process.

where H_{BHN} is the Brinell hardness number (BHN) of the CBH type work part. In the present paper, the value of BHN of the CBH type work part is 572 kgf/mm^2. The value of magnetic normal (MN) force is calculated as its average in the WG over tapered longitudinal surface (F_{nml}) and flat end surface (F_{nmf}) are calculated as 4.02 x 10^{-8} N and 7.53 x 10^{-8} N, respectively using Tables 4.2 and 4.3. Further, these values are used in Eqs. (4.50) and (4.51), the indented diameters ($D_{il,if}$) of the AAP over tapered longitudinal and flat end surfaces of the CBH type work part is calculated. The values of indented diameters are 3.46 x 10^{-8} m over the tapered longitudinal surface and 4.1 x 10^{-8} m on the flat end surface of the CBH type workpiece. The depth of indentation (D_{idl} or D_{idf}) can be calculated from Eqs. (4.52) and (4.53) and can be observed for both the tapered longitudinal and flat end CBH type work part surfaces from Fig. 4.7.

$$D_{idl} = \frac{d_{sc}}{2} - \frac{1}{2}(d_{sc}^2 - D_{il}^2)^{\frac{1}{2}} \tag{4.52}$$

$$D_{idf} = \frac{d_{sc}}{2} - \frac{1}{2}\left(d_{sc}^2 - D_{if}^2\right)^{\frac{1}{2}} \tag{4.53}$$

Using the value of D_{il} or D_{if}, the indentation depth of the abrasive particle (D_{idl} or D_{idf}) into the tapered longitudinal and flat end CBH type work part surfaces are found to be 1.996 x 10^{-11} m and 2.802 x 10^{-11} m respectively. Further, the cross-section area of the indentation portion (A_l or A_f) generated due to the indented AAP can be obtained from Eqs. (4.54) and (4.55) (Jain *et* al., 1999).

$$A_l = \frac{d_{sc}^2}{4} sin^{-1}\left\{\frac{2\times(D_{idl}(d_{sc}-D_{idl}))^{\frac{1}{2}}}{d_{sc}} - (D_{idl}(d_{sc}-D_{idl}))^{\frac{1}{2}}\left(\frac{d_{sc}}{2} - D_{idl}\right)\right\} \tag{4.54}$$

$$A_f = \frac{d_{sc}^2}{4} sin^{-1}\left\{\frac{2\times(D_{idf}(d_{sc}-D_{idf}))^{\frac{1}{2}}}{d_{sc}} - \left(D_{idf}(d_{sc}-D_{idf})\right)^{\frac{1}{2}}\left(\frac{d_{sc}}{2} - D_{idf}\right)\right\} \tag{4.55}$$

Thus, using Eqs. (4.54) and (4.55), the area of indentation for a single active abrasive particle is calculated as 1.298 x 10^{-13} m^2 for tapered longitudinal surface (A_l) and 1.538 x 10^{-13} m^2 for the flat end surface (A_f) of the CBH type work part. Further, the theoretical volume of material removal (V_{ml} and V_{mf}) for the total number of AAPs present on the tapered longitudinal surface (N_{lg}) and flat end surface (N_f) of the CBH type work part, respectively can be calculated using Eqs. (4.56) and (4.57).

$$V_{ml} = N_{lg} A_l L_{lg} \tag{4.56}$$

$$V_{mf} = N_f A_f L_{ft} \tag{4.57}$$

where N_{lg} and N_f is the number of AAPs during finishing of the tapered longitudinal and flat end CBH type work part surfaces respectively, A_l and A_f are the cross-sectional area of the indented part of the AAP (mm^2) along the tapered longitudinal and flat end CBH type work part surfaces respectively. L_{lg} and L_{ft} is the AAP's path length followed over the tapered longitudinal and flat end CBH type work part surfaces (mm), respectively. As per the continuity equation, the summation of all the grooves made due to indented abrasives on the CBH type work part surfaces are equivalent to material removed. For the calculation of volumetric material removed by the indented AAP in the n^{th} finishing time, the total AAP's indented depth ($D_{idl,idf}$) in the form of roughness is found as $D_{idl,idf} = 7(Ra_{l,f}^{n-1} - Ra_{l,f}^{n})$ (Jain *et* al., 1999), where $Ra_{l,f}^{n-1}$ is the initial surface roughness (SR) value of the longitudinal and flat end surface of the n^{th} finishing set and $Ra_{l,f}^{n}$ is the average SR value after n^{th} finishing set of the longitudinal and flat end surface of the CBH type workpiece. In each set, the finishing is performed for 20 min. Thus, the final material removal volume over the tapered longitudinal surface (V_{ml}) and flat end surface (V_{mf}) of the CBH type work part is obtained from Eqs. (4.58) and (4.59), respectively.

$$V_{ml} = L_w \pi (r_w + r_{w1}) 7 (Ra_l^{n-1} - Ra_l^{n}) \tag{4.58}$$

$$V_{mf} = \pi r_{w1}^2 7 \left(Ra_f^{n-1} - Ra_f^{n}\right) \tag{4.59}$$

where r_w is the radius towards the open end and r_{w1} is the internal CBH type work part radius towards its flat end (mm), L_w is the length covered over the longitudinal surface during the reciprocation motion of the MRG tool as shown in Fig. 4.1(a).

On equating the value of V_{ml} and V_{mf} from the Eqs. (4.56) and (4.57) with Eqs. (4.58) and (4.59), the expressions to calculate the surface roughness (SR) value from the developed theoretical model are obtained which are expressed in Eqs. (4.60) and (4.61) for n^{th} finishing set.

$$Ra_l^{n} = Ra_l^{n-1} - \frac{N_{lg} L_{lg} A_l}{7 L_w \pi (r_w + r_{w1})} \tag{4.60}$$

$$Ra_f^{n} = Ra_f^{n-1} - \frac{N_f L_{ft} A_f}{7\, \pi r_{w1}^2} \tag{4.61}$$

where A_l and A_f is the cross-sectional area of the path, N_{lg} and N_f is the total no. of AAPs, L_{lg} and L_{ft} is the path length followed by the AAP over the full length of the tapered longitudinal surface and flat end surface (diameter) of the CBH type work part respectively, L_w is the length covered over the tapered longitudinal CBH type work part surface with radius r_w to r_{w1} during MRG tool reciprocation and n is the finishing set number. Thus, from the developed theoretical SR model (Eqs. 4.60 and 4.61) for the present single electromagnetic magnetorheological grinding (MRG) tool based process, it is observed that the length of the path ($L_{lg,ft}$) followed by AAP is in relation with average SR value ($Ra_{l,f}^{n}$) in such a way that with an increase in path length, the $Ra_{l,f}^{n}$ decreases. Therefore, Eqs. (4.60) and (4.61) can be utilized to predict the surface roughness (SR) value of both interior surfaces (i.e., longitudinal and flat end surfaces) of the CBH type industrial components with the single electromagnetic MRG tool-based process.

4.3 Conclusions

Theoretical surface roughness (SR) model is developed for the present developed single electromagnetic magnetorheological grinding (MRG) tool-based process to finish the interior cylindrical blind hole (CBH) type work part surfaces. Further, to validate the theoretical SR model, the experiments were performed. After comparing the theoretical and experimental SR model results for tapered longitudinal and flat end CBH type work part surfaces using the present process, the following are the conclusions.

- Theoretically calculated values are validated using the experimentally measured values of the magnetic flux density (MFD) over the longitudinal and flat end surfaces of magnetorheological grinding tool. Thus, the model has capability to predict the magnetic flux density over the longitudinal and flat end surfaces of the magnetorheological grinding tool.
- The theoretically calculated and experimentally measured MFD values follow a reducing trend from the surfaces of the single electromagnetic MRG tool towards the CBH type work part surfaces. This confirms that the active abrasive particles (AAPs) are strongly gripped with the iron particles of the MRP fluid over the MRG tool surfaces and a magnetic normal force which helps in AAPs indentation acts over the CBH type workpiece surfaces. The asperities over the CBH type workpiece surfaces get removed by the predefined movements of these indented AAPs.

- Based on the mechanism, the magnetic normal force along with the forces produced while following the path due to the reciprocation motion of the rotating tool and the rotating workpiece helps to shear off material from the tapered longitudinal and flat end CBH type workpiece surfaces. This material removed by shearing off the asperities provide reduction in roughness value which can be predicted through the developed theoretical SR model.
- The developed theoretical SR model for the present developed single electromagnetic MRG tool-based process is found beneficial for prediction of the SR value for various CBH type precise industrial applications with internal tapered longitudinal and flat end surfaces. The fine finished CBH type industrial components with the present developed single electromagnetic MRG tool-based process may provide improved wear resistance, service life, and fine appealing moulded end products.

CHAPTER 5

EXPERIMENTATION TO EXAMINE THE PERFORMANCE OF THE DESIGNED MAGNETORHEOLOGICAL GRINDING TOOL FOR FINISHING THE INTERNAL SURFACES OF CYLINDRICAL BLIND HOLE TYPE WORKPIECES

In this chapter, the performance of the present designed magnetorheological grinding tool is experimentally analysed over the straight or tapered longitudinal and flat end surfaces of the cylindrical blind hole type workpiece. Furthermore, the optimum process parameters of the present developed magnetorheological grinding process are predicted using response surface methodology (RSM) technique (Dabnun, *et* al., 2005) and their effect on finishing performance over the internal longitudinal and flat end surfaces of the cylindrical blind hole type workpieces is studied.

5.1 Preliminary experimentation for performance analysis of the newly developed magnetorheological grinding tool

To investigate the performance of the newly designed grinding wheel type MR finishing (MRG) tool, the experimentation has been performed to finish both the surfaces of the cylindrical blind hole (CBH) type workpieces. The ferromagnetic mild steel material is used in the preliminary experimentation because of most of the industrial components like molds, femoral head tapered junctions, actuators etc. are made of a material which is ferromagnetic in nature. For the preliminary experimentation, the length and diameter of the CBH type workpieces are kept as 40 mm and 30 mm, respectively. Later, the traditional grinding process is used to achieve the initial roughness value of the CBH type workpiece. This value was measured by the Mitutoyo SJ410 surface roughness profilometer with the cut-off length of 0.25 mm. The initial average roughness values on both the surfaces of the CBH type workpieces are recorded in the range of 210 nm to 260 nm. Also, the scanning electron microscope (SEM) images were obtained and investigated for any improvement in the surface quality of the CBH type workpiece before and after finishing using the MRG tool. Further, for any improvement in the dimensional accuracy of the longitudinal surface of the CBH type workpieces, the circularity test is conducted using a coordinate measuring machine (CMM). In the present experimentation, the MR polishing (MRP) fluid is prepared considering the percentage volume concentration as 20 % of iron particles with mesh size of 500, 20 % abrasive particles (silicon carbide) with mesh size of 800, and 60 % base fluid (20 % of AP3 grease and 80 % of paraffin oil). The percentage of constituents of the MRP fluid are considered

from the literature (Bedi and Singh, 2018a). The MRP fluid is synthesized using a DC controlled mixer. This synthesized MRP fluid is utilized to finish the surfaces of the present selected ferromagnetic CBH type workpieces.

The experimental setup with the MRG tool to finish the interior surfaces of the cylindrical blind-hole (CBH) work parts is used as shown in Figs. 3.2 and 3.23 (Chapter 3). Initially, the preliminary experiments were conducted considering the MRG tool rotational speed (*T*), reciprocation speed of the tool (*R*), and the rotational speed of the CBH type workpiece (*W*) as parameters based on literature (Bedi and Singh, 2018b, Paswan and Singh, 2020). The rotational speed of the MRG tool and the CBH type workpiece governs the relative motion amid the longitudinal and across the flat end surfaces of the CBH type workpiece so that these are considered to be the important parameters. Also, the extent of the tangential shear force that is acting on the workpiece surface for shearing off the asperities through the active abrasive particles (AAPs), is governed by the MRG tool core rotational speed. The MRG tool reciprocation speed also helps the AAPs which shear off the surface asperities. Due to this, these parameters are considered to perform the design of experiments (DOE) to find the optimum parameters for the present developed MRF process utilizing the MRG tool. Thus, the response surface methodology (RSM) is used to find the optimum parameters for effectively finishing both surfaces of the CBH type workpiece using the newly designed MRG tool without and with grooves. Further in RSM, the central composite design (CCD) with five levels, and three parameters are utilized. In CCD, the levels of the parameters are selected based on the results obtained from the preliminary experiments for both the longitudinal and flat end surfaces of the CBH type workpiece. The selected levels of parameters in CCD opted for finishing the longitudinal and flat end surfaces of the CBH type workpieces with the MRG tool (grooved and without grooves) are reported in Tables 5.1 and 5.2, respectively.

Table 5.1 Process parameters and corresponding their parametric value for finishing the longitudinal surface of the CBH type workpiece using the MRG tool without and with grooves.

S. No.	Parameters	Units	Parametric range				
1.	MRG tool rotation speed ($T_{1,2}$)	RPM	200	300	400	500	600
2.	CBH type workpiece rotational speed ($W_{1,2}$)	RPM	20	50	80	110	140
3.	MRG tool reciprocation speed for longitudinal surface ($R_{1,2}$)	cm/min	6	8	10	12	14

In Table 5.1, the process parameters (T_1, W_1 and R_1) are designated for the finishing of the longitudinal surface of the CBH type workpieces using the non-grooved MRG tool, whereas process parameters (T_2, W_2 and R_2) are designated for the finishing of the longitudinal surface of the CBH type workpieces using the V-grooved MRG tool. Further, in Table 5.2, the process parameters (T_3, W_3 and R_3) are designated for the finishing of the flat end surface of the CBH type workpieces using the non-grooved MRG tool, whereas process parameters (T_4, W_4 and R_4) are designated for the finishing of the flat end surface of the CBH type workpieces using the V-grooved MRG tool.

Table 5.2 Process parameters and corresponding their parametric values for finishing the flat end surface of the CBH type workpiece using the MRG tool without and with grooves.

S. No.	Parameters	Units	Parametric range				
1.	MRG tool rotation speed ($T_{3,4}$)	RPM	300	400	500	600	700
2.	CBH type workpiece rotational speed ($W_{3,4}$)	RPM	30	60	90	120	150
3.	MRG tool reciprocation speed for flat end surface ($R_{3,4}$)	cm/min	6	8	10	12	14

Further, the rest of the parameters utilized in this MR finishing process is selected based on the literature, and their corresponding conditions for the present experimentation are mentioned in Table 5.3 (Bedi and Singh, 2018c; Singh and Singh, 2019b).

Table 5.3 The parameters and their condition for experimentations using the MRG tool with and without grooves.

Parameters	Condition
Gap between tool and workpiece surfaces	0.6 mm
Value of direct current supplied	2 A
Blind hole cylindrical workpiece	Ferromagnetic mild steel
Finishing medium	MR polishing fluid
Abrasive particles (Silicon carbide - SiC) in MRP fluid	800 mesh number
Iron particles in MRP fluid	500 mesh number

After selecting the five levels of three parameters in the CCD, the experiments are planned. Thus, a total of 80 (20 × 4) experiments are planned for the finishing of the longitudinal and flat end surfaces of the CBH type workpieces using the non-grooved and grooved MRG tool as reported in Tables 5.4 and 5.5. First, the experiments were conducted for finishing the longitudinal surface of the CBH type workpieces using the non-grooved and grooved MRG tool.

Table 5.4 Plan of experiments and their responses for the finishing of longitudinal surface of the CBH type workpiece using non-grooved MRG tool with the designated process parameters (T_1, W_1, R_1) and grooved MRG tool with the designated process parameters (T_2, W_2, R_2).

S. No.	$T_{1,2}$ (RPM)	$W_{1,2}$ (RPM)	$R_{1,2}$ (cm/ min)	Using MRG tool without grooves						Using MRG tool with grooves					
				Ra_i (nm)	Ra_{f1} (nm)	Ra_{f2} (nm)	Ra_{f3} (nm)	Avg Ra_f (nm)	$\%\Delta Ra$ (nm)	Ra_i (nm)	Ra_{f1} (nm)	Ra_{f2} (nm)	Ra_{f3} (nm)	Avg Ra_f (nm)	$\%\ \Delta Ra$ (nm)
1	500	50	12	230	200	190	190	193.33	15.94	210	160	170	140	156.67	25.40
2	300	110	8	240	210	220	200	210.00	12.50	230	170	190	180	180.00	21.74
3	400	140	10	210	160	180	170	170.00	19.05	210	160	150	140	150.00	28.57
4	400	80	10	260	190	200	190	193.33	25.64	240	150	160	160	156.67	34.72
5	400	80	10	240	180	200	170	183.33	23.61	240	150	160	180	163.33	31.94
6	400	80	10	240	180	190	160	176.67	26.39	220	130	150	150	143.33	34.85
7	400	80	14	220	160	180	170	170.00	22.73	240	170	150	180	166.67	30.56
8	600	80	10	240	170	190	190	183.33	23.61	250	160	180	160	166.67	33.33
9	400	80	10	230	160	170	190	173.33	24.64	220	140	130	160	143.33	34.85
10	200	80	10	210	170	180	180	176.67	15.87	210	160	170	140	156.67	25.40
11	400	80	10	230	180	160	190	176.67	23.19	250	170	150	190	170.00	32.00
12	300	110	12	230	200	190	170	186.67	18.84	240	190	170	160	173.33	27.78
13	400	20	10	210	180	190	200	190.00	9.52	220	170	190	180	180.00	18.18
14	500	110	8	240	170	200	200	190.00	20.83	210	150	150	140	146.67	30.16
15	300	50	12	210	160	180	150	163.33	22.22	230	170	140	160	156.67	31.88
16	400	80	10	250	190	200	170	186.67	25.33	220	120	150	160	143.33	34.85
17	500	110	12	240	190	200	180	190.00	20.83	240	170	160	170	166.67	30.56
18	400	80	6	210	180	160	180	173.33	17.46	250	190	180	180	183.33	26.67
19	300	50	8	230	190	210	180	193.33	15.94	240	180	190	170	180.00	25.00
20	500	50	8	230	190	180	190	186.67	18.84	220	150	170	150	156.67	28.79

The dimensions of the CBH samples used for the experiments over the longitudinal surface of the CBH type workpieces are 20 mm in diameter and 20 mm in length, i.e., 1257 sq. mm of the longitudinal surface area. Further, the same samples of 20 mm in diameter (i.e. 314 sq. mm of surface area) is used for finishing of the flat end surface of the CBH type workpieces with the non-grooved and grooved MRG tool. Each parametric combination of the planned experiments was conducted for 40 min over the longitudinal surface area of 1257 sq. mm and flat end surface area

of 314 sq. mm of the CBH type workpieces using the present developed experimental setup with the non-grooved and grooved MRG tool as shown in Figs. 3.2, 3.4 (d), 3.7(d) (chapter-3). During each 40 min of finishing set, the MR polishing fluid was renewed in every 20 min of finishing interval so that fresh active abrasives can be maintained during the 40 min of finishing operation.

Table 5.5 Plan of experiments and their responses for the finishing of flat end surface of the CBH type workpiece using non-grooved MRG tool with the designated process parameters (T_3, W_3, R_3) and grooved MRG tool with the designated process parameters (T_4, W_4, R_4).

S. No.	$T_{3,4}$ (RPM)	$W_{3,4}$ (RPM)	$R_{3,4}$ (cm/ min)	Using MRG tool without grooves						Using MRG tool with grooves					
				Ra_i (nm)	Ra_{f1} (nm)	Ra_{f2} (nm)	Ra_{f3} (nm)	Avg Ra_f (nm)	$\%\Delta Ra$	Ra_i (nm)	Ra_{f1} (nm)	Ra_{f2} (nm)	Ra_{f3} (nm)	Avg Ra_f (nm)	$\%\Delta Ra$
1	600	60	8	230	180	170	180	176.67	23.19	230	140	130	140	136.67	40.58
2	500	90	6	220	170	140	180	163.33	25.76	210	130	120	120	123.33	41.27
3	500	90	14	220	160	130	150	146.67	33.33	240	130	120	130	126.67	47.22
4	500	90	10	240	120	140	120	126.67	47.22	220	90	80	60	76.67	65.15
5	500	90	10	260	140	160	130	143.33	44.87	230	80	90	80	83.33	63.77
6	500	150	10	210	180	170	150	166.67	20.63	210	140	150	120	136.67	34.92
7	600	60	12	230	150	140	170	153.33	33.33	220	100	120	100	106.67	51.51
8	700	90	10	240	190	180	160	176.67	26.39	230	130	170	140	146.67	36.23
9	600	120	12	230	180	150	140	156.67	31.88	240	130	120	120	123.33	48.61
10	500	90	10	260	160	140	130	143.33	44.87	240	110	80	90	93.33	61.11
11	400	60	12	250	170	140	160	156.67	37.33	260	140	120	110	123.33	52.56
12	400	120	8	230	180	170	150	166.67	27.54	240	120	130	160	136.67	43.05
13	300	90	10	240	150	170	140	153.33	36.11	240	120	150	130	133.33	44.44
14	500	90	10	240	150	120	130	133.33	44.44	220	80	70	100	83.33	62.12
15	400	120	12	220	170	150	140	153.33	30.30	240	130	140	120	130.00	45.83
16	500	90	10	250	140	120	150	136.67	45.33	220	80	70	80	76.67	65.15
17	400	60	8	240	160	140	150	150.00	37.50	240	140	120	110	126.67	52.78
18	500	30	10	220	140	130	150	140.00	36.36	230	110	130	100	113.33	50.72
19	500	90	10	250	130	120	150	133.33	46.67	230	100	70	80	83.33	63.77
20	600	120	8	210	160	140	170	156.67	25.40	240	130	150	130	136.67	43.05

After the experiments are conducted on the initial ground surface (Ra_i) of CBH type workpieces, the roughness values (Ra_{f1}, Ra_{f2}, Ra_{f3}) were measured at three places on the finished surface of the CBH type workpieces for each parametric conditions as reported in Tables 5.4 and 5.5. The three-roughness values measured over the surface of the workpiece are not the same, so the average of these roughness values (Ra_{f1}, Ra_{f2}, Ra_{f3}) is considered the final average roughness value (R_{af}) as reported in Tables 5.4 and 5.5 respectively. Further, the response is considered in the form of percentage reduction in surface roughness as calculated from Eq. 5.1. Thus, after performing the

experimentation, the response of each experiment is obtained in the form of the percentage reduction in surface roughness (*%⊿Ra*). The *%⊿Ra* has calculated for the MRG tool without and with V-shaped grooves using Eq. (5.1).

$$\%\Delta Ra = \left[\frac{Ra_i - Ra_f}{Ra_i}\right] \times 100 \quad (5.1)$$

where *%⊿Ra* is the percentage reduction in average surface roughness, Ra_i is the initial average roughness value in nm and Ra_f is the final average roughness value in nm.

5.1.1. Results and discussion

Further, analysis of variance (ANOVA) was performed using the response *(%⊿Ra*) of the experimental data (Tables 5.4 and 5.5) for the longitudinal and flat end surfaces of the CBH type workpiece, respectively utilizing the MRG tool without and with grooves. While performing the ANOVA, the parameters with a p-value of the regression model less than 0.05 are considered significant, and the rest parameters with a p-value greater than 0.05 are considered non-significant. After neglecting the non- significant parameter, the ANOVA data is given in Tables 5.6 and 5.7 for the longitudinal and flat end surfaces of the CBH type workpieces using the MRG tool without and with grooves, respectively. The significant terms involved in the regression model while finishing the longitudinal surface of the CBH type workpieces using the MRG tool without and with grooves are T_1, W_1, R_1, T_1^2, W_1^2, R_1^2, T_1W_1, T_1R_1, T_2, W_2, R_2, T_2^2, W_2^2, R_2^2, T_2W_2, and T_2R_2 with the p-value less than 0.05 (Table 5.6). The predicted R-square values are 89.75% and 88.58% which describe the accuracy of the model developed for measuring the value of the responses on the longitudinal surface of the CBH type workpiece using the MRG tool without and with grooves respectively. After the regression analysis, the regression models are obtained for the longitudinal surface finishing of the CBH type workpieces using the MRG tool without and with grooves as expressed in Eqs. (5.2) and (5.3), respectively.

$$\%\Delta Ra_1 = -85.201 + 0.184T_1 + 0.294W_1 + 10.77R_1 - 1.523 \times 10^{-4}T_1^2 - 2.942 \times 10^{-3}W_1^2 - 0.318\,R_1^2 + 5.417 \times 10^{-4}T_1W_1 - 9.375 \times 10^{-3}T_1R_1. \quad (5.2)$$

Where $\%\,\Delta Ra_1$ is the percentage reduction in surface roughness, T_1 is the MRG tool rotational speed, W_1 is the workpiece rotational speed and R_1 is the tool reciprocation speed during finishing of the longitudinal surface of the CBH type workpiece using the MRG tool without grooves.

$$\%\Delta Ra_2 = -76.924 + 0.167\mathrm{T}_2 + 0.32\mathrm{W}_2 + 11.332\mathrm{R}_2 - 1.273 \times 10^{-4}T_2^2 - 3.081 \times 10^{-3}W_2^2 - 0.349R_2^2 + 5.417 \times 10^{-4}\mathrm{T}_2\mathrm{W}_2 - 9.375 \times 10^{-3}\mathrm{T}_2\mathrm{R}_2 \quad (5.3)$$

Where $\%\Delta Ra_2$ is the percentage reduction in surface roughness, T_2 is the MRG tool rotational speed, W_2 is the workpiece rotational speed and R_2 is the tool reciprocation speed during finishing of the longitudinal surface of the CBH type workpiece using the MRG tool with grooves.

Table 5.6. Analysis of variance (ANOVA) for percentage reduction in surface roughness over longitudinal surface of the CBH type workpiece using non-grooved MRG tool and grooved MRG tool.

Source	Using non-grooved MRG tool					Source	Using grooved MRG tool				
	Sum of square	DOF	Mean square	F value	Prob > F		Sum of square	DOF	Mean square	F value	Prob > F
Model	330.09	8	41.26	12.04	0.0002	Model	350.59	8	43.82	10.66	0.0003
T_1	22.56	1	22.56	6.58	0.0263	T_2	33.06	1	33.06	8.04	0.0162
W_1	22.56	1	22.56	6.58	0.0263	W_2	27.56	1	27.56	6.71	0.0252
R_1	27.56	1	27.56	8.04	0.0162	R_2	22.56	1	22.56	5.49	0.0390
T_1^2	58.30	1	58.30	17.01	0.0017	T_2^2	40.73	1	40.73	9.91	0.0093
W_1^2	176.26	1	176.26	51.42	< 0.0001	W_2^2	193.30	1	193.30	47.03	< 0.0001
R_1^2	40.73	1	40.73	11.88	0.0055	R_2^2	49.12	1	49.12	11.95	0.0054
T_1W_1	21.12	1	21.12	6.16	0.0304	T_2W_2	21.12	1	21.12	5.14	0.0445
T_1R_1	28.13	1	28.13	8.20	0.0154	T_2R_2	28.13	1	28.13	6.84	0.0240
Residual	37.71	11	3.43			Residual	45.21	11	4.11		
Lack of fit	28.38	6	4.73	2.53	0.1633	Lack of Fit	35.88	6	5.98	3.20	0.1111
Pure error	9.33	5	1.87			Pure Error	9.33	5	1.87		
Total	367.80	19				Total	395.80	19			

DOF is the abbreviation used for the degree of freedom.

Further, on performing the experiments over the flat end surface of the CBH type workpieces using the MRG tool without and with grooves, the predicted R-square values are 95.83% and 97.72% respectively. These describe the accuracy of the developed model for measuring the value of the responses in the form of percentage reduction in surface roughness. The significant terms involved in the regression model while finishing the flat end surface of the CBH type workpieces using the MRG tool without and with grooves are T_3, W_3, R_3, T_3^2, W_3^2, R_3^2, T_3W_3, T_3R_3, T_4, W_4, R_4, T_4^2, W_4^2, R_4^2, T_4W_4, and T_4R_4 with the p-value less than 0.05 (Table 5.7).

Thus, the regression models are obtained for the flat end surface finishing of the CBH type workpieces using the MRG tool without and with grooves as expressed in Eqs. (5.4) and (5.5), respectively.

$$\%\Delta Ra_3 = -104.159 + 0.197\mathrm{T}_3 + 0.451\mathrm{W}_3 + 17.028\mathrm{R}_3 - 3.818 \times 10^{-4}T_3^2 - 4.967 \times 10^{-3}W_3^2 - 1.0483R_3^2 + 6.667 \times 10^{-4}\mathrm{T}_3\mathrm{W}_3 + 0.01\mathrm{T}_3\mathrm{R}_3 \quad (5.4)$$

Where $\%\Delta Ra_3$ is the percentage reduction in surface roughness, T_3 is the MRG tool rotational speed, W_3 is the workpiece rotational speed and R_3 is the tool reciprocation speed during finishing of the flat end surface of the CBH type workpieces using the MRG tool without grooves.

Table 5.7 Analysis of variance (ANOVA) for percentage reduction in surface roughness over flat end surface of the CBH type workpiece using the non-grooved MRG tool and grooved MRG tool.

Source	Using non-grooved MRG tool					Source	Using grooved MRG tool				
	Sum of square	DOF	Mean square	F value	Prob > F		Sum of square	DOF	Mean square	F value	Prob > F
Model	1308.85	8	163.61	31.60	< 0.0001	Model	1843.89	8	230.49	58.81	< 0.0001
T_3	100.00	1	100.00	19.31	0.0011	T_4	49.00	1	49.00	12.50	0.0047
W_3	156.25	1	156.25	30.18	0.0002	W_4	144.00	1	144.00	36.74	< 0.0001
R_3	72.25	1	72.25	13.95	0.0033	R_4	72.25	1	72.25	18.43	0.0013
T_3^2	366.55	1	366.55	70.79	< 0.0001	T_4^2	857.78	1	857.78	218.85	< 0.0001
W_3^2	496.37	1	496.37	95.87	< 0.0001	W_4^2	717.21	1	717.21	182.99	< 0.0001
R_3^2	442.08	1	442.08	85.38	< 0.0001	R_4^2	589.21	1	589.21	150.33	< 0.0001
T_3W_3	32.00	1	32.00	6.18	0.0302	T_4W_4	24.50	1	24.50	6.25	0.0295
T_3R_3	32.00	1	32.00	6.18	0.0302	T_4R_4	32.00	1	32.00	8.16	0.0156
Residual	56.95	11	5.18			Residual	43.11	11	3.92		
Lack of fit	47.62	6	7.94	4.25	0.0668	Lack of fit	29.61	6	4.94	1.83	0.2623
Pure error	9.33	5	1.87			Pure error	13.50	5	2.70		
Total	1365.80	19				Total	1887.00	19			

DOF is the abbreviation used for the degree of freedom.

$$\%\Delta Ra_4 = -168.42 + 0.414\mathrm{T}_4 + 0.677\mathrm{W}_4 + 20.267\mathrm{R}_4 - 5.841 \times 10^{-4}T_4^2 - 5.934 \times 10^{-3}W_4^2 - 1.21R_4^2 + 5.83 \times 10^{-4}\mathrm{T}_4\mathrm{W}_4 + 1 \times 10^{-2}\mathrm{T}_4\mathrm{R}_4 \quad (5.5)$$

Where $\%\Delta Ra_4$ is the percentage reduction in surface roughness, T_4 is the MRG tool rotational speed, W_4 is the workpiece rotational speed and R_4 is the tool reciprocation speed during finishing of the flat end surface of the cylindrical blind holed (CBH) workpieces using the MRG tool with grooves. After the regression model, the effect of significant parameters on the $\%\Delta Ra$ obtained on surfaces of the CBH type workpieces are discussed and represented in the form of graphs.

The interaction effect on $\%\Delta Ra$ with respect to simultaneous variation in the tool rotational speed ($T_{1,2}$) and workpiece rotational speed ($W_{1,2}$) at constant tool reciprocation speed ($R_{1,2}$) of 10 cm/min for the longitudinal surface finishing of the CBH type workpieces using the non-grooved and grooved MRG tool as depicted in Figs. 5.1 (a) and (b), respectively. It can be seen that as the tool rotation speed ($T_{1,2}$) increases up to 460 rpm and 480 rpm simultaneously with workpiece rotation ($W_{1,2}$) up to 80 rpm, there is an increase in the trend of $\%\Delta Ra$ on the longitudinal surface finishing of the CBH type workpieces using the non-grooved and grooves MRG tool respectively. The

increase in the trend of $\%\Delta Ra$ is due to an upsurge in net relative motion on the active abrasive particles (AAPs) that acts over the longitudinal surface finishing of the CBH type workpieces. This upsurge in the net relative motion of the AAPs is due to the increase in net tangential force. Due to this, there is an improvement in surface finish as AAPs can easily shear off asperities from the longitudinal surface of the CBH type workpieces which leads to finishing and hence increasing the trend of $\%\Delta Ra$. However, after the optimum value, the net relative motion between AAPs and the longitudinal surface of the CBH type workpiece becomes so high that the interaction time between the AAPs and the asperities decreases. Due to which the AAPs cannot effectively shear off the asperities from the longitudinal surface of CBH type workpieces. Hence, there is a decrease in the trend of $\%\Delta Ra$. The same trend is followed during the finishing of the longitudinal surface of the CBH type workpieces with the grooved MRG tool. Further, the optimum parametric values for tool rotational speed (T_1) and workpiece rotational speed (W_1) during longitudinal surface finishing with the non-grooved MRG tool are found to be 460 rpm and 80 rpm respectively where the maximum value of the %age reduction in surface roughness can be observed from Fig. 5.1(a) at constant tool reciprocation speed (R_1) of 10 cm/min, whereas for the MRG tool with grooves, the optimum parametric values for the tool rotational speed (T_2) and workpiece rotational speed (W_2) are found to be 480 rpm and 80 rpm respectively as depicted in Fig. 5.1(b) at constant tool reciprocation speed (R_2) of 10 cm/min. Further, on comparing Figs. 5.1(a) and (b), Fig. 5.1(b) shows comparatively more increased in $\%\Delta Ra$ which indicates that the performance of the grooved MRG tool is higher than the non- grooved MRG tool over the longitudinal surface of the CBH type workpieces.

The simultaneous interaction effect of the tool rotation speed ($T_{1,2}$) and tool reciprocation speed ($R_{1,2}$) on $\%\ \Delta Ra$ along with constant workpiece rotational speed ($W_{1,2}$) of 80 rpm during longitudinal surface finishing of the CBH type workpieces using the MRG tool without and with grooves are presented in Figs. 5.1 (c) and (d), respectively. It can be seen that as the tool reciprocation speed increases up to 10 cm/min simultaneously with the tool rotational speed up to 460 rpm and 480 rpm, there is an increase in the trend of $\%\Delta Ra$ using the non-grooved and grooves MRG tool respectively. This increase in the trend of $\%\Delta Ra$ can be because of the increase in the tangential force and the axial force which are acting due to the tool rotational speed and tool reciprocation speed respectively. As the MRG tool rotates and reciprocates simultaneously, the rolling and sliding motion of the AAPs causes shearing off the asperities from the surface of the

CBH type workpiece. This results in an improvement in the surface finish by the abrasive particles in the MRP fluid column over the longitudinal surface of the CBH type workpiece. However, after 460 rpm and 480 rpm of tool rotational speed and 10 cm/min of tool reciprocation speed, the MRP fluid column on the cylindrical blind hole (CBH) workpiece surface is disturbed due to higher tangential force caused by the tool rotational speed.

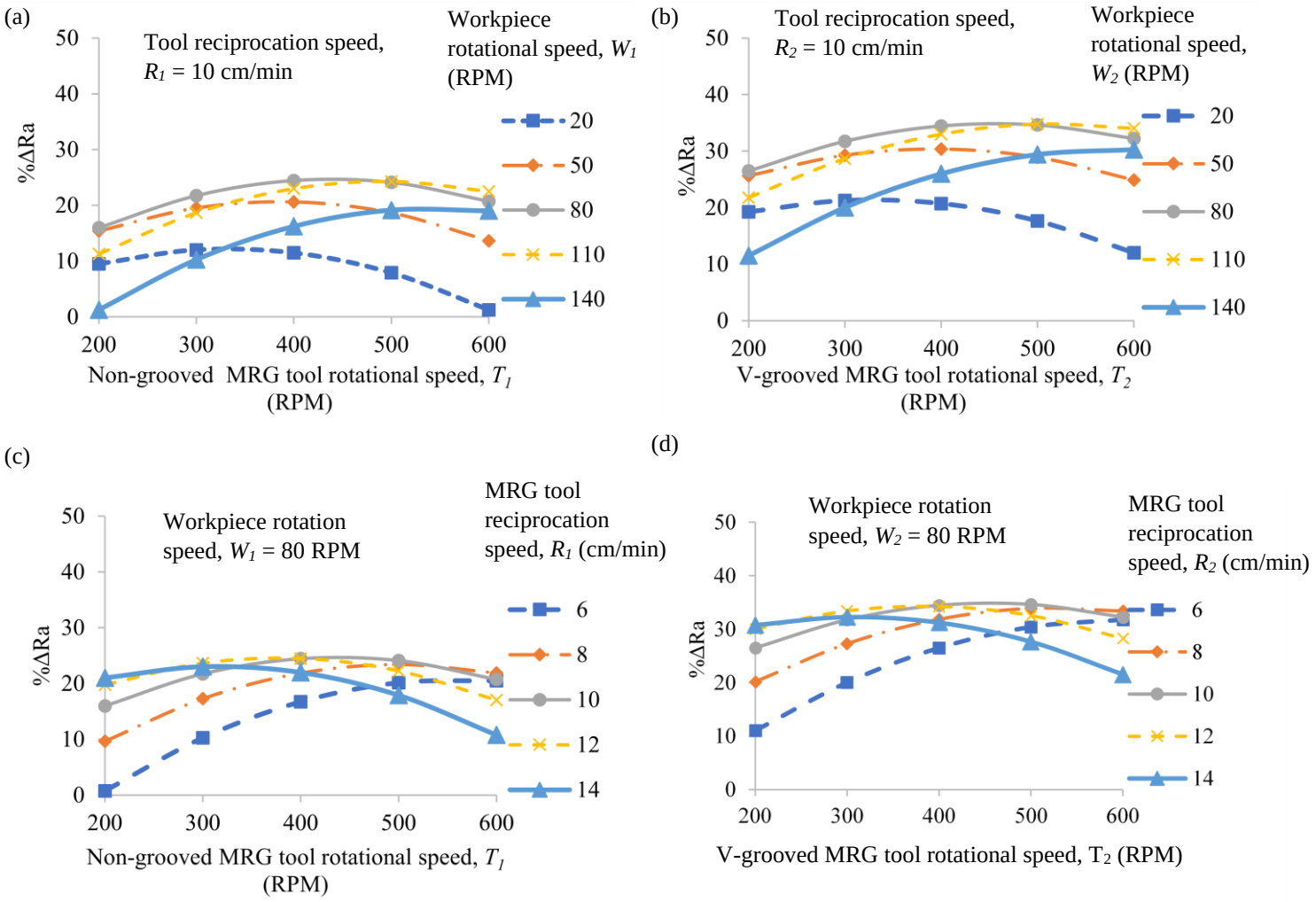

Figure 5.1. Effect of MRG tool rotational speed ($T_{1,2}$) at different workpiece rotation ($W_{1,2}$) on the percentage reduction in surface roughness ($\% \Delta Ra$) using MRG tool (a) without grooves, (b) with grooves, effect of MRG tool rotational speed ($T_{1,2}$) at different tool reciprocation speeds ($R_{1,2}$) on the percentage reduction in surface roughness using MRG tool (c) without grooves, and (d) with grooves over the longitudinal surface finishing of the cylindrical blind hole workpiece.

As the tool rotational speed increases, there is a decrease in the strength of the MRP fluid with abrasive particles. This event is followed by the increase in reciprocation speed of the tool which might counteract the magnetic strength to hold the abrasives with iron particles on the finishing surface of the MRG tool. Hence, there is a decrease in the trend of $\% \triangle Ra$. The same trend is followed for the longitudinal surface of the CBH type workpieces while finishing with the MRG tool with grooves. Thus, the optimum parametric values for the tool rotational speed (T_1) and tool reciprocation speed (R_1) for the MRG tool without grooves are found to be 460 rpm and 10 cm/min respectively where the maximum value of the %△Ra can be depicted in Fig. 5.1(c) at workpiece rotational speed (W_1) of 80 rpm. Whereas the optimum parametric values of tool rotational speed (T_2) and tool reciprocation speed (R_2) for the longitudinal surface finishing of the CBH type workpiece using the MRG tool with grooves are found as 480 rpm and 10 cm/min respectively where maximum $\%\triangle Ra$ can be observed in Fig. 5.1(d) at workpiece rotational speed (W_2) of 80 rpm. Also, on comparing Figs. 2 (c) and (d), the performance of the V-grooved MRG tool is found to be higher as it increases comparatively more $\% \triangle Ra$ (Fig. 5.1d).

Further, the interaction effect on $\%\triangle Ra$ with respect to variation in the tool rotational speed ($T_{3,4}$) and various workpiece rotational speed ($W_{3,4}$) at constant tool reciprocation speed ($R_{3,4}$) of 10 cm/min for the flat end surface finishing of the CBH type workpieces using the non-grooved and grooved MRG tool are depicted in Figs. 5.2 (a) and (b) respectively. It can be seen that as the tool rotation speed ($T_{3,4}$) increases up to 470 rpm and 490 rpm simultaneously with the workpiece rotation speed ($W_{3,4}$) up to 90 rpm, there is an increase in trend of $\% \triangle Ra$ using the non-grooved and grooved MRG tool respectively. The increase in the trend is due to an upsurge in the net tangential force acting on abrasive particles over the flat end surface of the CBH type workpiece. Due to this, the cutting shear force acting on the active abrasive particles (AAPs) helps to easily shear off the asperities from the flat end surface of the CBH type workpieces which leads to the increase in trend of % age reduction in surface roughness ($\% \triangle Ra$). However, after the optimum value, the net tangential force between the AAPs and the flat surface of the CBH type workpiece becomes so high that the iron particles loss their strength over the gripped AAPs. Due to this, the strength of the AAPs to effectively shear off the asperities from the flat end surface of CBH type workpieces are reduced. Hence, there is a decrease in the trend of $\% \triangle Ra$. The same trend is followed during the finishing of the flat end surface of the CBH type workpieces with the V-grooved MRG tool. Further, the optimum parametric values of tool rotational speed (T_3) and

workpiece rotational speed (W_3) for flat end surface finishing of the CBH type workpieces using the MRG tool without grooves are found to be 470 rpm and 90 rpm respectively where the maximum value of the *% ΔRa* can be depicted in Fig. 5.2(a) at tool reciprocation speed (R_3) of 10 cm/min. Whereas for the MRG tool with grooves, the optimum parametric values for the tool rotational speed (T_4) and workpiece rotational speed (W_4) are found to be 490 rpm and 90 rpm respectively as depicted in Fig. 5.2(b) at tool reciprocation speed (R_4) of 10 cm/min. Further, on comparing the effect on *% ΔRa* in Figs. 5.2(a) and (b), the performance of the grooved MRG tool is observed higher than the non- grooved MRG tool over the flat end surface of the CBH type workpieces.

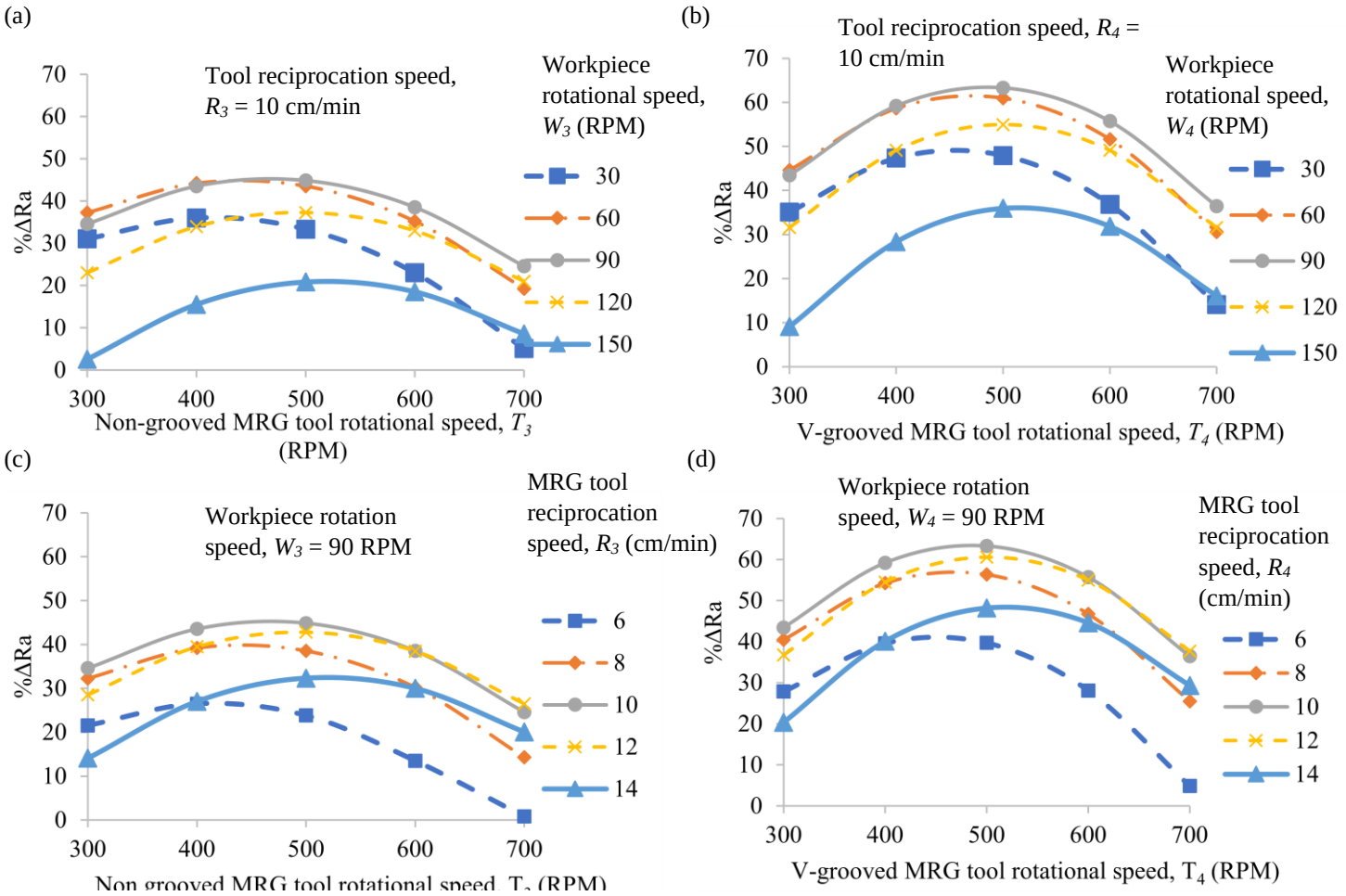

Figure 5.2. Effect of MRG tool rotational speed ($T_{3,4}$) at different workpiece rotation ($W_{3,4}$) on the percentage reduction in surface roughness (*% ΔRa*) using MRG tool (a) without grooves, (b) with grooves, effect of MRG tool rotational speed ($T_{3,4}$) at different tool reciprocation speed ($R_{3,4}$) on the percentage reduction in surface roughness using MRG tool (c) without grooves, and (d) with grooves over the flat end surface of the cylindrical blind hole workpieces.

The interaction effect of the tool reciprocation speed ($R_{3,4}$) and tool rotation speed ($T_{3,4}$) on $\% \triangle Ra$ along with constant workpiece rotational speed ($W_{3,4}$) of 90 rpm for the flat end surface finishing of the CBH type workpieces using the non-grooved and grooved MRG tool is presented in Figs. 5.2(c) and (d), respectively. It can be seen that as the tool reciprocation speed increases up to 10 cm/min simultaneously with the tool rotational speed up to 470 rpm and 490 rpm, there is an increase in the trend of $\% \triangle Ra$ using the non-grooved and grooved MRG tool due increase in the net cutting shear force. As the MRP fluid rotates and reciprocates simultaneously along with the magnetized flat end surface of the MRG tool, the AAPs causes shearing off the asperities from the flat end surface of the CBH type workpiece. This results in an improvement in the surface finish by the AAPs of the MRP fluid column. However, after 470 rpm and 490 rpm of tool rotational speed and 10 cm/min of tool reciprocation speed, the yield strength of the MRP fluid column decreases during finishing using the non-grooved and grooved MRG tool due to a more increase in net tangential force. Due to this the MRP fluid column is disturbed. Owing to this, the effectiveness of the AAPs to shear off the asperities from the flat end surface of the CBH type workpiece is reduced. Hence, there is a decrease in the trend of $\% \triangle Ra$.

The same trend is followed while finishing the flat end surface of the CBH type workpiece with the V-grooved MRG tool. Thus, the optimum values for the tool rotational speed (T_3) and tool reciprocation speed (R_3) for the MRG tool without grooves are found to be 470 rpm and 10 cm/min respectively where the maximum value of the %△Ra can be observed in Fig. 5.2 (c) at the workpiece rotational speed (W_3) of 90 rpm, whereas the optimum parametric values of tool rotational speed (T_4) and tool reciprocation speed (R_4) for the flat end surface finishing of the CBH type workpieces using the MRG tool with grooves are found as 490 rpm and 10 cm/min respectively where maximum $\% \triangle Ra$ as espied in Fig. 5.2 (d) at the workpiece rotational speed (W_4) of 90 rpm. Also, on comparing Figs. 5.2 (c) and (d), the performance of the V-grooved MRG tool is found to be higher as it increases a more $\% \triangle Ra$.

Further, using the predicted optimum process parameters, the experiments were performed thrice on the longitudinal surface of the cylindrical blind-hole (CBH) type workpieces with the non-grooved and V- grooved MRG tool to validate the results of the repeatability of the process as reported in Table 5.8. It can be observed that the percentage error (%age error) between the predicted response and the response from the experiments over the longitudinal surface of the CBH

type workpieces is in the range of 0.08 to 2.80 % for the MRG tool without grooves and 0.03 to 0.20% for the MRG tool with V- grooves using Eq. (5.6).

$$\%age\ error = \left|\frac{Experimental\ \%\Delta Ra - Predicted\ \%\Delta Ra}{Experimental\ \%\Delta Ra}\right| \quad (5.6)$$

Table 5.8 Validation of regression model for the developed process using the MRG tool without grooves and with V-grooves at optimum parameters over finishing the longitudinal surface of the cylindrical blind hole workpieces.

MRG tool surface	Time, T_t (min)	Finishing surface area (mm sq.)	$T_{1,2}$ (rpm)	$R_{1,2}$ (cm/min)	$W_{1,2}$ (rpm)	Roughness value (nm) on longitudinal surface		Exp. $\%\triangle Ra$ Eq. (5.1)	Pred. $\%\triangle Ra_{1,2}$ Eqs. (5.2,5.3)	%age error Eq. (5.6)
						Initial Ra_i	Final Ra_f			
Without any grooves	40	1257	460	10	80	230	173.33	24.64	24.62	0.08
	40	1257	460	10	80	240	180.00	25.00	24.62	1.52
	40	1257	460	10	80	250	186.67	25.33	24.62	2.80
With V-grooves	40	1257	480	10	80	230	150.00	34.78	34.79	0.03
	40	1257	480	10	80	240	156.67	34.72	34.79	0.20
	40	1257	480	10	80	220	143.33	34.85	34.79	0.17

Table 5.9 Validation of regression model for the developed process using the MRG tool without grooves and with V-grooves at optimum parameters over the flat end surface of the cylindrical blind hole workpieces.

MRG tool surface	Time T_t (min)	Finishing surface area (mm sq.)	$T_{3,4}$ (rpm)	$R_{3,4}$ (cm/min)	$W_{3,4}$ (rpm)	Roughness value (nm) on flat end surface		Exp. $\%\triangle Ra$ Eq. (5.1)	Pred. $\%\triangle Ra_{3,4}$ Eqs. (5.4,5.5)	%age error Eq. (5.6)
						Initial Ra_i	Final Ra_f			
Without any grooves	40	314	470	10	90	220	120.00	45.45	45.27	0.39
	40	314	470	10	90	250	133.33	46.67	45.27	3.00
	40	314	470	10	90	230	126.67	44.93	45.27	0.76
With V-grooves	40	314	490	10	90	230	83.33	63.77	63.43	0.53
	40	314	490	10	90	220	80.00	63.64	63.43	0.33
	40	314	490	10	90	250	90.00	64.00	63.43	0.89

Similarly, the experiments were performed thrice over the flat end surface of the CBH type workpieces utilizing the optimized parameters to validate the results of the repeatability of the process with the non-grooved and grooved MRG tool as reported in Table 5.9.

It can be observed that the %age error between the predicted response and the response from experiments over the flat end surface of the CBH type workpieces is in the range of 0.39 to 3.00% for the MRG tool without grooves and 0.33 to 0.89% for the MRG tool with V- grooves respectively. These show good agreements between the experimental results and regression models result for finishing both the longitudinal and flat end surfaces of the CBH type workpieces with the present developed MR grinding type process as reported in Tables 5.8 and 5.9, respectively. From Tables 5.8 and 5.9, it can also be observed that the experiments were performed thrice over the longitudinal and flat end surfaces of the CBH type workpieces at similar corresponding optimum parametric conditions using the MRG tool without and with grooves. The closeness of the three consecutive experimental results over the longitudinal and flat end surfaces of the CBH type workpieces show repeatability in the developed process performance.

Further, using the optimum parameters, entire longitudinal and flat end surfaces of the CBH type workpiece were finished with the MRG tool without and with grooves as reported in Table 5.10.

Table 5.10 Comparison in experimental performance of the developed process using the MRG tool without and with V-grooves at optimum parameters over the entire longitudinal surface (LS) and flat end surface (FES) of the cylindrical blind hole workpieces in terms of percentage reduction in surface roughness (%$\triangle R_a$) and finishing rate.

MRG tool surface	Surface of the CBH type workpiece	Time T_t (min)	Finishing on entire surface area (mm sq.)	$T_{1,2,3,4}$ (rpm)	$R_{1,2,3,4}$ (cm/min)	$W_{1,2,3,4}$ (rpm)	Surface roughness (nm)		Exp. $\%\triangle Ra$ Eq. (5.1)	Finishing rate (nm/min) Eq. (5.7)
							Initial Ra_i	Final Ra_f		
Without any grooves	LS	180	3770	460	10	80	260	140	46.15	0.67
	FES	60	707	470	10	90	220	100	54.54	2
With V-grooves	LS	180	3770	480	10	80	240	90	62.50	0.83
	FES	60	707	490	10	90	230	60	73.91	2.83

The obtained higher $\%\triangle Ra$ results and finishing rate validate the ability and effectiveness of the process with the V-grooved MRG tool for finishing both the surfaces of CBH type workpieces

over the non-grooved MRG tool. The finishing rate obtained after the present MR finishing (MRF) process is calculated using Eq. (5.7).

$$Finishing\ rate = \left[\frac{R_{ai}-R_{af}}{T_t}\right] \quad (5.7)$$

where T_t is the time taken in min to finish a surface till the final surface roughness value is achieved by the MRG tool.After MR finishing with the MRG tool over both the surfaces of the CBH type workpiece, the experimental results are reported in the form of surface roughness (SR) profiles, scanning electron microscopy (SEM) images, and images of the circularity.

The SR profiles of the initial ground surface and minimum surface roughness values achieved on the longitudinal and flat end surfaces of the CBH type workpiece after finishing with the initially designed grinding wheel type MR finishing (MRG) tool without any grooves are shown in Figs. 5.3 (a) – (d). The initial roughness value is measured as 260 nm on a longitudinal surface and 220 nm on the flat end surface of the CBH type workpiece which is further reduced to 140 nm and 100 nm respectively after finishing is performed using the MRG tool without any grooves (Table 5.10). These final surface roughness profiles were achieved after 180 min of finishing on the longitudinal surface area of 3770 sq. mm and 60 min on flat end surface area of 707 sq. mm of the CBH type workpiece at the corresponding optimum parameters using the MRG tool without any grooves. The improvement in surface finishing can be seen by comparing the initial and final SR profiles of the longitudinal surface (Figs. 5.3a and b) and the flat end surface (Figs. 5.3c and d) of the CBH type workpiece. Further, using Eqs. (5.1) and (5.7), the $\% \ \Delta R_a$ and finishing rate are calculated for the MRG tool without grooves. The calculated $\% \ \Delta R_a$ after MR finishing with the MRG tool without grooves on the longitudinal surface is 46.15 %, and on the flat end surface is 54.54 % as reported in Table 5.10. The finishing rate is calculated using Eq. (5.7) for the MRG tool without grooves on the longitudinal surface as 0.67 nm/min, and on the flat end surface of the CBH type workpiece is 2 nm/min. These results of $\%\Delta R_a$ and finishing rate are achieved on the longitudinal surface and flat end surface of the CBH type workpieces with the MRG tool without any grooves are reported in Table 5.10.

Further, the surface roughness (SR) profiles of the initial ground surface and the minimum surface roughness values achieved on the longitudinal and flat end surfaces of the CBH type workpiece after finishing with the improved design of MRG tool with V-shaped grooves are shown in Figs. 5.4(a) - (d). The initial and final SR profiles after 180 min of finishing on the longitudinal surface

area of 3770 sq. mm of the CBH type workpiece at the corresponding optimum parameters using the improved MRG tool with V-shaped grooves are presented in Figs. 5.4(a) and (b).

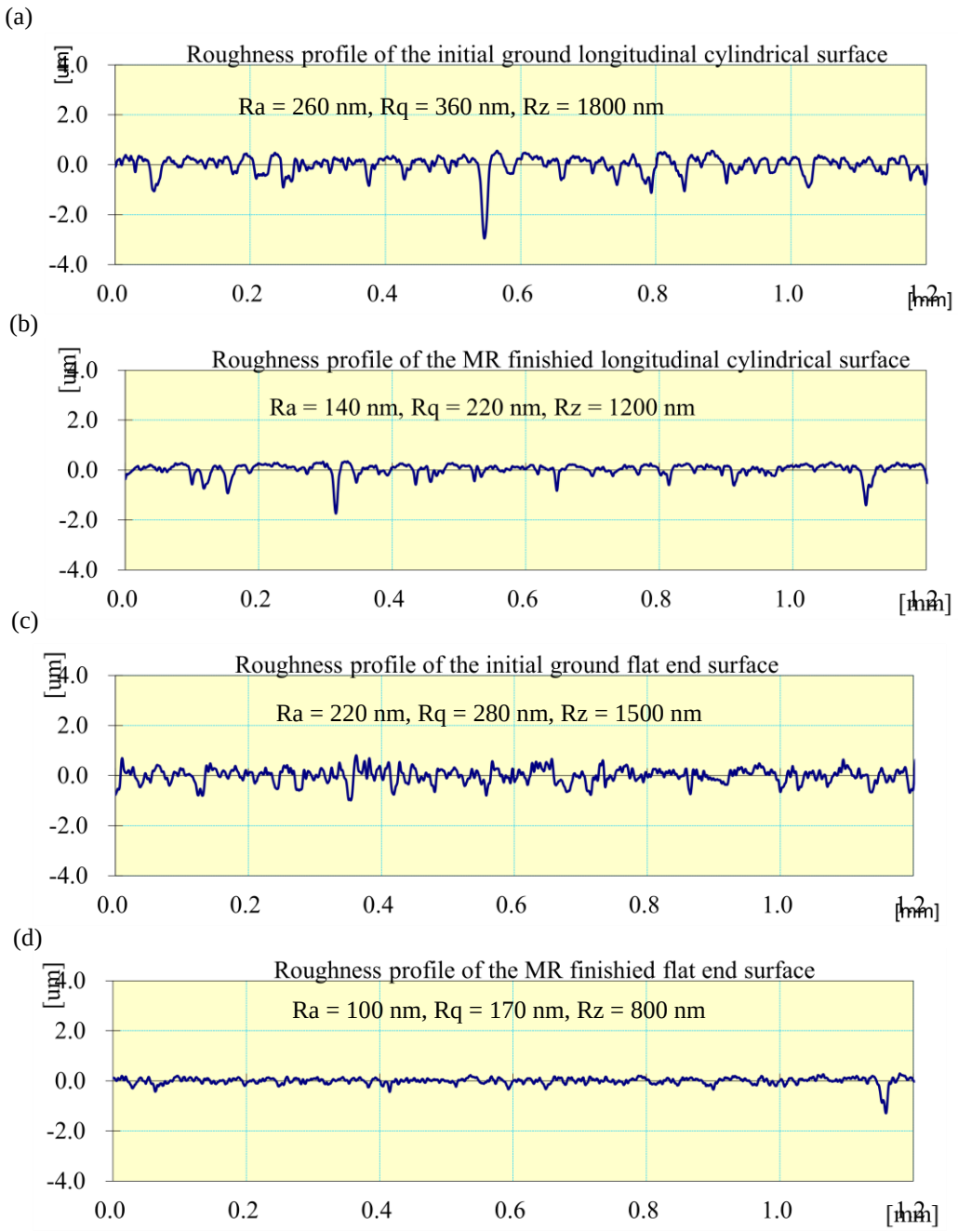

Figure 5.3. The surface roughness profiles of the cylindrical blind hole (CBH) workpiece (a) the initial longitudinal ground surface, (b) the finally MR finished longitudinal surface area of 3770 mm sq. after 180 min finishing, (c) initial flat end ground surface, and (d) finally MR finished flat end surface area of 707 mm sq. after 60 min of finishing using the MRG tool without grooves at optimized parameters.

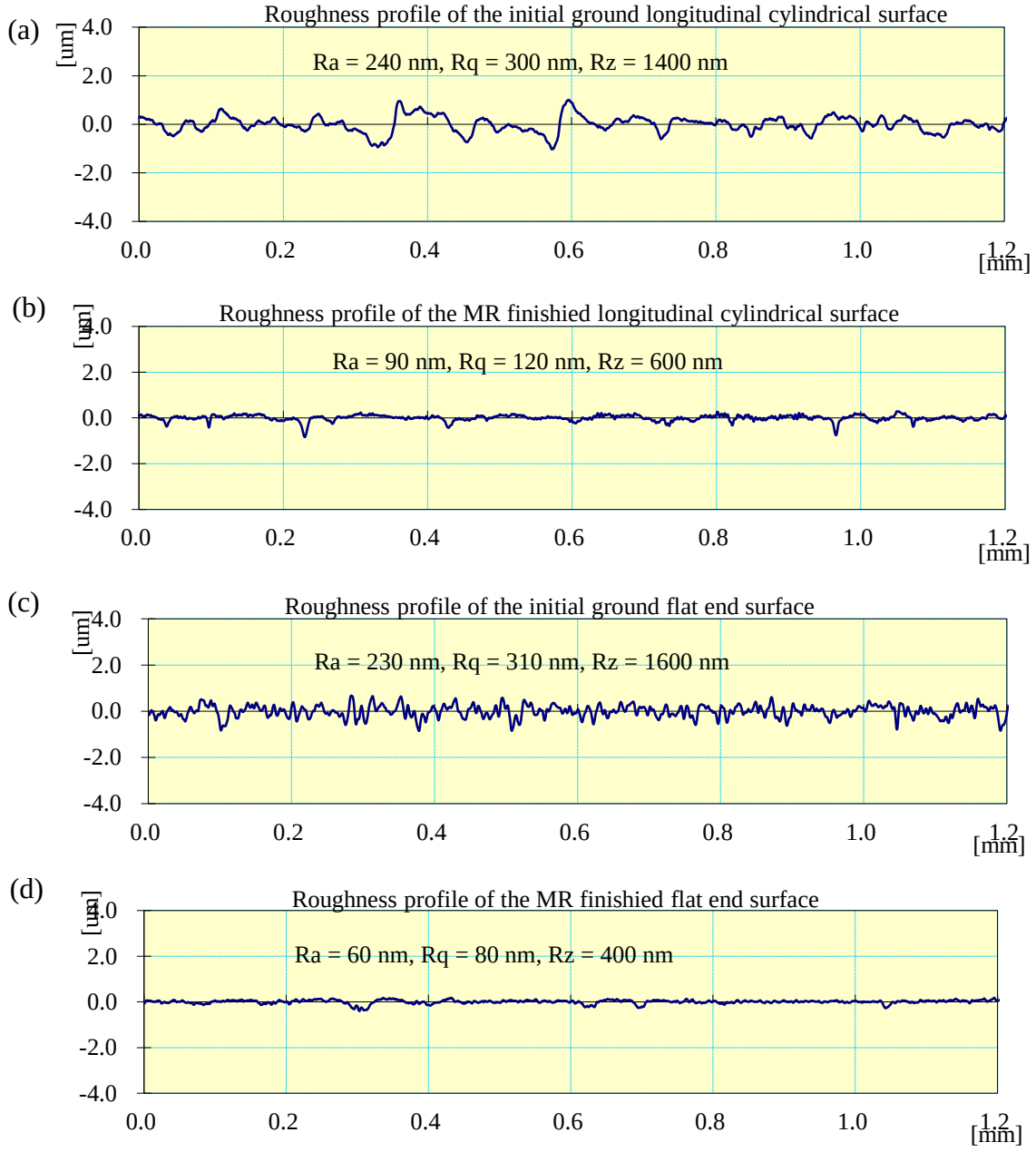

Figure 5.4. The surface roughness profiles of the cylindrical blind hole (CBH) workpiece (a) the initial longitudinal ground surface, (b) the finally MR finished longitudinal surface area of 3770 mm sq. after 180 min of finishing, (c) initial flat end ground surface, and (d) finally MR finished flat end surface area of 707 mm sq. after 60 min of finishing using the present process with V-grooved MRG tool at optimized parameters.

The initial average roughness value was measured as 240 nm after the grinding process on the longitudinal surface of the CBH type workpiece as shown in Fig. 5.4(a). The peak to valley height presents in the initial SR profile is seen due to the presence of asperities on the longitudinal surface

of the CBH type workpiece. When the finishing is performed on the longitudinal surface area of 3770 sq. mm of the CBH type workpiece using the MRG tool with V-shaped grooves, the SR value is reduced to 90 nm in 180 min as shown in Fig. 5.4(b). The peak to valley height gets reduced in the final SR profile of the longitudinal surface of the CBH type workpiece. This signifies that surface asperities get sheared off as the peaks of the final roughness profile has been reduced significantly. Thus, the surface finish of the longitudinal surface of the CBH type workpiece gets enhanced significantly while using the MRG tool with V-shaped grooves. A similar enhancement in surface finishing can be seen across the flat end surface area of 707 sq. mm of the CBH type workpiece. The initial SR profile after grinding and final SR profile after 60 min of MR finishing at the corresponding optimum parameters with the same MRG tool having V-shaped grooves over the flat end surface of the CBH type workpiece can be espied in Figs. 5.4(c) and (d). The initial SR value on the flat end surface of the CBH type workpiece is measured as 230 nm which gets reduced to 60 nm in 60 min finishing on the flat end surface area of 707 sq. mm of the CBH type workpiece using the MRG tool with V-shaped grooves. Thus, the final SR profile with Ra value of 60 nm (Fig. 5.5d) reveals that the asperities get slashed away more significantly from the flat end surface of the CBH type workpiece after finishing is performed with the MRG tool with V-shaped grooves.

These roughness asperities are slashed away due to the relative motion amid the strongly attached MRP fluid over the MRG tool with V-shaped grooves surface and the surfaces of the CBH type workpiece. The %△Ra is calculated as 62.50 % on the longitudinal surface and 73.91 % on the flat end surface of the CBH type workpiece as reported in Table 5.10. The performance in terms of finishing rate of the MRG tool with V-shaped grooves are calculated as 0.83 nm/min on the longitudinal surface and 2.83 nm/min on the flat end surface of the CBH type workpiece and reported in Table 5.10. These results of *% ⊿Ra* and finishing rate also show the effectiveness of the process while finishing is performed on the longitudinal surface and flat end surface of the CBH type workpieces using the MRG tool with V-shaped grooves. Thus, the industrial applications like the molds are used for manufacturing the plastic parts in industries which can be fine finished using the presently developed process with the V-grooves MRG tool. The MR finished surface with a reduced coefficient of friction can also help in improving the flowability of the molten plastic in the mold cavity.

The surface characteristics of the cylindrical blind holed (CBH) work parts are also analyzed before and after the MR finishing performed with the presently developed process. The surface morphology was studied using the micrograph images as obtained from the scanning electron microscopy (SEM) test. The SEM images of the initial ground and after 180 min of finishing on the longitudinal surface area of 3770 sq. mm of the CBH type workpiece at the corresponding optimized parameters with the MRG tool without any grooves are shown in Figs. 5.5(a) - (b). Similarly, the SEM images of the initial ground and after 60 min of finishing on the flat end surface area of 707 sq. mm of the CBH type workpiece using the same MRG tool without any grooves are shown in Figs. 5.5(c) - (d).

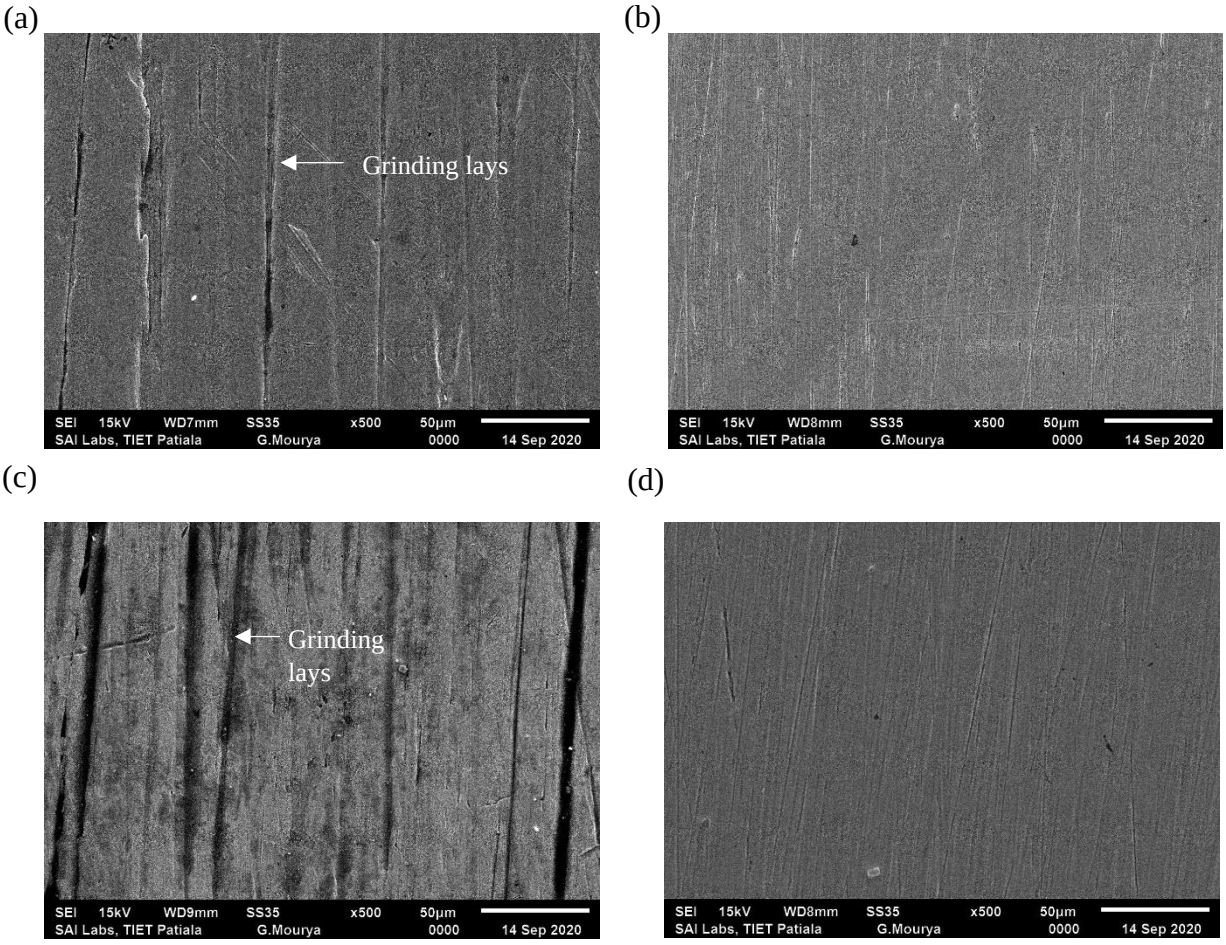

Figure 5.5 Scanning electron microscopy images at ×500 of cylindrical blind hole (CBH) workpiece (a) initial longitudinal ground surface, (b) finally MR finished longitudinal surface area of 3770 mm sq. after 180 min of finishing, (c) the initial flat end and (d) finally MR finished flat end surface area of 707 mm sq. after 60 min of finishing using the grinding wheel type MR finishing (MRG) tool without grooves at optimized parameters.

The improvement in surface texture can be seen by comparing the initial ground surface and final longitudinal surface (Figs. 5.6a and b) as well as the flat end surface (Figs. 5.5 c and d) of the CBH type workpiece. From the initial SEM image as depicted in Figs. 5.5 (a) and (c), the initial ground surface has the vertical lays texture (plowing marks) that were formed due to the traditional cylindrical grinding process throughout the longitudinal and flat end surfaces of the CBH type workpiece. These plowing marks are formed due to the plastically deformed material as the work part material piles up to the sides of the bonded abrasives on the grinding wheel to form small grooves on the finishing surfaces of the CBH type workpiece. But, after applying the present process with the initially designed MRG tool (without grooves), the deep vertical grooves present on the initial ground surfaces have been eliminated as shown in Figs. 5.5(b) and (d), respectively.

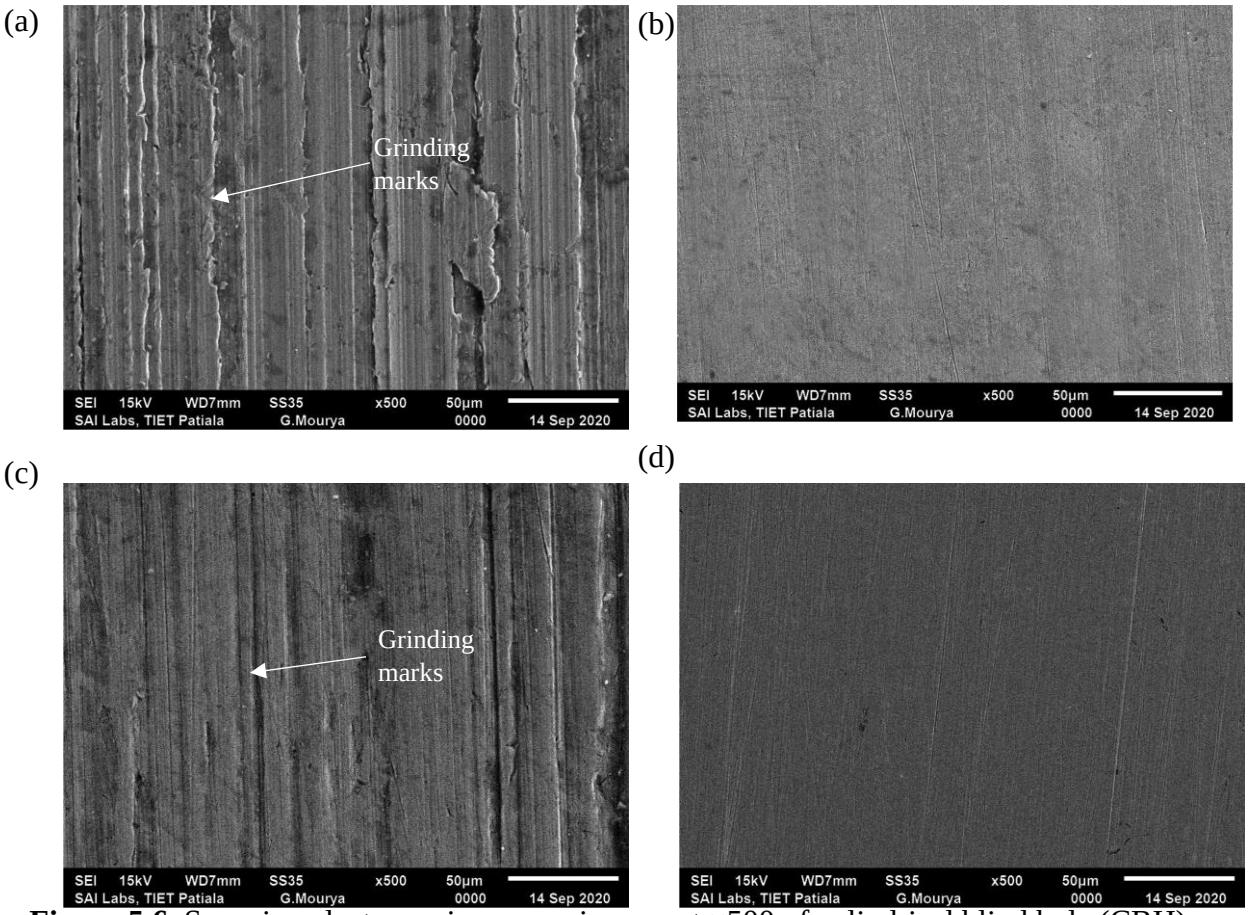

Figure 5.6. Scanning electron microscopy images at ×500 of cylindrical blind hole (CBH) workpiece (a) initial longitudinal ground surface, (b) finally MR finished longitudinal surface area of 3770 mm sq. after 180 min of finishing, (c) the initial flat end and (d) finally MR finished flat end surface area of 707 mm sq. after 60 min of finishing using the present MRG tool with V-grooves at optimized parameters.

The improved longitudinal and flat end MR finished surfaces have been achieved as compared with the initial ground surfaces of the CBH type workpiece. Further, the SEM images of the initial ground and after 180 min of finishing on the longitudinal surface area of 3770 sq. mm of the CBH type workpiece using the MRG tool with V-shaped grooves are shown in Figs. 5.6(a) - (b). Similarly, the SEM images of the initial ground and after 60 min of finishing on the flat end surface area of 707 sq. mm of the CBH type workpiece using the same MRG tool with V-shaped grooves are shown in Figs. 5.6(c) - (d). After the grinding process, grinding lays are observed as shown in Figs. 5.6(a) and (c) across the longitudinal as well as flat end surfaces of the CBH type workpiece. But, after the MR finishing using the MRG tool with V-grooves across the longitudinal and flat end surfaces of the CBH type workpiece, the grinding lays are removed and the finely finished surfaces are achieved as depicted in Figs. 5.6(b) and (d). The micrographs of the final MR finished surfaces of the CBH type workpiece using the V-grooved MRG tool shows more fine surface characteristics than using the MRG tool without any grooves (Figs. 5.5 and 5.6).Hence, on comparing the results obtained from the surface roughness profiles and SEM images, it is evident that the improved MRG tool with V-grooves can perform better finishing than the MRG tool without grooves. Thus, the overall results with respect to the reduction in roughness values and enhancement in surface morphology confirms the better efficacy of the present developed process using a MRG tool with V-shaped grooves for fine finishing the internal surfaces of the cylindrical blind hole (CBH) work parts.

The CBH type industrial components like molds need higher dimensional accuracy in the internal cylindrical surface to improve their functional performance and dimensional accuracy of the end products (Sirwal and Singh, 2018). So, the circularity test is performed on the finished longitudinal surface of the CBH type workpiece with the V-grooved MRG tool using a coordinate measuring machine (CMM). This test predicts the closeness of the actual obtained circular shape in the internal longitudinal surface of the CBH type workpiece with reference to the true circle. The closeness of the actual circular shape of the cylindrical workpiece surface to that of the true circle describes the dimensional accuracy. The initial and final images of the circularity plot after 180 min of finishing on the internal longitudinal surface area of 3770 sq. mm of the CBH type workpiece using the MRG tool with V-shaped grooves are shown in Figs. 5.7(a) - (f), respectively.

Circularity images of the initial ground longitudinal surface of cylindrical blind hole (CBH) type workpiece

Circularity images of final MR finished longitudinal surface of CBH type workpiece using MRG tool with V-grooves

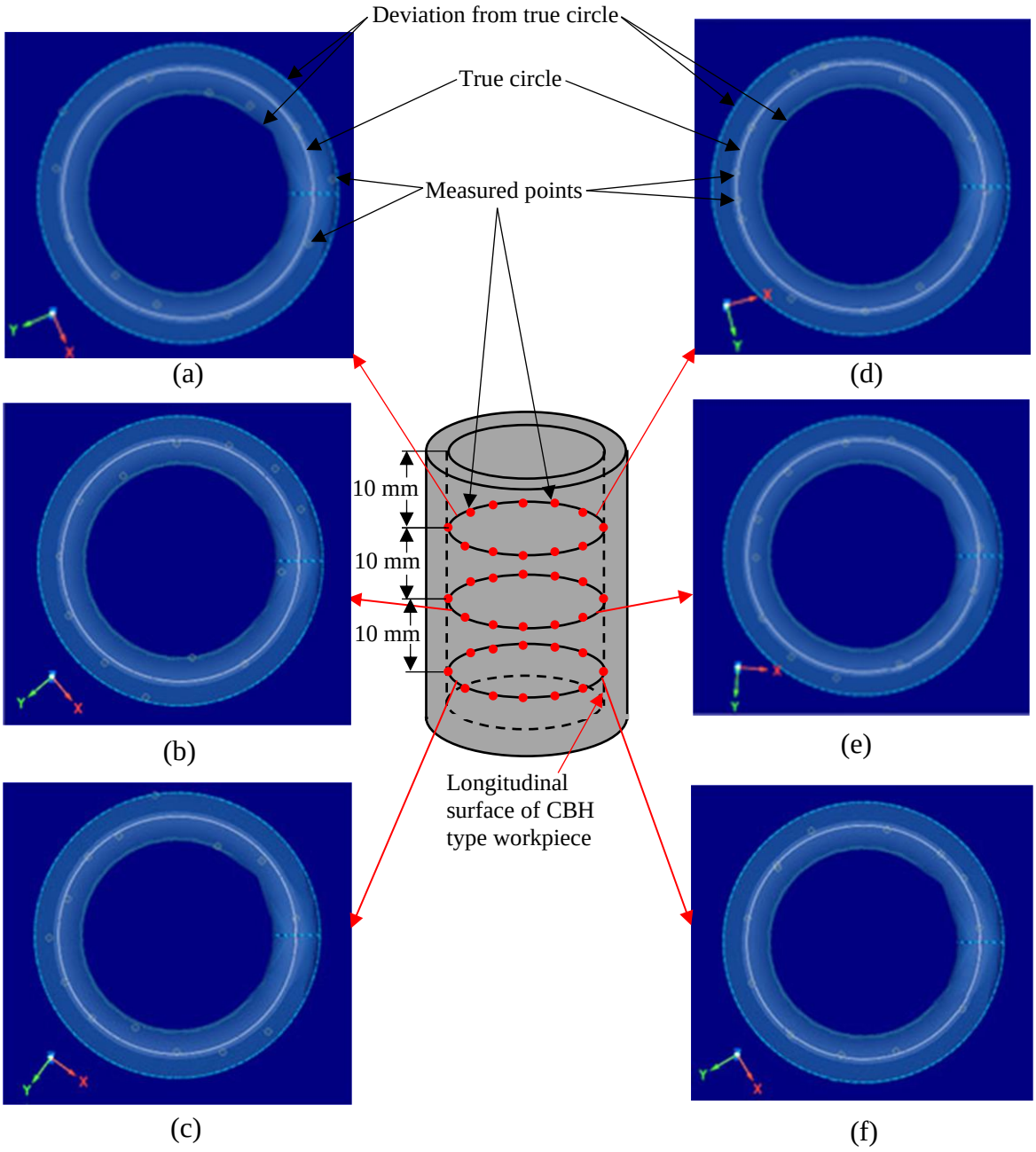

Figure 5.7. Circularity images of initial ground surface at (a) 10 mm, (b) 20 mm and (c) 30 mm, and final MR finished longitudinal surface at (d) 10 mm, (e) 20 mm and (f) 30 mm of the cylindrical blind hole workpiece after 180 min finishing using the MRG tool with V-grooves.

The circularity measurements were performed at three different levels on the internal longitudinal surface of the CBH type workpiece i.e. at 10 mm, 20 mm, and 30 mm from the top surface as shown in Fig. 5.7. On each level, there are 13 different measurements recorded using the CMM probe along the internal longitudinal surface of the CBH type workpiece. The results of circularity images of the initial ground longitudinal surface of the cylindrical blind holed (CBH) workpiece are shown in Figs. 5.7(a) - (c). It can be observed that the recorded points (measured points) have deviated from the true circle, and the value of circularity is found in the range of 0.0415 to 0.0378. But after finishing the longitudinal internal surface of the CBH type workpiece using the MRG tool with V-grooves, the recorded points (measured points) are achieved with the more closeness to the true circle as can be seen in Figs. 5.7(d) - (f), and the final value of circularity is found in the range of 0.0137 to 0.0119. Hence, the results of the circularity test in terms of improvement in dimensional accuracy confirm that the present developed process with V-grooves MRG tool can be found more useful in manufacturing industries for improving the functional performance of the cylindrical blind holed (CBH) type molds and dimensional accuracy of the end products as produced from the molds. Thus, the developed process with the V-grooved MRG tool is found to be useful in fine finishing the surfaces of the CBH type workpieces such as the housing of steering racks, actuators, valve seats, and molds. The CBH type molds are used for the manufacturing of plastic parts like drosophila vials, bottle caps, etc. The functional properties like high load-bearing capacity, service life, replication quality, ejection force, and flowability of the molten plastic in the case of molds can be improved with the help of this developed process using a V-grooved grinding wheel type MR finishing (MRG) tool. Further, this process with the V-grooved MRG tool can also be found useful in manufacturing industries where fine finishing is required on the longitudinal and flat end internal surfaces of the cylindrical blind holed work parts for improving their usability.

5.1.2 Conclusions

In the present work, the developed magnetorheological grinding (MRG) tool-based finishing process has been employed and successfully demonstrated experimentally for better performance CBH type workpieces. The following conclusions are drawn.

- The average percentage reduction in the surface roughness value and enhancement in finishing rate using the improved single newly designed MRG tool with V-grooves at

optimized parameters are found more useful for fine finishing on both the surfaces of the CBH work parts than the MRG tool without any grooves.

- The SEM images reveal enhancement in surface characteristics of the MR finished longitudinal and flat end surfaces of the CBH work parts using the MRG tool with V grooves. Also, the circularity test on the longitudinal surface reveals that the dimensional accuracy is achieved after finishing performed using the MRG tool with V grooves.
- The results obtained from the experimentation reveals that the present developed process using a single grinding wheel type MR finishing tool with V-grooves can be found more useful to fine finish the inner longitudinal and flat end surfaces of the various industrial cylindrical blind holed work parts such as molds, dies, automobile actuators, valve seats, etc.

5.2 Experimentation for validating the theoretical analysis of surface roughness in magnetorheological grinding tool-based finishing process

5.2.1 Experimentation

To validate the theoretical surface roughness model for the newly developed magnetorheological finishing process with single electromagnetic MR grinding (MRG) tool, the experiments are performed over both the tapered longitudinal and flat end CBH type work part surfaces. For performing the experimentation, EN-31 steel is used as the material for the CBH type work part. The longitudinal CBH type work part surface is given an angle of 4.4 degree, thus providing a tapered angle to this surface. To finish this tapered longitudinal CBH type work part surface, a rotating vice is utilized as depicted in Fig. 5.8. This vice is provided with an angle of 4.4 degrees based on the angle of the tapered longitudinal surface to be finished. This helps in maintaining uniform working space, thus providing uniformity in the finish over the tapered longitudinal CBH type work part surface with the presently single electromagnetic MRG tool. This angle of the vice is later set to 0 degree for the finishing of the flat end CBH type work part surface (Fig. 5.8). For performing the experimentation, the MRP fluid is prepared using 19 % by volume concentration (vol. con.) of SiC abrasive particles, 26 % by vol. con. of EIPs and 55 % of the base fluid (paraffin

as 80 % and 20 % of AP3 grease). This composition of MRP fluid is mixed with the help of a mixing chamber. Further, the initial roughness values after performing the grinding process on both the CBH type work part surface were recorded using Mitutoyo SJ410 surface tester.

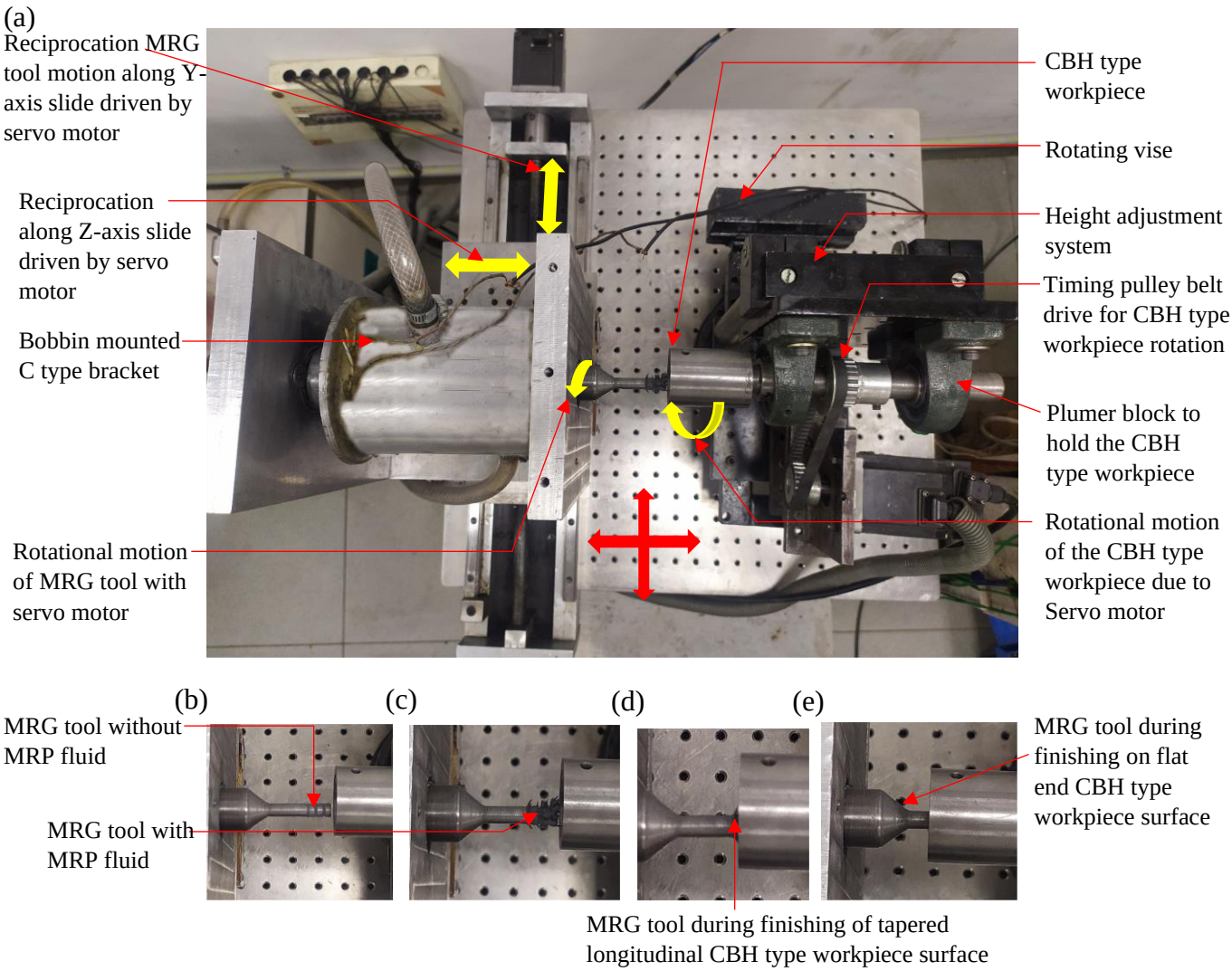

Figure 5.8. Photograph of (a) complete experimental setup of the grinding wheel type magnetorheological (MR) finishing (MRG) process, the tool (b) without MR polishing (MRP) fluid, (c) with stiff MRP fluid, and (d) during finishing of the tapered longitudinal and (e) during finishing of the flat end cylindrical blind hole (CBH) type work part surfaces.

The surface roughness (SR) values achieved after the grinding process over the tapered longitudinal surface (lateral area of 1594.43 mm^2) is 390 nm and over the flat end surface area of 254.47 mm^2 is 350 nm. The average of this initial SR value is utilized in the theoretical SR model. After the measurements of the initial roughness values, the finishing process parameters utilized

for the finishing of tapered longitudinal and flat end CBH type work part surfaces using the present single electromagnetic MRG tool are stated in Table 5.11. Considering the duration of each finishing set of 20 min, the SR value after each set of the MR finishing is measured. These surface roughness (SR) values are measured on the same points located on the CBH type work part surfaces. These experimental SR values achieved after MR finishing are compared with that obtained through the surface roughness model after each finishing time. Further, to validate the results, the surface texture is visualized using the scanning electron microscope (SEM) images before and after the MRF process utilizing the MRG tool.

Table 5.11 Finishing parameters used for finishing both the CBH type work part surfaces using the MRG tool.

Finishing parameters	**Conditions**	
	Longitudinal surface	**Flat end surface**
Rotational speed of the MRG tool (RPM)	520	1050
Reciprocation speed of the MRG tool (cm/min)	16	18
Rotational speed of the CBH type workpiece (RPM)	80	100
Direct current (A)	2.8	2.5
Working gap (mm)	1	0.9

5.2.2 Results and discussion

To analyze the effect of the novel MRG tool-based finishing process in the change of surface roughness for the CBH type workpieces theoretical analysis is performed on chapter 4. The surface roughness model was developed (Eqs. 4.60 and 4.61) for present process (chapter 4). Using equations (Eqs. 4.60 and 4.61), the theoretical values are calculated and compared with the experimental obtained surface roughness values. The surface roughness (SR) values are measured after the completion of each finishing time and are reported in Tables 5.12 and 5.13. First, the finishing is performed over the tapered longitudinal CBH type work part surface. After finishing on the tapered longitudinal surface area of 1595.43 mm^2 of the CBH type work part with the present MRG tool, the final *Ra* value was found as 90 nm. Whereas the final *Ra* from the theoretical SR model (Eq. 4.60) was found as 99 nm. The percentage error after finishing upto 100 min with

the present single electromagnetic MRG tool over the tapered longitudinal CBH type work part surface was calculated using Eq. 5.8.

$$Percentage\ error = \frac{|Experiment\ Ra\ value - Theoretical\ Ra\ value|}{Experiment\ Ra\ value} \times 100 \quad (5.8)$$

Table 5.12 Validation of theoretical surface roughness with the experimental results over the tapered longitudinal surface of the cylindrical blind hole type work part with the present single electromagnetic MRG tool-based process.

Finishing time (min)	n^{th} finishing set	Experimental measured surface roughness, *Ra* value (nm)	Theoretical calculated surface roughness, *Ra* value (nm) Eq. (4.60)	Percentage error Eq. (5.8)
0	-	390	390	-
20	1	300	331	10.33
40	2	250	273	9.20
60	3	200	215	7.50
80	4	150	157	4.67
100	5	90	99	10.00

Table 5.13 Validation of theoretical surface roughness with the experimental results over the flat end surface of the cylindrical blind hole type workpiece with present single electromagnetic MRG tool-based process.

Finishing time (min)	n^{th} finishing set	Experimental measured surface roughness, *Ra* value (nm)	Theoretical calculated surface roughness, *Ra* value (nm) Eq. (4.61)	Percentage error Eq. (5.8)
0	-	350	350	-
20	1	240	252	5.00
40	2	140	154	10.00
60	3	50	56	12.00

The percentage error between the experimental and theoretically calculated R_a value is found in the range of 4.67 % to 10.33 % after finishing is performed for 100 mins over the tapered longitudinal CBH type work part surface as reported in Table 5.12. Further, the experiment is performed for the flat end CBH type work part surface with an initial SR value of 350 nm. After 60 min of finishing time over the interior flat end circular surface of the same CBH type work part

using the same single electromagnetic MRG tool, the *Ra* value over the surface was found as 50 nm. The theoretical value of surface roughness over the flat end CBH type work part surface was calculated as 56 nm which is obtained. The percentage error amid the experimentally and theoretically calculated value is found in the range of 5.00 % to 12.00 % after 60 min (each set of 20 min) of finishing time with the same single electromagnetic MRG tool. The comparison of the values of the theoretical SR model with the experimental SR values after n^{th} finishing set is stated in Tables 5.12 and 5.13. This comparison of the theoretical and experimental results for both the longitudinal and flat end CBH type work part surfaces is showing a close agreement with each other, which validates the predicted developed model. Further, the significant reduction in SR values obtained through the theoretical SR model and experiment, it is evident that the MRF process utilizing a single electromagnetic MRG tool can be used for finishing both tapered longitudinal surface and flat end surface of the CBH type work part. The reduction in SR values is achieved by the simultaneous reciprocation motion of the rotating MRG tool and rotating CBH type work part which insisted the AAPs to follow the helical path over the interior tapered longitudinal surface and the spiral path over flat end surface of the CBH type work part.

Owing to the relative AAPs motion over the CBH type work part surfaces, the AAPs follow the helical path length which is calculated from Eq. (4.46). While following the helical path, the AAPs collide with the asperities present over the tapered longitudinal surface of the CBH type workpiece. Owing to shearing off the asperities from the tapered longitudinal surface of the CBH type workpiece, the surface roughness gets reduced. Similarly, the reduction in surface roughness can be achieved over the flat end CBH type workpiece surface while following the spiral path by the AAP's for which the length is calculated from Eq. (4.49). So, with this enhancement in the removal of material of the roughness peaks, the finishing is improved over the interior CBH type work part surfaces. This reduction in surface roughness can also be analysed by comparing the SR profiles of the initial ground and final MR finished tapered longitudinal and flat end CBH type work part surfaces as espied in Fig. 5.9(a-d).

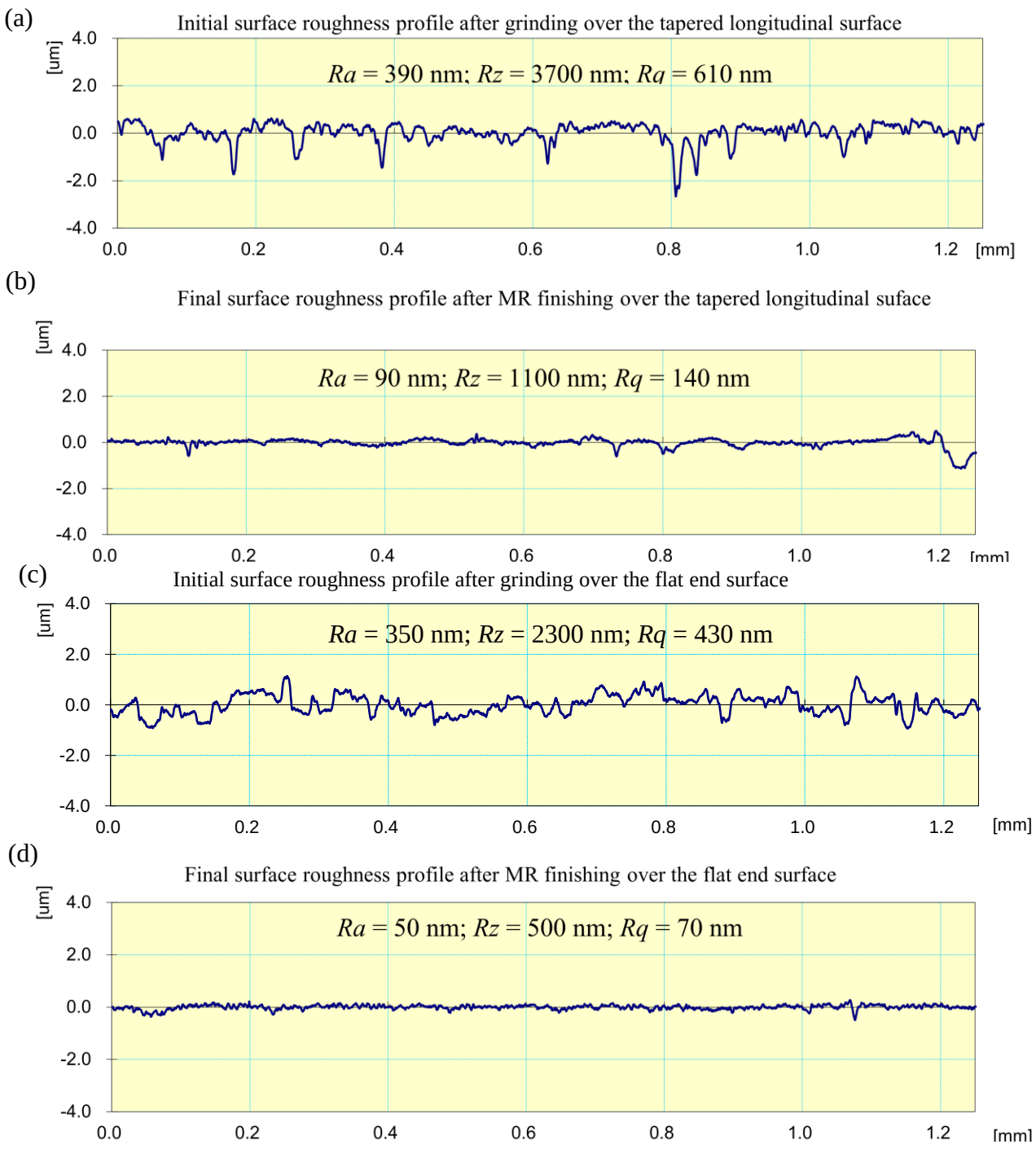

Fig. 5.9. Surface roughness profile of the (a) initial tapered longitudinal surface after grinding, (b) tapered longitudinal surface after 100 mins of magnetorheological (MR) finishing with MRG tool over the surface area of 1595.43 mm^2, (c) initial flat end surface after grinding, and (d) flat end surface after 60 mins of MR finishing with the MRG tool over the surface area of 254.47 mm^2.

Further, to visually analyse the surface texture for both the CBH type work part surfaces, the SEM was performed at a magnification of 1500X. The images obtained from SEM in Fig. 5.10 (a-d) present the initial ground and final MR finished tapered longitudinal and flat end CBH type work part surfaces.

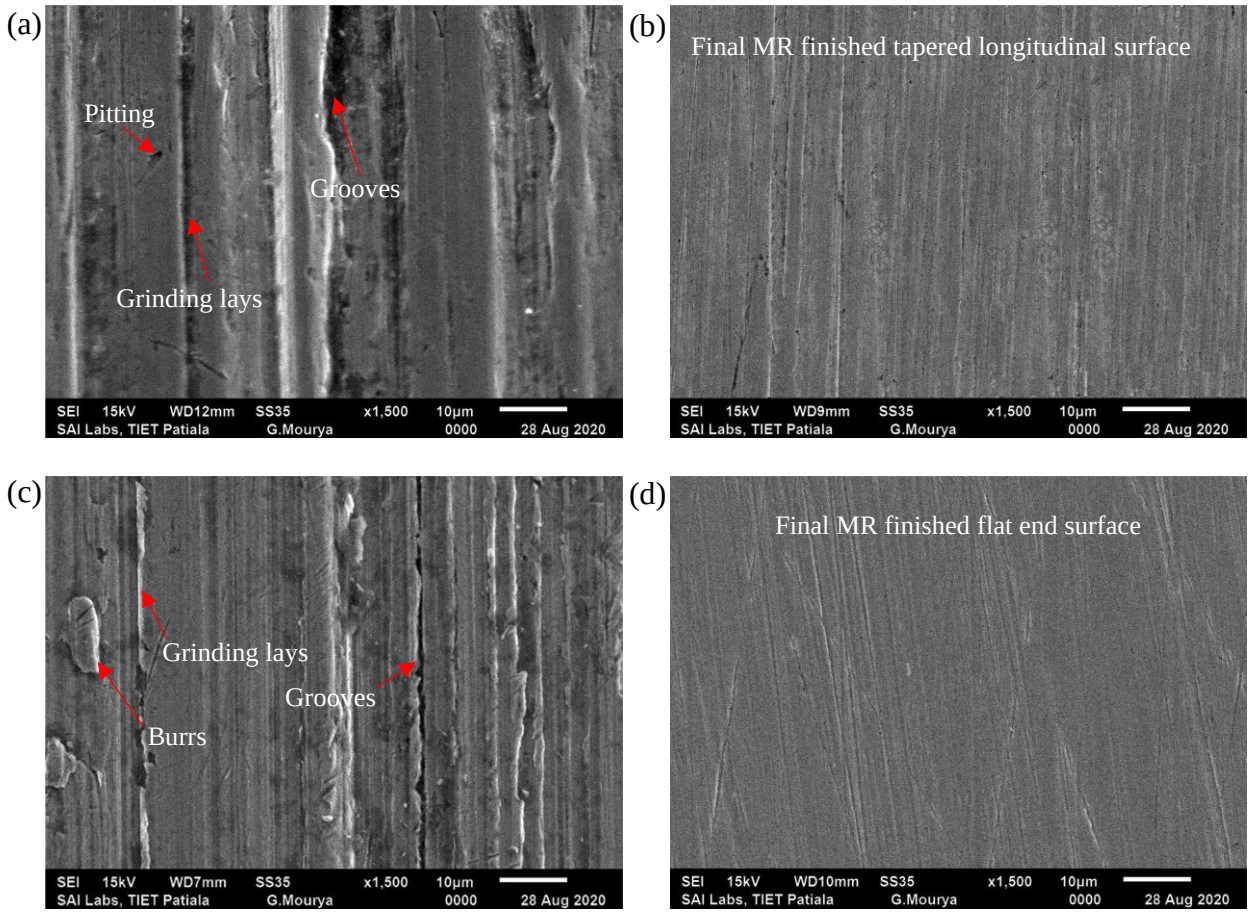

Fig. 5.10. Scanning electron microscope (SEM) images of the (a) initial longitudinal surface after grinding, (b) final magnetorheological (MR) finished longitudinal surface for 100 min over surface area of 1594.47 mm^2, (c) initial flat end surface after grinding and (d) final flat end surface after MR finishing for 60 min over the surface area of 254.47 mm^2 with the present developed process using single electromagnetic MRG tool.

It can be visualized that the initial surfaces after the grinding process on the EN-31 CBH type work part have various types of surface defects like grinding lays, grooves, burrs etc. that can be seen in Figs. 5.11 (a) and (c). After finishing the internal tapered longitudinal CBH type work part surface, the SEM image of the final MR finished surface after 100 min of finishing time can be observed

in Fig. 5.10 (b). Later, the flat end CBH type work part surface is finished with the same single electromagnetic MRG tool for 60 min of finishing time. The improvement in surface texture over the flat end CBH type work part surface can be observed by comparing Figs. 5.10 (c) and (d). The significant improvement in surface texture can be observed by comparing the initial ground (Fig. 5.10 (a) and (c)) and final MR finished (Figs. 5.10 (b) and (d)) SEM images of the tapered longitudinal and flat end surfaces of the CBH type workpiece. This is owing to the removal of surface defects like grinding lays, grooves, burrs, etc from the surfaces of the CBH type workpiece surfaces. Thus, these results of SEM images describe that the presently developed single electromagnetic MRG tool-based process can enhance the quality of the CBH type work part surfaces

Thus, after finishing with the developed MRG process, the enhancement in surface finish can be observed from the surface roughness profile obtained over the final MR finished surfaces as espied in Figs. 5.9 (b) and (d). Further, the enhancement in surface quality can also be observed from the final scanning electron microscope images over the final MR finished surfaces. Thus, from these results it is evident that the developed MRG tool is capable to remove the grinding lays from the surfaces of the CBH type workpiece. These defects over the tapered longitudinal and flat end surfaces of the CBH type workpiece are removed owing to the control over the magnetic normal force in the MRG process as compared to the hand-held grinding process. The developed theoretical SR model for the present single electromagnetic MRG tool-based process is validated experimentally. This can be confirmed by the closeness of the % error obtained for the reduction in surface roughness value as reported in Tables 5.12 and 5.13 for the tapered longitudinal and flat end surfaces of the CBH type workpiece, respectively. Thus, this developed theoretical SR model of the single electromagnetic MRG tool-based process can provide a prediction of the SR value for the tapered or straight longitudinal and flat end surfaces of the CBH type industrial components. The resistance to wear and service life may also enhance after fine finishing the industrial cylindrical blind hole type parts.

5.2.3 Conclusions

From the experimental analysis performed to confirm the theoretical study in chapter 3, and to test the feasibility of the present developed MRG based finishing process which is useful in finishing the tapered CBH type workpieces of variable diameters, following conclusions have been made.

- Reduction in SR value obtained experimentally after finishing with the single electromagnetic MRG tool from 390 nm to 90 nm in 100 min of finishing time over the tapered longitudinal and from 350 nm to 50 nm in 60 min of finishing time over flat end CBH type work part surface. This reduction in SR value obtained through experimentation reveals that the single electromagnetic MRG tool is effective to perform finishing on both the CBH type work part surfaces.
- The percentage error between the experimentally and theoretically (obtained through the theoretical SR model) calculated SR values were found in the range of 4.67 to 10.33 and 5 to 12 over the tapered longitudinal and flat end surfaces of the CBH type workpiece respectively. These values of percentage error show good agreement between the theoretical and experimentally measured SR values.
- The enhancement in scanning electron microscopy images before and after MR finishing for 100 and 60 min of finishing time over tapered longitudinal and flat end surfaces of the CBH type workpiece respectively using a single electromagnetic MRG tool is achieved. This confirmed that the present developed single electromagnetic MRG tool-based process can provide fine finishing over both internal surfaces of the CBH type workpiece.

CHAPTER 6

PARAMETRIC STUDY OF THE DEVELOPED MAGNETORHEOLOGICAL GRINDING TOOL-BASED PROCESS FOR FINE FINISHING THE VARIOUS TYPE OF TYPICAL BLIND HOLE SURFACES

In this chapter, various type of typical blind hole industrial workpieces is finely finished using the present developed magnetorheological grinding (MRG) tool-based finishing process. The typical blind hole type industrial workpieces finished in this work are tapered cylindrical mold cavities for spray bottle cap hoods and light covers, and blind hole type ball cup surface of the ball transfer units. The fine finishing of the blind hole surface of these components improves the operative performance for their respective application in industries.

6.1 Parametric investigation for fine finishing of the typical tapered mold cavity for spray bottle cap hoods using the newly developed magnetorheological grinding (MRG) tool-based process

In the manufacturing industries, most of the mass-produced discrete parts need moulds. These moulds are used for the production processes such as forging, casting, and injection moulding of plastic end products (Altan *et* al., 2001). Further, due to the competitive scenarios of the market, maintaining higher quality, dimensional accuracy and the low cost of the end product is desired. Thus, the permanent moulds present a very crucial aspect of the entire production chain. The permanent moulds find their usefulness in the manufacturing of plastic parts like bottle caps, containers, etc. (Maan and Singh, 2018). The surface finishing of the injection moulds directly affects the surface appearance of the end product (Shiou and Chen, 2003). The reduction in microcracks, residual stresses, and friction can lead to higher performance and longer operating life of the mould cavity (Mennig and Stoeckhert, 2013). Also, reduced friction between the surfaces of the cylindrical blind hole (CBH) type mould cavity and plastic melt may cause easy ejection of plastic parts from it. To achieve these requirements, it is necessary to fine-finish the surfaces of the mould cavities (Wang *et* al., 2015). The hardness of the material used for manufacturing the permanent moulds is higher which makes the finishing process a tedious task. Also, the processes used to finish such parts need very highly skilled operators (Martínez-Mateo, 2011). To attain finely finished surfaces of the plastic parts, the surface roughness of the mould must be in the nanometer range (Schulz, 1995). But yet traditional finishing process being used

for the permanent mould finishing is hand-held grinders which may cause some defects such as heat-affected zones (HAZ), microstructural changes and microcracks, etc. (Sirwal *et* al., 2020). Also, this process has hard bonded abrasives that are used for the finishing of the mould surfaces. Owing to this, the process cannot fulfill the need for fine finishing the surfaces of the mould cavity with controlled finishing forces (Jain, 2008). Therefore, to deal with limitations involved in traditional process while finishing the CBH type mould cavity, the present developed magnetorheological grinding (MRG) tool-based finishing process is utilized.

In the present work, the MRG tool-based process is utilized for fine finishing of the internal tapered longitudinal as well as flat end surfaces of the CBH type mould cavity. The fine finishing of the tapered longitudinal surface of the CBH type mould cavity is a challenging task as compared to a straight surface in relation to maintaining a constant working gap. This constant working gap helps to provide uniform finishing over the entire CBH type mould surface. In order to fulfill this requirement, the present experimental setup can help in fine finishing the internal tapered longitudinal CBH type workpiece surface. The typical CBH type mould cavity used in the present work is made up of EN-31 material which is utilized for the manufacturing of the spray bottle cap hoods. Fine finishing of such moulds may reduce intermixing of two or more-coloured plastic melt and also there is improvement in the aesthetic appearance of the final end product (Grover and Singh, 2017c).

Further, the response surface methodology technique is used to predict the percentage concentration of the abrasives and electrolytic iron particles (EIPs) in the MRP fluid for fine finishing both the surfaces of the EN-31 CBH type mould cavity. Also, the same technique is used for finding the optimum parametric conditions required for fine finishing of the tapered longitudinal and flat end surfaces of the CBH type mould cavity. After finding the optimum parametric conditions for fine finishing on both the surfaces of the CBH type mould cavity, these are experimentally validated. Further, the surface roughness profile and surface characteristics are analyzed for any improvement in surfaces of the CBH type mould cavity. Also, to check for any improvement in dimensional accuracy of the CBH type mould cavity, the circularity test is conducted. Thus, the present process may help in enhancing the mould life and the surface quality of the end products which produces from the mould cavities.

6.1.1 Materials and methods

6.1.1.1 Selection of materials and workpiece preparations

Injection moulding is one of the important processes for manufacturing of the plastic products. These moulds can be used for the manufacturing of plastic parts like bottle caps, containers, vials etc (Maan *et* al., 2017). According to the Society of the plastic industries, the permanent mould produces around 100,000 products in its span after surface finishing (Martínez-Mateo, 2011; Shiou and Chen, 2003). The material for the permanent moulds that are used in manufacturing industries is very hard and tough. Because of these properties of the permanent mould material, the working life of the mould becomes higher as there occurs high resistance to wear. Thus, the materials used for the manufacturing of mould is EN-31 and P20 (Shiou and Chen, 2003). So, the selection of material for experimentation in the present work is based on the final mould cavity which is made up of EN-31 material. The chemical composition of EN-31 steel is obtained using optical emission spectroscope (Foundry master) and it is reported in Table 6.1.

Table 6.1 Chemical composition of EN-31 material.

Fe	C	Si	Mn	P	S	Cr	Mo	Ni	Al	Co
96.7	0.977	0.284	0.433	0.0523	0.0242	1.37	0.0168	0.0222	0.0032	0.0085
Cu	Nb	Ti	V	W	Pb	Sn	B	Ca	Zr	As
0.0398	0.0049	0.0145	0.0020	0.015	0.025	0.004	0.0019	0.0001	0.002	0.0159

In the present work, the EN-31 mould cavity is fine finished using the presently developed MRG tool. The open-end diameter of mould cavity is kept as 0.021 m, whereas the diameter towards the flat end surface of the cylindrical blind hole (CBH) type mould cavity is kept as 0.018 m as shown in Fig. 6.1. The depth of this tapered mould cavity is 0.026 m. In the schematic diagram of the mould cavity, a taper angle of 4.4 degree can be observed in Fig. 6.1. Further, for the design of experiments, the dimensions of the fabricated samples for the tapered longitudinal and flat end surfaces of the CBH type mould cavity is the same. These samples after machining are heat-treated to gain hardness. The initial Vickers hardness of this steel is measured in the range of 287 to 334 HV. High hardness in the range of 589 to 649 HV is achieved after the tempering process and measured using the micro-hardness instrument (Mitutoyo HM210). The EN-31 steel after hardening can be subjected to severe abrasion (wear resistant) and high surface loading (Guo and

Liu, 2002). After hardening, these samples are finished to the initial surface roughness value with the help of the grinding process. Later, the initial surface roughness value is measured over the tapered longitudinal and flat end surfaces of the CBH type workpieces using the Mitutoyo SJ 400 surface roughness measuring instrument with cut-off length as 0.25 mm. Thus, the measured initial surface roughness values over the tapered longitudinal surface of the samples are achieved in the range of 340 to 410 nm and 300 to 360 nm over the flat end surface of the CBH type mould cavity.

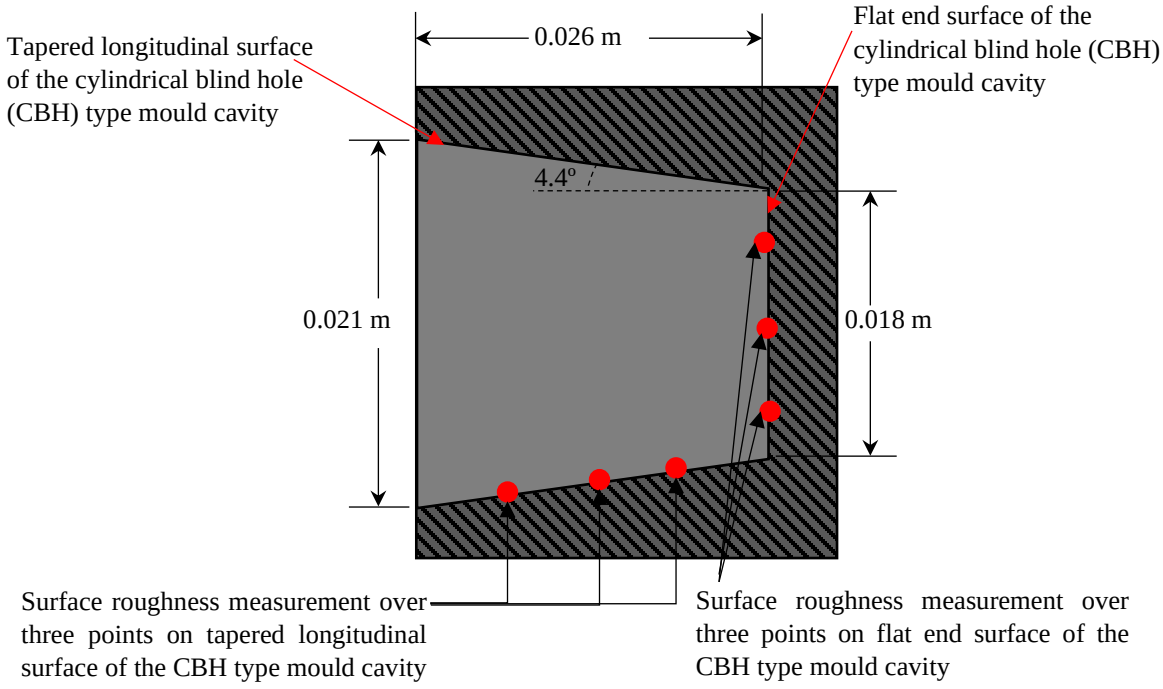

Figure 6.1. Dimensions of the cylindrical blind hole (CBH) type mould cavity for finishing with the magnetorheological grinding (MRG) process and surface roughness measurement on their surfaces.

6.1.2 Experimentation

The experimental setup for the MRG tool-based finishing process is used for the finishing of internal tapered longitudinal and flat end surfaces of the cylindrical blind hole (CBH) type mould cavity is presented in Fig. 6.2 (a). This is little modified form of the setup for finishing the tapered CBH type mold cavities than the reported in chapter-3. The Z-axis slide used in the experimental setup is driven by a servo motor (S_1) for providing the reciprocation motion to the MRG tool during fine finishing of the tapered longitudinal surface of the CBH type mould cavity. Further, the Y-

axis slide is driven by a servo motor (S_2) which is used to provide reciprocation motion to the MRG tool during finishing of the flat end surface of the CBH type mould cavity. The MRG tool core is provided with rotational motion through the timing pulley belt drive driven by the servo motor (S_3).

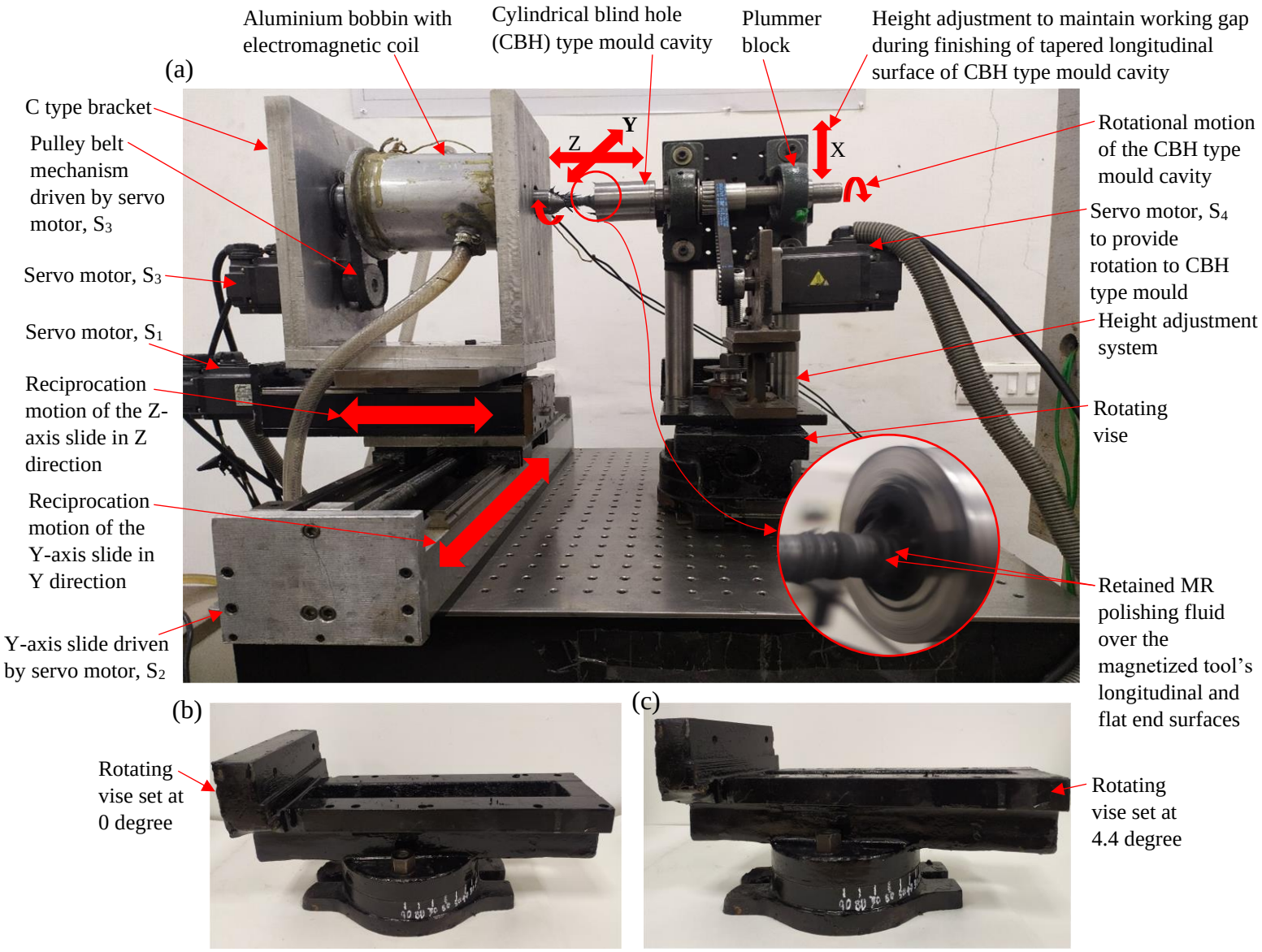

Fig. 6.2 Photograph of the (a) experimental setup during finishing with the magnetorheological grinding (MRG) process over the internal tapered longitudinal and flat end surfaces of the CBH workpiece, (b) vise fixed at 0 degree for finishing the flat end surface and (c) vise fixed at 4.4 degree of rotation for the MR finishing over tapered longitudinal surface of the CBH type mould cavity.

Further, for finishing the tapered longitudinal surface of the CBH type mould cavity, a rotating vise is used as shown in Figs. 6.2 and 6.3. This rotating vise is marked with degrees on its base as shown in Figs. 6.2 (b-c). Thus, this rotating vise helps in aligning (uniform working gap) the tapered longitudinal surface of the CBH type mould cavity parallel with the longitudinal surface of the MRG tool as shown in Fig. 6.3(a).

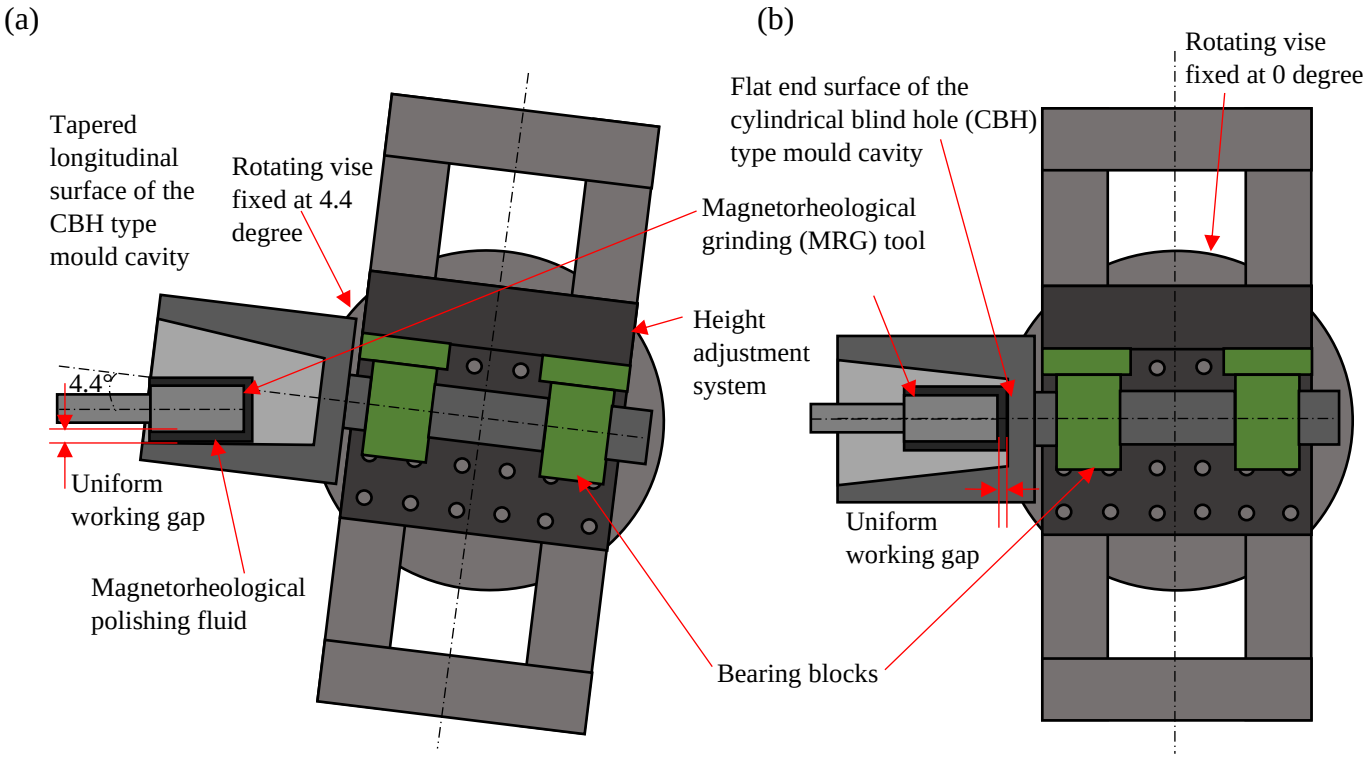

Fig. 6.3 Schematic diagram of the experimental setup of the magnetorheological grinding process during finishing of the (a) tapered longitudinal surface, and (b) internal flat end surface of the CBH type mould cavity.

If the tapered longitudinal surface of the CBH type mould cavity is not aligned with the longitudinal surface of the MRG tool, the magnetic flux density over the length of the finishing tool surface cannot be found uniform due to the non-uniform working gap with the ferromagnetic work part surface. Thus, this may lead to uneven finishing over the entire tapered longitudinal surface of the CBH type mould cavity. So, the vice makes it possible to achieve fine and uniform finishing over the tapered longitudinal surface of the CBH type mould cavities.

6.1.3 Design of experiments for selecting the concentration of the EIPs and abrasive particles in MRP fluid

The composition of the MRP fluid plays a key role in the MR finishing process. The ability of the MR finishing processes is determined by the rheological properties of MRP fluid. When the MRP fluid is applied over the finishing surface of the magnetized tool, dipoles are created. The electrolytic iron particles (EIPs) form chain structures by dipole interaction under the influence of applied magnetics flux density (MFD) (Jain, 2009). These EIP chain structures strongly grip the abrasive particles that perform finishing. The yield strength of the EIP chain structures depends on the strength of the MFD produced due to the induced current in the electromagnetic coil (Yan *et* al., 2007). Thus, the MRP fluid is optimized for finishing the EN-31 mould cavity workpiece using the response surface methodology (RSM) technique where central composite design (CCD) has been utilized. This technique is based on statistics and mathematics which helps in analysis and to develop the mathematical model (Hazir and Ozcan, 2019; Paswan and Singh, 2021). To perform the RSM, the central composite design (CCD) method with 2 parameters and 5 levels were opted to optimize the percentage volume concentration (PVC) of abrasive particles and electrolytic iron particles (EIPs) in MRP fluid for finishing the flat end CBH type mould cavity workpiece surface made up of EN-31 material. The range of PVC for abrasive particles (SiC-mesh size 800) and electrolytic iron particles (EIP- mesh size as 500) are selected based on the literature review (Pandey *et* al., 2013; Singh *et* al., 2012). The percentage contribution of abrasive particles (C) is in the range of 15 to 25 % whereas that of the EIPs (*E*) is selected in the range of 20 to 30% as reported in Table 6.2.

Table 6.2 Percentage concentration of electrolytic iron particles, abrasive particles and their range for finishing of the EN-31 cylindrical blind hole type mold cavity.

Components of magnetorheological polishing fluid		Ranges				
		-2	-1	0	1	2
Percentage concentration of electrolytic iron particles	*E*	20	22.5	25	27.5	30
Percentage concentration of abrasive particles	*C*	15	17.5	20	22.5	25

The rest is the base fluid (paraffin and AP3 grease) which can be calculated for constituting 100% of the MRP fluid. Thirteen experiments were performed over the EN-31 material used for the CBH

type mould cavity as reported in Table 6.3. The experiments are performed using the experimental setup as shown in Fig. 6.2. Experiments were performed for 40 min with the tool rotational speed of 800 rpm, workpiece rotational speed of 90 rpm, tool reciprocation speed of 10 cm/min. The current to the electromagnet was kept as 2A and the working gap of 0.9 mm.

The maximum percentage reduction in surface roughness (SR) value (*%ΔRa*) for the percentage contribution of abrasive particles and EIPs in the fluid during finishing of the interior tapered longitudinal and flat end CBH type sample surfaces was used as a response and calculated from Eq. 6.1.

$$\%\Delta Ra_{c,l,f} = \frac{(Ra_i - Ra_{c,l,f})}{Ra_i} \times 100 \quad (6.1)$$

where $\%\Delta Ra_{c,l,f}$ is the percentage reduction in SR while finding the percentage of MRP fluid components on the tapered longitudinal or flat end CBH type mould workpiece surface, Ra_i is the initial average SR value over the cylindrical blind hole (CBH) type workpiece surface before MR finishing in nm and $Ra_{c,l,f}$ is the final average SR value over the CBH type workpiece surface after MR finishing in nm.

Table 6.3 Plan of experiments and their response for MR finishing over the EN-31 material using the present MRG process.

S. No.	Percentage concentration of			Initial *Rai* (nm)	Final *Ra* value				*%ΔRa*$_c$ (Eq. 6.1)
	C	*E*	Base fluid		Ra_1 (nm)	Ra_2 (nm)	Ra_3 (nm)	Avg. Ra_c (nm)	
1	25.00	25.00	50.00	350	270	250	240	253.33	27.62
2	20.00	25.00	55.00	320	130	170	150	150.00	53.13
3	20.00	25.00	55.00	310	150	140	170	153.33	50.54
4	17.50	27.50	60.00	300	200	170	180	183.33	38.89
5	20.00	25.00	55.00	320	170	160	170	166.67	47.92
6	22.50	27.50	50.50	340	230	200	210	213.33	37.25
7	20.00	30.00	50.00	350	210	220	200	210.00	40.00
8	20.00	20.00	60.00	300	220	240	210	223.33	25.56
9	15.00	25.00	60.00	330	210	180	190	193.33	41.41
10	20.00	25.00	55.00	330	160	200	170	176.67	46.46
11	22.50	22.50	55.00	320	220	210	240	223.33	30.21
12	17.50	22.50	60.00	310	200	190	220	203.33	34.41
13	20.00	25.00	55.00	300	150	170	160	160.00	46.67

To get the best possible outcomes for the *%ΔRa*, the prediction of the optimum PVC of EIPs and abrasive particles in the MRP fluid was done after the regression analysis. Thus, the developed regression model was used to obtain the maximum *%ΔRa* from Eq. 6.2.

$$\%\Delta Ra_c = -610 + 22.033C + 34.433E - 0.58C^2 - 0.66E^2 \quad (6.2)$$

where *C* is the PVC of abrasive particles fluid and *E* is the PVC of EIPs in the MRP fluid.

Figure 6.4(a) depicts the effect of the PVC of SiC abrasive particles (*C*) on the *%ΔRa* at 25 % of EIPs (*E*). It can be observed that as the PVC of SiC abrasive particles increases up to the value of 20 %, the trend of the *%ΔRa* increases. This is because as the PVC of *C* increases initially, the abrasive particles get trapped in the EIP chain structures. Owing to this, the abrasive particles are tightly gripped by the EIPs during finishing operation as there are less discontinuous chains. This led to the increment in the trend of the *%ΔRa*. However, as there is further increase in the PVC of abrasive particles, the number of active abrasives among the EIPs increases. This leads to weakening of the lattice structure of the EIPs which may cause reduction in the shear strength of the MRP fluid (Kumar *et* al., 2019). Further, an increase in *C*, a large gap between the EIPs may occur which reduces the magnetic interaction force. This leads to a decrease in the strength of the MRP fluid. Owing to this, there is a reduction in material removal which leads to a decrement in the trend of the *%ΔRa*. Thus, the maximum value of the *%ΔRa* was achieved at 19 % of the concentration of abrasive particles.

Figure 6.4(b) depicts the effect of the percentage value contribution (PVC) of EIPs (*E*) on the *%ΔRa* at 20 % contribution of abrasive particles (*C*). It can be seen that as the PVC of *E* increases up to the value of 25 %, the trend of the *%ΔRa* increases. Due to the lower PVC of EIPs, the columnar structure of EIPs is thinner and weaker. This weak chains of EIPs are incapable to grip the SiC abrasive particles rigidly during finishing. But further with the increase in the PVC of EIPs, there is an increment in the cutting shear strength and normal magnetic forces (Huang *et* al., 2005). Also, with an increase in the PVC of EIPs in the MRP fluid, the magnetic permeability of the MRP fluid also increases owing to which the EIP chains become continuous (Khan and Jha, 2018). Further, these EIPs tend to form stronger chains along the magnetic flux lines produced from the magnetic tool surface. Thus, owing this, there is an upsurge in the yield stress of the MRP fluid. This helps to grip the AAPs more strongly in the EIP chains. These firmly gripped AAPs help in cutting the asperities from the surface of the CBH type mould cavity during finishing which results in an increment in the trend of the *%ΔRa*. However, when the PVC of EIPs goes beyond

25 %, the trend of *%ΔRa* decreases. Owing to this decrease in trend up to 25 % of the PVC of the EIPs, all the AAPs are sufficiently gripped by the EIP chain structures. On further adding the EIPs to the MRP fluid aggregates the existing EIP chains which lead to a decrease in the number of overall cutting edges of AAPs which are used for finishing a surface. This leads to a decrease in the removal of material from the workpiece surface. Owing to which there is a decrease in the trend of the *%ΔRa*. Thus, the maximum value of the *%ΔRa* was achieved at 25 % PVC of EIPs. The quadratic model equation after the regression analysis is used to maximize the *%ΔRa*. Thus, the optimized PVC of the abrasive particles and EIPs are found as 19 % and 26 % with base fluid as 55 % in the MRP fluid to be used during MR finishing of the EN-31 CBH type workpiece surface with the developed MRG tool. Further, this composition of MRP fluid is used for experimentation.

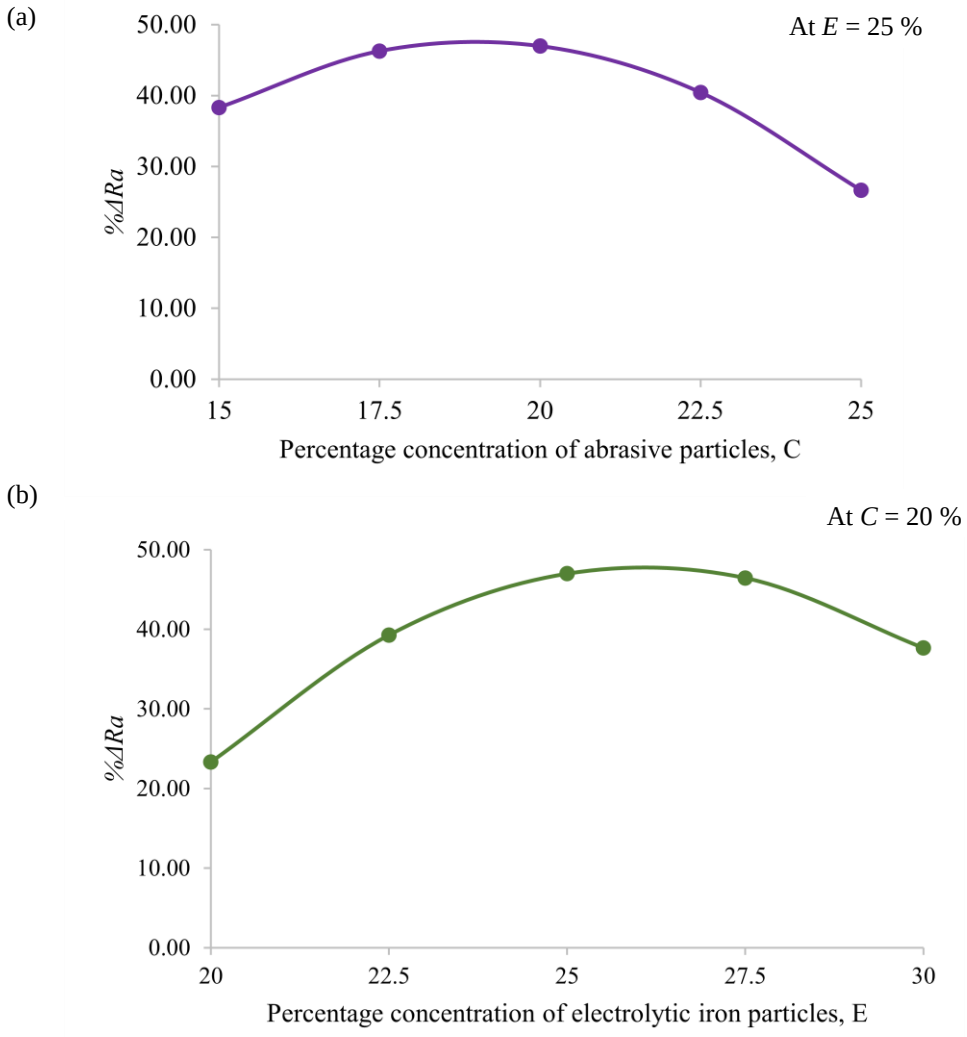

Fig. 6.4 Effect of percentage concentration of (a) the abrasive particles (*C*) and (b) the electrolytic iron particles (*E*) on the percentage reduction in surface roughness *(%ΔRa*).

6.1.4 Design of experiments to predict the finishing process parameters

To find the optimum parameters for the finishing of the interior tapered longitudinal and flat end surfaces of the EN-31 blind hole type mould cavity with the MRG tool, the response surface methodology (RSM) is performed. The parameters considered for the design of experiments are current (*I*), working gap (*G*), rotational speed of the CBH type mould cavity (*W*), rotational speed (*T*) and reciprocation speed (*R*) of the MRG tool. For performing the experimentation, the range of the finishing parameters are considered based on the preliminary experimentation and literature (Maan *et* al., 2017; Chana and Singh, 2019; Bedi and Singh, 2018a). The range of the current, working gap, rotational speed of the CBH type mould cavity, rotational and reciprocation speed of the MRG tool is selected and reported in Tables 6.4 and 6.5. To perform the RSM, the central composite design (CCD) method with 5 parameters and 5 levels was opted to optimize the process parameters for the finishing of both the surfaces of the mould cavity.

Table 6.4 Experimental parameters and their range for finishing the EN-31 tapered longitudinal surface of the cylindrical blind hole workpiece.

Finishing process parameters	Range				
	-2	-1	0	1	2
Rotation of the magnetorheological grinding (MRG) tool (RPM), T_l	300	450	600	750	900
Reciprocation of the MRG tool (cm/min), R_l	5	10	15	20	25
Rotation of the cylindrical blind hole workpiece (RPM), W_l	30	60	90	120	150
Current (A), I_l	1.5	2	2.5	3	3.5
Working gap (mm), G_l	0.3	0.6	0.9	1.2	1.5

Further, a total of 100 (50 x 2) experiments were performed for finishing over the interior tapered longitudinal and flat end surfaces of the cylindrical blind hole (CBH) type workpiece. For each experimental condition as reported in Tables 6.6 and 6.7, the finishing is performed over the interior tapered longitudinal and flat end blind hole type sample surfaces for 40 min of finishing time.

Table 6.5 Experimental parameters and their range for finishing the EN-31 flat end surface of the cylindrical blind hole workpiece.

Finishing process parameters	Range				
	-2	-1	0	1	2
Rotation of the magnetorheological grinding (MRG) tool (RPM), T_f	300	600	900	1200	1500
Reciprocation of the MRG tool (cm/min), R_f	5	10	15	20	25
Rotation of the cylindrical blind hole workpiece (RPM), W_f	40	70	100	130	160
Current (A), I_f	1.5	2	2.5	3	3.5
Working gap (mm), G_f	0.3	0.6	0.9	1.2	1.5

The dimensions of the samples for the longitudinal surface are 0.021 m (open end) and 0.018 m (towards the flat end) in diameter with a length of 0.026 m (Fig. 6.1). Whereas for the flat end surface of the CBH type samples, the diameter is considered as 0.018 m. After the experiments are conducted, the surface roughness (SR) values are measured using Mitutoyo SJ-400 surftest (cut off length of 0.25 mm) at three different points on the surfaces of the CBH type samples as it can be observed in Fig. 6.1. The three-SR values measured over the workpiece surface are not the same, so the percentage reduction in SR ($\%\Delta Ra$) is considered as reported in Tables 6.6 and 6.7.

Table 6.6 Plan of experiments and their response for tapered longitudinal surface of the EN-31 cylindrical blind hole type mold cavity workpieces.

S. No.	Finishing process parameters					Initial Ra_i (nm)	Final Ra value				$\%\Delta Ra_l$ (Eq. 6.1)
	T_l (rpm)	W_l (rpm)	R_l (cm/min)	I_l (A)	G_l (mm)		Ra_1 (nm)	Ra_2 (nm)	Ra_3 (nm)	Avg. Ra_l (nm)	
1	600	90	25	2.50	0.90	350	260	240	250	250.00	28.57
2	750	120	10	3.00	1.20	380	340	300	320	320.00	15.79
3	300	90	15	2.50	0.90	370	270	290	250	270.00	27.03
4	450	60	20	2.00	1.20	410	320	290	310	306.67	25.20
5	600	90	15	2.50	0.30	400	350	320	340	336.67	15.83

6	750	120	10	3.00	0.60	380	340	320	310	323.33	14.91
7	600	90	15	2.50	1.50	370	270	260	290	273.33	26.13
8	450	60	10	3.00	1.20	340	220	240	230	230.00	32.35
9	600	90	15	2.50	0.90	350	240	210	230	226.67	35.24
10	600	150	15	2.50	0.90	380	290	270	280	280.00	26.32
11	600	30	15	2.50	0.90	360	260	290	270	273.33	24.07
12	600	90	15	2.50	0.90	370	240	260	250	250.00	32.43
13	450	120	10	2.00	1.20	400	340	330	350	340.00	15.00
14	450	60	20	3.00	0.60	350	270	260	230	253.33	27.62
15	750	120	20	2.00	0.60	390	310	280	290	293.33	24.79
16	600	90	15	2.50	0.90	410	260	300	280	280.00	31.71
17	750	60	10	2.00	0.60	380	290	320	300	303.33	20.18
18	750	60	10	3.00	0.60	360	280	290	310	293.33	18.52
19	450	120	20	3.00	0.60	340	250	270	280	266.67	21.57
20	450	60	10	3.00	0.60	370	290	260	270	273.33	26.13
21	750	60	10	3.00	1.20	390	300	270	310	293.33	24.79
22	900	90	15	2.50	0.90	380	320	310	290	306.67	19.30
23	750	120	20	2.00	1.20	350	260	300	270	276.67	20.95
24	750	60	20	2.00	0.60	360	290	290	280	286.67	20.37
25	450	60	20	2.00	0.60	370	310	270	300	293.33	20.72
26	750	60	20	3.00	0.60	400	340	320	350	336.67	15.83
27	450	60	10	2.00	0.60	340	280	260	290	276.67	18.63
28	600	90	15	1.50	0.90	360	310	270	280	286.67	20.37
29	600	90	5	2.50	0.90	390	290	310	300	300.00	23.08
30	750	120	10	2.00	0.60	410	350	310	340	333.33	18.70
31	600	90	15	3.50	0.90	380	290	260	270	273.33	28.07

32	450	120	10	3.00	1.20	340	270	280	280	276.67	18.63
33	600	90	15	2.50	0.90	370	260	250	240	250.00	32.43
34	450	120	20	3.00	1.20	350	280	260	290	276.67	20.95
35	750	120	20	3.00	1.20	400	320	300	340	320.00	20.00
36	600	90	15	2.50	0.90	360	260	250	240	250.00	30.56
37	450	120	20	2.00	1.20	410	340	310	330	326.67	20.33
38	450	120	10	3.00	0.60	370	310	290	300	300.00	18.92
39	750	120	10	2.00	1.20	390	330	320	300	316.67	18.80
40	750	120	20	3.00	0.60	380	300	280	320	300.00	21.05
41	600	90	15	2.50	0.90	350	240	230	250	240.00	31.43
42	450	120	10	2.00	0.60	400	320	340	320	326.67	18.33
43	600	90	15	2.50	0.90	360	220	250	240	236.67	34.26
44	750	60	20	3.00	1.20	410	300	330	320	316.67	22.76
45	600	90	15	2.50	0.90	350	250	230	240	240.00	31.43
46	750	60	10	2.00	1.20	370	310	280	300	296.67	19.82
47	450	60	20	3.00	1.20	360	260	270	250	260.00	27.78
48	750	60	20	2.00	1.20	390	330	310	290	310.00	20.51
49	450	60	10	2.00	1.20	340	250	270	260	260.00	23.53
50	450	120	20	2.00	0.60	360	280	310	270	286.67	20.37

This *%ΔRa* is considered as a response for the RSM technique. After finding the optimum parameters and validating the experiments, the circularity test is conducted over the tapered longitudinal surface of the CBH type mould cavity using Accurate spectra 5.6.4 coordinate measuring machine (CMM).

Table 6.7 Plan of experiments and their response for flat end surface of the EN-31 cylindrical blind hole type mould cavity workpieces.

156	Finishing process parameters					Initial	Final *Ra* value				$\%\Delta Ra_f$
	T_f (RPM)	R_f (cm/min)	W_f (RPM)	I_f (A)	G_f (mm)	Ra_i (nm)	Ra_1 (nm)	Ra_2 (nm)	Ra_3 (nm)	Avg. Ra_f (nm)	(Eq. 6.1)
1	900	100	20	2.5	0.9	310	70	100	90	86.67	72.04
2	300	100	20	2.5	0.9	340	230	240	220	230.00	32.35
3	600	130	25	3	1.2	310	200	220	230	216.67	30.11
4	600	70	25	3	1.2	330	260	230	240	243.33	26.26
5	1200	130	15	2	0.6	350	180	170	190	180.00	48.57
6	600	70	25	2	0.6	310	160	180	160	166.67	46.24
7	1200	130	25	3	0.6	340	110	120	100	110.00	67.65
8	900	100	20	2.5	0.9	320	80	60	90	76.67	76.04
9	600	70	25	3	0.6	300	170	140	160	156.67	47.78
10	900	100	20	2.5	0.3	350	120	110	140	123.33	64.76
11	900	100	20	1.5	0.9	360	260	230	240	243.33	32.41
12	1200	130	25	2	1.2	310	160	140	150	150.00	51.61
13	900	100	30	2.5	0.9	320	100	120	90	103.33	67.70
14	600	130	15	2	1.2	330	230	250	210	230.00	30.30
15	1200	70	25	2	0.6	340	190	160	170	173.33	49.02
16	1200	70	25	3	1.2	310	170	140	150	153.33	50.54
17	1200	70	25	2	1.2	350	240	250	240	243.33	30.48
18	1200	70	15	3	0.6	320	180	200	170	183.33	42.71
19	600	70	25	2	1.2	330	220	190	210	206.67	37.37
20	1200	70	15	3	1.2	340	150	130	140	140.00	58.82
21	900	100	20	2.5	0.9	310	80	70	80	76.67	75.27
22	600	130	25	2	1.2	320	200	190	220	203.33	36.46

23	900	100	20	2.5	1.5	350	230	210	240	226.67	35.24
24	900	100	20	2.5	0.9	340	120	110	130	120	64.71
25	600	130	15	3	0.6	330	210	190	210	203.33	38.38
26	1200	130	25	3	1.2	310	110	90	80	93.33	69.89
27	600	70	15	2	0.6	320	160	130	140	143.33	55.21
28	900	100	20	3.5	0.9	350	140	120	100	120.00	65.71
29	1200	130	25	2	0.6	360	150	140	120	136.67	62.04
30	900	100	10	2.5	0.9	330	140	130	150	140.00	57.58
31	600	130	15	2	0.6	340	170	180	160	170.00	50.00
32	600	130	15	3	1.2	300	200	190	170	186.67	37.78
33	900	40	20	2.5	0.9	310	220	180	200	200.00	35.48
34	1200	130	15	3	1.2	350	150	160	140	150.00	57.14
35	900	100	20	2.5	0.9	310	70	90	60	73.33	76.34
36	900	160	20	2.5	0.9	330	140	120	150	136.67	58.59
37	900	100	20	2.5	0.9	320	90	90	80	86.67	72.92
38	1200	70	25	3	0.6	340	160	140	130	143.33	57.84
39	600	70	15	3	0.6	360	200	170	180	183.33	49.07
40	600	130	25	2	0.6	310	140	120	130	130.00	58.06
41	1500	100	20	2.5	0.9	300	170	130	150	150.00	50.00
42	1200	70	15	2	0.6	350	240	210	230	226.67	35.24
43	600	70	15	3	1.2	330	190	180	170	180.00	45.45
44	900	100	20	2.5	0.9	340	90	80	90	86.67	74.51
45	1200	70	15	2	1.2	320	220	200	180	200.00	37.50
46	900	100	20	2.5	0.9	310	90	80	70	80.00	74.19
47	1200	130	15	3	0.6	350	220	210	200	210.00	40.00
48	1200	130	15	2	1.2	300	160	180	170	170.00	43.33
49	600	70	15	2	1.2	330	200	210	180	196.67	40.40

50	600	130	25	3	0.6	340	210	170	190	190.00	44.12

The analysis of variance (ANOVA) is performed using the response (*%ΔRa*) of the experimental data for the interior tapered longitudinal and flat end CBH type workpiece surfaces, after 40 min of the MRG process (Tables 6.6 and 6.7). After performing the ANOVA, the parameters with a p-value of the regression model less than 0.05 are considered significant, and the rest parameters with a p-value greater than 0.05 are considered non-significant. After neglecting the non-significant parameter, the ANOVA data are given in Tables 6.8 and 6.9 for finishing the interior tapered longitudinal and flat end surfaces of the samples using the MRG tool. The significant terms involved in the regression model are T_l, W_l, R_l, I_l, G_l, T_l^2, W_l^2, R_l^2, I_l^2, G_l^2, T_lW_l, T_lI_l, W_lR_l, W_lI_l and W_lG_l with the p-value less than 0.05 (Table 6.8). The R-square value is 90.35 % which describe the accuracy of the model developed for measuring the value of the responses on the interior tapered longitudinal EN-31 CBH type samples surface using the MRG tool. Further, the significant terms involved in the regression model for the flat end surface of the CBH type samples are T_f, W_f, R_f, I_f, G_f, T_f^2, W_f^2, R_f^2, I_f^2, G_f^2, T_fW_f, T_fR_f, T_fI_f, T_fG_f, W_fR_f, R_fG_f, and I_fG_f with the p-value less than 0.05 (Table 6.9). The R-square value is 90.10 % which describe the accuracy of the model developed for measuring the value of the responses on the flat end CBH type mould samples surface using the MRG tool. After the regression analysis, the regression models are obtained for the finishing of the interior tapered longitudinal and flat end CBH type mould cavity surfaces using the MRG tool as expressed in Eqs. 6.3 and 6.4, respectively.

$$\%\triangle \mathrm{Ra}_l = -149.53 + 0.132\mathrm{T}_l + 0.364\mathrm{W}_l + 1.837\mathrm{R}_l + 62.15I_l + 75.33\mathrm{G}_l - 1.0167\times 10^{-4}\mathrm{T}_l^2 - 2.264\times 10^{-3}\mathrm{W}_l^2 - 0.077\mathrm{R}_l^2 - 8.65\mathrm{I}_l^2 - 33.75\mathrm{G}_l^2 + 2.917\times 10^{-4}\mathrm{T}_l\mathrm{W}_l - 0.018\mathrm{T}_l\mathrm{I}_l + 7.083\times 10^{-3}\mathrm{W}_l\mathrm{R}_l - 0.067\mathrm{W}_l\mathrm{I}_l - 0.125\mathrm{W}_l\mathrm{G}_l \quad (6.3)$$

where $\%\Delta Ra_l$ is the percentage reduction in SR, W_l is the rotational speed of the tapered longitudinal CBH type mould cavity surface, T_l and R_l is the rotational and reciprocation speed of the MRG tool, I_l is the current and G_l is the working gap between the longitudinal MRG tool surface and the interior tapered CBH type sample surface.

$$\%\triangle \mathrm{Ra}_f = -125.385 - 3.069\times 10^{-3}\mathrm{T}_f + +0.755\mathrm{W}_f + +1.86\mathrm{R}_f + 81.275\mathrm{I}_f + 57.791\mathrm{G}_f - 8.562\times 10^{-5}\mathrm{T}_f^2 - 6.896\times 10^{-3}\mathrm{W}_f^2 - 0.088\mathrm{R}_f^2 - 22.825\mathrm{I}_f^2 - 60.625\mathrm{G}_f^2 + 3.507\times 10^{-4}\mathrm{T}_f\mathrm{W}_f + 2.021\times 10^{-3}\mathrm{T}_f\mathrm{R}_f + 0.026\mathrm{T}_f\mathrm{I}_f + 0.035\mathrm{T}_f\mathrm{G}_f + 0.02\mathrm{W}_f\mathrm{R}_f - 1.938\mathrm{R}_f\mathrm{G}_f + 17.708\mathrm{I}_f\mathrm{G}_f \quad (6.4)$$

where $\%\Delta Ra_f$ is the percentage reduction in SR, W_f is the rotational speed of the flat end CBH type mould cavity surface, T_f and R_f is the rotational and reciprocation speed of the MRG tool, I_f is the current and G_f is the working gap between the flat end MRG tool surface and the CBH type sample surface.

Table 6.8 Analysis of various (ANOVA) for percentage improvement in the surface finishing on tapered longitudinal surface of the EN-31 cylindrical blind hole type mold cavity.

Source	Sum of square	Degree of freedom	Mean square	*F* value	*p* value	Remarks	Percentage contribution
Model	1330.37	15	88.69	21.22	< 0.0001	Significant	
T_l	72.90	1	72.90	17.44	0.0002		5.41
W_l	62.50	1	62.50	14.95	0.0005		4.64
R_l	32.40	1	32.40	7.75	0.0087		2.41
I_l	36.10	1	36.10	8.64	0.0059		2.68
G_l	40.00	1	40.00	9.57	0.0039		2.97
T_l^2	167.44	1	167.44	40.06	< 0.0001		12.44
W_l^2	132.84	1	132.84	31.78	< 0.0001		9.87
R_l^2	117.04	1	117.04	28.00	< 0.0001		8.69
I_l^2	149.64	1	149.64	35.80	< 0.0001		11.11
G_l^2	295.24	1	295.24	70.64	< 0.0001		21.93
$T_l W_l$	55.12	1	55.12	13.19	0.0009		4.09
$T_l I_l$	60.50	1	60.50	14.48	0.0006		4.49
$W_l R_l$	36.12	1	36.12	8.64	0.0059		2.68
$W_l I_l$	32.00	1	32.00	7.66	0.0091		2.38
$W_l G_l$	40.50	1	40.50	9.69	0.0037		3.01
Residual	142.11	34	4.18				
Lack of fit	126.11	27	4.67	2.04	0.1662	Not significant	
Error	16.00	7	2.29				1.19
Total	1472.48	49					

Table 6.9 Analysis of various (ANOVA) for percentage improvement in the surface finishing on flat end surface of the EN-31 cylindrical blind hole type mold cavity.

Source	Sum of square	Degree of freedom	Mean square	*F* value	*p* value	Remarks	Percentage contribution
Model	9696.1	17	570.36	17.12	< 0.0001	significant	
T_f	697.23	1	697.23	20.93	< 0.0001		7.12
W_f	275.63	1	275.63	8.27	0.0071		2.82
R_f	148.23	1	148.23	4.45	0.0428		1.51
I_f	378.22	1	378.22	11.35	0.002		3.86
G_f	731.02	1	731.02	21.95	< 0.0001		7.47
T_f^2	1900.36	1	1900.36	57.05	< 0.0001		19.42
W_f^2	1232.56	1	1232.56	37	< 0.0001		12.59
R_f^2	155.76	1	155.76	4.68	0.0382		1.59
I_f^2	1041.96	1	1041.96	31.28	< 0.0001		10.65
G_f^2	952.66	1	952.66	28.6	< 0.0001		9.73
T_fW_f	318.78	1	318.78	9.57	0.0041		3.26
T_fR_f	294.03	1	294.03	8.83	0.0056		3.00
T_fI_f	472.78	1	472.78	14.19	0.0007		4.83
T_fG_f	318.78	1	318.78	9.57	0.0041		3.26
W_fR_f	282.03	1	282.03	8.47	0.0065		2.88
R_fG_f	270.28	1	270.28	8.11	0.0076		2.76
I_fG_f	225.78	1	225.78	6.78	0.0139		2.31
Residual	1065.92	32	33.31				
Lack of Fit	974.42	25	38.98	2.98	0.0699	not significant	
Error	91.5	7	13.07				0.93
Total	10762.02	49					

6.1.4.1 Effect of significant parameters on process performance over the tapered longitudinal surface

Figure 6.5 (a) depicts the effect on the percentage reduction in surface roughness ($\%\Delta Ra_l$) due to the simultaneous variation in the MRG tool rotation speed (T_l) and the rotational speed of the CBH type mould cavity (W_l). The MRG tool reciprocation speed (R_l), current (I_l) and working gap (G_l) were kept constant at 15 cm/min, 2.5 A and 0.9 mm, respectively. As an upsurge in the values of T_l and W_l upto 600 rpm and 90 rpm is initially observed, there is an increasing trend in $\%\Delta Ra_l$. This increase in trend of $\%\Delta Ra_l$ is due to the increment in net tangential force which further increases the cutting shear force that results in enhanced shearing off the asperities for the interior tapered longitudinal EN-31 CBH type mould cavity surface. On further increasing the values of T_l and W_l above 600 rpm and 90 rpm simultaneously, there is a decrease in trend in $\%\Delta Ra_l$ as shown in Fig. 6.5 (a). This decrement in the trend of $\%\Delta Ra_l$ is observed as there is an upsurge in the cutting shear force. This owes to the increment in net tangential force which may detach the active abrasive particles (AAPs) due to centrifugal effect from the electrolytic iron particles (EIPs) in the MRP fluid due to the simultaneous rotation of the MRG tool and the CBH type mould cavity. This adversely affects the finishing action being performed over the tapered longitudinal CBH type mould cavity surface. Thus, the maximum value of $\%\Delta Ra_l$ is achieved when the MRG tool rotation speed (T_l) and rotational speed of the CBH type mould cavity (W_l) is at 600 rpm and 90 rpm.

Figure 6.5 (b) depicts the effect on the $\%\Delta Ra_l$ due to simultaneous variation in the MRG tool rotation speed (T_l) and current (I_l). The MRG tool reciprocation speed (R_l), rotational speed of the CBH type mould cavity (W_l) and working gap (G_l) were kept constant at 15 cm/min, 90 rpm and 0.9 mm, respectively. As in Fig. 6.5 (b) initially, if there is a simultaneous increase in T_l and I_l upto 600 rpm and 2.5 A, an incremental trend of the $\%\Delta Ra_l$ is observed. This trend is followed due to the increment in net tangential force and current which further increases the cutting shear strength of the MRP fluid and magnetic normal force (acting due to magnetization of the MRG tool over the AAPs). The increase in magnetic field due to increase in current enhances the gripping strength of the EIPs along with an increase in the cutting shear force acting over the AAPs that helps in the shearing off the asperities from the surface of the EN-31 CBH type mould cavity. Thus, owing to this an increase in trend of $\%\Delta Ra_l$ is observed. On further increasing the values of T_l and I_l above 600 rpm and 2.5 A simultaneously, there is a decrease in trend of $\%\Delta Ra_l$ as shown in Fig. 6.5 (b). This decrement in the trend of $\%\Delta Ra_l$ is observed as the cutting shear force and the magnetization

of the MRG tool increases simultaneously. This is owing to the increment in tangential force along with the magnetization, which not only removes the asperities but also uproots excess material from the tapered longitudinal CBH type mould cavity surface which results in pit formation (Maan and Singh, 2018). So, this causes a decrement in $\%\Delta Ra_l$. Thus, the maximum value of $\%\Delta Ra_l$ is attained when the MRG tool rotation speed (T_l) and current (I_l) are at 600 rpm and 2.5 A.

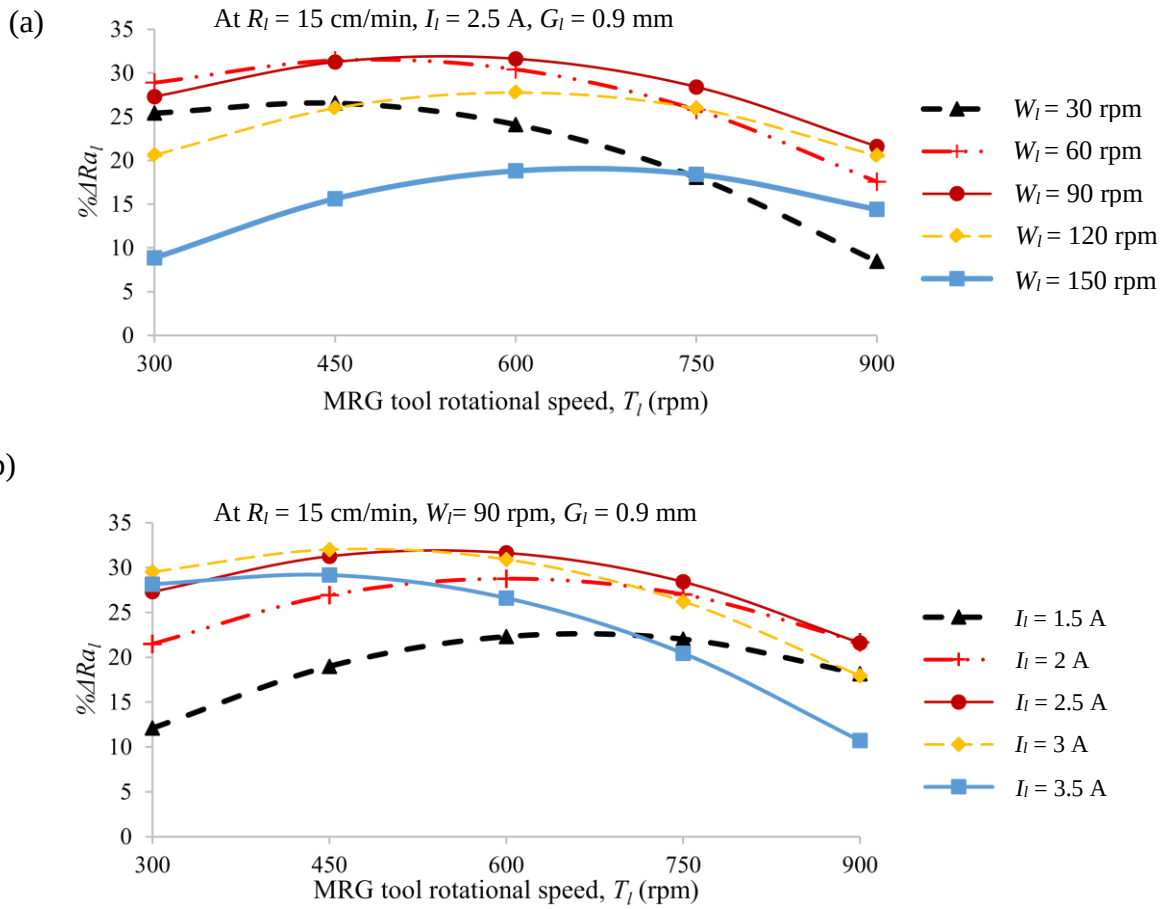

Figure. 6.5 Effect of MRG tool rotation (T_l) on percentage reduction in surface roughness ($\%\Delta Ra_l$) at (a) varying rotation of the cylindrical blind hole (CBH) type mould cavity (W_l) and (b) varying current (I_l) during finishing of the tapered longitudinal surface of the EN-31 CBH type mould cavity using the present MRG process.

Figure 6.6 (a) depicts the effect on $\%\Delta Ra_l$ due to simultaneous variation in the rotation speed of the CBH type mould cavity (W_l) and MRG tool reciprocation speed (R_l). The MRG tool rotational speed (T_l), current (I_l) and working gap (G_l) were kept constant at 600 rpm, 2.5 A and 0.9 mm, respectively. In Fig. 6.6 (a), initially as W_l and I_l simultaneous increase upto 90 rpm and 15 cm/min, the upsurge in the trend of the $\%\Delta Ra_l$ is observed. The upsurge in trend followed by $\%\Delta Ra_l$ is due

to the increment in rotational speed of the CBH type mould cavity (W_l) and tool reciprocation speed (R_l) simultaneously. This results in an increment in the number of passes over the tapered longitudinal rotating CBH type mould cavity surface. Thus, owing to this an increase in trend of $\%\Delta Ra_l$ is observed. On further increase in the values of W_l and R_l above 90 rpm and 15 cm/min simultaneously, there is a decrease in trend in $\%\Delta Ra_l$ as shown in Fig. 6.6(a). This decrement in trend of $\%\Delta Ra_l$ is seen as a combined motion generated due to the rotation of the CBH type mould cavity and reciprocation of the MRG tool. This is owing to the increase in the pitch (d) which causes non-uniform interaction of the AAPs with the asperities present on the interior tapered longitudinal surface of the CBH type mould cavity which results in a reduction in $\%\Delta Ra_l$. Thus, the maximum value of $\%\Delta Ra_l$ is attained when the rotational speed of the CBH type mould cavity (W_l) and the MRG tool reciprocation speed (R_l) is at 90 rpm and 15 cm/min respectively.

Figure 6.6 (b) represents the effect on $\%\Delta Ra_l$ due to simultaneous variation in the rotational speed of the CBH type mould cavity (W_l) and current (I_l). The MRG tool rotational speed (T_l), MRG tool reciprocation speed (R_l) and working gap (G_l) were kept constant at 600 rpm, 15 cm/min and 0.9 mm, respectively. In Fig. 6.6 (b) initially, as W_l and I_l simultaneous increases upto 90 rpm and 2.5 A, an upsurge in trend of the $\%\Delta Ra_l$ is observed. The upsurge in the trend followed by $\%\Delta Ra_l$ is due to the increment in the rotational speed of the CBH type mould cavity (W_l) and current (I_l) simultaneously. Due to the increase in current, an upsurge in magnetic field which helps the EIPs to grip the abrasives. Thus, the abrasive particles point towards the CBH type mould cavity surface. When these strongly gripped abrasives collide with the asperities present on the interior tapered longitudinal surface of the cavity rotating with higher speed results in greater material removal from its surface. Owing to this, an incremental trend is followed by $\%\Delta Ra_l$. On further increasing the values of W_l and I_l above 90 rpm and 2.5 A simultaneously, there is a decrease in trend in $\%\Delta Ra_l$ as shown in Fig. 6.6(b). This decrement in the trend of $\%\Delta Ra_l$ is due to the increase in speed of the AAPs to collide with the asperities present on the rotating CBH type mould cavity along with the increase in current. This owes to the removal of extra material from the tapered longitudinal surface of the CBH type mould cavity which may result in the formation of micro-grooves. Hence, causing a reduction in the trend of $\%\Delta Ra_l$. Thus, the maximum value of $\%\Delta Ra_l$ is attained when the rotational speed of the CBH type mould cavity (W_l) and current (I_l) are at 90 rpm and 2.5 A respectively.

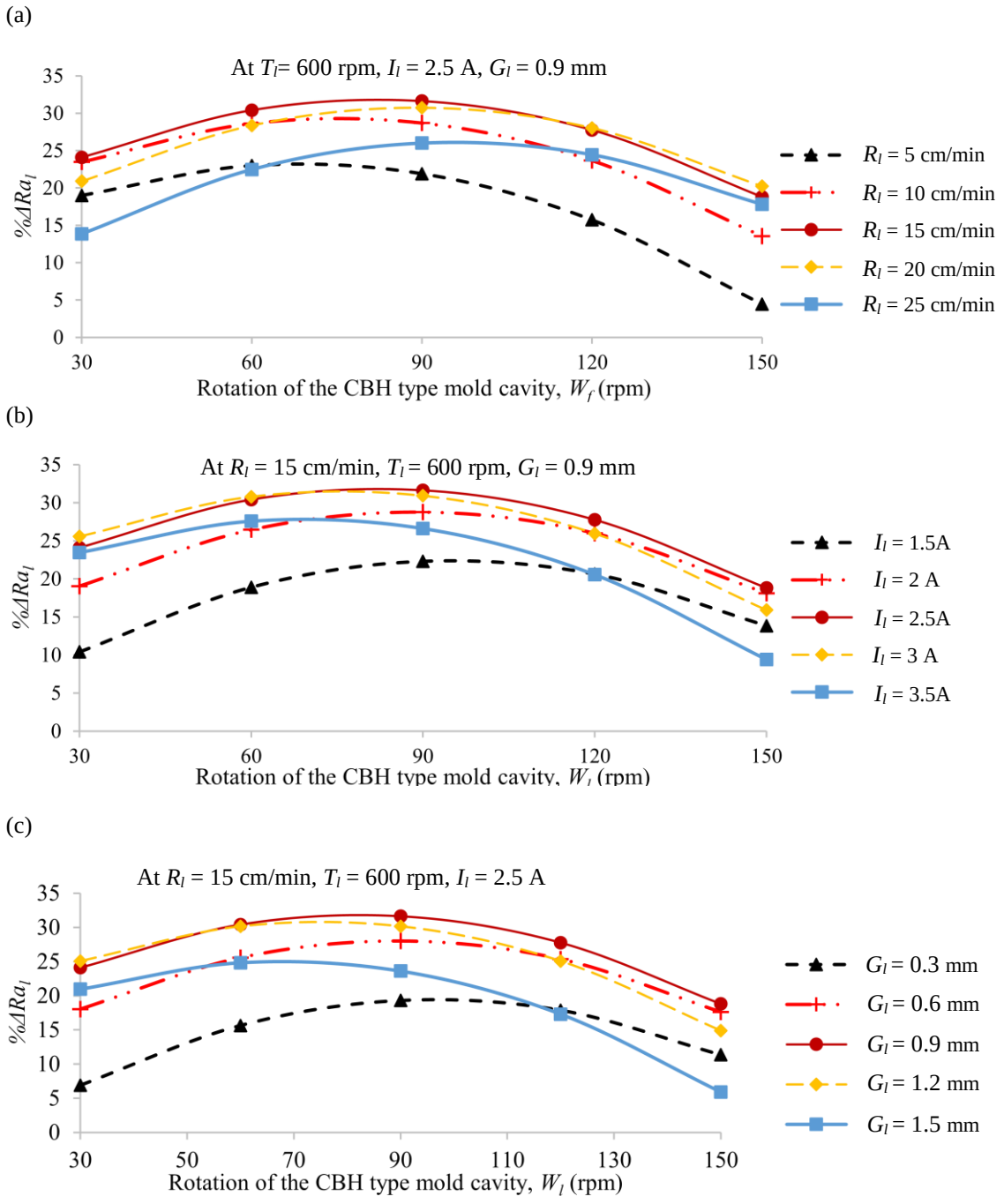

Figure 6.6 Effect of rotation of the CBH mould cavity on *%ΔRa*$_l$ at varying (a) reciprocation speed of the MRG tool, (b) current, and (c) working gap during finishing the longitudinal surface of the EN-31 cylindrical blind hole (CBH) type mould cavity using the present MRG process.

Figure 6.6 (c) depicts the effect on the $\%\Delta Ra_l$ due to the simultaneous variation in the rotational speed of the CBH type mould cavity (W_l) and the working gap (G_l). The MRG tool rotational speed (T_l), MRG tool reciprocation speed (R_l) and current (I_l) were kept constant at 600 rpm, 15 cm/min and 2.5 A, respectively. Initially, as there is a simultaneous increase in W_l and G_l upto 90 rpm and 0.9 mm, an incremental trend of the $\%\Delta Ra_l$ can be observed from Fig. 6.6(c). This trend observed is due to the simultaneous increase in the rotation of the CBH type mould cavity as well as the working gap between its surface and the longitudinal MRG tool surface. As the rotation of the CBH type mould cavity increases, the net tangential force increases simulations with the working gap. Initially as the working gap is less, the MRP fluid is in squeezed form between the finishing surface of the MRG tool and the workpiece surface. As the working gap increases along with the simultaneous increase in rotational speed of the CBH type mould cavity workpiece, the MRP fluid get loose resulting in reduced indentation pressure over the CBH type mould cavity surface causing a reduction in the formation of pits (Sidpara and Jain, 2012). This is followed by the increase in distance travelled by the AAPs over the rotating CBH type mould cavity workpiece surface. Thus, leads to rise in trend of the $\%\Delta Ra_l$ which can be observed in Fig. 6.6(c). Further, as the values of W_l and G_l are increased above 90 rpm and 0.9 mm simultaneously, there is a decrease in trend in $\%\Delta Ra_l$ as depicted in Fig. 6.6(c). This decrease in the trend of $\%\Delta Ra_l$ is due to the reduction in interaction of the AAPs with the asperities present on the tapered longitudinal surface of the CBH type mould cavity. This is owing to an increase in the working gap between the MRG tool surface and the asperities present on the rotating tapered longitudinal CBH type mould cavity surface. Thus, the maximum value of $\%\Delta Ra_l$ is attained when the rotation speed of the CBH type mould cavity (W_l) and the working gap (G_l) are at 90 rpm and 0.9 mm respectively.

6.1.4.2 Effect of significant parameters on process performance over the flat end surface

Figure 6.7 (a) presents the effect on $\%\Delta Ra_f$ due to simultaneous variation in the MRG tool rotational speed (T_f) and rotational speed of the cylindrical blind hole (CBH) type mould cavity (W_f). The MRG tool reciprocation speed (R_f), working gap (G_f) and current (I_f) were kept constant at 20 cm/min, 0.9 mm and 2.5 A, respectively. Initially, as there is a simultaneous increase in T_f and W_f upto 900 rpm and 100 rpm, an incremental trend of the $\%\Delta Ra_f$ can be observed from Fig. 6.7(a). This trend observed is due to the increase in relative motion of the T_f and W_f. As the rotation of the workpiece increases simulations with T_f, the net tangential force increases. Thus, this causes

an upsurge in the shearing off the asperities from the flat end surface of the CBH type mould cavity. Thus, an incremental trend of the $\%\Delta Ra_f$ can be seen. Further, the values of T_f and W_f increases beyond 900 rpm and 100 rpm simultaneously, there is a decreasing trend in $\%\Delta Ra_f$ as can be espied in Fig. 6.7(a). This decrease in the trend of $\%\Delta Ra_f$ as the net relative motion becomes so high which results in deformation of the magnetorheological polishing (MRP) fluid column. Hence, this reduces the capability of the AAPs present in the MRP fluid to shear off the asperities from the flat end CBH type mould cavity surface. Thus, the maximum value of $\%\Delta Ra_f$ is attained when MRG tool rotational speed (T_f) and rotation speed of the CBH type mould cavity (W_f) are at 900 rpm and 100 rpm respectively.

Figure 6.7(b) presents the effect on the $\%\Delta Ra_f$ due to simultaneous variation in the MRG tool rotational speed (T_f) and reciprocation speed (R_f). The rotational speed of the CBH type mould cavity (W_f), working gap (G_f) and current (I_f) were kept constant at 100 rpm, 0.9 mm and 2.5 A, respectively. Initially, as there is simultaneous increase in T_f and R_f upto 900 rpm and 20 cm/min, an incremental trend of the $\%\Delta Ra_f$ can be observed from Fig. 6.7(b). This trend observed as the AAPs start following a uniform path with pitch (b) over the surface of the workpiece due to increase in T_f and R_f. Thus, an incremental trend of the $\%\Delta Ra_f$ can be seen. Further, as the values of T_f and W_f increases beyond 900 rpm and 100 rpm simultaneously, there is a decrease in trend of $\%\Delta Ra_f$ as can be espied in Fig. 6.7(b). This decrease in trend of $\%\Delta Ra_f$ is due to the non-uniformity of the path followed by the AAPs over the surface of the CBH type mould cavity workpiece owing to reciprocation speed of the present MRG tool. This is followed by the increase in rotational speed of the MRG tool. Hence, this reduces the capability of the AAPs present in the MRP fluid to shear off the asperities from the flat end CBH type mould cavity surface. Thus, the maximum value of $\%\Delta Ra_f$ is attained when MRG tool rotational speed (T_f) and rotation speed of the CBH type mould cavity (W_f) are at 900 rpm and 100 rpm respectively.

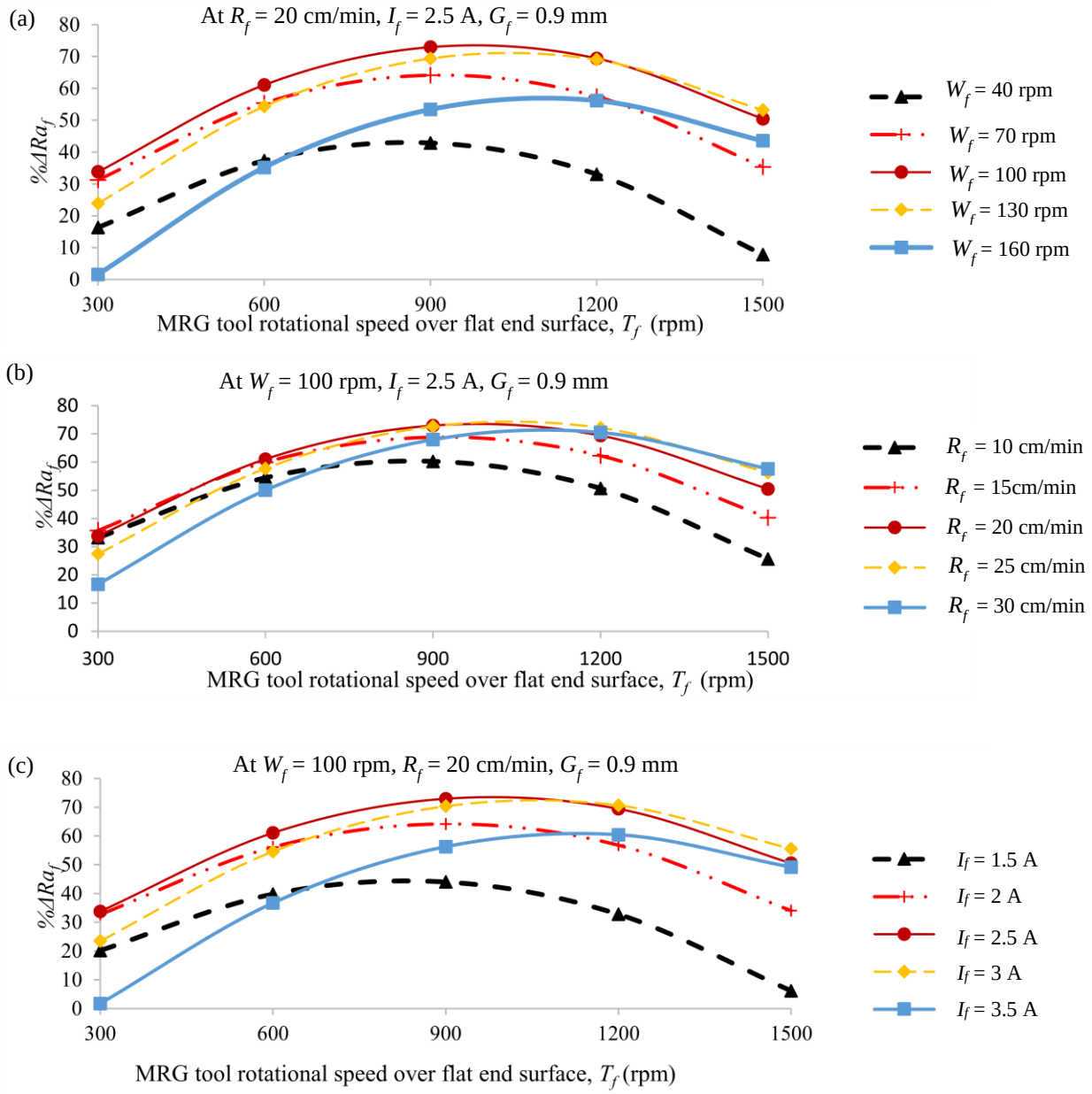

Fig. 6.7 Effect of MRG tool rotation (T_f) on percentage reduction in surface roughness (%ΔRa$_f$) at (a) varying rotation of the cylindrical blind hole (CBH) mould cavity (W_f), (b) reciprocation speed of the MRG tool, (c) varying current (I_f) during finishing over the flat end surface of the EN-31 CBH type mould cavity using the present MRG process.

Figure 6.7(c) presents the effect on *%ΔRa$_f$* due to the simultaneous variation in the MRG tool rotational speed (T_f) and current (I_f). The rotational speed of the CBH type mould cavity (W_f),

working gap (G_f) and reciprocation speed of the MRG tool (R_f) were kept constant at 100 rpm, 0.9 mm and 20 cm/min, respectively. Initially the upsurge in the values of T_f and I_f upto 900 rpm and 2.5 A results in an incremental trend of the $\%\Delta Ra_f$ as can be observed from Fig. 6.7(c). This trend is observed as there is an increment in strength to hold the AAPs with the EIP chains present in the MRP fluid due to increase in current. The increment in the strength of AAPs simultaneously with an increase in MRG tool rotation results in higher material removal from the flat end surface of the CBH type mould cavity. Thus, an incremental trend of the $\%\Delta Ra_f$ can be seen. Further as the values of T_f and I_f increases beyond 900 rpm and 2.5 A simultaneously, there is a decrease in trend in $\%\Delta Ra_f$ as can be espied in Fig. 6.7(c). This decline in the trend of $\%\Delta Ra_f$ is due to the saturation of the MFD near to 2.5 A current along with the increased MRG tool rotation. Thus, owing to this the AAPs undergo centrifugal effect which leads to ineffective interaction with the asperities present over the flat end CBH type mould cavity surface. This results in less material removal from the CBH type mould cavity workpiece surface. Thus, the maximum value of $\%\Delta Ra_f$ is attained when MRG tool rotational speed (T_f) and current (I_f) are at 900 rpm and 2.5 A respectively.

Figure 6.8(b) presents the effect on the $\%\Delta Ra_f$ due to the simultaneous variation in the rotational speed of the CBH type mould cavity (W_f) and the MRG tool reciprocation speed (R_f). The MRG tool rotational speed (T_f), current (I_f) and working gap (G_f) were kept constant at 900 rpm, 2.5 A and 0.9 mm, respectively. Initially the upsurge in the values of W_f and R_f upto 100 rpm and 20 cm/min results in the escalation in trend of the $\%\Delta Ra_f$ which can be espied in Fig. 6.8(b). This trend is followed by the $\%\Delta Ra_f$, as the number of passes over the flat end surface of the CBH type mould cavity increases with the simultaneous increase in W_f and R_f. Thus, this owes to an upsurge in the trend of the $\%\Delta Ra_f$. On further increasing the values of W_f and R_f beyond 100 rpm and 20 cm/min simultaneously, there is a decrease in trend of $\%\Delta Ra_f$ as can be observed in Fig. 6.8(b). This trend of $\%\Delta Ra_f$ is because of the increase in pitch (b) between the two arms of the spiral path formed over the flat end surface of the CBH type mould cavity. Hence, this causes non-uniformity of path over the flat end CBH type mould cavity surface which results in reduction of material removal rate with respect to the trend before increment in values of W_f and R_f. Thus, the maximum value of $\%\Delta Ra_f$ is attained when the rotational speed of the CBH type mould cavity (W_f) and MRG tool reciprocation speed (R_f) are at 100 rpm and 20 cm/min respectively.

Figure 6.8(c) presents the effect on $\%\Delta Ra_f$ due to the MRG tool reciprocation speed (R_f) and working gap (G_f). The MRG tool rotational speed (T_f), current (I_f) and rotational speed of the CBH type mould cavity (W_f) was kept constant at 900 rpm, 2.5 A and 100 rpm, respectively. Initially, the upsurge in the values of R_f and G_f upto 20 cm/min and 0.9 mm results to an incremental trend of the $\%\Delta Ra_f$ which can be espied in Fig. 6.8(c). This is due to the increase in cutting shear force and reduction in indentation due to decrement in F_{mf} (F_{mf} decreases as working gap increases). This leads to fine finishing the surface of the CBH type mould cavity workpiece. Thus, this results to an upsurge in the trend of the $\%\Delta Ra_f$. On further increasing the values of R_f and G_f beyond 20 cm/min and 0.9 mm simultaneously, there is a decrease in trend in $\%\Delta Ra_f$ as can be observed in Fig. 6.8(c). This is because of the cutting shear force that increases along with the increase in the working gap. As the working gap increases, the weakly held AAPs over the surface of the MRG tool collide with the asperities over the flat end CBH type mould cavity surface. This results in less penetration of the abrasives into the workpiece surface resulting in less material removal. Thus, the maximum value of $\%\Delta Ra_f$ is attained when rotational speed of the CBH type mould cavity (W_f) and the MRG tool reciprocation speed (R_f) is found at 100 rpm and 20 cm/min respectively.

Figure 6.8(d) presents the effect on the $\%\Delta Ra_f$ due to the simultaneous variation in current (I_f) and working gap (G_f). The rotational speed of the CBH type mould cavity (W_f), MRG tool rotational (T_f) and reciprocation (R_f) speed was kept constant at 100 rpm, 900 rpm and 20 cm/min, respectively. Initially, from Fig. 6.8(d) an upsurge in the values of I_f and G_f upto 2.5 A and 0.9 mm resulting to an increment in the trend of the $\%\Delta Ra_f$. The current and the working gap governs the magnetic flux strength of the EIP chains. The EIPs present over the finishing surface of the MRG tool strongly grip the abrasive particles. Thus, these strongly held abrasive particles under incremental magnetic flux density shear off the asperities from the flat end surface of the CBH type mould cavity resulting in the rise of $\%\Delta Ra_f$. On further increasing the values of I_f and G_f beyond 2.5 A and 0.9 mm simultaneously, there is a decrease in the trend of $\%\Delta Ra_f$ as can be observed in Fig. 6.8(d). This may occur due to the reduced effect of current on the magnetic flux strength with simultaneous increment in the working gap. Hence, causing a slump in the magnetic flux strength within the finishing zone resulting in reduced shearing off the roughness peaks from the flat end CBH type mould cavity surface. Thus, the maximum value of $\%\Delta Ra_f$ is attained when current (I_f) and working gap (G_f) is at 2.5 A and 0.9 mm respectively.

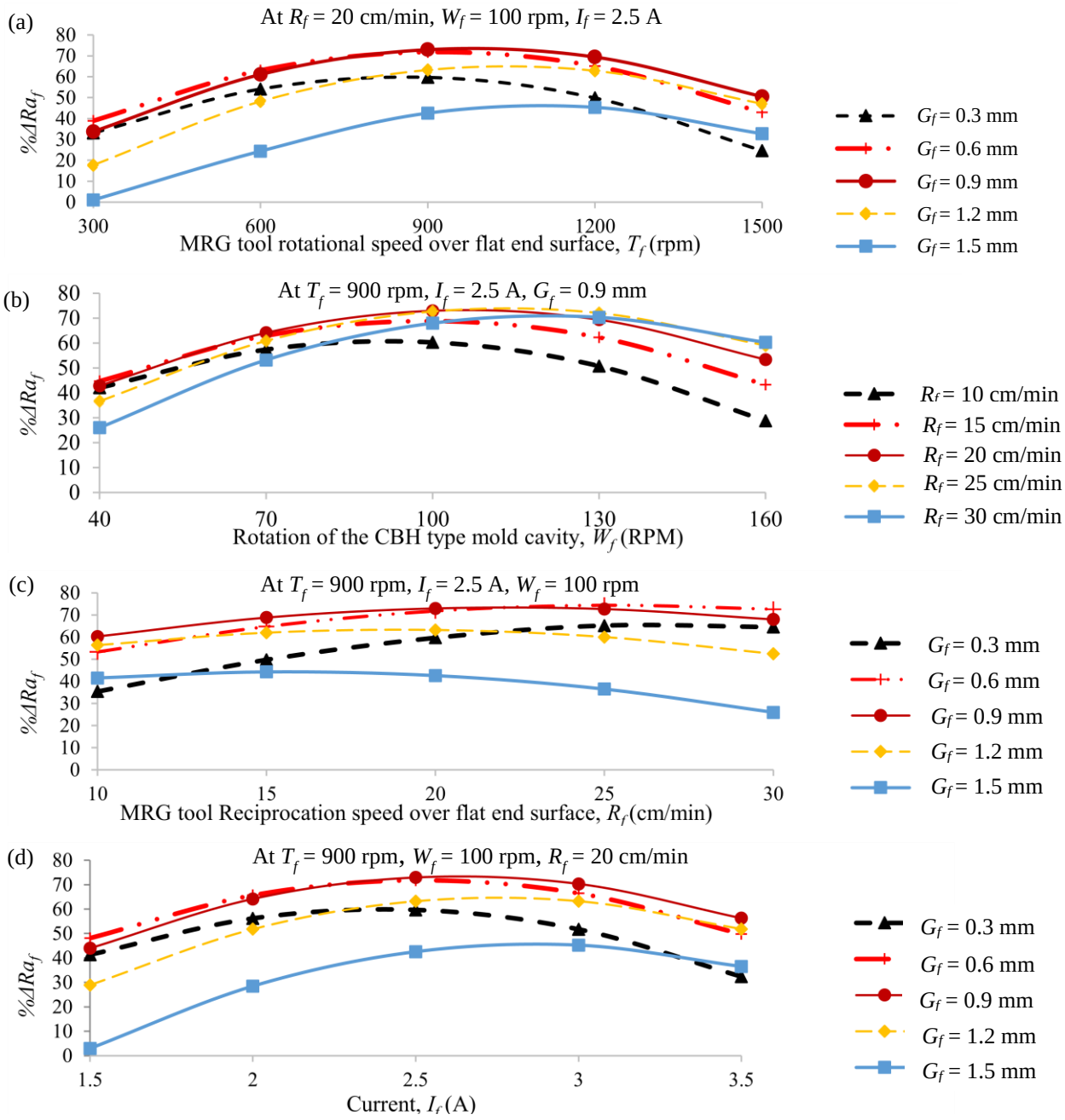

Fig. 6.8 (a) Effect of MRG tool rotation (T_f) on percentage reduction in surface roughness ($\%\Delta Ra_f$) by varying the working gap (G_f), (b) effect of rotation of the CBH type mould cavity (W_f) on $\%\Delta Ra_f$ by varying reciprocation speed of the MRG tool (R_f), (c) effect of R_f on $\%\Delta Ra_f$ by varying G_f and (d) effect of current (I_f) on $\%\Delta Ra_f$ by varying G_f during finishing over the flat end surface of the EN-31 CBH type mould cavity using the present MRG process.

6.1.5 Optimum process parameters and their validation

After analysis of the regression model, the optimum parameters are predicted in order to investigate the best combination of parameters which gives the maximum %age reduction in surface roughness ($\%\Delta Ra_{l,f}$). In order to obtain the minimum value of the surface roughness, the quadratic mathematical model is obtained from the experimental data which would maximize the $\%\Delta Ra_{l,f}$ for the tapered longitudinal and flat end CBH type mould cavity surfaces.

Maximization of the $\%\Delta Ra_l$ for tapered longitudinal surface of the CBH type mould cavity is subject to

$300 \text{ rpm} \leq T_l \leq 900 \text{ rpm}$

$30 \text{ rpm} \leq W_l \leq 150 \text{ rpm}$

$5 \text{ cm/min} \leq R_l \leq 25 \text{ cm/min}$

$1.5 \text{ A} \leq I_l \leq 3.5 \text{ A}$

$0.3 \text{ mm} \leq G_l \leq 1.5 \text{ mm}$

The optimum parameters for the finishing of the tapered longitudinal CBH type mould cavity surface were predicted based on the effects of process parameters on the $\%\Delta Ra_l$ from Figs. 6.5 and 6.6 along with the regression model of the tapered longitudinal surface of the CBH type mould cavity. The optimized parameters were found as the rotational speed of the CBH type mould cavity 80 rpm, current 2.8 A, working gap 1 mm, rotational and reciprocation speeds of the MRG tool are 520 rpm and 16 cm/min, respectively. Simultaneous, maximization of the $\%\Delta Ra_f$ for the flat end surface of the CBH type mould cavity is subject to

$300 \text{ rpm} \leq T_f \leq 1500 \text{ rpm}$

$40 \text{ rpm} \leq W_f \leq 160 \text{ rpm}$

$5 \text{ cm/min} \leq R_f \leq 25 \text{ cm/min}$

$1.5 \text{ A} \leq I_f \leq 3.5 \text{ A}$

$0.3 \text{ mm} \leq G_f \leq 1.5 \text{ mm}$

The optimum parameters for the finishing of the interior flat end surface of the CBH type mould cavity were predicted based on the effects of process parameters on the $\%\Delta Ra_f$ from Figs. 6.7 and

6.8 along with the regression model of the flat end surface of the CBH type mould cavity. The optimized parameters were found as the rotational speed of the CBH type mould cavity of 100 rpm, current of 2.5 A, working gap of 0.9 mm, rotational and reciprocation speeds of the MRG tool are 1050 rpm and 18 cm/min, respectively. After predicting the optimized parameters, the confirmatory tests were conducted for 40 min of finishing time to check the repeatability of the developed regression models for the interior tapered longitudinal and flat end surfaces of the CBH type mould cavity. This is done by performing finishing experiments over three samples each for the interior tapered longitudinal and flat end surfaces of the EN-31 CBH type mould cavity. The $\%\Delta Ra_f$ was measured after experimentation and calculated theoretically from the regression Eqs. (6.3) and (6.4). The percentage error is calculated using Eq. (6.5) between the experimental and theoretically obtained results over interior tapered longitudinal (TLS) and flat end (FS) surfaces of the CBH type mould cavity ranges from 1.11 to 3.64 % and 0.95 to 2.71 %, respectively. Thus, the percentage error shows that there is good agreement between the regression model and the experimentally.

$$Percentage\ error\ (\%age\ error) = \frac{\left|(Experimental\ \%\Delta Ra_{l,f} - Predicted\ \%\Delta Ra_{l,f})\right|}{Experimental\ \%\Delta Ra_{l,f}} \times 100 \qquad (6.5)$$

Further, using the predicted optimum parameters, the finishing is performed over the interior tapered longitudinal and flat end surfaces of the EN-31 CBH type mould cavity to achieve the minimum value of surface roughness utilizing the same experimental setup with the MRG tool. The initial surface roughness measured after grinding over the interior tapered longitudinal surface of the CBH type mould cavity is 350 nm (1595 sq. mm). Further, after MR finishing with the optimized process parameters on the tapered longitudinal surface of the EN-31 CBH type mould cavity was finished to 80 nm in 100 min of the finishing time. The initial ground and final MR finished surface roughness profiles are obtained over the tapered longitudinal surface of the CBH type mould cavity are shown in Figs. 6.9 (a) and (b), respectively. The surface roughness profile in Fig. 6.9 (b) of the final MR finished longitudinal surface of the CBH type mould cavity shows the improvement in surface finish. The percentage reduction in surface roughness achieved after 100 min of finishing time is 77.14 % (Eq. 6.1) and the finishing rate is calculated as 2.7 nm/min from Eq. 6.6 over the tapered longitudinal surface area of 1595 sq. mm of the CBH type mould cavity.

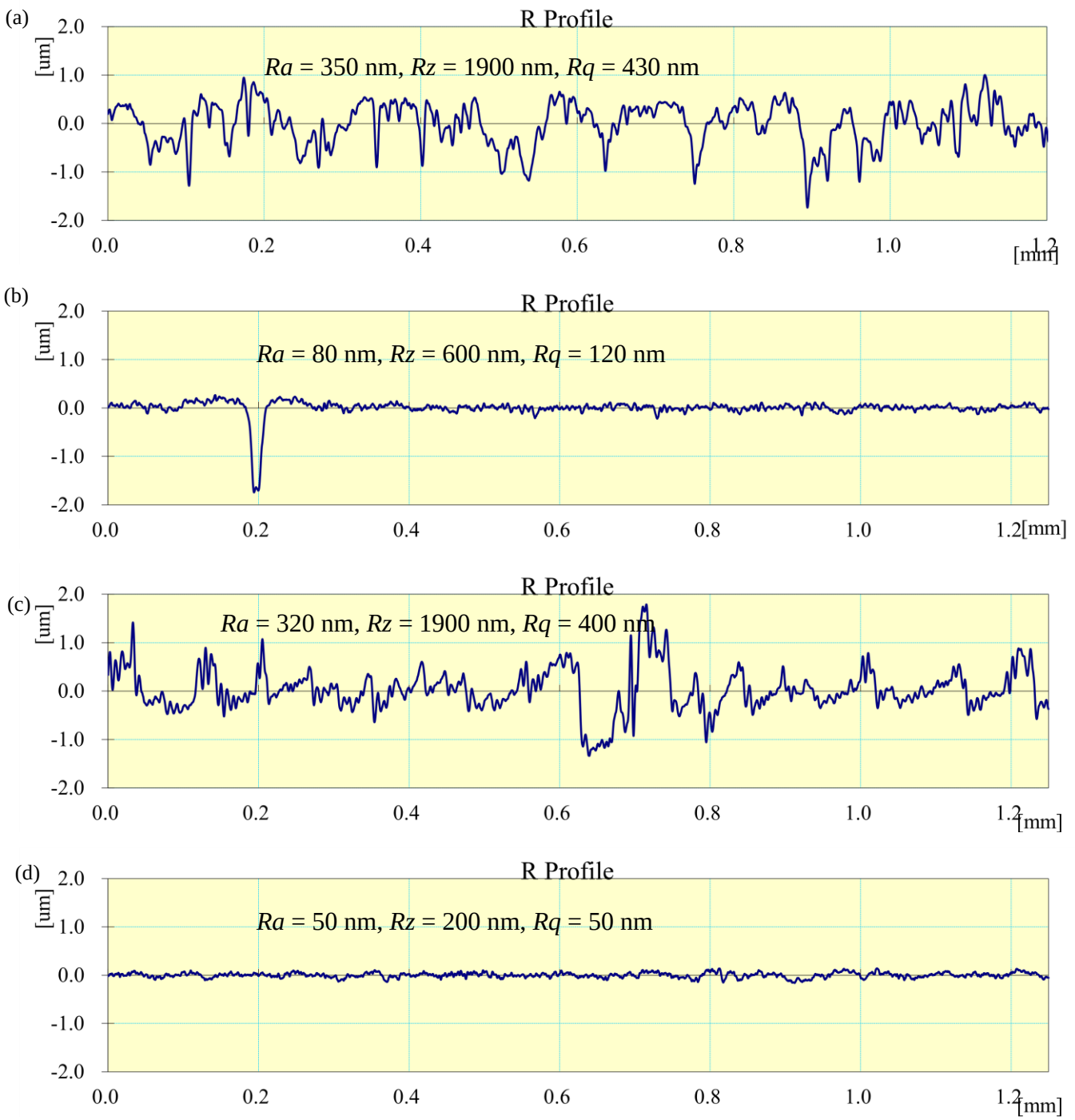

Fig. 6.9 Surface roughness profiles of the EN-31 cylindrical blind hole (CBH) type workpiece (a) the initial tapered longitudinal ground surface, (b) the finally MR finished tapered longitudinal surface area of 1595 mm sq. after 100 min, (c) initial flat end ground surface, and (d) finally MR finished flat end surface area of 254 mm sq. after 60 min of finishing using the present MRG process with optimized parameters.

$$Finishing\ rate = \frac{(Ra_i - Ra_{l,f})}{Total\ time\ take\ for\ finishing} \tag{6.6}$$

Further, the flat end surface of the EN-31 CBH type mould cavity is finished using the setup as shown in Fig. 6.2. The initial surface roughness value measured after grinding over the flat end surface of the CBH type mould cavity is 320 nm. After MR finishing with the optimized parameters, the roughness value is reduced to 50 nm over the flat end surface (254 sq. mm) of the CBH type mould cavity after 60 min of finishing time.

The initial ground and final MR finished roughness profiles are obtained over the flat end surface of the CBH type mould cavity as shown in Figs. 6.9(c) and (d). The surface roughness profile in Fig. 6.9(d) of the final MR finished flat end surface of the CBH type mould cavity (Fig. 6.9c) presents the improvement in surface finish. The percentage reduction in surface roughness ($\%\Delta Ra_f$) over the flat end surface of the CBH type mould cavity is obtained as 84.37% and the finishing rate of 4.5 nm/min after 60 min of finishing time. Further, the improvement in MR finished surface of the tapered longitudinal and flat end surfaces of the EN-31 CBH type mould cavity can be observed from its mirror image as shown in Fig. 6.10. Figure 6.10 (a) is the initial surfaces after the grinding process and Fig. 6.10 (b) is the final MR finished images of the CBH type mould cavity. On comparing Figs. 6.10 (a) and (b), the improvement in the surface quality of the CBH type mould cavity can be observed. Also, Fig. 6.10(c) presents the spray bottle safety hood as the final end product which can be obtained from such CBH type mould cavities.

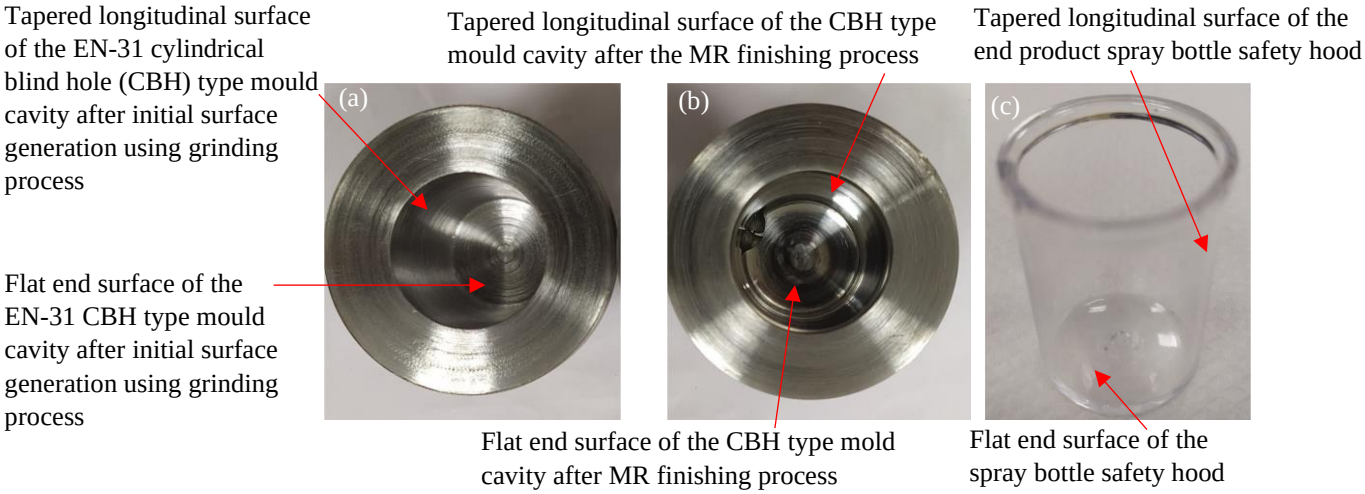

Fig. 6.10 Photograph of the CBH type mould cavity (a) initially after grinding process, (b) after the present MR finishing process and (c) the final end product spray bottle safety hood.

Further, the improvement in surface characteristics can be observed on comparing the initial and final images obtained from the scanning electron microscope (SEM). For comparison of the initial

and final images of SEM, the images can be observed in Fig. 6.11(a-d) at magnification of 500X. The initial images of the tapered longitudinal and flat end surfaces of the CBH type mould cavity can be observed in Figs. 6.11 (a) and (c). Here, pitting, grooves and grinding lays can be observed over the initial tapered longitudinal and flat end surfaces of the EN-31 CBH type mould cavity. Further, the finishing is performed with the magnetorheological grinding (MRG) process with optimum parameters over both the surfaces of the CBH type mould cavity. After performing the MR finishing process, the initial and final SEM images of the interior tapered longitudinal and flat end surfaces of the CBH type mould cavities are compared. On comparing the final images of the tapered longitudinal and flat end surfaces of the CBH type mould cavities in Figs. 6.11 (b) and (d), the improved surface after MR finishing can be observed. All the defects which were observed in Figs. 6.11 (a) and (c) after grinding process are removed in Figs. 6.11 (b) and (d). Thus, the smooth surfaces are achieved. So, the present MRG process is found effective to finish such mould cavities with interior tapered longitudinal and flat end surfaces.

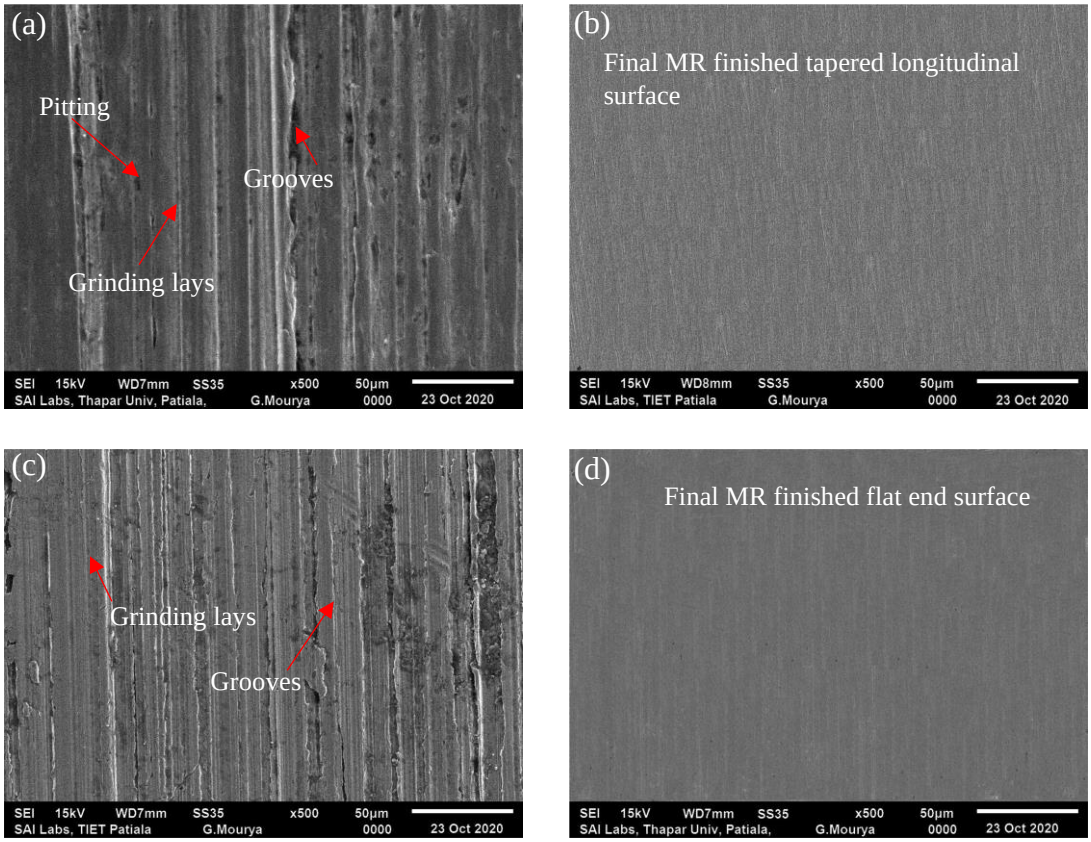

Fig. 6.11 SEM images at magnification of X500 (a) on the initial grinded surface, (b) after MR finishing with the MRG tool over the tapered longitudinal with surface area of 1595 sq. mm, (c) on the initial grinded surface and (d) after MR finishing on the flat end surfaces with surface area of 254 sq. mm of the cylindrical blind hole type mould cavity with the MRG tool.

Further to confirm the dimensional accuracy on the interior tapered longitudinal surface of the CBH type mould cavity, the circularity test was conducted. The circularity is performed to predict the closeness of the real circle to the true circle of the interior tapered longitudinal surface of the CBH type mould cavity. This closeness of the real circle to the true circle describes about the dimensional accuracy of the CBH type mould cavity (Martorelli *et* al., 2017). The images of the circularity were measured and depicted in Figs. 6.12(a, b). Figure 6.12 (a) shows the circularity image of the initial ground surface. The initially measured value of circularity after grinding was found as 0.0444 mm. It can be observed from Fig. 6.12 (a) that most of the recorded points from the real circle have deviated from the true circle. However, in Fig. 6.12 (b), it can be seen that there is a significant enhancement in the circularity as most of the recorded points are lying close to the true circle. Also, the value of the circularity was found as 0.0154 mm. Hence, from Fig. 6.12, it is evident that the tapered longitudinal surface of EN-31 CBH type workpieces are finished effectively with the present MRG process. Also, the process is useful for improving the dimensional accuracy of the CBH type mould cavity surfaces.

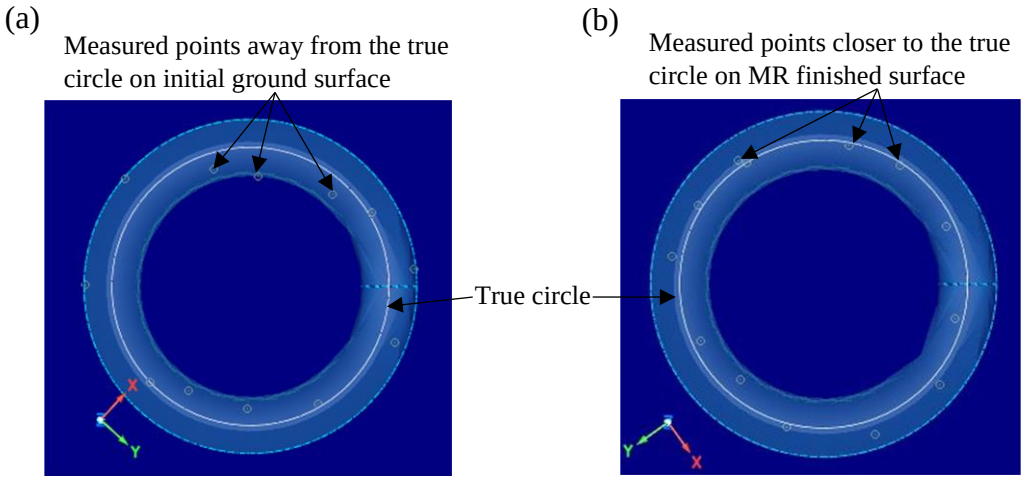

Fig. 6.12 Circularity image of (a) initial ground surface and (b) final MR finished tapered longitudinal surface at T_l = 520 rpm, W_l = 80 rpm, R_l = 16 cm/min, I_l = 2.8 A and G_l = 1mm of the cylindrical blind hole (CBH) type mould cavity using the magnetorheological grinding (MRG) process.

6.1.6 Improvement in functional performance of mould cavity

The fine finished surfaces of the mould cavity is used in the injection moulding process which helps in achieving an improved surface and uniform dimension throughout the cross-sectional area of the end product. The surface roughness affects the wear rate required for the separation of a plastic part from the mould cavity of the injection moulding process as expressed in Eq. (6.7) (Chowdhury, 2010).

$$W_v = \frac{kLt}{R}\left[\frac{R}{Vt}\right]^{-b} \tag{6.7}$$

where W_v is the wear rate (mm^3/sec), t is the time in seconds, V is the sliding velocity, L is the normal load, R is the RMS of the tested surface, b and k are arbitrary constants. Further, Eq. 6.7 is used to find the reaction force which is expressed in Eq. 6.8 (Al-Samarai *et* al., 2012).

$$F_R = \frac{W_v}{V\,W_s} \tag{6.8}$$

where F_R is the reaction force in N, W_v is the wear rate (mm^3/sec) and W_s is the specific wear (mm^3/N-mm). Further, the frictional force (F_f) is directly affected by the coefficient of friction (μ) as expressed in Eq. (6.9).

$$\mu = \frac{F_f}{F_R} \tag{6.9}$$

where F_f is the frictional force in N and F_R is the reaction force that occurs due to surface roughness of the mould and μ is a coefficient of friction.

During the moulding process of the plastic parts, the moulded parts are ejected from the mould cavity with the help of the ejection system. Thus, the ejection force is used to separate the moulded plastic parts from the mould cavity. The ejection force (F_{Ej}) is expressed in Eq. (6.10) (Jones, 2012; Bakharev and Astbury, 2013).

$$F_{Ej} = \frac{E_s A_t \mu \alpha_s \Delta T}{\frac{d}{2t_e}\left(1-\frac{\upsilon_s}{2}\right)} \tag{6.10}$$

where F_{Ej} is the ejection force in N, E_s is the elastic modulus of the end product in N/mm^2, A_t is the total surface area of the end product in contact with the mould cavity in mm^2, α_s is the linear thermal expansion coefficient of the end product in mm/ºC and ΔT is the temperature difference between the temperature molten plastic and solidified end product temperature in ºC. d, t_e, and υ_s are the equivalent diameter in mm, the wall thickness in mm and Poisson's ratio of the material of the end product, respectively. From Eq. (6.10), it is evident that the ejection force is directly proportional to the coefficient of friction. The reduction in the coefficient of friction with reduction

in surface roughness can reduce the ejection force. This further can help in the easy ejection of moulded parts.

Also, if the mould surface is rough, the molten plastic experience greater frictional stress which reduces the flowability on the surfaces of the mould cavity. Hence if the mould surface is finely finished, the resistance offered by the mould surface is low which can lower the frictional stress. This can enhance the flowability of the molten plastic. The frictional stress (τ_f) can be estimated using Eq. (6.11) in Eq. (6.12) (Bergstrom *et* al., 2001).

$$\tau_f = \eta \dot{y} \tag{6.11}$$

$$\tau_f = \frac{F_f}{A_r} \tag{6.12}$$

where τ_f is frictional stress acting on the molten plastic and mould surface, η is the viscosity of molten plastic, $\dot{y}$ is the velocity gradient in the direction of molten plastic flow and A_r is the area of the mould cavity. As the frictional force reduces, there is a reduction in the value of the frictional stress as given in Eq. (6.12). The maximum stress can be calculated using Eq. (6.13) (Bergstrom *et* al., 2001).

$$\sigma_{sm} = \frac{2\,\tau_f L}{R_f} \tag{6.13}$$

where σ_{sm} is the maximum stress on the flow of molten plastic in N/mm^2 and R_f is the radius of the cavity in mm. The magnitude of force F_c acting on the molten plastic due to friction produced by the mould surface can be calculated using Eq. (6.14) (Bergstrom *et* al., 2001).

$$F_c = \sigma_{sm} \pi {R_f}^2 L \tag{6.14}$$

As the magnitude of the force F_c is directly proportional to the maximum stress. Thus, the reduction in the value of μ can reduce the force acting on the flow of the molten plastic (F_c). Hence, the molten plastic can experience low resistance to flow on the surfaces of the blind-hole injection moulds. After the MR finishing process, the surface is finely finished which can allow the molten plastic to flow easily. As it has been seen that the frictional force and the ejection force are influenced by the value of μ. The reduction in the value of the ejection force can help to separate the end product from the mould cavity more easily. The coefficient of friction can also affect the replication quality and life span of the moulds. Also, the improvement in the functional properties like higher load-bearing capacity, ejection force and flowability of the molten plastic in the case of moulds can be achieved with the help of the present developed MR finishing process. Hence, the present advancement in the developed MR finishing process utilizing the MRG tool finds its

greater application in fine finishing the interior tapered longitudinal and flat end surfaces of the EN-31 cylindrical blind-hole (CBH) type industrial applications like permanent moulds used for the manufacturing of the plastic spray bottle cap hoods, containers etc.

6.1.7 Conclusions

The present magnetorheological grinding (MRG) tool-based process is used to finish the internal tapered longitudinal and flat end cylindrical blind hole (CBH) type mould cavities (made up of EN-31 material). Response surface methodology technique with the central composite design is used to find the optimum process parameters and their influence on the percentage reduction in surface roughness is analysed. Further, the process parameters are predicted to effectively finish the surfaces of the EN-31 CBH type mould cavity using the developed MR grinding process. The following conclusions show the effectiveness of the present developed MR finishing process for improving the quality of the CBH type mould cavities after fine finishing.

- The regression analysis with the response surface methodology reveals that the optimized concentration of the abrasives and electrolytic iron particles (EIPs) as 19% and 26%, respectively with the concentration of base fluid as 55% in MR polishing fluid proved higher percentage reduction in the surface roughness on the EN-31 material using the MRG tool.

- The effective MR finishing is achieved over interior tapered longitudinal surface of the EN-31 CBH type mould cavity using the predicted optimum parameters such as the rotational speed of the mould cavity, current, working gap, tool rotational and reciprocation speed are 80 rpm, 2.8 A, 1 mm, 520 rpm and 16 cm/min with the present MRG process. Further, the same MRG process is found effective for fine finishing the flat end surface of the EN-31 CBH type mould cavity utilizing the predicted optimized parameters as 100 rpm, 2.5 A, 0.9 mm, 1050 rpm and 18 cm/min respectively.

- The percentage reduction in surface roughness achieved over the interior tapered longitudinal (1595 sq. mm) and flat end (254 sq. mm) surfaces of the CBH type mould cavity using the MRG tool is 77.14% after 100 min and 84.37% after 60 min respectively. Further, the finishing rate found on both the surfaces of the CBH type mould cavity is 2.7

nm/min and 4.5 nm/min, respectively. These results describe that the surface roughness decreases significantly after MR finishing with the present MRG tool.

- The SEM images and photographs reveal that a smooth tapered longitudinal and flat end surfaces of the CBH type mould cavities are achieved after the MR finishing utilizing the MRG tool. This smoothness in surface characteristics describe the enhancement in CBH type mould cavity surfaces.

- The improvement in the image obtained through circularity test performed over the tapered longitudinal surface of the CBH type mould cavity reveals that the dimensional accuracy is achieved after MR finishing using the present MRG process.

- The overall results reveal the usefulness of the MR finished CBH type mould cavity for improving the efficacy of the injection moulding process and enhance the surface quality of the end products.

6.2 Parametric investigation for fine finishing of the typical tapered mold cavity for light covers using the newly developed magnetorheological grinding (MRG) tool-based process

In aviation industry, the lights provide visual guidance for the pilots to land, taxi, and take off at the airport. These lights are classified as approaching light systems, landing area lights, runway lights, obstruction, and taxiway lights based on their use at the airport. As these lights serve various purposes at the airport, so lights (ground runway lights) should be visible from an optimum distance. Also, the lighting system should not be bulky (Ji *et* al., 2012; Mahtab, 2015). To fulfill this requirement, the surface of the light cover should be clear and defect-free so that uniform light can spread outwards from the cover surface with minimum energy losses. So, the traditional lights utilizing the bulky glass cover are replaced with a cover made up of polycarbonate material (Ji *et* al., 2012). As these covers are made up of polycarbonate material, so the processes used for their manufacturing are the thermoforming and injection moulding process (Mahtab, 2015). The thermoforming and injection moulding processes provide benefits such as utilization of maximum material, easy production of complicated geometric products, low cost of production, precise and accurate parts (Acker *et* al., 2016; Singh and Singh, 2019b; Murthy and Rao, 2017). Considering these advantages of the thermoforming and injection moulding process, tool steel is generally used as mould material after tempering up to maximum hardness. After attaining these properties by the tool steel mould, it has sufficient toughness to withstand loading (Marashi *et* al., 2017). So, in

the present work, H13 tool steel is used as mould material because it offers high-temperature resistance, high corrosion resistance, and high wear resistance (Marashi *et* al., 2017). The moulds with fine finished surfaces have a direct impact on the final product's appearance and efficacy (Shiou and Chen, 2003). The reduction in microcracks, residual stresses, and friction can improve mould cavity efficiency and can provide prolonged operating life (Mennig and Stoeckhert, 2013; Jain *et* al., 2017). Also, because of the reduced friction between both the surfaces of the cylindrical blind hole (CBH) type mould cavity and the plastic melt, the plastic parts can be ejected more easily. Therefore, to deal with limitations involved in traditional process while finishing the (CBH) type mould cavity, the present developed magnetorheological grinding (MRG) tool-based finishing process is utilized.

Further, to fulfill the finishing requirement of the H13 typical CBH type mould cavity, the present MR grinding (MRG) tool is employed. As the MR grinding process is newly developed, so the best process parameters are predicted (response surface methodology (RSM) for the inner tapered longitudinal (TL) and flat end surfaces of the CBH type mould cavity made up of the H13 material. For predicting the best process parameters, the RSM technique is employed in the proposed work for effective fine finishing on both the surfaces of the H13 CBH type mould cavity. The obtained predicted best parametric conditions are used in final experimentation for effective fine finishing on both surfaces of the CBH type mould cavity. In addition, the surface roughness profile and surface characteristics are examined to investigate the improvement in the surfaces of the H13 CBH type mould cavities. These results present that this approach may help in enhancing the mould life and improving the surface quality of end products (light covers) produced using H13 CBH type mould cavities.

6.2.1 Materials and Methods

6.2.1.1 Selection of material and workpiece preparation

Injection moulding of plastic parts is one of the prominent processes of the manufacturing industry (Maan *et* al., 2017). These moulds may be used to make plastic parts such as covers of lights used in automobile components, communication technology parts, aviation industry, medical and electronics parts (Mahtab, 2015). According to the society of plastic industries, a permanent mould can manufacture 100,000 components after surface finishing in its service life (Martínez-Mateo *et*

al., 2011). Permanent moulds used in the manufacturing industry are made of very hard and durable material. Also, the moulds require a material that has high strength at elevated temperatures, wear-resistance, and is cost-efficient (Mazur *et* al., 2017). Because of these properties of the permanent mould material, the mold's working life is extended. Owing to these properties, the H13 material is chosen for experimentation which is used for making the typical cylindrical blind hole (CBH) type mould cavity.

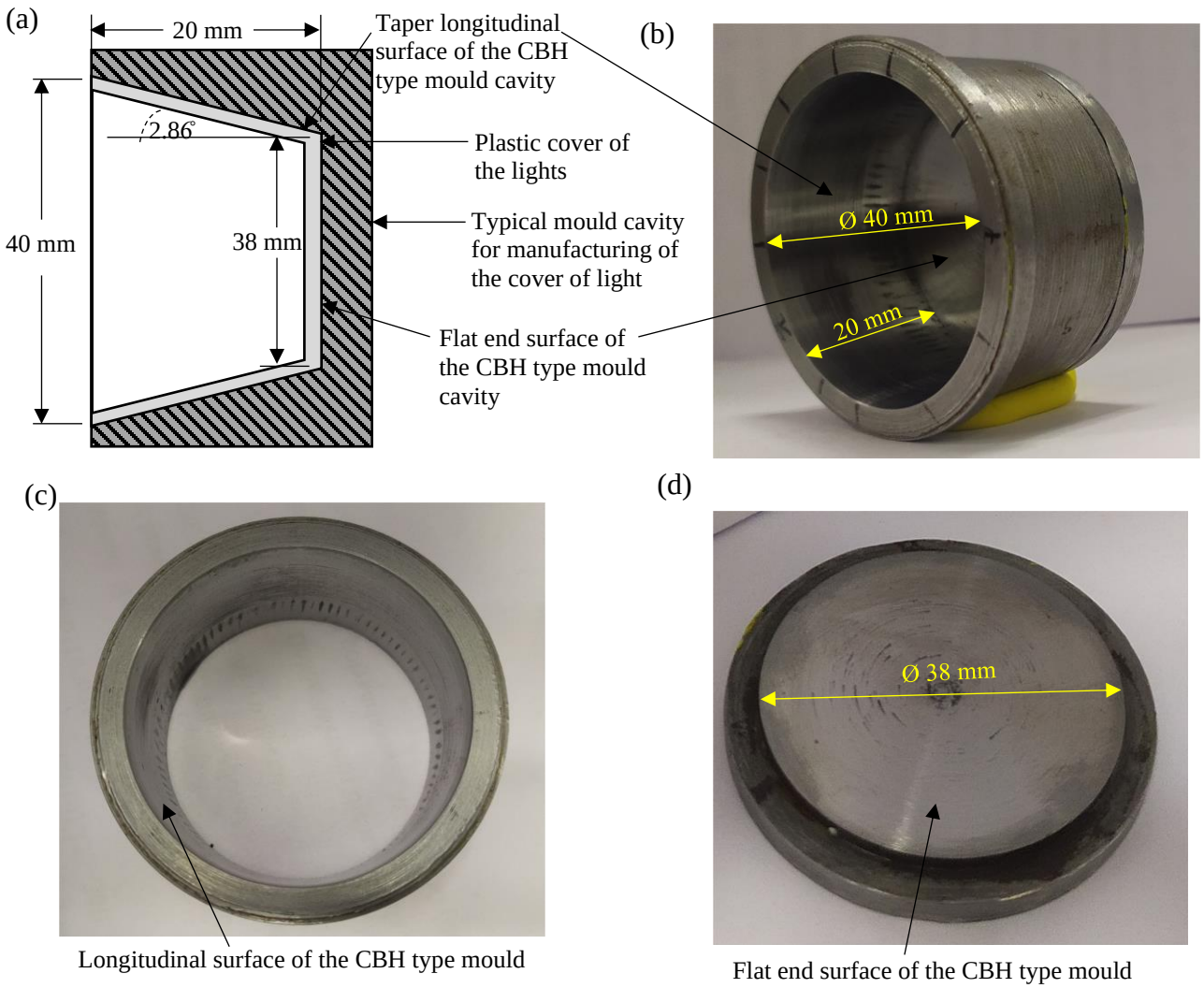

Fig. 6.13 (a) Schematic diagram, (b) actual image of the typical cylindrical blind hole (CBH) type mould cavity, along with (c) the tapered longitudinal surface, and (d) flat end surface for making cover of lights (made-up of plastic part).

Table 6.10 presents the chemical composition of AISI H13 steel (Yang and Zhang, 2004). The Vickers hardness value of the AISI H13 steel ranges from 424 to 549 HV (Chana and Singh, 2019).

Owing to the hardness of the H13 steel, properties like wear resistance, and sufficient toughness are attained (Guo and Liu, 2002). The specifications of the H13 typical mould cavity are used in this work for fine finishing with the present magnetorheological grinding tool is shown in Fig. 6.13 (a). The open-end diameter of the typical mould cavity is 40 mm, while the diameter towards the flat end surface of the CBH type mould cavity is 38 mm. This tapered mould cavity has a depth of 20 mm. In Fig. 6.13, a taper angle of 2.86 degrees can be seen in the schematic diagram of the mould cavity. The image of the typical CBH type mould cavity can be observed from Fig. 6.13(b). Further, the images of the tapered longitudinal surface and flat end surface of the typical CBH type mould cavity can be espied in Figs. 6.13 (c) and (d).

For the design of experiments, the dimensions of the manufactured samples for the tapered longitudinal (TL) is having a diameter at the open end as 40 mm and towards the flat end as 39 mm diameter with a height of 10 mm. Further, for the flat end surfaces of the CBH type mould cavity, the diameter of the manufactured samples is 38 mm. With the help of the grinding process, these samples are finished to the initial surface roughness value.

The initial surface roughness value is then determined using the Mitutoyo SJ 400 surface roughness measuring instrument over the TL and flat end surfaces of the CBH type samples. For measuring the surface roughness value, the cut-off length used is 0.25 mm with a gaussian filter. The measured initial surface roughness values over the TL surface of the samples are in the range of 390 to 470 nm, while the flat end surface of the CBH type mould cavity is in the range of 300 to 360 nm.

Table 6.10. Chemical composition of the AISI H13 steel (Yang and Zhang, 2004).

Elements	Composition (%)
Carbon	0.36
Chromium (Cr)	5.7
Molybdenum (Mo)	1.6
Silicon (Si)	0.8
Manganese (Mn)	0.2
Vanadium (V)	1.1

6.2.2 Experimental setup

The cylindrical blind hole (CBH) type mould cavity's internal tapered longitudinal (TL) and flat end surfaces can be fine finished using the magnetorheological grinding (MRG) experimental

setup as espied in Fig. 6.14 (a). To mate the longitudinal surface of the MRG tool with the TL surface of the CBH type mould cavity, the height adjustment system and the rotating vise is used.

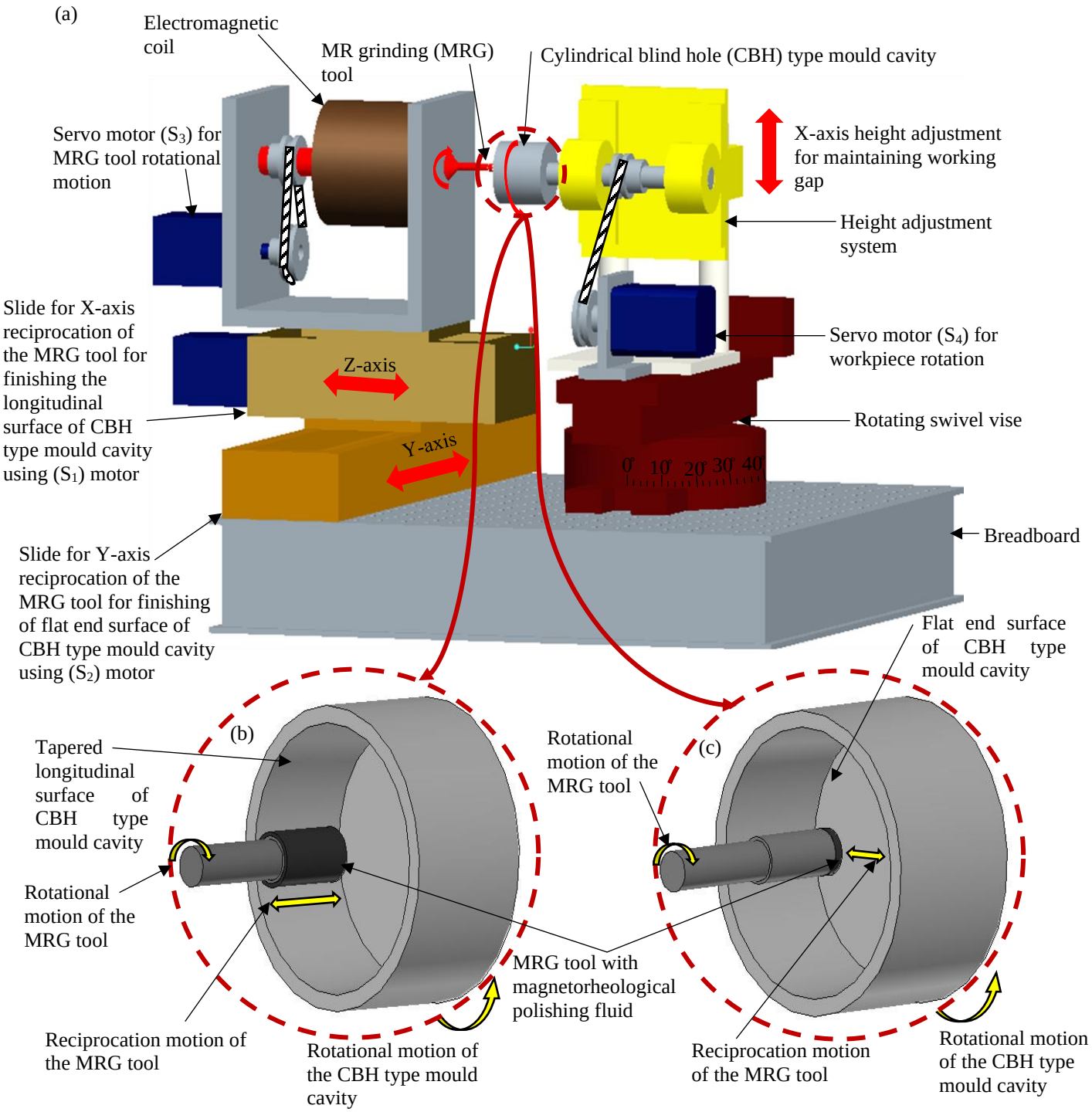

Fig. 6.14 (a) CAD model of the magnetorheological grinding (MRG) experimental setup used for the finishing of typical cylindrical blind hole (CBH) type mould cavity for light covers having (b) tapered longitudinal surface, and (c) flat end surface.

After mating the MRG tool with the CBH type mould cavity can be espied through the CAD model in Fig. 6.14 (b). This contributes to a uniform working gap between the longitudinal surface of the MRG tool and the TL surface of the CBH type mould cavity, resulting in uniform magnetic flux density. Owing to uniform magnetic flux density, even finishing can be achieved over the entire TL surface of the CBH type mould cavity. Further, the vise is rotated to its initial position (0̊) which helps in fine finishing the flat end surface of the CBH type mould cavity as can be observed in Fig. 6.14 (c). Later, the controlled direct current (DC) power supply is used to provide the current to the electromagnetic coil. Direct current is supplied to the copper coil for the magnetizing tool core after the experimental setup for fine finishing of the CBH type mould cavity. The copper coil produces heat during the magnetization of the tool core due to the flow of current through it. The coolant that flows through the bobbin containing the electromagnetic coil regulates the heat.

Further, in the MR finishing (MRF) process, the composition of the MRP fluid plays a critical part. The rheological properties of MRP fluid decide the capability of MRF processes (Jain, 2009, Yan *et* al., 2007). As H13 material is used for the mould cavity workpiece. So, from the literature, the composition of the MRP fluid is considered. Thus, the MRP fluid comprises 30 % volume concentration (VC) of EIPs, 15 % VC of abrasive particles (silicon carbide), and 55 % VC of carrier fluid (80 % paraffin and 20 % AP3 grease). The mesh size of EIPs used is 400 and that of the abrasive particles is 800 (Chana and Singh, 2019). This concentration of the MRP fluid is utilized to fine finish the TL and flat end surfaces of the H13 typical CBH type mould cavity using the present magnetorheological grinding (MRG) tool.

Next, the Taguchi optimization technique was used to examine the finishing process parameters on the H13 die steel for the mould cavity used for making light covers. The magnetic force is proportional to the current ($I_{l,f}$) intensity to finish the tapered longitudinal (TL) and flat end surfaces of the cylindrical blind hole (CBH) type mould cavity. The tangential shear force acting via active abrasive particles on the workpiece surface is governed by the rotational speed of the MRG tool surface ($T_{l,f}$) and the workpiece surface ($W_{l,f}$). The axial force exerted upon the active abrasive particles is controlled by the reciprocating speed of the MRG tool ($R_{l,f}$). The finishing process parameters are selected based on the literature (Chana and Singh, 2019). Further for range selection of the process parameters required to fine finish the TL and flat end surfaces of the CBH type mould cavity using the MRG process, preliminary experiments need to be performed. To perform the preliminary experiments, the initial surface roughness values are recorded and

reported in Tables 6.11 and 6.12. Further, the preliminary experiments the composition of the MRP fluid as 30 % VC of EIPs, 15 % VC of abrasive particles, and 55 % VC of carrier fluid.

Table 6.11 Initial trials and their results for selecting the suitable process parameters for the MR finishing of the tapered longitudinal surface of the CBH type mould cavity.

S. No.	Parameters				Surface roughness value	
	Tool rotational speed, T_l (rpm)	Tool reciprocation speed, R_l (cm/min)	Workpiece rotation speed, W_l (rpm)	Current, I_l (A)	Initial Ra_i (nm)	Final Ra_f (nm)
1	200	10	30	3	390	300
2	200	15	90	2	430	320
3	300	20	45	3.5	460	390
4	500	25	60	0.5	410	330
5	800	5	75	1	420	340

Table 6.12 Initial trials and their results for selecting the suitable process parameters for the MR finishing of the flat end surface of the CBH type mould cavity.

S. No.	Parameters				Surface roughness value	
	Tool rotational speed, T_f (rpm)	Tool reciprocation speed, R_f (cm/min)	Workpiece rotation speed, W_f (rpm)	Current, I_f (A)	Initial Ra_i (nm)	Final Ra_f (nm)
1	300	10	150	3.0	340	290
2	700	25	70	1.0	350	280
3	1100	35	30	1.5	300	230
4	2000	30	90	2.0	310	280
5	1500	15	120	3.5	330	270

During the experiment, the working gap is another finishing process parameter that is kept constant at 0.6 mm for each trail. After preliminary experiments are performed for 20 min over each sample, the final roughness values are reported in Tables 6.11 and 6.12 for the finishing of the TL and flat end surfaces of the CBH type workpiece, respectively. So, based on this preliminary experimentation, the range for the process parameters is selected and is reported in Tables 6.13 and 6.14.

Table 6.13 Experimental process parameters and their range for finishing the tapered longitudinal surface of the cylindrical blind hole type mould cavity.

S. No.	Parameters	Units	Range		
1	Tool rotational speed (T_l)	rpm	200	500	800
2	Tool reciprocation speed (R_l)	cm/min	5	15	25
3	Workpiece rotation speed (W_l)	rpm	30	60	90
4	Current (I_l)	A	0.5	2.0	3.5

Table 6.14 Experimental process parameters and their range for finishing the flat end surface of the cylindrical blind hole type mould cavity.

S. No.	Parameters	Units	Range		
1	Tool rotational speed (T_f)	rpm	400	1000	1600
2	Tool reciprocation speed (R_f)	cm/min	15	25	35
3	Workpiece rotation speed (W_f)	rpm	70	100	130
4	Current (I_f)	A	1.5	2.5	3.5

Further, to attain the optimum process parameters for finishing the tapered longitudinal and flat end surfaces of the cylindrical blind hole (CBH) type workpiece using the MRG tool, the Taguchi technique is utilized. It suggests a plan of experiments by using the highly fractional factorial orthogonal design with factors in column and treatments combinations in rows. Using the Taguchi technique, the optimum parameters can be obtained for fine finishing the mould cavity workpiece surfaces. The larger the better method is opted to evaluate the best combination of the finishing process parameters. The L27 orthogonal array is used to investigate the effects of 4 parameters, each of which has 3 levels. Signal to noise (S/N) ratio which are log functions of the desired output serves as an objective function for optimization. The plot between the mean of the response and the finishing process parameters is obtained using the S/N ratio and the larger the better technique. In the generated L27 orthogonal array, 27 parametric combinations are made. The experimentation is performed over the TL surface each for 60 min of finishing time. But on the flat end surface, the finishing is performed for 40 min of finishing time. The experimentation on each sample is performed in sets for 20 min each.

The average of the surface roughness value is obtained for three trials. For each combination, three roughness values (Ra_1, Ra_2, Ra_3) are recorded using Mitutoyo SJ 400 roughness measurement instrument as reported in Tables 6.15 and 6.16. For measuring the surface roughness value, the cut-off length used is 0.25 mm with gaussian filter. The average of the three-surface roughness values (Ra_1, Ra_2, Ra_3) is calculated and reported in Tables 6.15 and 6.16. This average of surface

roughness value is utilized to obtain the percentage reduction in surface roughness (*%ΔRa*) as calculated using Eq. (6.15).

$$\%\Delta Ra = \left(\frac{Ra_i - Ra_f}{Ra_i}\right) \times 100 \quad (6.15)$$

where R_{ai} is the initial surface roughness before MR finishing in nm and R_{af} if the final surface roughness after MR finishing in nm. Tables 6.15 and 6.16 report the experimental plan and response values for the TL and flat end surfaces of the CBH type mould cavity.

Table 6.15 Experimental plan and its response for finishing the tapered longitudinal surface of the cylindrical blind hole type mould cavity.

S. No.	Tool rotational speed (T_l), rpm	Tool reciprocation speed (R_l), cm/min	Workpiece rotation speed (W_l), rpm	Current (I_l), A	Initial surface roughness, Ra_i in nm	Surface roughness value in nm			Avg. Ra_f	*%ΔRa*
						Ra_1 (nm)	Ra_2 (nm)	Ra_3 (nm)		
1	200	5	30	0.5	390	240	230	210	226.67	41.88
2	200	5	30	0.5	410	230	250	220	233.33	43.09
3	200	5	30	0.5	440	250	240	230	240.00	45.45
4	200	15	60	2.0	420	160	180	170	170.00	59.52
5	200	15	60	2.0	400	150	170	160	160.00	60.00
6	200	15	60	2.0	430	160	180	150	163.33	62.02
7	200	25	90	3.5	460	270	250	280	266.67	42.03
8	200	25	90	3.5	440	260	270	260	263.33	40.15
9	200	25	90	3.5	430	250	240	220	236.67	44.96
10	500	5	60	3.5	410	230	220	200	216.67	47.15
11	500	5	60	3.5	470	270	250	260	260.00	44.68
12	500	5	60	3.5	390	200	220	210	210.00	46.15
13	500	15	90	0.5	400	190	170	180	180.00	55.00
14	500	15	90	0.5	430	200	180	190	190.00	55.81
15	500	15	90	0.5	460	210	190	230	210.00	54.35
16	500	25	30	2.0	440	230	220	220	223.33	49.24
17	500	25	30	2.0	470	220	240	250	236.67	49.65
18	500	25	30	2.0	460	210	230	220	220.00	52.17
19	800	5	90	2.0	450	260	250	270	260.00	42.22
20	800	5	90	2.0	420	230	240	250	240.00	42.86

21	800	5	90	2.0	410	250	230	260	246.67	39.84
22	800	15	30	3.5	390	170	140	160	156.67	59.83
23	800	15	30	3.5	440	180	190	170	180.00	59.09
24	800	15	30	3.5	470	200	220	210	210.00	55.32
25	800	25	60	0.5	420	240	210	230	226.67	46.03
26	800	25	60	0.5	430	220	210	240	223.33	48.06
27	800	25	60	0.5	460	230	240	260	243.33	47.10

Table 6.16 Experimental plan and its response for finishing the flat end surface of the cylindrical blind hole type mould cavity.

S. No.	Tool rotational speed (T_f), rpm	Tool reciprocation speed (R_f), cm/min	Workpiece rotation speed (W_f), rpm	Current (I_f), A	Initial surface roughness, Ra_i in nm	Surface roughness value in nm			Avg. Ra_f	$\%\Delta Ra$
						Ra_1 (nm)	Ra_2 (nm)	Ra_3 (nm)		
1	400	15	70	1.5	340	190	180	200	190.00	44.12
2	400	15	70	1.5	300	170	160	180	170.00	43.33
3	400	15	70	1.5	360	210	220	200	210.00	41.67
4	400	25	100	2.5	320	160	170	150	160.00	50.00
5	400	25	100	2.5	350	180	160	170	170.00	51.43
6	400	25	100	2.5	310	160	150	130	146.67	52.69
7	400	35	130	3.5	360	190	210	180	193.33	46.30
8	400	35	130	3.5	330	170	190	160	173.33	47.47
9	400	35	130	3.5	320	190	160	180	176.67	44.79
10	1000	15	100	3.5	350	150	130	110	130.00	62.86
11	1000	15	100	3.5	340	110	120	130	120.00	64.71
12	1000	15	100	3.5	300	100	130	90	106.67	64.44
13	1000	25	130	1.5	360	150	160	140	150.00	58.33
14	1000	25	130	1.5	320	110	140	130	126.67	60.42
15	1000	25	130	1.5	350	140	130	160	143.33	59.05
16	1000	35	70	2.5	310	130	140	100	123.33	60.22
17	1000	35	70	2.5	340	150	120	140	136.67	59.80
18	1000	35	70	2.5	360	140	150	160	150.00	58.33
19	1600	15	130	2.5	320	190	170	150	170.00	46.88
20	1600	15	130	2.5	350	160	200	180	180.00	48.57

21	1600	15	130	2.5	330	180	170	190	180.00	45.45
22	1600	25	70	3.5	340	160	200	170	176.67	48.04
23	1600	25	70	3.5	300	190	170	150	170.00	43.33
24	1600	25	70	3.5	310	200	160	170	176.67	43.01
25	1600	35	100	1.5	320	160	180	190	176.67	44.79
26	1600	35	100	1.5	350	200	170	180	183.33	47.62
27	1600	35	100	1.5	330	180	160	190	176.67	46.46

Further, the Mitutoyo SJ 400 instrument is also used for measuring the waviness with cut off length as 0.8 mm. Next, the circularity is investigated using the Accurate coordinate measuring machine (CMM).

6.2.3 Results and discussion

The larger the better approach was used to forecast the best finishing process parameter combination for completing the tapered longitudinal and flat end surfaces of the CBH type mould cavity with the MRG process. Figures 5 (a) and (b) show the mean S/N ratio for each parameter conditions. For the maximum response value, the parameter value with the highest S/N ratio is selected. The maximum response value of the percentage reduction in surface roughness (*%ΔRa*) is determined by the larger S/N ratio.

6.2.3.1 Effect of finishing process parameters

In MR finishing of the CBH type mould cavity, the effect of finishing process parameters such as the rotational speed of the mould cavity, current, rotational, and reciprocation speed of the MRG tool is investigated. In the MR finishing process, each process parameter has its own contribution in finishing the surfaces of the CBH type mould cavity. The effect of each process parameter can be espied in Figs. 6.15 (a) and (b) for the tapered longitudinal (TL) and flat end surfaces of the H13 CBH type workpiece, respectively.

The source of the tangential shear force is the rotational speed of the MRG tool ($T_{l,f}$) over the oppositely rotating CBH workpiece which helps to govern the relative motion of the active abrasive particles (AAPs). These AAPs during their rotational motion over the rotating TL and flat end surfaces helps in shearing the asperities. It can be observed from Figs. 6.15 (a) and (b), the rotation speed of the MRG tool (200 rpm) over the TL and 400 rpm of the flat end surfaces of the CBH type workpieces, respectively present that the graph is on the lower side. But as the values of the rotational speed of the MRG tool increases up to 500 rpm and 1000 rpm, the graph attains

the maximum value. The shearing of the asperities is increased owing to the upsurge in relative motion between the AAPs and the CBH type mould cavity surfaces. But on further increase in the value of the rotational speed of the MRG tool, the graph presents reduction. This reduction in the graph after attaining level 3 (800 rpm on longitudinal surface and 1600 rpm on flat end surface) may be due to the higher tangential force which may reduce the indentation force of the AAPs of magnetorheological polishing (MRP) fluid on the finishing surface of the workpiece. Owing to the reduction of the indentation force, the AAPs find it ineffective to fine finish both the surfaces of the CBH type workpiece.

Further, a similar trend of the graph can be observed for the tool reciprocation speed ($R_{l,f}$) over the tapered longitudinal (TL) and flat end surfaces of the CBH type mould cavity using the present MRG process as shown in Figs. 6.15 (a) and (b). The maximum value of the S/N ratio can be observed at level 2 (i.e., 15 cm/min on the TL surface and 25 cm/min on the flat end surface) of the MRG tool reciprocation speed. At level 1 of the MRG tool reciprocation speed, the number of passes over the CBH type mould cavity surfaces is too low that the asperities are not sheared off completely. But as the MRG tool reciprocation speed increases to 15 cm/min over the TL surface and 25 cm/min over the flat end surface of the CBH type workpiece, the S/N ratio is higher. This higher S/N ratio is owing to the uniform removal of asperities from the TL and flat end surfaces of the CBH type mould cavities. On further increasing the MRG tool reciprocation speed to level 3, the MRP fluid column is disturbed. Thus, resulting in less interaction of the AAPs with the asperities over the CBH type workpiece surface. Thus, the predicted optimum MRG tool reciprocation speed is 15 cm/min for the TL surface and 25 cm/min for flat end CBH type mould cavity surface. Initially, the rotational speed of the CBH type mould cavity for the longitudinal surface is 30 rpm and for the flat end surface is 70 rpm. But the increase in trend can be observed in Figs. 6.15 (a) and (b), owing to the increase in the rotational speed of the CBH type mould cavity. This is owing to the increase in the relative motion of the AAPs to collide with the asperities present over the TL and flat end surfaces of the CBH type mould cavity. On further upsurge in the rotational speed of the CBH type mould cavity, the relative motion becomes so high that the AAPs become incapable to shear off the asperities. This is owing to the distortion of the MRP fluid column. Thus, the predicted optimum rotation speed of the CBH type mould cavity for the tapered longitudinal (TL) surface is 60 rpm and for the flat end surface is 100 rpm. Next, the magnetic field in this MR finishing process is controlled by the current ($I_{l,f}$).

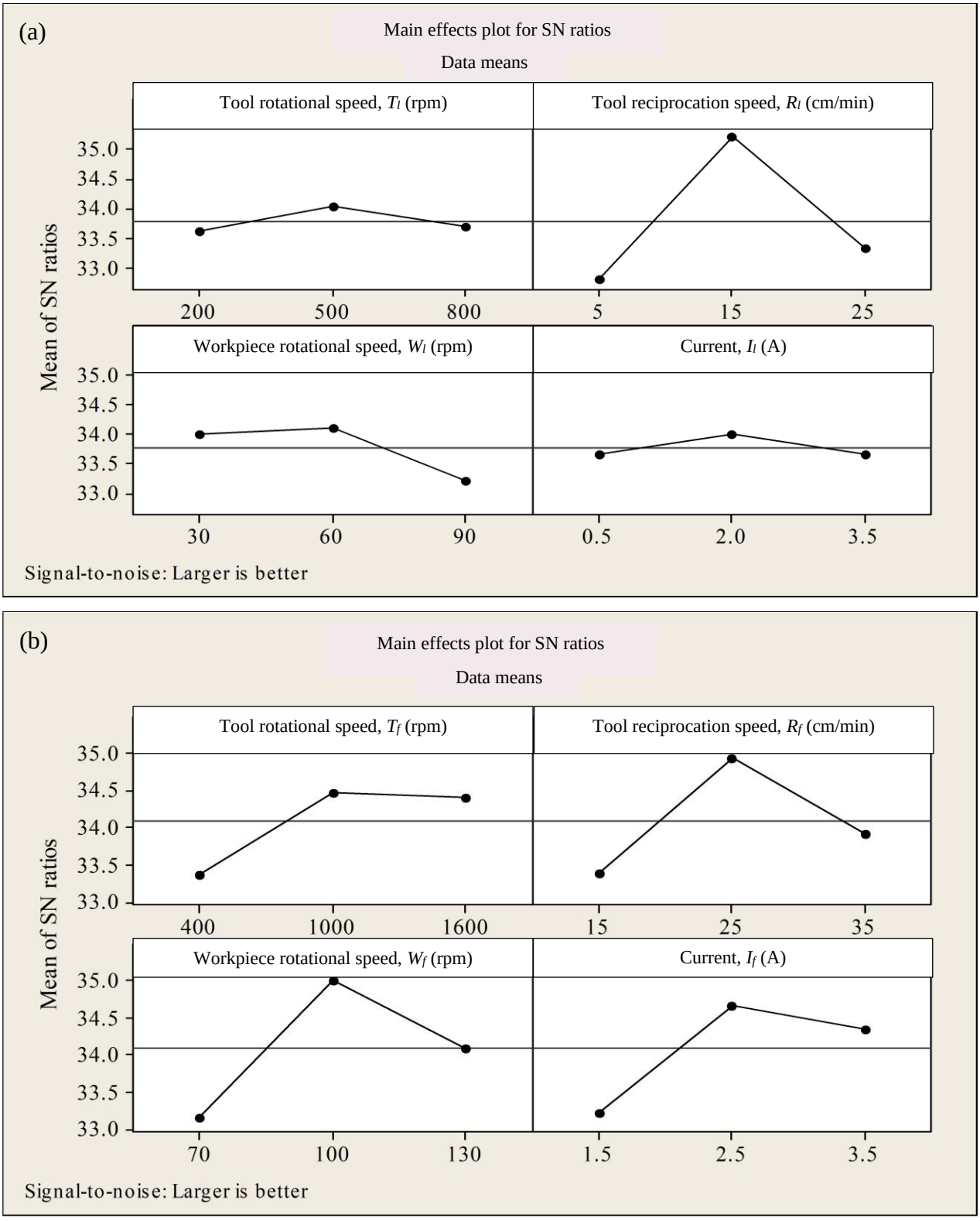

Fig. 6.15 Plot of the mean of S/N ratio with the different finishing parameters using larger the better technique after the MR finishing of typical mould cavity for the light cover having (a) tapered longitudinal and (b) flat end surfaces.

From Figs. 6.15 (a) and (b), it can be observed that the value of current for the longitudinal and flat end surfaces of the CBH type mould cavity are 0.5 A and 1.5 A, respectively. These values present, low S/N ratio as compared to levels 2 and 3. This may be owing to the less magnetic field produced within the working gap resulting in less gripping of AAPs over the finishing surfaces of the workpiece. On further increasing the values of current to 2 A and 2.5 A for the TL surface and flat end surface, the AAPs are gripped strongly. Thus, this results in an increase of response trend in the graph as shown in Figs. 6.15 (a) and (b). When the value of current reaches 3.5 A for both the surfaces of the CBH type mould cavity, the generated magnetic field is high. Owing to this high magnetic field the AAPs indent more over the CBH type mould cavity surfaces. This causes the deformation of the surface causing a decrement in the improvement of surface roughness value. Thus, the predicted optimum value of current is 2 A for the TL surface and 2.5 A for the flat end surface of the CBH type mould cavity surface.

Finally, the predicted optimum process parameters for the finishing of TL surface of the H13 CBH type mould cavity are rotational speed as 60 rpm, current of 2 A, rotational and reciprocation speed of the MRG tool as 500 rpm and 15 cm/min, respectively. Further, the predicted optimum process parameters for the finishing of the flat end surface of the H13 CBH type mould cavity are rotational speed of CBH type mould cavity as 100 rpm, current of 2.5 A, rotational and reciprocation speed of the MRG tool as 1000 rpm and 25 cm/min, respectively. These predicted best optimum process parameters found over both the surfaces of the H13 CBH type mould cavity is used to perform the final experimentation and the results are obtained in the form of surface roughness value, surface roughness profile, optical microscope images, and mirror images. Also, circularity and waviness are conducted over the TL surface to check the dimensional accuracy.

6.2.3.2 Observation of surface roughness on tapered longitudinal CBH type mould cavity

Further, the optimal process parametric combination for the tapered longitudinal (TL) surface of the H13 cylindrical blind hole (CBH) type mould cavity is predicted as the current of 2 A, CBH type workpiece mould cavity rotational speed of 60 rpm, MRG tool rotational speed and reciprocation speed are 500 rpm and 15 cm/min, respectively. The experiments were carried out on the longitudinal surface of the CBH type mould cavity (Fig. 6.13) for 140 min using these selected best parametric conditions. During the MR finishing, the surface roughness parameters as the average surface roughness (R_a), maximum height of the roughness value (R_q), the root mean square roughness value (R_z) values were recorded every 20 min as shown in Fig. 6.16 (a). It can

be observed from Fig. 6.16 (a) that the reduction in surface roughness is more in the initially finishing cycles. From this reduction in surface roughness, it is evident that the shearing out of the steep roughness peaks requires less cutting shear force. The sharpness of the roughness peaks is reduced and the shear area is enhanced in subsequent finishing cycles.

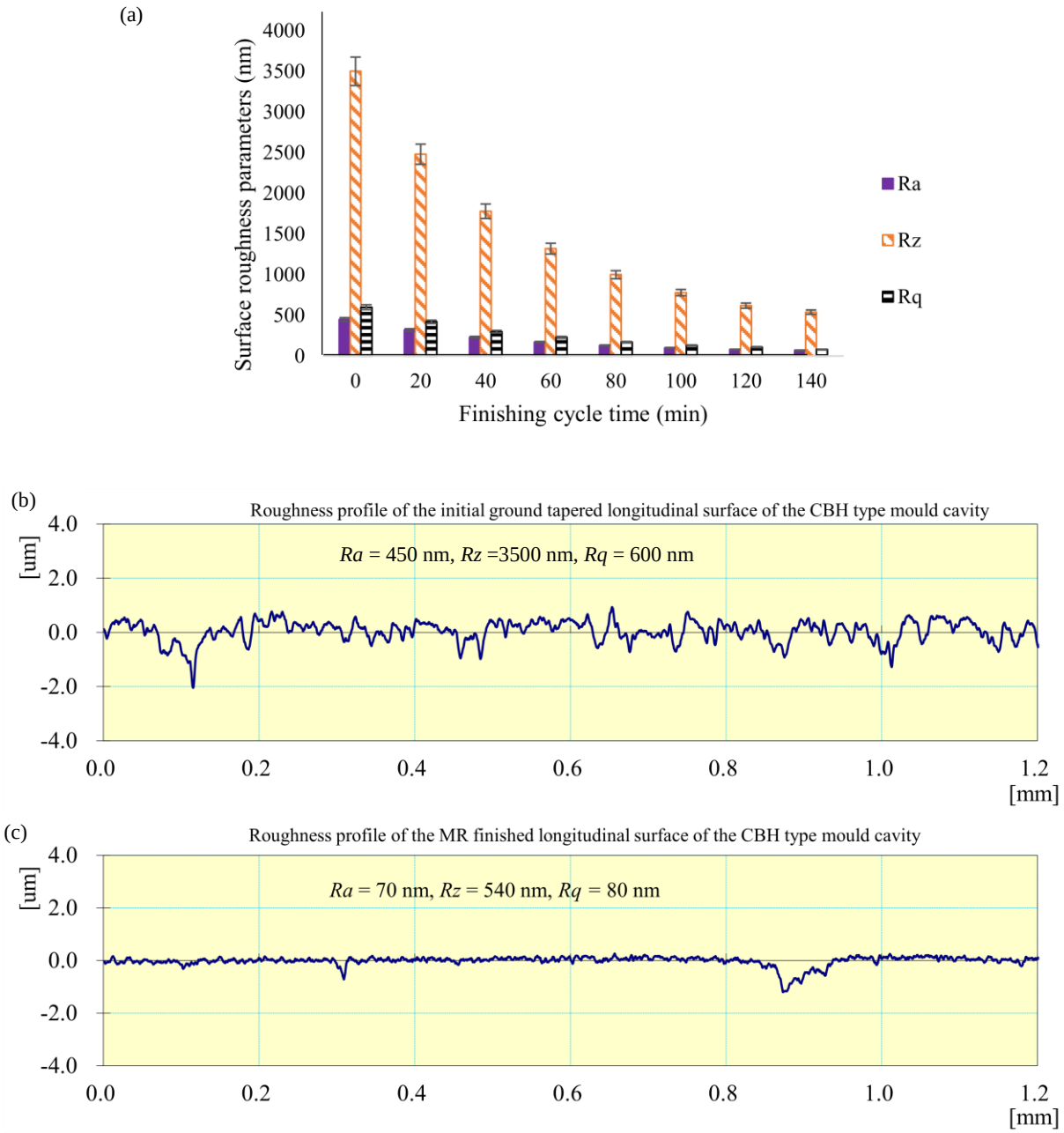

Fig. 6.16 (a) Reduction in surface roughness values at different finishing cycle time, surface roughness profiles of the (b) initial, (c) final MR finished tapered longitudinal surface of the typical mould cavity for the light cover after 140 min of the MR grinding process.

As a result, greater shearing force is required to shear off the roughness peaks. With the present MR finishing process utilizing the MRG tool, the R_a value was reduced from an initial ground value of 450 nm to 70 nm in 140 min of finishing time. The other roughness parameters after the MR finishing process such as R_z and R_q were lowered from original values of 3500 nm and 600 nm to 540 nm and 80 nm in 140 min of finishing time over the TL surface area of 2453 sq. mm of the cylindrical blind hole type mould cavity (Fig. 6.13). The percentage reduction in surface roughness (*%ΔRa*) is obtained as 84.44 % over the TL surface of the H13 CBH type mould cavity. The roughness profiles of the initial ground and MR finished TL CBH type workpiece surfaces are espied in Figs. 6.16 (a) and (b), respectively. It can be observed from Fig. 6.16 (b) that there is huge variation in the initial surface roughness profile from the centerline. But after MR finishing with the present developed MRG tool-based process, the variation in the final surface roughness profile is reduced. On comparing the initial surface roughness profile in Fig. 6.16 (b) and the final surface roughness profile in Fig. 6.16 (c), the improvement in surface finish can be observed

6.2.3.3 Observation of surface roughness on flat end CBH type mould cavity

After finishing over the tapered longitudinal (TL) CBH type mould cavity surface, the finishing is performed over its flat end surface while using the same MRG tool. For the flat end surface, the optimal process parametric combination is used as the current of 2.5 A, CBH type workpiece mould cavity rotational speed of 100 rpm, MRG tool rotational speed of 1000 rpm, and reciprocation speed of 25 cm/min, respectively. The experiments were carried out on the flat end surface of the CBH type mould cavity (Fig. 6.13) for 80 min using the selected best parametric conditions. After each 20 minutes of finishing time, the surface roughness values of the flat end surface of the CBH type mould cavity are recorded. The reduction in surface roughness value over the flat end CBH type mould cavity surface can be observed from Fig. 6.17 (a). In Fig. 6.17 (a), a similar trend (higher shearing out of the steep roughness peaks in initial finishing cycles) can be observed over the flat end surface of the CBH type mould cavity. Further, with the present MR finishing process after 80 min of finishing time, the initial ground average surface roughness (R_a) value was lowered from 320 nm to 60 nm. The other roughness parameters like the root mean square value (R_q) and the maximum height of the roughness value (R_z) was lowered from original values of 420 nm and 2500 nm to 70 nm and 450 nm, respectively. The *%ΔRa* is attained as 81.25 % over the flat end surface of the H13 typical CBH type mould cavity with surface area 1134 sq. mm. Further, the roughness profiles obtained over the initial ground and final MR finished flat end

CBH type mould cavity surface are compared from Fig. 6.17 (b) and (c). It can be espied that the variation in the final roughness profile (Fig. 6.17 (c)) obtained over the MR finished flat end CBH type mould cavity surface is reduced.

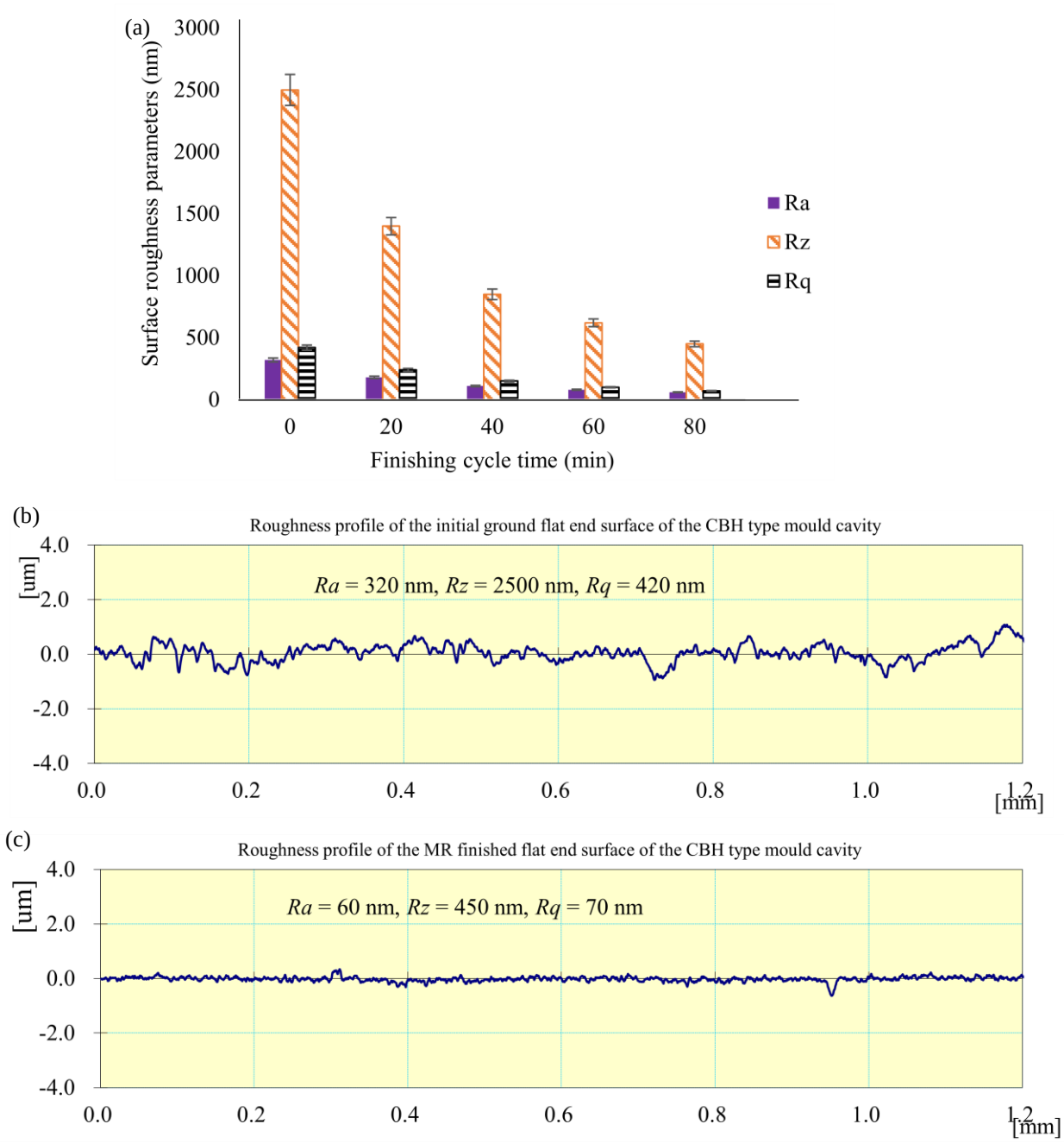

Fig. 6.17 (a) Reduction in surface roughness values at different finishing cycle time, surface roughness profiles of the (b) initial, (c) final MR finished flat end surface of the typical mould cavity for the light cover after MR finishing with magnetorheological grinding process in 80 min of finishing time.

So, the reduction in surface roughness parameter values and the improvement in surface roughness profile demonstrate that the TL and flat end CBH type mould cavity surfaces are significantly improved owing to the MRG process. So, the reduction in surface roughness parameter values and the improvement in surface roughness profile represent that the present MRG tool is capable of fine finishing the TL and flat end surfaces of the CBH type mould cavity for light covers.

6.2.3.4 Observation of surface characteristics and dimensional accuracy on the CBH type mould cavity surfaces

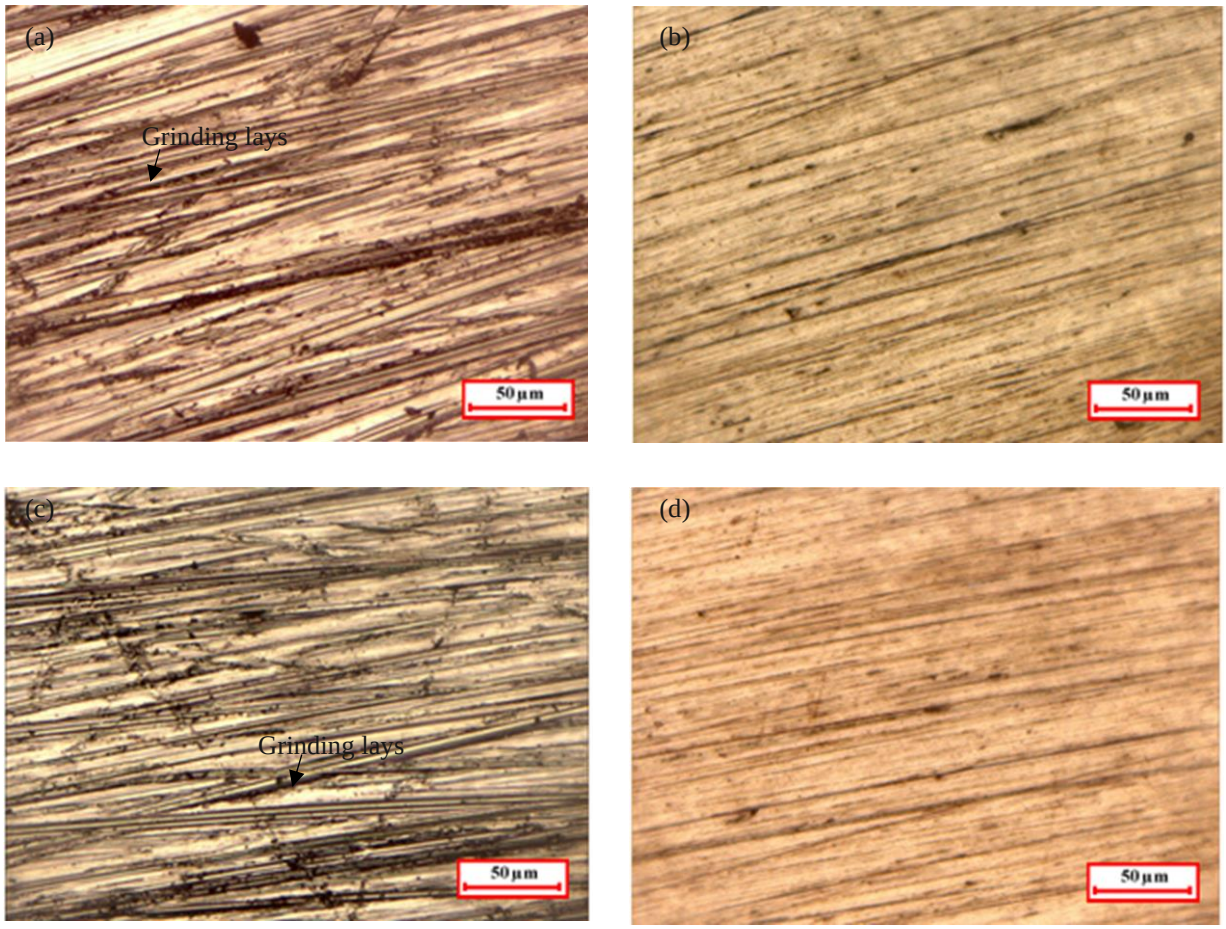

Fig. 6.18 Optical microscope images of the (a) initial, (b) final MR finished tapered longitudinal surface, (c) initial and (d) final MR finished flat end surface of the typical H13 mould cavity for the light cover.

In Figs. 6.18 (a-d), optical microscope images using Zeiss Leica instrument are obtained over the ground surface and MR finished surfaces of the CBH type mould cavity after MR finishing using the magnetorheological grinding (MRG) tool with the magnification of 100X. Figures 6.18 (a) and (b) present the optical microscope images of the initial ground surface and MR finished tapered

longitudinal (TL) CBH type mould cavity surface, respectively. Further, from Figs. 6.18 (c) and (d), optical microscope images can be observed over the flat end CBH type mould cavity of the initial ground and MR finished surfaces, respectively. In Fig. 6.18 (a) and (c), the grinding marks can be observed over the TL and flat end surfaces of the CBH type mould cavity. Due to these marks, there may be problems like an increase in injection force, the reduced service life of the mould cavity, the poor aesthetic appearance of the end product, etc. However, after MR finishing, the enhancement in the surface texture of the TL and flat end surfaces of the CBH type mould cavity can be observed in Figs. 6.18 (b) and (d). The improvement in the surface texture of both the surfaces of the CBH type mould cavity is owing to the elimination of grinding marks after MR finishing with the MRG tool. This improved surface may help reduce the value of the coefficient of friction over the MR finished surface which can further assist in enhancing the flowability of the molten plastic in the mould cavities (Mennig and Stoeckhert, 2013).

Further, a reflection image test is performed to see the effect of finishing using the MRG tool on the CBH type mould cavity surfaces. Figures 6.19 (a) and (b) show the initial and final mirror images on the TL surface of the CBH type mould cavity.

Similarly, Figs. 6.19 (c) and (d) show the initial and final mirror images on the flat end surface of the CBH type mould cavity. In this test, the reflection of the lettering ‘TIET' is created over the TL and flat end surfaces in the initial images as espied in Figs. 6.19 (a) and (c). But it can be observed that the text appears blurred. This may be owing to surface defects produced during the grinding process while the initial surfaces were generated. However, after utilising the MRG tool, these faults are removed, and the reflection of the text ‘TIET' is read clearly over the MR finished CBH type mould cavity surfaces, as shown in Figs. 6.19(b) and (d). Thus, on comparing the initial and final mirror images, it is clear that the TL and flat end surfaces of the CBH type mould cavity of H13 steel is improved after finishing using the present MRG tool. Thus, the surface characteristic of the MR finished CBH type mould cavity surfaces was considerably enhanced, as evident from the optical microscope and mirror images. The optical microscope and mirror images show that the MR grinding tool is effective in fine finishing the TL and flat end surfaces of the CBH type mould cavity. As the surfaces of the CBH type mould cavity are fine finished, so the end products with good aesthetic appearance and clear surfaces can be achieved. This clear and transparent surface may help in the uniform spreading of light out of the polycarbonate cover manufactured using CBH type mould cavities (Walter *et* al., 2007).

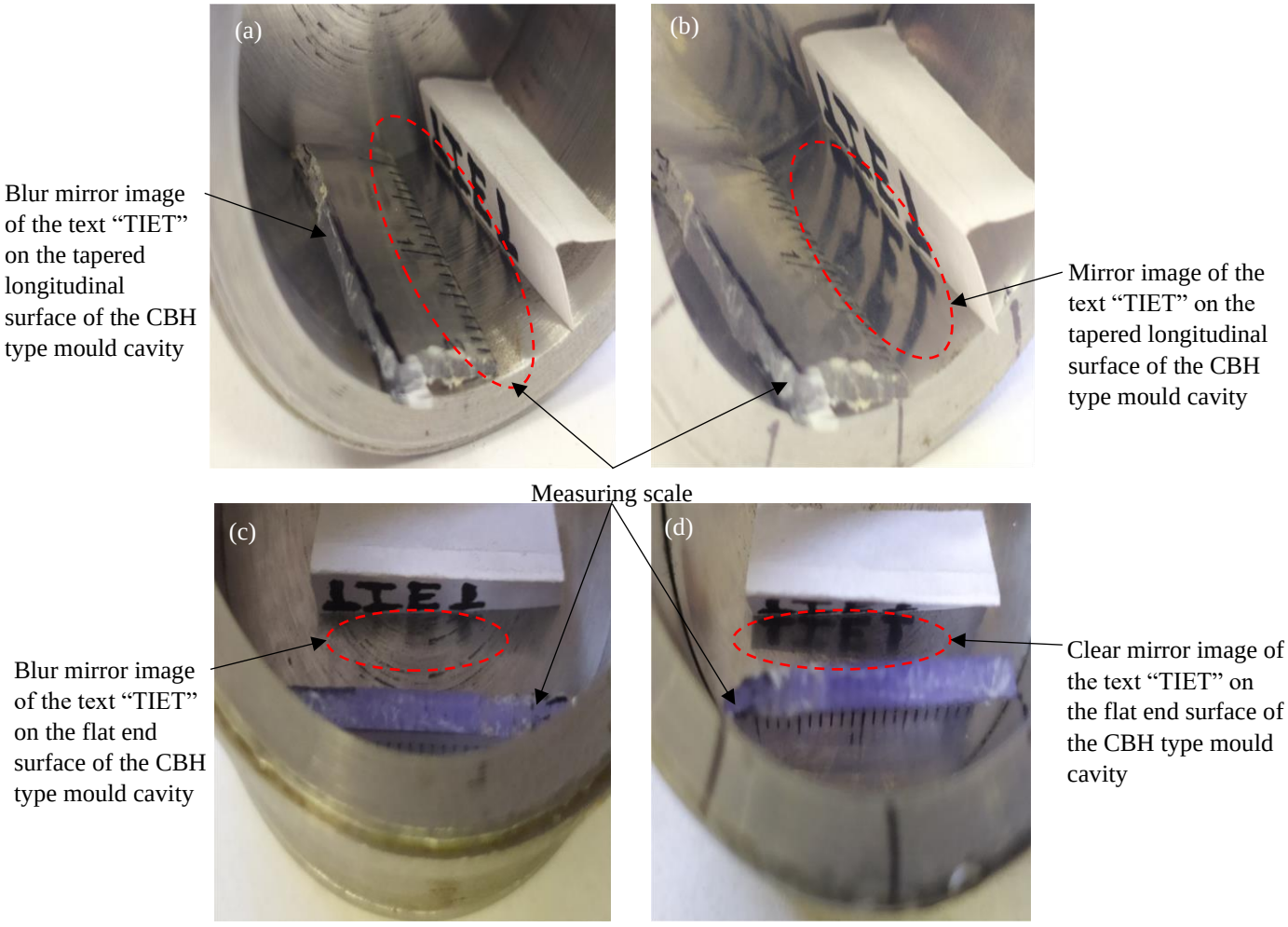

Fig. 6.19 Reflection image test of the (a) initial, (b) final MR finished tapered longitudinal surface after 140 min, (c) initial and (d) final MR finished flat end surface of the typical mould cavity for light cover after 80 min of MR finishing with the magnetorheological grinding process.

The CBH type industrial moulds require higher dimensional precision in the internal cylindrical surface to increase their functional performance and the dimensional accuracy of the end products (Mahtab, 2015). So, using a coordinate measuring machine (CMM), the circularity test is done on the finished tapered longitudinal surface of the typical CBH type mould cavity. This test presents how close the actual circular of the internal TL CBH type mould cavity surface is to the true circle.

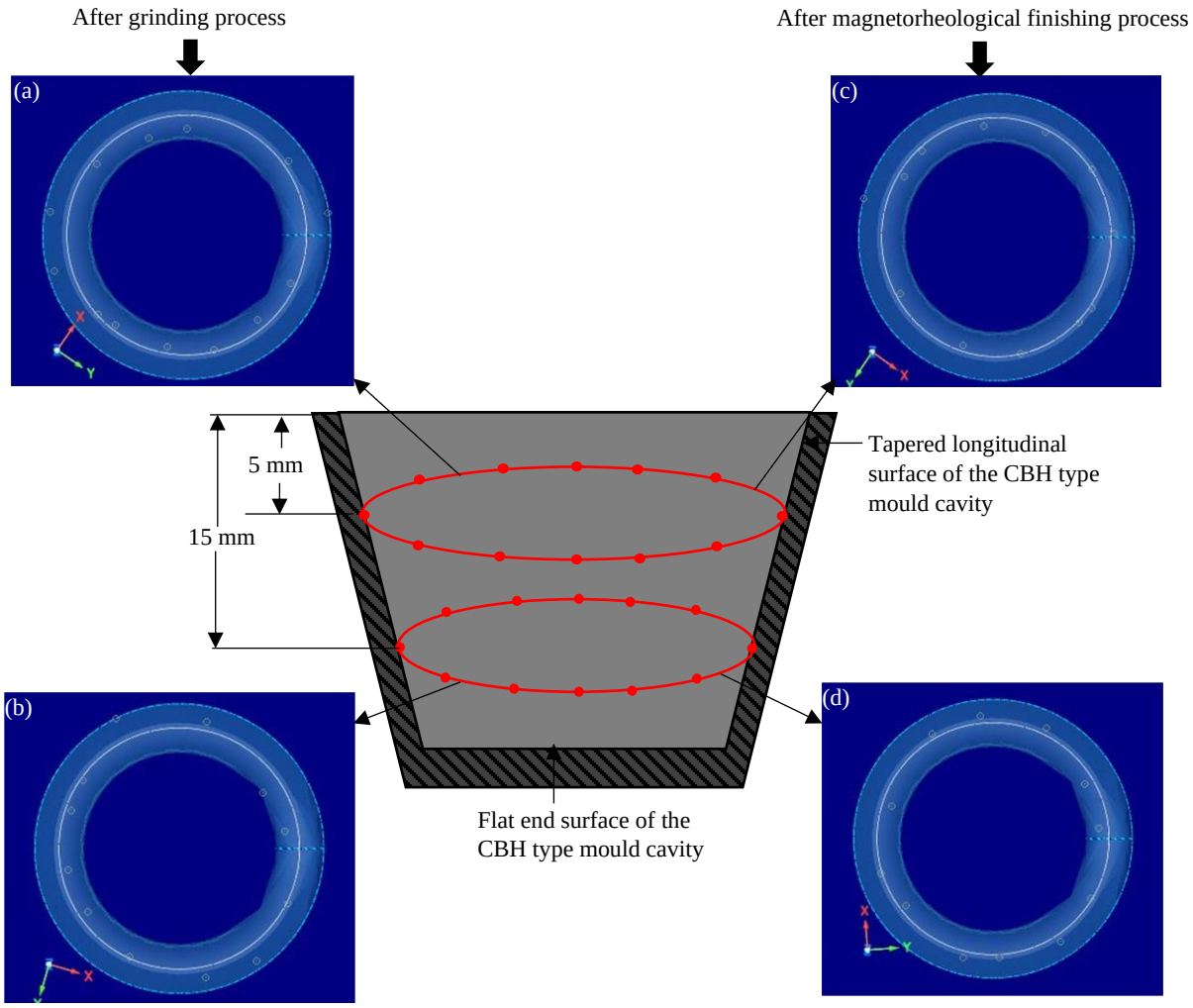

Fig. 6.20 Circularity test over initial surface at (a) 5 mm, (b) 15 mm and the final MR finished surface at (c) 5 mm and (d) 15 mm over the tapered longitudinal surface of the typical mould cavity for the light cover.

The circularity is defined as the distance between the actual circle formed over the cylindrical workpiece surface and the true circle. Figures 6.20 (a) - (d) show the initial and final images of the circularity plot after 140 min of finishing on the internal TL surface area of 2453 sq. mm of the CBH type mould cavity (Fig. 6.13) using the MRG tool. Circularity measurements were taken on the internal TL surface of the CBH workpiece at two different levels i.e., at 5 mm and 15 mm from the top surface as indicated in Fig. 6.20. On each level, the CMM probe was used to record 12 distinct measurement points along the interior TL surface of the CBH type mould cavity. Also Figs. 6.20 (a) and (b) present the results of circularity images of the initial ground TL surface of the CBH type mould cavity. It can be seen that the recorded points (measured points) are more

away from the true circle, with deviation values of circularity ranging from 0.0243 to 0.0275 mm. The recorded points (measured points) are closer to the true circle after finishing the inner TL surface of the CBH type mould cavity with the MRG tool, as shown in Figs. 6.20 (c) - (d), and the final deviation value of circularity is found in the range of 0.0075 to 0.0081 mm. As reduction is recorded in the deviation value of the circularity, so there is an improvement in surface quality over the TL CBH type mould cavity surface after MR finishing with the present MRG process.

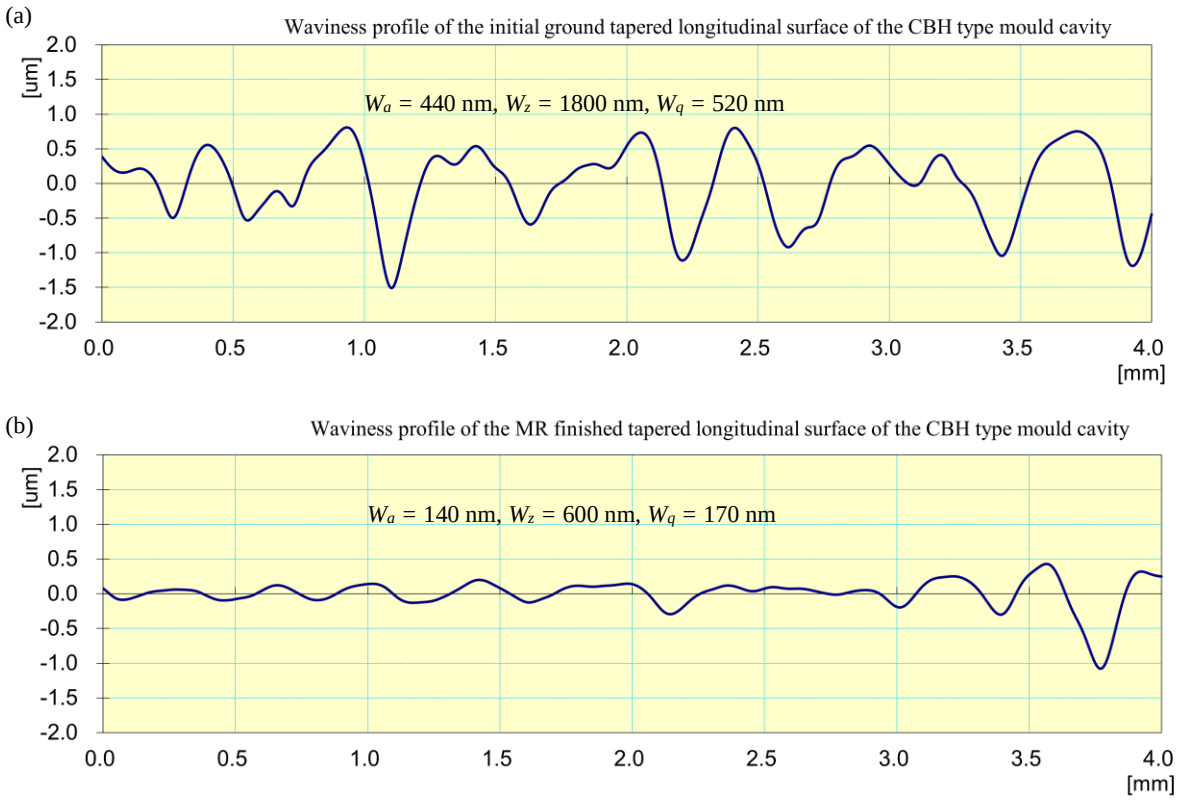

Fig. 6.21 Waviness test over the (a) initial surface, and (b) on the final MR finished tapered longitudinal surface of the typical mould cavity for the light cover.

Further, the waviness is performed over the TL surface of the CBH type mould cavity after MR finishing using the MRG process. The waviness (W_a) on the initial ground surfaces is found as 440 nm which is reduced to 140 nm. The waviness is measured after 140 min of finishing time using the Mitutoyo SJ 400 instrument keeping cut-off length as 0.8 mm. The initial values for the rest of the waviness parameters like root mean square (W_q) and the total height of profile (W_z) are 1800 nm and 600 nm, respectively. The values of W_q and W_z are reduced to 600 nm and 170 nm,

respectively. The waviness profiles in Fig. 6.21 (a) and (b) obtained over the initial ground and final MR finished TL surface of the CBH type mould cavity, respectively present the improvement in surface quality after MR finishing with the MRG process. Thus, from the results of circularity and waviness, the present MRG tool is found effective in improving the dimensional accuracy of the H13 cylindrical blind hole (CBH) type mould cavities. This may further help in improving the dimensional accuracy of the final end products.

6.2.4. Functional performance improvement

The finely finished surfaces of the mould cavity are utilised in the injection moulding process, which helps in achieving a better surface and uniform dimension across the cross-sectional area of the end product. From Eq. (6.16), it can be observed that the frictional force (F_{fr}) is directly affected by the coefficient of friction (μ).

$$\mu = \frac{F_{fr}}{F_{rt}} \tag{6.16}$$

where μ is the coefficient of friction, and F_{fr} is the frictional force in N. To calculate the frictional force, the reaction force over the mould cavity is expressed in Eq. (6.17) (Al-Samarai *et* al., 2012).

$$F_{rt} = \frac{kL_n t_s}{VW_s R_q}\left[\frac{R}{Vt}\right]^{-b} \tag{6.17}$$

where F_{rt} is the reaction force that occurs due to surface roughness of the mould, W_s is the specific wear (mm3/N-mm), and L_n is the normal load, R_q is the root mean square roughness of the tested surface, t_s is the time in seconds, V is the sliding velocity, b and k are arbitrary constants.

The moulded components are extracted out from the mould cavity with the help of the ejection system during the plastic moulding process. To extract the moulded plastic components from the mould cavity, the ejection force is used. The ejection force (F_{Ej}) is expressed in Eq. (6.18) (Bakharev and Astbury, 2013).

$$F_{Ej} = \frac{E_S A_t \mu \alpha_s \Delta T}{\frac{d}{2t_e}\left(1-\frac{\upsilon_s}{2}\right)} \tag{6.18}$$

where F_E is the ejection force (N), E_s is the elastic modulus of the end product (N/mm^2), A_t is the total surface area of the end product in contact with the mould cavity (mm^2), α_s is the linear thermal expansion coefficient of the end product (mm/^{o}C) and ΔT is the temperature difference between the temperature molten plastic and solidified end product temperature (^{o}C). d, t_e, and υ_s are the

equivalent diameter (mm), the wall thickness of mould cavity in mm and Poisson's ratio of the material of the end product, respectively. From Eq. (6.18), the ejection force is proportional to the coefficient of friction. The ejection force can be reduced by lowering the coefficient of friction owing to the low surface roughness value. This can also help in the ejection of moulded end products with ease.

In addition, if the mould surface is rough, the molten plastic can be subjected to more frictional stress, reducing flowability on the mould cavity surfaces. But, if the mould surface is finely finished it results in low frictional stress, thus the resistance experienced by the melt over this surface is low. So, Eq. (6.19) may be used to calculate the amount of force acting on the flow of the molten plastic (F_{mp}) owing to friction produced by the mould surface (Bergstrom *et* al., 2001).

$$F_{mp} = \frac{2\,F_{fr} L_n^2 \pi R_m}{A_m} \tag{6.19}$$

where A_m is the area of the mould cavity, and R_m is the radius of the cavity in mm.

As the magnitude of the force F_{mp} is directly proportional to the maximum stress. Thus, the reduction in the value of μ can reduce the force acting on the flow of the molten plastic (F_{mp}). As a result, the molten plastic can flow freely on the surfaces of the cylindrical blind hole (CBH) type moulds. The surface is finely finished after the MR finishing process, allowing molten plastic to flow freely. As can be observed, the value of the coefficient of friction affects the frictional force and the ejection force. The coefficient of friction affects the quality of replication and the mold's life span. In the case of moulds, the present MR finishing process can also be utilized to improve the functional properties such as ejection force, and flowability of the molten plastic. Hence, the present process utilizing the MRG tool finds its application to fine finish the interior tapered longitudinal and flat end surfaces of the H13 cylindrical blind-hole (CBH) type permanent moulds used for the manufacturing of the light cover used in the aviation industry.

6.2.5 Conclusions

The magnetorheological grinding (MRG) tool-based process is utilized to fine finish the tapered longitudinal (TL) and flat end surfaces of the H13 cylindrical blind hole (CBH) type mould cavity. For fine finishing both the surfaces of the CBH type mould cavity, the best process parameters are obtained using the Taguchi technique. After the MR finishing process utilizing MRG tool, the

surface characteristics obtained over the final MR finished mould cavity surfaces were compared to the initial ground surfaces. From this study, the following conclusions were drawn which inspires the use of the present MR finishing process for finishing the H13 CBH type mould cavities used in industry.

- The effective MR finishing is achieved over the interior tapered longitudinal surface of the CBH type mould cavity made up of H13 steel using the predicted optimum parameters such as the mould cavity rotational speed, current, tool rotational, and reciprocation speed are 60 rpm, 2 A, 500 rpm and 15 cm/min with the present MRG process. Further, the same MRG tool is found effective for fine finishing the flat end surface of the same CBH type mould cavity utilizing the predicted optimized parameters as 1000 rpm, 2.5 A, 100 rpm, and 25 cm/min, respectively.

- The percentage reduction in surface roughness achieved over the interior TL (2453 sq. mm) and flat end (1134 sq. mm) surfaces of the CBH type mould cavity using the MRG tool is 84.44 % after 140 min and 81.25 % after 80 min respectively. These results describe that the surface roughness decreases significantly after MR finishing with the present MRG process.

- The optical microscope images and mirror images reveal the smoothness of the tapered longitudinal and flat end finished surfaces of the H13 CBH type mould cavities are achieved after using the MRG process. This smoothness in surface characteristics describes the enhancement in the surfaces of the CBH type mould cavity.

- The improved circularity images and waviness profile performed over the TL surface of the H13 CBH type mould cavity reveals about the dimensional accuracy is achieved after MR finishing using the present MRG process.

- The reduction in the ejection force and improvement in flowability of melt plastic can be achieved over the MR finished CBH type mould cavity after MR finishing with the MRG process. The overall results reveal the usefulness of the MR finished CBH type mould cavity for enhancing the moulding process and surface quality of the end products. This may further provide clear light covers for uniform light spread.

6.3 Fine finishing of the typical blind hole type ball cup surface of ball transfer unit for improving its functional performance using the newly developed magnetorheological grinding (MRG) tool-based process

In the manufacturing and aerospace industries, positioning equipment is utilized to load/unload, orient, feed or control the cargo within a workplace for handling, storing, and transportation (Eko Saputro and Daneshvar, 2016; Rajeev, 2018). The major type of position equipment are used as the ball transfer units (BTUs), turntables, manipulators, industrial robots, etc. The BTUs are used as integral parts of the feed devices, aircraft cargo bay, cargo ships, conveyor systems, and vehicles that hold cargo (Brewer, 2016). The BTU is comprised of parts such as the main body with a hemispherical-shaped ball cup, a load ball, the supporting balls, and a cover installed over the main body whose schematic sectioned view can be observed in Fig. 6.22 (Masciarelli). The BTU performs its operation as the cargo rolls over the load ball which is in contact with the support balls. These support balls are further in contact with the ball cup surface.

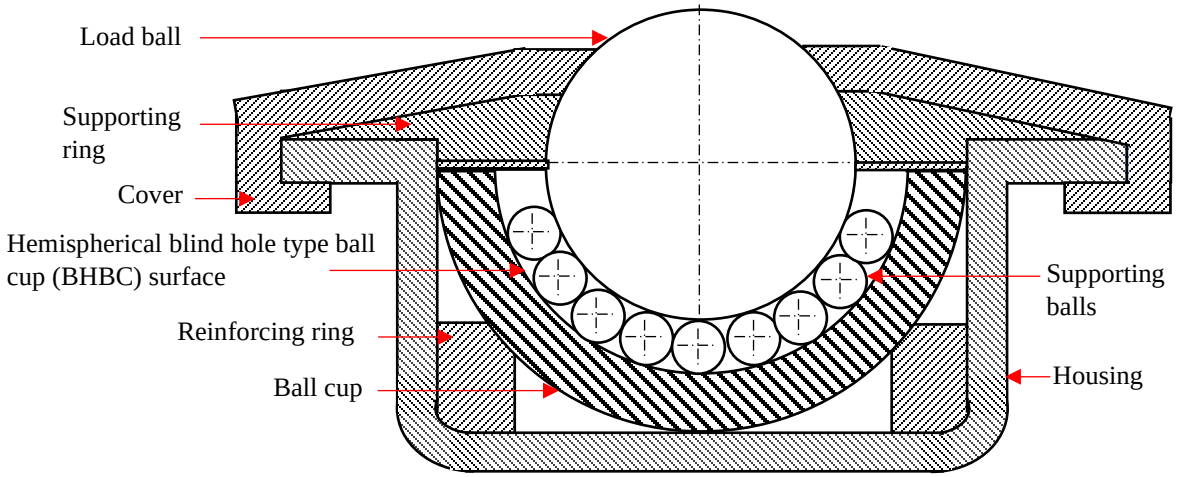

Fig. 6.22 Schematic sectioned view of the ball transfer unit (BTU) with various parts.

In the ball transfer unit (BTU), the finely finished ball cup surface along with its dimensional accuracy is highly required to resist corrosion, noise, and vibration (Mapelli and Barella, 2007; Turnbull *et* al., 2020). This also helps in reducing the resistance produced between the small balls and the ball cup surface due to a reduction in friction (2016). Further, it can enhance functional performance and service life by reducing wear and total frictional torque. Also, the power

consumed to transport the load over the BTU can reduce. To achieve a fine finished internal hemispherical blind hole type ball cup (BHBC) surface of the BTU, the roughness value is considered to be in the nanometer range (Tauviqirrahman and Ichsan, 2019). For finishing the interior BHBC work part surface, the grinding is used (Examiner and Hughes, 1999). But, achieving the fine-finished interior hemispherical surface of such type of BHBC workpieces is a tedious task with this grinding process. So, to perform this process, highly technically skilled workers are required. After performing the grinding process, geometrical imperfections like micro folded material and grooves are left out on the workpiece surface (Bedi and Singh, 2018b). This can lead to metal debris generation, vibration, noise, etc. while BTU is used in its functional application (Jurko *et* al., 2016). Also, there is no in-process control over the finishing forces in the grinding process (Maan *et* al., 2017, Grover and Singh, 2017c). Thus, fine finishing without surface defects may not be achieved with this traditional finishing process. As the load acts on the BTU, the fine finishing of the BHBC surface becomes important because it acts as a critical surface for the source of vibrations. So, the roughness of the BHBC surface is considered as the critical controlling parameter during the manufacturing process because it can affect the life span (Jurko *et* al., 2016). Therefore, to deal with limitations involved in traditional process while finishing, the present developed magnetorheological grinding (MRG) tool-based finishing process is utilized.

In the present study, a typical blind hole type ball cup (BHBC) workpiece surface of BTU made using stainless steel 304-grade material is used. To fine finish over its internal surface, a magnetorheological (MR) finishing process with the designing of a new tool is used. Hence, after enhancing the surface quality with a dimensional accuracy of the BHBC workpiece surface, the functional performance of the BTUs can be enhanced. Further, fine finishing of the BHBC workpiece surface can also reduce the coefficient of friction (COF). This can help to eliminate metal debris generation, reduction in running torque, reduction in operating temperature, lubrication requirement, etc. during BTU operation (Grover and Singh, 2017c). The fine finishing can result in proper relative motion among the small balls and ball cup surface of the BTU. So, fine finishing of the ball cup surface can enhance the life span of the BTUs, resulting in lower replacement costs.

Thus, in the present process, a new MR hemispherical finishing (MRHF) tool with converging sides is designed to achieve a high and uniform density of magnetic flux over its end surface. Also, the MRHF tool must be able to maintain the uniform working gap (WG) amid its end surface and

the interior ball cup workpiece surface of the BTU. This uniformity in the WG can provide uniform magnetic force over the workpiece surface. Thus, this may result in uniform finishing over the entire BHBC workpiece surface. The uniformity in finishing can provide improvement in the dimensional accuracy of the BHBC workpiece surface. Also, the MRHF tool is made with the electromagnet coil because it provides in-process control over the magnetic force in fine finishing of the different BHBC workpiece materials like stainless steel 304 and nylon as compared to the permanent magnet-based tool with a constant magnetic flux density (MFD) source. Further, in the present work, the response surface methodology technique is employed to predict the finishing parameters for the best results while fine-finishing the stainless steel 304-grade BHBC workpiece. After finding the optimum finishing parameters over the surface of the BHBC workpiece of the BTU, these parameters are experimentally validated. Later, the efficacy of the present MRHF process with the predicted optimum parameters is analyzed in fine finishing the interior BHBC work part surface with the surface roughness (SR) profiles and surface characteristics. Further, the dimensional accuracy is analyzed using the circularity test for the BHBC workpiece of the BTU.

6.3.1. Materials and methods

6.3.1.1 Material selection and workpiece preparation

The material used for making the blind hole type ball cups (BHBC) of ball transfer units (BTUs) is stainless steel 304-grade material. The properties of stainless steel 304-grade material make it useful for applications in BTUs. To fabricate the typical BHBC work part of BTU, the stainless steel 304-garde rod of 32 mm diameter was used. The internal hemispherical surface of the BHBC workpiece was prepared with the help of a computerized numeric control milling machine. The carbide ball end milling tool was used for manufacturing the typical BHBC work part with an internal surface of 25 mm diameter. After attaining the requisite diameter of the interior typical BHBC work part surface, the grinding operation was performed for initial surface generation. Further in the present electromagnetic MRF process, the magnetic flux density (MFD) has a significant role to retain the MRP fluid over the tool surface. Owing to this requirement, a material of tool core is required which is having capability to get magnetize by an electromagnet. So, the magnetorheological hemispherical finishing (MRHF) tool core is made up of mild steel material.

6.3.2 Experimental setup

After deciding the dimensions of the MRHF tool surface through MFEA, the experimental setup is prepared for the finishing of the interior BHBC work part surface which can be observed in Fig.

6.23. The aluminium C type structure is used for holding the MRHF tool in its position and a pair of ball bearings are used for its free rotation. The DC supply is provided to obtain the magnetization over the MRHF tool surface. The MRHF tool's magnetized surface holds the MRP fluid rigidly. The height adjustment system is used for aligning the center axis of the MRHF tool with that of the BHBC workpiece. The work part is mounted on the height adjustment system with the help of adjustable plumber blocks. In between these plumber blocks, a V-type pulley belt mechanism is used to provide rotational motion to the BHBC workpiece. Thus, the present experimental setup with the different controlled motions mechanism can perform MR finishing over the surface of the BHBC workpieces. Furthermore, the finishing parameters for the experimentation are selected based upon the literature (Singh *et* al., 2012) and preliminary experiments. The parameters considered are rotation of the magnetorheological hemispherical finishing (MRHF) tool (T_r), rotation of the blind hole type ball cup (BHBC) workpiece (R_w), and current (I). The range for the T_r and I were selected considering the literature review (Singh *et* al., 2012) and the experiments. The value of T_r is kept in the range of 300 to 700 rpm. Further, the magnetic field over the MRHF tool surface relies upon the intensity of I flowing through the electromagnet coil. The working gap (WG) was maintained constant at 0.6 mm during the experimentations.

The current in the electromagnetic coil is liable to the rise and fall of the magnetic flux density (MFD) in the WG of 0.6 mm amid the MRHF tool surface and the internal BHBC work part surface. This is helpful in the indenting of AAPs over the BHBC workpiece surface. Further, the value of the MFD was measured on the finishing surface of the newly developed MRHF tool using a gauss meter. No significant change was measured in the MFD after 3 A current is attained. So, this is considered as the upper limit of the current. Therefore, the range of the I is considered from 1 to 3 A. The workpiece is provided with rotational motion as it additionally contributes to reducing the roughness peaks with an increase in the AAPs relative motion. The range of the workpiece rotational speed was carefully chosen in the range of 40 to 160 rpm (Das *et* al., 2012). Thus, Table 6.17 states the finishing parameters and their selected range. For experimentation, the shape of the MRHF tool without MRP fluid is espied in Fig. 6.24(a).

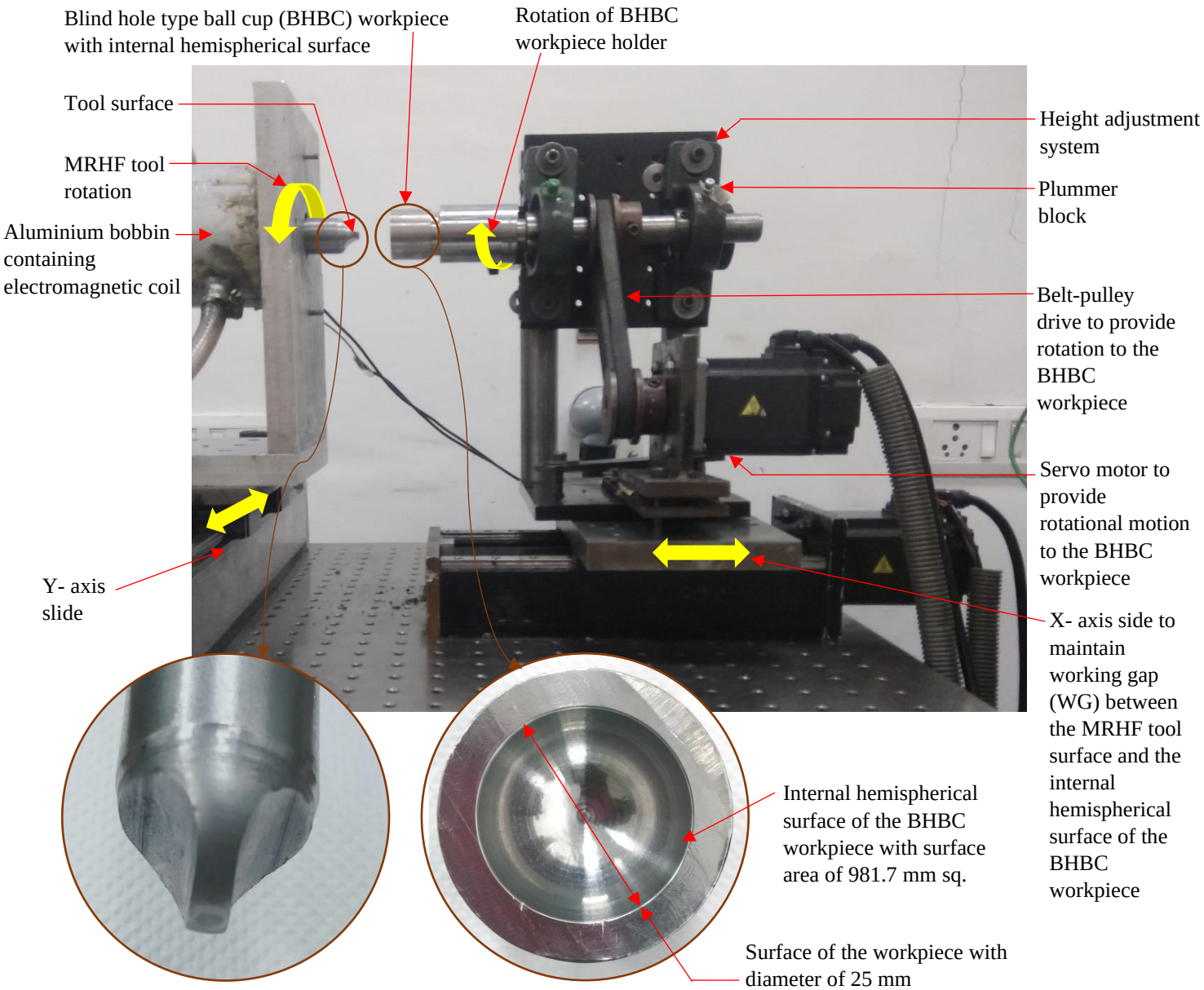

Fig. 6.23 Experimental setup with the magnetorheological hemispherical finishing (MRHF) tool for the finishing of the internal hemispherical surface of the blind hole type ball cup (BHBC) workpiece.

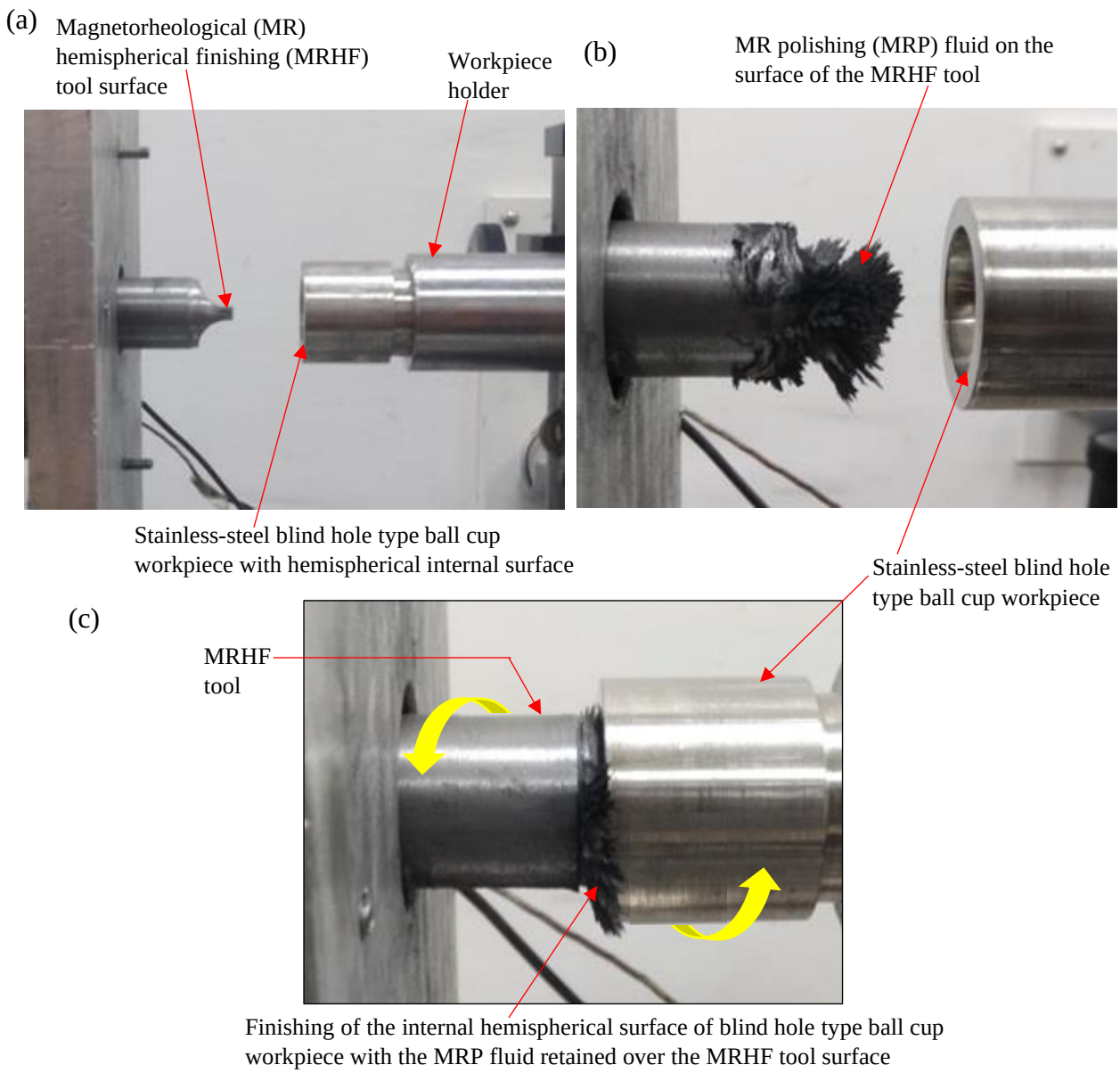

Fig. 6.24 The experimental images of (a) shape of the MR hemispherical finishing (MRHF) tool surface, (b) the stiffened MR polishing (MRP) fluid on the MRHF tool surface and (c) action of the MRHF tool during finishing on the internal hemispherical surface of the blind hole type ball cup workpiece.

Also, the BHBC workpiece is fixed in the workpiece holder as espied in Fig. 6.24(a). The rotation to the BHBC workpiece is provided through this workpiece holder as espied in Fig. 6.23. Further in Fig. 6.24(b), the MRP fluid-laden MRHF tool is magnetized using an electromagnetic coil. After magnetization of the MRHF tool, the rigid MRP fluid over its surface can be espied in Fig 6.24(b). The MRP fluid-laden MRHF tool surface is aligned with the BHBC workpiece surface using a Y-axis slide as espied in Fig. 6.23. The 0.6 mm WG is maintained amid the MRHF tool and the

BHBC work part surfaces using the X-axis slide as espied from Fig. 6.23. After maintaining the 0.6 mm WG, the finishing is performed over the BHBC workpiece surface using the MRHF tool as presented in Fig. 6.24(c). For optimizing the finishing process parameters, central composite design (CCD) in the response surface methodology (RSM) technique is opted to finish the interior BHBC work part surface utilizing the present MRHF process. With the 3 parameters and 5 levels, CCD is followed for predicting the optimum parameters needed to effectively finish the interior BHBC work part surface as stated in Table 6.17.

Table 6.17 Parameters and their corresponding levels.

Finishing parameters	Unit	Levels				
		-2	-1	0	1	2
Rotation of the magnetorheological hemispherical finishing (MRHF) tool (T_r)	RPM	300	400	500	600	700
Rotation of the blind hole type ball cup (BHBC) workpiece (R_w)	RPM	40	70	100	130	160
Current (I)	A	1	1.5	2	2.5	3

The other parameters involved in the finishing process and their condition utilized in experimentation are reported in Table 6.18. Twenty experiments were executed on the interior BHBC workpiece surface area of 981.7 sq. mm as mentioned in Table 6.19. Each experiment has been performed for 40 min. After every 20 min, the MRP fluid was renewed in order to utilize fresh active abrasives in every finishing set time.

Table 6.18 Other parameters and their condition used in the experimentation.

Parameters	Condition
Material of ball cup workpiece of the ball transfer unit	Stainless steel 304
Finishing medium	Magnetorheological polishing (MRP) fluid
Abrasive particles	SiC of mesh size 800
Iron particles	Mesh size of 500
Working gap (WG)	0.6 mm

After performing these experiments, the values of the average surface roughness (Ra_{f1}, Ra_{f2}, Ra_{f3}) were measured at three places over the interior surface of the BHBC work parts as stated in Table 6.19.

Table 6.19. Design of experiments and their responses.

Run	Finishing process parameters			Initial roughness value, Ra_i (μm)	Final surface roughness				
	T_r (rpm)	R_w (rpm)	I (A)		Ra_{f1} (μm)	Ra_{f2} (μm)	Ra_{f3} (μm)	Avg. Ra_f (μm)	$\%\Delta Ra$ (Eq. 6.20)
1	600.00	130.00	2.50	0.290	0.130	0.110	0.140	0.127	56.32
2	400.00	70.00	2.50	0.310	0.160	0.150	0.170	0.160	48.39
3	400.00	130.00	2.50	0.280	0.130	0.140	0.120	0.130	53.57
4	500.00	100.00	3.00	0.290	0.100	0.090	0.110	0.100	65.52
5	500.00	40.00	2.00	0.310	0.170	0.160	0.180	0.170	45.16
6	500.00	100.00	2.00	0.280	0.120	0.130	0.110	0.120	57.14
7	500.00	100.00	2.00	0.320	0.110	0.150	0.130	0.130	59.38
8	500.00	100.00	2.00	0.300	0.130	0.110	0.140	0.127	57.78
9	500.00	100.00	2.00	0.270	0.110	0.120	0.100	0.110	59.26
10	600.00	70.00	1.50	0.290	0.160	0.140	0.180	0.160	44.83
11	500.00	100.00	1.00	0.280	0.170	0.180	0.160	0.170	39.29
12	600.00	70.00	2.50	0.310	0.130	0.120	0.140	0.130	58.06
13	700.00	100.00	2.00	0.300	0.150	0.160	0.170	0.160	46.67
14	400.00	130.00	1.50	0.270	0.140	0.130	0.150	0.140	48.15
15	300.00	100.00	2.00	0.290	0.210	0.200	0.220	0.210	27.59
16	500.00	160.00	2.00	0.300	0.130	0.140	0.120	0.130	56.67
17	400.00	70.00	1.50	0.310	0.200	0.190	0.210	0.200	35.48
18	500.00	100.00	2.00	0.270	0.120	0.130	0.110	0.120	55.56
19	500.00	100.00	2.00	0.280	0.100	0.120	0.140	0.120	57.14
20	600.00	130.00	1.50	0.310	0.140	0.170	0.150	0.153	50.54

T_r is used for rotation of the magnetorheological hemispherical finishing (MRHF) tool, R_w is used for rotation of the blind hole type ball cup (BHBC) workpiece and I is used for current.

These measured values on the interior BHBC work part surface are not found exactly the same, so the average of these roughness values (Ra_{f1}, Ra_{f2}, Ra_{f3}) is considered the final avg. roughness value (Ra_f) as stated in Table 6.19. Finally, the %age reduction in avg. surface roughness *(%ΔRa*) is chosen as an outcome or response. The *%ΔRa* can be calculated from Eq. (6.20).

$$\%\Delta Ra = \frac{(Ra_i - Ra_f)}{Ra_i} \times 100 \quad (6.20)$$

where Ra_i is the avg. roughness (*Ra*) value before the MRF process in µm, Ra_f is the final avg. roughness (*Ra*) value after the MRF process in µm. Further, to study the surface characteristic of the interior BHBC workpiece surface, the scanning electron microscope (SEM) is utilized. Also, to analyze the dimensional accuracy of the surface of the BHBC workpiece, the coordinate measuring machine is utilized.

6.3.3 Results and discussion

Further, the analysis of variance (ANOVA) was executed for the obtained experimental responses ($\%\Delta R_a$). The statically significant p-value was considered to be less than 0.05.

Table 6.20. Analysis of variance (ANOVA) for the percentage reduction in surface roughness value ($\%\Delta R_a$) while MR finishing the interior surface of the blind hole type ball cup (BHBC) workpiece.

Source	Sum of square	Degree of freedom	Mean square value	F-value	p-value	%age cont. (Eq. 6.22)
Model	1619.31	8	202.41	53.98	< 0.0001	
T_r	248.06	1	248.06	66.14	< 0.0001	15.32
R_w	126.56	1	126.56	33.75	0.0001	7.81
I	473.06	1	473.06	126.13	< 0.0001	29.21
T_r^2	614.39	1	614.39	163.84	< 0.0001	37.94
R_w^2	65.47	1	65.47	17.46	0.0015	4.04
I^2	31.18	1	31.18	8.31	0.0149	1.92
T_rR_w	21.13	1	21.13	5.63	0.0369	1.30
R_wI	28.13	1	28.13	7.50	0.0193	1.74
Residual	41.26	11	3.75			
Lack of fit	29.92	6	4.99	2.20	0.2023	
Error	11.33	5	2.27			0.69
Total	1660.57	19				

The ANOVA is given in Table 6.20 after removing the non-significant parameters. The p-value of the model is <0.05, this represents that the quadratic model is significant. The significant terms involved in the regression model while finishing the interior blind hole type ball cup (BHBC) work part surface are T_r, R_w, I, T_r^2, R_w^2, I^2, T_rR_w, and R_wI with a p-value < 0.05 (Table 6.20). The R-squared value is 97.38 % and Adj. R- squared is 95.47 % which defines the fitness of the equation. Thus, this represents that the quadratic model is significant. Using CCD, a quadratic model has been made using ANOVA. For predicting the *%⊿SR*, a quadratic equation is obtained as given in Eq. (6.21).

$$\%\triangle Ra = -206.086 + 0.592\,T_r + 0.973\,R_w + 41.193\,I - 4.989\,x\,10^{-4}T_r^2 - 1.793\,x\,10^{-3}R_w^2 - 4.454I^2 - 5.417\,x\,10^{-4}T_rR_w - 0.125R_wI \quad (6.21)$$

where T_r is used for rotation of the magnetorheological hemispherical finishing (MRHF) tool, R_w is used for rotation of the blind hole type ball cup (BHBC) workpiece and I is used for current.

The percentage contribution (*%age cont.*) is also obtained from the ANOVA Table 6.19 that expresses the %age weightage of each finishing parameter used in the model of *%⊿Ra*. It is expressed as in Eq. (6.22).

$$\%age\ cont. = \frac{Sum\ of\ square\ (SoS)}{Total\ SoS} \times 100 \quad (6.22)$$

The *%age cont.* of all the significant parameters used in the MR finishing process are calculated and the results of it are plotted in Fig. 6.25(a). A clustered bar chart is used for expressing the results. Here in Fig. 6.25(a), it can be espied that the rotation of the magnetorheological hemispherical finishing (MRHF) tool (T_r and T_r^2) is the most significant parameter with the contribution of 53.58 %, followed by current (I and I^2) with the contribution of 30.92 % and the rotation of the blind hole type ball cup (BHBC) workpiece with the contribution of 11.77 %. The percentage of error in the quadratic model is 0.70 %. Further, in the following section after the investigation of the regression model, the interaction of significant parameters with respect to the *%⊿Ra* has been discussed.

The graph in Fig. 6.25(a) represents the interaction effect on $\%\triangle R_a$ due to the MRHF tool rotation (T_r) and rotation of the blind hole type ball cup (BHBC) workpiece (R_w) at current (I) 3 A. As the T_r increases, the *%⊿Ra* increases from 300 to 550 rpm along with R_w of 100 rpm but on further increment in T_r from 550 to 700 rpm, there is a decrement in *%⊿Ra*. This behaviour of variation in *%⊿Ra* owes to the fact that as the T_r increases from 300 to 550 rpm along with the speed of the

BHBC workpiece rotation, the interaction of the AAPs with the roughness peaks over the work part surface rises. But as the speed of the tool rotation exceeds beyond 550 rpm till 700 rpm accompanied by R_w of 100 rpm, the tangential force rises more which may increase the higher relative motion amid the tool and workpiece. Owing to the increase in higher relative motion, there is less interaction of the asperities over the workpiece with the AAPs. Also, when the speed of the MRHF tool rotation exceeds 550 rpm, the tangential effect owing to tangential force splashes the magnetorheological polishing (MRP) fluid away from the workpiece surface. This renders the MRHF tool ineffective to finish the workpiece surface. Hence, the $\%\triangle Ra$ decreases beyond the 550 rpm of T_r. On the other hand, as the value of T_r reaches in the range of 300 to 550 rpm along with the value of R_w as 100 rpm, the MRP fluid gains sufficient force to effectively shear the roughness peaks. Thus, an incremental in the $\%\triangle R_a$ was observed. But for the value of R_w as 130 rpm and 160 rpm with T_r as 550 rpm, the $\%\triangle R_a$ decreases. This is due to insufficient interaction time and disturbance of the MRP fluid to finish the internal hemispherical workpiece surface. When the R_w is in the range of 40 rpm to 100 rpm, the MRP fluid effectively shears the asperity from the workpiece surface with 550 rpm of the tool rotation as there is a rise in the $\%\triangle R_a$. But as the R_w speed reaches 100 rpm with the T_r as 550 rpm, the maximum value of the $\%\triangle R_a$ is observed as shown in Fig. 6.25 (a). Thus, this clearly signifies that the optimum value of the two parameters is predicted that are desired for the effective MR finishing of the BHBC surfaces.

In another Fig. 6.25(b), the interaction of the current (I) and rotation of the BHBC workpiece (R_w) can be observed in relation to the $\%\triangle R_a$ at 550 rpm of the tool rotation speed. As the value of the current rises to 3 A, there is an increment in the $\%\triangle R_a$. As I increases, the magnitude of the magnetic field rises which can cause an increment in the magnetic indentation force. Owing to this, there is a rise in indentation by the abrasives over the interior BHBC work part surface. As the R_w and the current increases, there is a gradual increment in the $\%\triangle R_a$ upto 100 rpm of workpiece rotation. But such a pattern is not observed when the R_w reaches beyond 100 rpm with a current beyond 2.5 A. It can be observed that there is a decrement in the $\%\triangle R_a$. The reason behind this may be due to the high workpiece rotational speed that causes improper interaction of the abrasive particles with the surface asperities of the workpiece. This improper interaction is due to the short interaction time between the abrasive and the surface asperities.

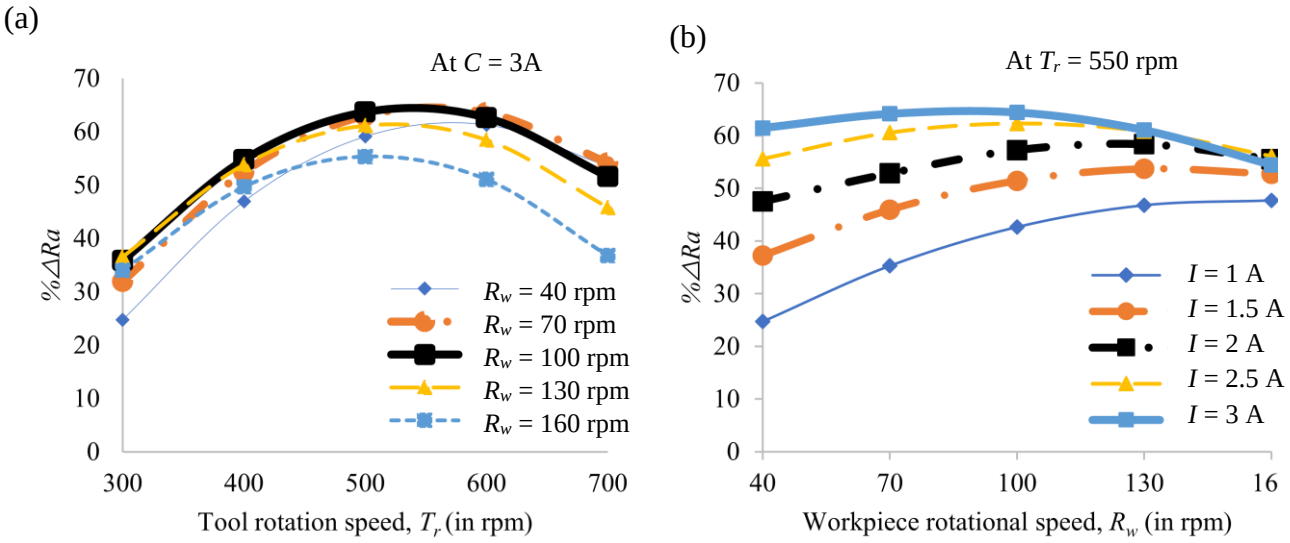

Fig. 6.25 (a) Effect of the tool rotational speed (T_r) on %age reduction in surface roughness (%ΔR$_a$) by varying the workpiece rotational speed (R_w), and (b) effect of the workpiece rotational speed (R_w) on *%ΔRa* by varying the current (I).

After finding the best contributing parameter from the regression model. The optimum finishing parameters were predicted from the quadratic model. By utilizing the quadratic mathematical regression model, the maximum *%*ΔR_a was obtained at rotation of the magnetorheological hemispherical finishing (MRHF) tool of 550 rpm, the rotation speed of the blind hole type ball cup (BHBC) workpiece of 100 rpm along with the 3 A current. Five confirmatory experiments using the optimum finishing parametric conditions were carried out to validate the outcome of the regression model. The experimental *%*ΔR_a was evaluated on the surface of the initial and the final MR finished. On the other hand, the theoretical *%*ΔR_a value was calculated using the regression model from Eq. (6.21). These values of experimental *%*ΔR_a and theoretical *%*ΔR_a are compared and stated in Table 6.21. Also, the *%age error* among the experimental *%*ΔR_a and predicted *%*ΔR_a is calculated from Eq. (6.23) and is stated in Table 6.21.

$$\%age\ error = \frac{|Experimental\ \%\Delta Ra - Predicted\ \%\Delta Ra|}{Experimental\ \%\Delta Ra} \times 100 \qquad (6.23)$$

The *%age error* among the experimental and theoretical results is found in the range of 1.36 to 4.34 %. Thus, this states that experimental *%ΔRa* and predicted *%ΔRa* are found in close agreement with each other. The closeness of the five-consecutive experimental *%ΔRa* values as

reported in Table 6.21 reveals the reproducibility of the developed MRHF tool for surface finishing of the BHBC workpieces.

Table 6.21 Validation of regression model with optimum process parameters.

Exp.	Time (min)	Finishing parametric conditions			Experimental $\%\Delta R_a$. (Eq. 6.20)	Predicted $\%\Delta R_a$. (Eq. 6.21)	%age error (Eq. 6.23)
		Rotational speed of the tool (T_r) rpm	Rotational speed of the workpiece (R_w) rpm	Current (I) A			
1	40	550	100	3	62.36	64.41	3.28
2	40	550	100	3	63.54	64.41	1.37
3	40	550	100	3	64.58	64.41	1.36
4	40	550	100	3	61.73	64.41	4.34
5	40	550	100	3	65.71	64.41	1.99

6.3.3.1 Observation of surface roughness on blind hole type ball cup (BHBC) workpiece

Further, utilizing these optimized finishing parameters, the final internal surface of the blind hole type ball cup (BHBC) workpiece was finished which has a diameter of 25 mm. Figure 6.26 presents the time accomplished to fine finish the interior BHBC work part surface.

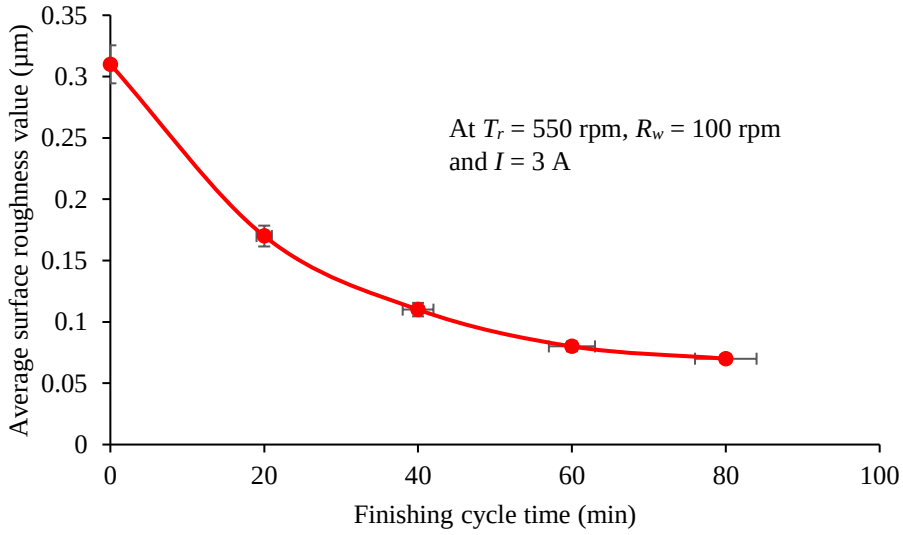

Fig. 6.26. Reduction in surface roughness with time over the internal hemispherical surface of the blind hole type ball cup workpiece after finishing with the magnetorheological hemispherical finishing tool at optimum parameters.

After each 20 min of finishing time using the MRHF tool, the SR value was recorded. The final roughness value was achieved after performing the MRF process for 80 min on the BHBC work part surface area of 981.7 mm sq. No further changes were observed with these predicted parametric conditions thereafter over the BHBC workpiece surface. The SR parameters such as the average SR value (*Ra*), root mean square value (*Rq*), and an average maximum height of the profile (*Rz*) is analyzed before and after the present MRF process. The parameter *Ra* is the surface roughness average of measured peaks and valleys over the BHBC workpiece surface. *Rq* is the root mean square of a surface measured peaks and valleys. The *Ra* and *Rq* parameters can be used to detect general variations in the overall profile height characteristics of this BHBC workpiece surface. Further, the *Rz* is the average of the five tallest peaks and five lowest valleys present over the sampling length of the BHBC workpiece surface. Thus, the *Rz* parameter helps to determine the uniformity in peaks and valleys over the sampling length. For measuring the surface roughness (SR) parameters over the BHBC workpiece surface, a block with V-groove is used to place the BHBC workpiece horizontal over the Mitutoyo SJ 410 roughness measuring instrument setup. During the measurement of SR parameters, the probe is allowed to move perpendicular to the concentric lays. Further, the Gaussian filtration is used by the SR measurement instrument over the measured profile and the final roughness profile is obtained. After the SR measurement, the final SR parameters (*Ra*, *Rq*, and *Rz*) were recorded as 0.070 µm, 0.120 µm, and 0.700 µm from the initial ground SR parameters of 0.310 µm, 0.540 µm, and 3.6 µm (Fig. 6.27). The maximum $\%\triangle R_a$ parameters achieved over the internal hemispherical surface area of 981.7 mm sq. (diameter of 25 mm) of the BHBC workpiece is 77.41 %, 77.78 %, and 80.55 %. The finishing rate of the MRHF process over the BHBC workpiece surface is obtained as 0.003 µm/min using Eq. 6.24.

$$Finishing\ rate = \frac{(Ra_i - Ra_f)}{Total\ finishing\ time} \tag{6.24}$$

The SR profiles are espied in Figs. 6.27(a) and (b) of the initial ground and final MR finished internal blind hole type ball cup (BHBC) workpiece surface. The initial profile in Fig. 6.27 (a) indicates that the surface is non-uniform with more deviation of peaks and valleys from the mean line as seen from the SR profile. But, after the MRF process is executed over the BHBC workpiece surface using the MRHF tool, the final SR profile in Fig. 6.27(b) is significantly reduced with less deviation of peaks and valleys i.e., almost closer to the mean line. Thus, on comparing the initial and final SR profiles in Figs. 6.27 (a) and (b), an improvement in the finally obtained roughness profile from the initial SR profile on the interior BHBC work part surface of the BTU can be

observed. This reduction in surface roughness may enhance the sliding speed of the supporting balls and reduce the traction force amid the supporting balls and the BHBC work part surface of the BTU. Thus, it is evident that the performance of the BTU can enhance with the enhancement of the surface finishing of the BHBC workpiece using the present developed process with a new MRHF tool (Yunlong *et* al., 2018).

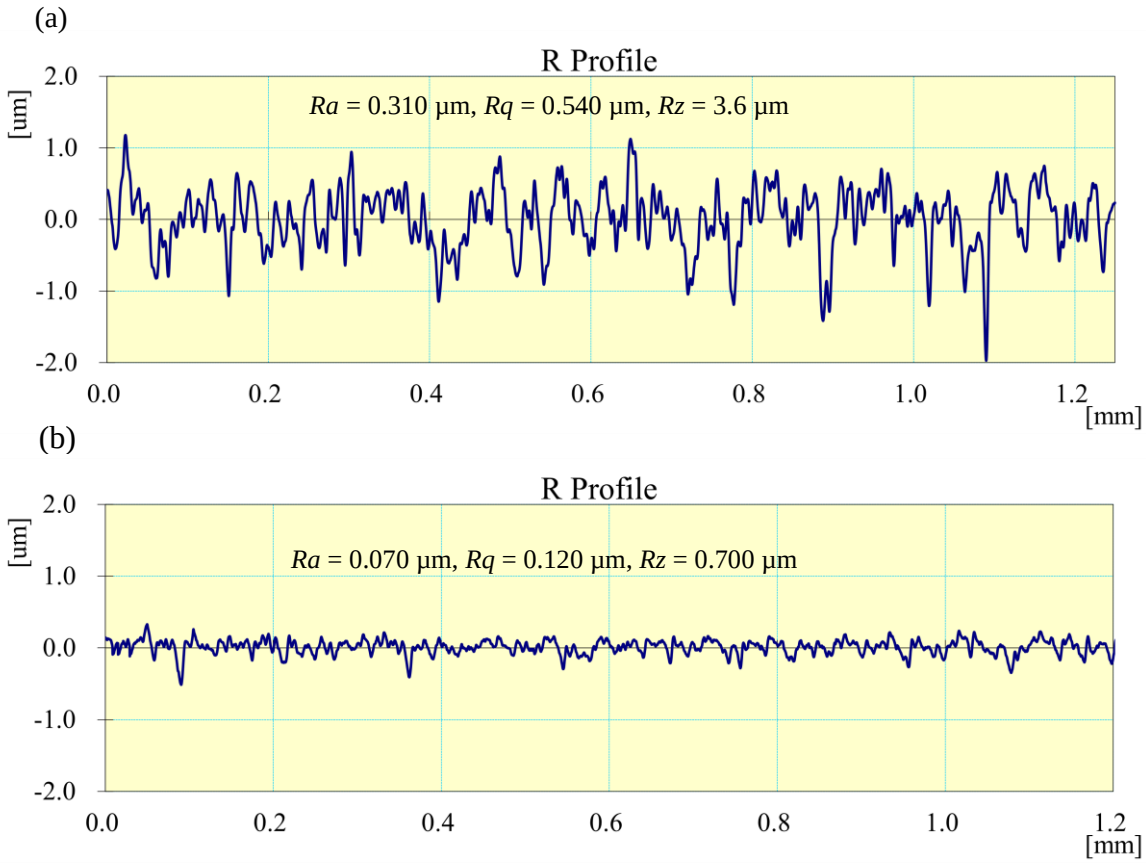

Fig. 6.27 Surface roughness profiles of the (a) initial ground and (b) finally MR finished hemispherical surface area of 981.7 mm sq. over the blind hole type ball cup workpiece after 80 min MR finishing at optimized parameters of T_r as 550 rpm, R_w as 100 rpm and current as 3 A with working gap of 0.6 mm.

6.3.3.2 Observation of surface characteristics and dimensional accuracy on blind hole type ball cup (BHBC) workpiece

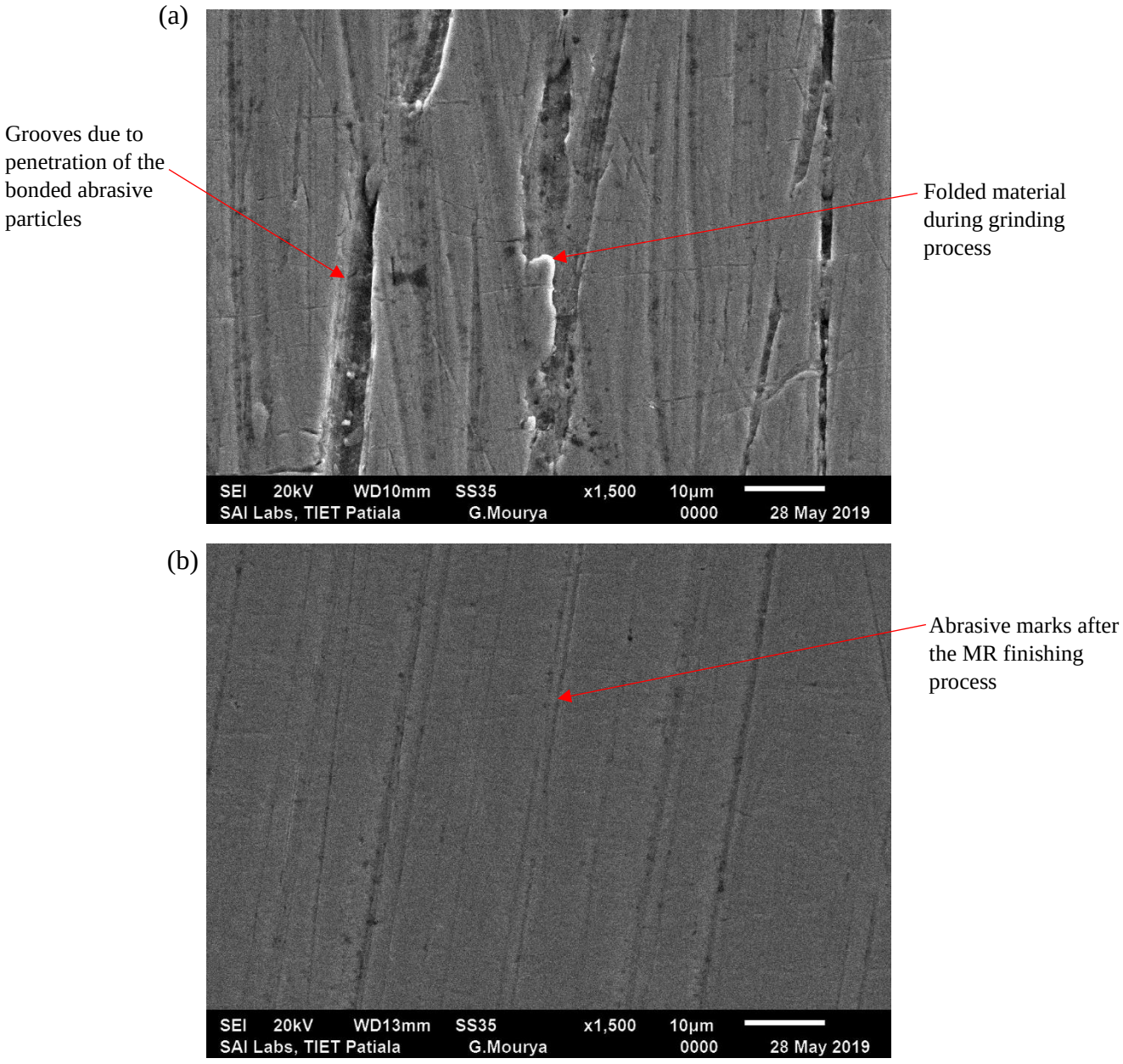

Fig. 6.28 Scanning electron microscopy images of the (a) initial ground and (b) finally finished hemispherical surface area 981.7 mm sq. of the blind hole workpiece with the magnetorheological hemispherical finishing tool at optimized parameters of T_r as 550 rpm, R_w as 100 rpm and current as 3 A with working gap of 0.6 mm in 80 min.

Further, the surface characteristics are analyzed on the interior BHBC work part surface utilizing a scanning electron microscope (SEM). The SEM images of the BHBC work part surface were

obtained before and after the MR finishing (MRF) process at an optical scale of 1500 X which can be observed in Figs. 6.28 (a) and (b). The grooves over the interior ground BHBC surface and folded material can be observed in the SEM image as seen from Fig. 6.28 (a). These defects over the workpiece surface in the initial SEM image are owing to the grinding wheel's bonded abrasives. These abrasives penetrate the workpiece surface and form grooves. Also, due to plastic deformation of the material by the penetrated abrasives, the material gets accumulated over the sides of these grooves, thus resulting in the material folding over the work part surface. But in the case of the MRF process, there is controlled penetration of the abrasive particles into the BHBC surface. Thus, after the interior BHBC surface is finished with the MRHF tool, these defects are removed as espied in Fig. 6.28 (b). Also, some lay marks are observed in Fig. 6.28(b) after finishing with the MRHF tool which shows that the abrasive particles shear the asperities present over the BHBC workpiece surface. Further, on comparing the initial and final SEM images from Figs. 6.28(a) and (b) respectively, an enhancement in the quality of the BHBC work part surface of BTU is observed after finishing with the MRHF tool.

Further, the reflection image test is conducted over the BHBC workpiece surface to see the finishing effect after the MRHF tool is used. Here, the initial and final mirror images on the BHBC surface can be observed in Figs. 6.29 (a) and (b).

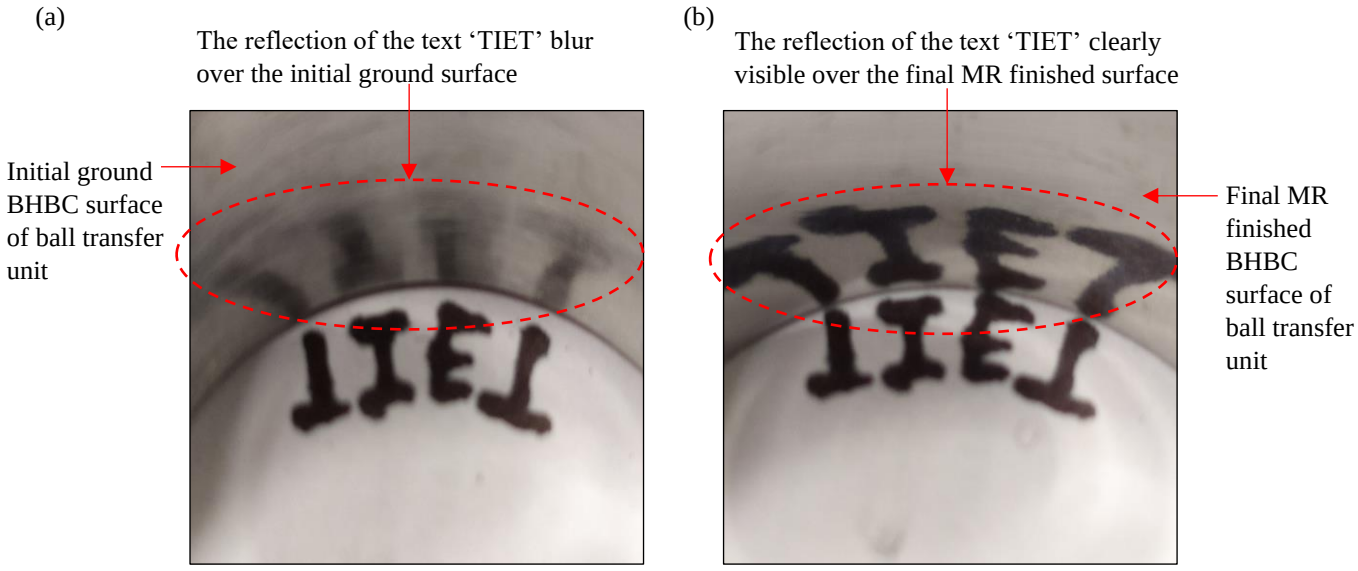

Fig. 6.29 Mirror images of the (a) initial ground and (b) finally finished blind hole type ball cup workpiece surface using the present process with a magnetorheological hemispherical finishing tool at optimized parameters of T_r as 550 rpm, R_w as 100 rpm and current as 3 A with working gap of 0.6 mm in 80 min.

In the initial image from Fig. 6.29 (a), the text 'TIET' is blurred when observed in the reflection formed over the BHBC workpiece surface. This might be due to the surface defects produced during the initial surface generation by the grinding process. But after performing the present process using the MRHF tool these defects are removed, so the reflection of the text 'TIET' is clearly visible over the MR finished work part surface as it can be seen in Fig. 6.29 (b). Further, on comparing the initial and final mirror images, it is evident that the improvement is achieved over the surface of the BHBC workpiece after finishing using the presently designed MRHF tool. Thus, from the results of the SEM and reflection test, it is revealed that a smooth surface is obtained over the BHBC workpiece after finishing using the presently designed MRHF tool. This smooth BHBC workpiece surface may prevent stress fluctuations during the BTU operation (Yunlong *et* al., 2018).

Further, the circularity test was carried out over the ground and the finally MR finished work part surface. This test is conducted utilizing the coordinate measuring machine to check the dimensional accuracy over the internal blind hole type ball cup (BHBC) workpiece surface. The circularity is used to measure the actual circular surface closeness relative to the true circle. So, this describes that the interior BHBC work part surface is dimensionally accurate. The points for the circularity test were recorded over the BHBC workpiece surface at two levels as shown in Figs. 6.30 (a) and (b). A total of 12 points were recorded for the circularity test for each level using the coordinate measuring machine probe. The circularity of the initial ground surface can be espied from Fig. 6.30(a) and the average value was found to be in the range of 0.395.

After observing Fig. 6.30(a), it can be seen that the majority of points mentioned over the actual circle are away from the true circle. Nevertheless, in Fig. 6.30(b), as the majority of reported points are near the true circle, it is evident that the higher circularity is achieved after performing the MRF process on the interior BHBC work part surface. Also, the average circularity value was detected as 0.1075. Therefore, from Fig. 6.30, it can be inferred that the present MRHF tool is used to improve the dimensional accuracy of the interior BHBC workpiece surface. If the dimensional accuracy of the BHBC workpiece surface is poor due to the higher surface roughness, the vibrations and noise in components may occur when the BTU is under operating conditions. These vibrations may cause deformation of the support balls of the BTU which may further deteriorate the life of its rest components (Yan *et* al., 2020). So, the MRHF tool is utilized to finish the interior

BHBC work part surface of the BTU in order to enhance its performance in relation to functionality (Turnbull *et* al., 2020; Bucinskas *et* al., 2010; Migal *et* al., 2021).

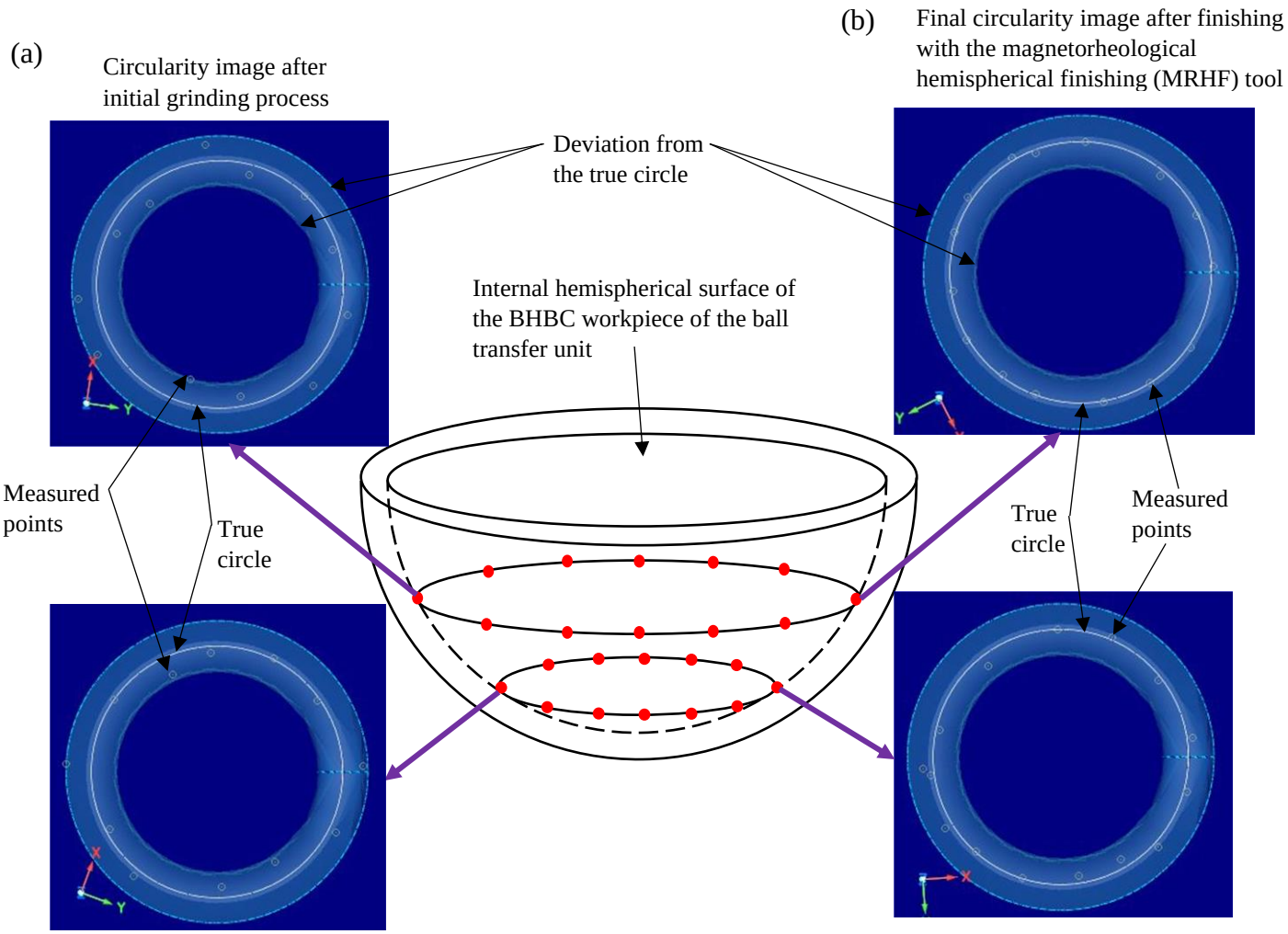

Fig. 6.30 Circularity images of the (a) initial ground and (b) final MR finished internal hemispherical surface of the blind hole type ball cup (BHBC) workpiece at optimum parameters as T_r = 550 rpm, R_w = 100 rpm and I = 3 A after 80 min of finishing with the developed magnetorheological hemispherical finishing (MRHF) tool.

6.3.4 Functional performance

The enhancement in the quality of the interior blind hole type ball cup (BHBC) work part surface can enhance the functional performance of the ball transfer unit (BTU). As the SR value influences the coefficient of friction (COF), so low value of COF may result in smooth movement of the small

balls on the interior BHBC work part surface (Singh and Singh, 2019b). Thus, the frictional force (F_{Fr}) is directly proportional to the coefficient of friction factor as expresses in Eq. (6.25).

$$F_{Fr} = \mu F_r \tag{6.25}$$

where μ is the COF over the surface of the interior BHBC workpiece, F_r is the reaction force acting due to contact amid the small supporting balls and the BHBC workpiece surface. As F_{Fr} is directly proportional to COF, so a low amount of friction may be experienced for the low value of COF by the transporting load when it comes in contact with the large ball.

Further, the total frictional torque in BTU may cause power loss owing to the rough contacting surfaces of its components, this may cause an adverse effect on its functional efficacy and service life. The total frictional torque (T_{fq}) is directly proportional to co-efficient of friction as expressed in Eq. 6.26. If the total frictional torque is high, the travelling speed of the transporting cargo over the large ball of the BTU may reduce. This reduction in travelling speed of transporting cargo, may cause a loss of power. This total frictional torque (T_{fq}) being applied by the BTU can be calculated using Eq. 6.26 (Khurmi and Gupta, 2005).

$$T_{fq} = \frac{1}{3}\mu LD \tag{6.26}$$

where L is the equivalent dynamic load in N and D is the diameter of the bearing surface. Further, using the total frictional torque (Eq. 6.26), the power loss due to friction (P_t) in watts can be calculated using Eq. 6.27 (Khurmi and Gupta, 2005).

$$P_t = \frac{2\pi N_c T_{fq}}{60} \tag{6.27}$$

where N_c is the speed of the transporting cargo in contact with the larger ball of the BTU and T_{fq} is the total frictional torque in N-m.

Further, the heat generation due to friction and wear occurs in relative motion between the ball transfer unit (BTU) components. This heat generation within the BTU leads to a rise in temperature. Thus, the rise in temperature in the BTU may deteriorate the BHBC surface by causing its premature breakage (Kim *et* al., 2015). So, the reduction in heat generated (H_{btu}) during BTU operation can take place by reducing the coefficient of friction (COF). The heat generation in BTU can be calculated using Eq. 6.28 (Khurmi and Gupta, 2005).

$$H_{btu} = \mu L N_s \tag{6.28}$$

where μ is the COF on interior BHBC work part surface, L is the equivalent dynamic load in N, N_s is the conveying speed in m/s.

Thus, after fine finishing of the blind hole type ball cup (BHBC) surface with the presently designed MRHF tool, the COF can reduce with the reduced surface roughness value from 0.310 µm to 0.070 µm. This may result in the enhancement of functional performance of the ball transfer unit. The functional performance includes a reduction in frictional force, total frictional torque, power loss due to friction, and heat generation under operating conditions. Further, a finely finished surface of a ball cup of BTU may help in reducing the generation of metal debris, reducing vibration, noise, temperature during operation, and lubrication requirement. Thus, a ball transfer unit with improved service life and functionality can be achieved after fine finishing with the present process using a new magnetorheological hemispherical finishing (MRHF) tool. Also, the enhanced service life can reduce the replacement cost of the BTUs. Furthermore, the same MRHF tool can also be used in the future to finely finish the different sizes of the internal hemispherical surface of the BHBC workpieces. This can be achieved by providing the swivel motion to the BHBC workpieces. To provide the swivel motion to the BHBC workpiece, an additional axis is to be added to the present MR finishing setup.

6.3.5 Conclusions

The present study includes the fine finishing of the internal blind hole type ball cup (BHBC) work parts surface using the magnetorheological hemispherical finishing (MRHF) tool. The regression model was used to predict the optimized finishing process parametric conditions for fine finishing the interior BHBC work part surface using the present MRHF designed tool. After obtaining the optimized parameters using the regression model, the parameters were validated to fine finish the BHBC work part surface. The following are the conclusions that illustrate the usefulness and efficacy of the developed MRHF tool utilized for the fine finishing BHBC work parts surface.

- The %age error in experimental and predicted results of the percentage reduction in surface roughness is obtained as 1.36 to 4.34 %. This reveals the reproducibility of the present developed MRHF process to finish the BHBC work parts surface.
- The surface roughness value of the interior BHBC stainless steel-grade 304 workpiece surface is lower down to 0.070 µm from pre-experimentally recorded value of 0.310 µm in 80 min of MR finishing cycle time after utilizing the optimized parametric values of the current, workpiece, and tool rotational speed of 3 A, 100 rpm and 550 rpm respectively. Thus, the present developed process with a new MRHF tool is found effective in fine

finishing the interior BHBC work part surface made up of stainless steel 304-grade. This reduced roughness value may enhance the functional performance of the BTU.

- An enhanced final MR finished SEM image and the reflection test reveals an enhancement in the BHBC workpiece surface of BTU after finishing with the MRHF tool. This may reduce the stress fluctuations produced over the BHBC workpiece surface while BTU is in operating condition. This also helps in reducing the friction, and lubrication requirements. Thus, there can be an increase in the service life of the BTU.
- The closeness of the recorded points in the final circularity image with the true circle over the interior BHBC work part surface reveals its dimensional improvement after utilizing the MRHF process with a new tool. Thus, the noise and vibrations may reduce due to the improvement in the dimensional accuracy of the BHBC workpiece surface of the BTU.
- The BTU with the fine finished BHBC surface can be utilized as integral parts of feed devices, aircraft cargo bay and cargo ships. Also, in future, the present developed MRHF tool can be used for fine finishing of the different sizes of the BHBC surface of the different BTUs by providing swivel motion to the workpiece.

CHAPTER 7

CONCLUSIONS AND SCOPE OF FUTURE WORK

7.1 Conclusions

A new magnetorheological grinding (MRG) tool-based finishing process was developed to improve the functional ability and productivity of the cylindrical blind hole type workpieces. Initially, the different trials of finite element analysis were performed to develop the optimum design of the magnetorheological grinding tool. Further, the theoretical analysis was performed to investigate the effect of the different process parameters on the finishing performance and productivity of the cylindrical blind hole-type workpieces. Next, for finishing the tapered longitudinal type workpieces, the improved swivel vise fixture was fabricated which demonstrates effective finishing of the tapered shape cylindrical blind hole (CBH) type workpieces. The preliminary experiments successfully demonstrated the effectiveness of the single electromagnetic-based MRG tool to fine finish both longitudinal and flat end surfaces of the CBH type workpieces. Further, the study for investigation of optimum process parameters has been performed on the typical tapered blind hole type EN-31 and H-13 steel mold cavities which are the most useful molds for producing plastic parts such as spray bottle cap hoods, light covers, etc. Thus, the developed MRG tool-based finishing process has been successfully exhibited for the fine finishing of the various types of the CBH type workpieces. Following specific conclusions have been made based on the results obtained from the present research work.

- The magnetostatic finite element analysis and experimental validation of the magnetic flux density across magnetorheological grinding (MRG) tool surfaces with V-grooves confirms its high magnitude and uniformity. This reveals that the present single electromagnetic MRG tool is in good agreement while performing the finishing over the interior longitudinal and flat end surfaces of the CBH type workpieces.
- The capability of the present developed MRG tool to finish both longitudinal as well as the flat end surface of the CBH workpiece makes this tool to be useful in a great variety of industrial products which require fine finishing with higher dimensional accuracy.

- The MRG tool finishes the longitudinal cylindrical blind hole type workpiece surface eccentrically. As a result, the MRG tool may be used on a variety of workpieces with varying diameters. Also, using the rotating swivel vice helps the MRG tool to maintain a constant working gap between the tapered longitudinal CBH type workpiece surface and the longitudinal surface of the MRG tool. This aids in the uniform finishing of the tapered longitudinal CBH type workpiece surface.
- Based on the mechanism, the magnetic normal force acts along with other forces owing to the reciprocation motion of the rotating tool and the rotating workpiece. These forces are produced while the abrasive particles follow the helical path over the tapered longitudinal surface and spiral path over the flat end surface. This helps in shearing off material by the abrasive particles.
- Over the tapered longitudinal and flat end surfaces of the CBH type workpiece, the percentage error between experimentally and theoretically estimated roughness values were found to be in the ranges of 4.67 to 10.33 and 5 to 12. This % error reveals that the theoretical and experimentally measured surface roughness levels were in good agreement.
- In this study, the optimum parameters of the MRG tool-based finishing process for the EN-31 CBH type mould cavity were found to be 25 percent concentration of SiC abrasive particles in MR polishing (MRP) fluid, and 20 percent concentration of electrolytic iron particles in MRP fluid. Further for longitudinal surface, the optimum parameters were found as 520 rpm tool rotating speed, 16 cm/min reciprocation speed of the tool, 80 rpm workpiece rotating speed, 2.8 A magnetizing current, and 1 mm working gap. For flat surface, the optimum parameters were found as 1050 rpm tool rotating speed, 18 cm/min reciprocation speed of the tool, 100 rpm workpiece rotating speed, 2.5 A magnetizing current, and 0.9 mm working gap. The effective MR finishing is achieved over interior surfaces of the EN-31 CBH type mould cavity using these predicted optimum parameters.
- The error obtained between the experimental and the predicted % change in surface roughness in the present work is found within 1.11 to 3.64 % for longitudinal surface and 0.95 to 2.71 % for flat surface which concludes that the developed regression model is decently accurate. Therefore, the predicted optimized process parameters for finishing the CBH type workpiece of EN-31 mold surface is found in good order.

- The straight or tapered cylindrical blind hole type workpieces with different diameters are finely finished with the present MRG tool. This verifies that the MRG process can be utilized for the finishing of CBH-type workpieces with different diameters.
- The improvement in surface roughness profile, scanning electron microscope images, and circularity images validate that the present developed single electromagnetic MRG tool is capable of fine finishing the CBH type workpiece with an almost defect-free surface and better dimensional accuracy.
- The overall results obtained with the present developed MRG tool shows its usefulness for finishing the inner longitudinal and flat end surfaces of the various typical industrial CBH type workpieces such as molds, dies, actuators, and femoral head tapered junction, etc. These fine finished CBH type industrial components with the present developed single electromagnetic MRG tool-based process may provide improved wear resistance, service life, and fine appealing molded end products.

7.2 Scope of future work

The new magnetorheological grinding (MRG) tool-based finishing process has demonstrated its capacity to finish the various CBH workpieces with enhanced finishing performance and productivity. The following are some of the future work scopes that might be pursued to improve the finishing performance of the present process.

- The current tool can finish workpiece surfaces with internal cylindrical blind holes up to 40 mm in length. To finish the longer lengths of cylindrical blind hole type workpieces, the tool design could be enhanced further.
- Further experimentation on various industrial blind hole type components can be performed to determine the viability of the current magnetorheological fluid-based finishing technique and to validate the real-time performance.
- Fluid replacement characterization can be performed. This can provide the requisite time required to replace the fluid for effective finishing of the workpiece surfaces.

REFERENCES

Acker, R., Martin, S., Meltke, K., and Wolf, G. (2016). Casting of Fe–CrMnNi and ZrO2-Based Metal–Matrix Composites and Their Wear Properties. *Steel Research International*, *87*(8), 1111-1117.

Alam, Z., and Jha, S. (2017). Modeling of surface roughness in ball end magnetorheological finishing (BEMRF) process. *Wear, 374*, 54-62.

Alauddin, M., El Baradie, M. A., and Hashmi, M. S. J. (1996). Optimization of surface finish in end milling Inconel 718. *Journal of Materials Processing Technology*, *56*(1-4), 54-65.

Al-Samarai, R. A., Haftirman, K. R. A., and Al-Douri, Y. (2012). The influence of roughness on the wear and friction coefficient under dry and lubricated sliding. *Int. J. Sci. Eng. Res*, *3*(4), 1-6.

Altan, T., Lilly, B., and Yen, Y. C. (2001). Manufacturing of dies and molds. *CIRP Annals*, *50*(2), 404-422.

Bakharev, A., and Astbury, D. (2013). Simulation of ejection of moldings using combination of mold filling and thermo-mechanical analyses. In *AIP Conference Proceedings*, *1532* (1), 555-560). American Institute of Physics.

Barletta, M., Guarino, S., Rubino, G., andTagliaferri, V. (2007). Progress in fluidized bed assisted abrasive jet machining (FB-AJM): Internal polishing of aluminium tubes. *International Journal of Machine Tools and Manufacture*, *47*(3-4), 483-495.

Bedi, T. S., & Singh, A. K. (2018c). Development of magnetorheological fluid-based process for finishing of ferromagnetic cylindrical workpiece. *Machining Science and Technology*, *22*(1), 120-146.

Bedi, T. S., and Singh, A. K. (2016). Magnetorheological methods for nanofinishing–a review. *Particulate Science and Technology*, *34*(4), 412-422.

Bedi, T. S., and Singh, A. K. (2018a). A new magnetorheological finishing process for ferromagnetic cylindrical honed surfaces. *Materials and Manufacturing Processes*, *33*(11), 1141–1149. https://doi.org/10.1080/10426914.2016.1269925

Bedi, T. S., and Singh, A. K. (2018b). Magnetorheological finishing of ferromagnetic blind-hole type surfaces. *Materials and Manufacturing Processes*, *33*(11), 1169–1176. https://doi.org/10.1080/10426914.2017.1328120

Bergstrom, J., Thuvander, F., Devos, P., and Boher, C. (2001). Wear of die materials in full scale plastic injection moulding of glass fibre reinforced polycarbonate. *Wear*, *251*(1-12), 1511-1521.

Brewer, S. (2016) Ball Transfer Unit for Cargo Bay. U.S. Patent 9238551.

Bučinskas, V., Mirzaei, S., and Kirchner, K. (2010). Some aspects of bearing noise generation. In *Solid State Phenomena*, *164*, 278-284, Trans Tech Publications Ltd.

Buj-Corral, I., Vivancos-Calvet, J., and Coba-Salcedo, M. (2014). Modelling of surface finish and material removal rate in rough honing. *Precision Engineering*, *38*(1), 100-108.

Cabanettes, F., Dimkovski, Z., and Rosén, B. G. (2015). Roughness variations in cylinder liners induced by honing tools' wear. *Precision Engineering*, *41*, 40-46.

Chana, A., and Singh, A. K. (2019). Magnetorheological nano-finishing of tube extrusion punch for improving its functional applications in press machine. *International Journal of Advanced Manufacturing Technology*, *103*.

Chen, M., Liu, H., Su, Y., Yu, B., and Fang, Z. (2016). Design and fabrication of a novel magnetorheological finishing process for small concave surfaces using small ball-end permanent-magnet polishing head. *International Journal of Advanced Manufacturing Technology*, *83*(5–8), 823–834. https://doi.org/10.1007/s00170-015-7573-5

Cheng, H., Yeung, Y., and Tong, H. (2008). Viscosity behavior of magnetic suspensions in fluid assisted finishing. *Progress in Natural Science*, *18*, 91-96.

Chowdhury, M. A. (2010). The effect of natural frequency of the experimental set-up on the wear rate. *Industrial lubrication and tribology*.

Dabnun, M. A., Hashmi, M. S. J., and El-Baradie, M. A. (2005). Surface roughness prediction model by design of experiments for turning machinable glass–ceramic (Macor). *Journal of Materials Processing Technology*, *164*, 1289-1293.

Das, M., Jain, V. K., and Ghoshdastidar, P. S. (2010). Nano-finishing of stainless-steel tubes using rotational magnetorheological abrasive flow finishing process. *Machining Science and Technology*, *14*(3), 365–389.

Das, M., Jain, V. K., and Ghoshdastidar, P. S. (2011). The out-of-roundness of the internal surfaces of stainless-steel tubes finished by the rotational-magnetorheological abrasive flow finishing process. *Materials and Manufacturing Processes*, *26*(8), 1073–1084. https://doi.org/10.1080/10426914.2010.537141

Das, M., Jain, V. K., and Ghoshdastidar, P. S. (2012). Nanofinishing of flat workpieces using rotational–magnetorheological abrasive flow finishing (R-MRAFF) process. *The International Journal of Advanced Manufacturing Technology*, *62*(1), 405-420.

Eko Saputro, T., and Daneshvar Rouyendegh, B. (2016). A hybrid approach for selecting material handling equipment in a warehouse. *International Journal of Management Science and Engineering Management*, *11*(1), 34-48.

Examiner, P.; Hughes, S. T. (1999) Method for Manufacturing a Hemisphere of a Hemispheric Bearing. U.S. Patent 5907905.

Gadelmawla, E. S., Koura, M. M., Maksoud, T. M., Elewa, I. M., and Soliman, H. H. (2002). Roughness parameters. *Journal of Materials Processing Technology*, *123*(1), 133-145.

Gupte, P. S., Wang, Y., Miller, W., Barber, G. C., Yao, C., Zhou, B., and Zou, Q. (2008). A study of torn and folded metal (TFM) on honed cylinder bore surfaces. *Tribology transactions*, *51*(6), 784-789.

Gorana, V. K., Jain, V. K., and Lal, G. K. (2004). Experimental investigation into cutting forces and active grain density during abrasive flow machining. *International Journal of Machine Tools and Manufacture*, *44*(2-3), 201-211.

Grabon, W., Pawlus, P., and Sep, J. (2010). Tribological characteristics of one-process and two-process cylinder liner honed surfaces under reciprocating sliding conditions. *Tribology International*, *43*(10), 1882–1892.

Grover, V., and Singh, A. K. (2017a). Improved design of magnetorheological honing tool based on finite element analysis and experimental analysis of its performance. *International Journal of Advance Manufacturing Technology*, *100,* 1067-1080.

Grover, V., and Singh, A. K. (2018a). Improved magnetorheological honing process for nanofinishing of variable cylindrical internal surfaces. *Materials and Manufacturing Processes*, *33*(11), 1177–1187. https://doi.org/10.1080/10426914.2017.1339322

Grover, V., and Singh, A. K. (2017b). A novel magnetorheological honing process for nano-finishing of variable cylindrical internal surfaces. *Materials and Manufacturing Processes*, *32*(5), 573-580.

Guo, X., Yan, G., and He, W. (2008). A position telemetric method for implantable microcapsules in the gastrointestinal tract. *Measurement Science and Technology*, *19*(4), 045201.

Guo, Y. B., and Liu, C. R. (2002). Mechanical properties of hardened AISI 52100 steel in hard machining processes. *J. Manuf. Sci. Eng.*, *124*(1), 1-9.

Hashimoto, F., Yamaguchi, H., Krajnik, P., Wegener, K., Chaudhari, R., Hoffmeister, H. W., and Kuster, F. (2016). Abrasive fine-finishing technology. *CIRP Annals - Manufacturing Technology*, *65*(2), 597–620.

Hazir, E., and Ozcan, T. (2019). Response surface methodology integrated with desirability function and genetic algorithm approach for the optimization of CNC machining parameters. *Arabian Journal for Science and Engineering*, *44*(3), 2795-2809.

Heng, L., Kim, Y. J., and Mun, S. D. (2017). Review of Superfinishing by the Magnetic Abrasive Finishing Process. *High Speed Machining*, *3*(1), 42–55. https://doi.org/10.1515/hsm-2017-0004

Huang, J., Zhang, J. Q., and Liu, J. N. (2005). Effect of magnetic field on properties of MR fluids. *International Journal of Modern Physics B*, *19*(1), 597-601.

Jackson, M. J., and Hitchiner, M. P. (2012). *High performance grinding and advanced cutting tools*. Springer Science & Business Media.

Jain, N. K., Jain, V. K., and Jha, S. (2007). Parametric optimization of advanced fine-finishing processes. *The International Journal of Advanced Manufacturing Technology*, *34*(11), 1191-1213.

Jain, R. K., Jain, V. K., and Dixit, P. M. (1999). Modeling of material removal and surface roughness in abrasive flow machining process. *International Journal of Machine Tools and Manufacture*, *39*(12), 1903-1923.

Jain, V. K. (2008). Abrasive-based nano-finishing techniques: an overview. *Machining Science and Technology*, *12*(3), 257-294.

Jain, V. K. (2009). Magnetic field assisted abrasive based micro-/nano-finishing. *Journal of Materials Processing Technology*, *209*(20), 6022–6038.

Jaworski, J., and Trzepieciński, T. (2016). Surface layer properties of low-alloy high-speed steel after grinding. *acta mechanica et automatica*, *10*(4).

Jeevanantham, S., Sivaram, N. M., Smart, D. R., and Nallusamy, S. (2017). Optimization of internal grinding process parameters on C40E steel using taguchi technique. *International Journal of Applied Engineering Research*, *12*(19), 8660-8664.

Jha, S., and Jain, V. K. (2004). Design and development of the magnetorheological abrasive flow finishing (MRAFF) process. *International Journal of Machine Tools and Manufacture*, *44*, 1019–1029. https://doi.org/10.1016/j.ijmachtools.2004.03.007

Jha, S., and Jain, V. K. (2006a). Nanofinishing Techniques. In *Micromanufacturing and Nanotechnology* (pp. 171–195). Springer. https://doi.org/https://doi.org/10.1007/3-540-29339-6_8

Jha, S., and Jain, V. K. (2006b). Modeling and simulation of surface roughness in magnetorheological abrasive flow finishing (MRAFF) process. *Wear*, *261*, 856–866. https://doi.org/10.1016/j.wear.2006.01.043

Jha, S.; Jain, V. K., and Komanduri, R. (2007). Effect of extrusion pressure and number of finishing cycles on surface roughness in magnetorheological abrasive flow finishing (MRAFF) process. *The International Journal of Advanced Manufacturing Technology*, *33*(7–8): 725–729.

Ji, C., Zhao, M., Peng, T., Wang, F., Li, C., and Liu, S. (2012). Design of one novel LED airport runway centerline light suitable for various applications. In *2012 13th International Conference on Electronic Packaging Technology & High Density Packaging* (pp. 1421-1424). IEEE.

Jones, P. (2010) Mould design guide. Celanese 53:84.

Jurko, J., Panda, A., Valíček, J., Harničárová, M., and Pandová, I. (2016). Study on cone roller bearing surface roughness improvement and the effect of surface roughness on tapered roller bearing service life. *The International Journal of Advanced Manufacturing Technology*, *82*(5-8), 1099-1106.

Kadhum, A. H., Hamad, Y. M., and Naif, N. K. M. (2015). The Effect of Magnetic Abrasive Finishing on the Flat Surface for Ferromagnetic and non-Ferromagnetic materials. *Al-Nahrain Journal for Engineering Sciences*, *18*(1), 66-75.

Kang, J., and Yamaguchi, H. (2012). Internal finishing of capillary tubes by magnetic abrasive finishing using a multiple pole-tip system. *Precision Engineering*, *36*(3), 510-516.

Kang, J., George, A., and Yamaguchi, H. (2012a). High-speed internal finishing of capillary tubes by magnetic abrasive finishing. *Procedia CIRP*, *1*, 414-418.

Khan, D. A., and Jha, S. (2018). Synthesis of polishing fluid and novel approach for nanofinishing of copper using ball-end magnetorheological finishing process. *Materials and Manufacturing Processes*, *33*(11), 1150-1159.

Khatri, N., Manoj, J. X., Mishra, V., Garg, H., and Karar, V. (2018). Experimental and simulation study of nanometric surface roughness generated during magnetorheological finishing of silicon. *Materials Today: Proceedings*, *5*(2), 6391-6400.

Khurmi, R. S.; Gupta, J. K. (2005) A Textbook of Machine Design; Eurasia Publishing House (Pvt.) Ltd., India.

Kim, J. D., Kang, Y. H., Bae, Y. H., and Lee, S. W. (1997). Development of a magnetic abrasive jet machining system for precision internal polishing of circular tubes. *Journal of Materials Processing Technology*, *71*(3), 384-393.

Kim, K. S., Lee, D. W., Lee, S. M., Lee, S. J., and Hwang, J. H. (2015). A numerical approach to determine the frictional torque and temperature of an angular contact ball bearing in a spindle system. *International Journal of Precision Engineering and Manufacturing*, *16*(1), 135-142.

Kumar, A., Alam, Z., Khan, D. A., and Jha, S. (2019). Nanofinishing of FDM-fabricated components using ball end magnetorheological finishing process. *Materials and Manufacturing Processes*, *34*(2), 232-242.

Kurore, T., Imanaka, O., and Tachibana, S. (1983). Magnetic field-assisted fine finishing. *Bulletin of the Japan Society of Precision Engineering*, *17*(1), 49-50.

Lee, J., and S. Malkin. (1993). Experimental investigation of the bore honing process. 406-414.

Li, W., Li, X., Yang, S., and Li, W. (2018). A newly developed media for magnetic abrasive finishing process: Material removal behavior and finishing performance. *Journal of Materials Processing Technology*, *260*, 20-29.

Linke, B. S., and Dornfeld, D.A. (2012). Application of axiomatic design principles to identify more sustainable strategies for grinding. *Journal of Manufacturing Systems 31*(4), 412-419.

Linke, B. S.; Corman, G. J.; Dornfeld, D. A., and Tönissen, S. (2013). Sustainability indicators for discrete manufacturing processes applied to grinding technology. *Journal of Manufacturing Systems, 32*(4), 556-563.

Linke, B. S.; Garretson, I.; Torner, F., and Seewig, J. (2017). Grinding energy modeling based on friction, plowing, and shearing. *ASME Journal of Manufacturing Science Engineering, 139*(12), 121009.

Loveless, T. R., Williams, R. E., and Rajurkar, K. P. (1994). A study of the effects of abrasive-flow finishing on various machined surfaces. *Journal of Materials Processing Tech.*, *47*(1–2), 133–151. https://doi.org/10.1016/0924-0136(94)90091-4

Maan, S., and Singh, A. K. (2018). Nano-surface finishing of hardened AISI 52100 steel using magnetorheological solid core rotating tool. *The International Journal of Advanced Manufacturing Technology*, *95*(1), 513-526.

Maan, S., Singh, G., and Singh, A. K. (2017). Nano-surface-finishing of permanent mold punch using magnetorheological fluid-based finishing processes. *Materials and Manufacturing Processes*, *32*(9), 1004-1010.

Mahtab, R. (2015). Design and testing of heliport approach light in compliance with civil aviation rules.

Mali, H. S., and Manna, A. (2009). Current status and application of abrasive flow finishing processes: a review. *Proceedings of the Institution of Mechanical Engineers, Part B: Journal of Engineering Manufacture*, *223*(7), 809-820.

Mapelli, C., and Barella, S. (2007). Failure analysis of a ball transfer unit. *Engineering Failure Analysis*, *14*(4), 579-587.

Marashi, J., Yakushina, E., Xirouchakis, P., Zante, R., and Foster, J. (2017). An evaluation of H13 tool steel deformation in hot forging conditions. *Journal of Materials Processing Technology*, *246*, 276-284.

Martínez-Mateo, I., Carrión-Vilches, F. J., Sanes, J., and Bermúdez, M. D. (2011). Surface damage of mold steel and its influence on surface roughness of injection molded plastic parts. *Wear*, *271*(9-10), 2512-2516.

Martorelli, M., Gerbino, S., Lanzotti, A., Patalano, S., and Vitolo, F. (2017). Flatness, circularity and cylindricity errors in 3D printed models associated to size and position on the working plane. In *Advances on Mechanics, Design Engineering and Manufacturing* (pp. 201-212). Springer, Cham.

Masciarelli, C. (1987) Anti-Friction Element. U.S. Patent 4660994.

Mazur, M., Brincat, P., Leary, M., and Brandt, M. (2017). Numerical and experimental evaluation of a conformally cooled H13 steel injection mould manufactured with selective laser melting. *The International Journal of Advanced Manufacturing Technology*, *93*(1), 881-900.

Mehra, D., Mahapatra, M. M., and Harsha, S. P. (2018). Effect of wear parameters on dry abrasive wear of RZ5-TiC in situ composite. *Industrial Lubrication and Tribology*.

Mennig, G., and Stoeckhert, K. (Eds.). (2013). *Mold-making handbook*. Carl Hanser Verlag GmbH Co KG.

Migal, V., Lebedev, A., Shuliak, M., Kalinin, E., Arhun, S., and Korohodskyi, V. (2021). Reducing the vibration of bearing units of electric vehicle asynchronous traction motors. *Journal of Vibration and Control*, *27*(9-10), 1123-1131.

Mulik, R. S., and Pandey, P. M. (2013). Experimental investigations into the finishing force and torque in magnetic abrasive finishing process. *In ASME 2013 International Mechanical Engineering Congress and Exposition.* American Society of Mechanical Engineers Digital Collection.

Murthy, I. N., and Rao, J. B. (2017). Molding and casting behavior of ferro chrome slag as a mold material in ferrous and non-ferrous foundry industries. *Materials and Manufacturing Processes*, *32*(5), 507-516.

Nadolny, K., and Kieraś, S. (2020). New approach for cooling and lubrication in dry machining on the example of internal cylindrical grinding of bearing rings. *Sustainable Materials and Technologies*, *24*, 00166. https://doi.org/10.1016/j.susmat.2020.e00166

Nadolny, K., Kapłonek, W., Królczyk, G., and Ungureanu, N. (2018). The effect of active surface morphology of grinding wheel with zone-diversified structure on the form of chips in traverse internal cylindrical grinding of 100Cr6 steel. *Proceedings of the Institution of Mechanical Engineers, Part B: Journal of Engineering Manufacture*, *232*(6), 965-978.

Niranjan, M. S., and Jha, S. (2014). Flow Behaviour of Bidisperse MR Polishing Fluid and Ball End MR Finishing. *Procedia Materials Science*, *6*, 798–804.

Okada, A., Uno, Y., McGeough, J. A., Fujiwara, K., Doi, K., Uemura, K., and Sano, S. (2008). Surface finishing of stainless steels for orthopedic surgical tools by large-area electron beam irradiation. *CIRP annals*, *57*(1), 223-226.

Pandey, S., Kant, S., Mishra, V., Khatri, N., and Ramagopal, S. V. (2013). Parametric optimization of ball end magneto rheological finishing process on EN-31. *Int J Rece Technol Eng*, *2*(2), 2277-3878.

Paswan, S. K., and Singh, A. K. (2020). Theoretical and experimental investigations on nano-finishing of internal cylindrical surfaces with a newly developed rotational magnetorheological honing process. *Proceedings of the Institution of Mechanical Engineers, Part C: Journal of Mechanical Engineering Science*, *234*(2), 363-383.

Paswan, S. K., and Singh, A. K. (2021). Investigation of Optimized Parameters for Magnetorheological Finishing the Internal Surface of the Cast-Iron Cylindrical Molds. *Arabian Journal for Science and Engineering*, *46*(3), 2147-2164.

Paswan, S. K., Bedi, T. S., and Singh, A. K. (2017). Modeling and simulation of surface roughness in magnetorheological fluid based honing process. *Wear*, *376*, 1207-1221.

Paswan, S.K., and Singh, A.K. (2019) Analysis of surface finishing mechanism in a newly developed rotational magnetorheological honing process for its productivity improvement. *Wear*, *426*, 68-82.

Rajeev, B. (2018) Aircraft Floor Panel with Ball Transfer Unit. U.S. Patent 9963232.

Rhoades, L. (1991). Abrasive flow machining: a case study. *Journal of Materials Processing Technology*, *28*, 107–116.

Sabri, L., Mezghani, S., and Mansori, M. El. (2010). A study on the influence of bond material on honing engine cylinder bores with coated diamond stones. *Surface and Coatings Technology*, *205*(5), 1515–1519.

Sabri, L., Mezghani, S., El Mansori, M., and Zahouani, H. (2011). Multiscale study of finish-honing process in mass production of cylinder liner. *Wear*, *271*(3–4), 509–513. https://doi.org/10.1016/j.wear.2010.03.026

Sankar, M. R., Jain, V. K., and Ramkumar, J. (2009). Experimental investigations into rotating workpiece abrasive flow finishing. *Wear*, *267*(1–4), 43–51.

Sankar, M. R., Jain, V. K., and Ramkumar, J. (2010). Rotational abrasive flow finishing (R-AFF) process and its effects on finished surface topography. *International journal of machine tools and manufacture*, *50*(7), 637-650.

Sankar, M. R., Jain, V. K., and Ramkumar, J. (2016). Nano-finishing of cylindrical hard steel tubes using rotational abrasive flow finishing (R-AFF) process. *The International Journal of Advanced Manufacturing Technology*, *85*(9–12), 2179–2187. 249 https://doi.org/10.1007/s00170-015-8189-5

Saraswathamma, K., Jha, S., and Rao, P. V. (2015). Experimental investigation into ball end magnetorheological finishing of silicon. *Precision Engineering*, *42*, 218-223.

Schulz, H. (1995). High-speed milling of dies and moulds—cutting conditions and technology. *CIRP annals*, *44*(1), 35-38.

Shiou, F. J., and Chen, C. H. (2003). Freeform surface finish of plastic injection mold by using ball-burnishing process. *Journal of materials processing technology*, *140*(1-3), 248-254.

Sidpara, A., and Jain, V. K. (2011). Experimental investigations into forces during magnetorheological fluid-based finishing process. *International Journal of Machine Tools and Manufacture*, *51*(4), 358-362.

Sidpara, A., and Jain, V. K. (2012). Nano–level finishing of single crystal silicon blank using magnetorheological finishing process. *Tribology International*, 47, 159–166.

Sidpara, A., and Jain, V. K. (2012). Theoretical analysis of forces in magnetorheological fluid-based finishing process. *International Journal of Mechanical Sciences*, *56*(1), 50-59.

Sidpara, A., Das, M., and Jain, V. K. (2009). Rheological characterization of magnetorheological finishing fluid. *Materials and Manufacturing Processes*, *24*(12), 1467–1478. https://doi.org/10.1080/10426910903367410

Singh, A. K., Jha, S., and Pandey, P. M. (2010). Nanofinishing Process for 3D Freeform Surfaces Using Ball End MR Finishing Tool. In *Proceedings of the 36th International MATADOR Conference* (pp. 67-70). Springer, London.

Singh, A. K., Jha, S., and Pandey, P. M. (2012). Parametric analysis of an improved ball end magnetorheological finishing process. *Proceedings of the Institution of Mechanical Engineers, Part B: Journal of Engineering Manufacture*, *226*(9), 1550-1563.

Singh, A. K., Jha, S., and Pandey, P. M. (2012). Performance evaluation of improved ball end magnetorheological finishing process. *World Academy of Science and Technology*, *6*, 1193-97.

Singh, A. K., Jha, S., and Pandey, P. M. (2013). Mechanism of material removal in ball end magnetorheological finishing process. *Wear*, *302*(1-2), 1180-1191.

Singh, G., Kumar, H., Kansal, H. K., and Srivastava, A. (2020). Effects of chemically assisted magnetic abrasive finishing process parameters on material removal of inconel 625 tubes. *Procedia Manufacturing*, *48*, 466-473.

Singh, M., and Singh, A. K. (2019a). Improved magnetorheological finishing process with rectangular core tip for external cylindrical surfaces. *Materials and Manufacturing Processes*, *34*(9), 1049-1061.

Singh, M., and Singh, A. K. (2019b). Magnetorheological finishing of micro-punches for enhanced performance of micro-extrusion process. *Materials and Manufacturing Processes*, *34*(14), 1646-1657.

Singh, M., and Singh, A. K. (2019a). Performance investigation of magnetorheological finishing of rolls surface in cold rolling process. *Journal of Manufacturing Processes*, *41*, 315-329.

Singh, M., and Singh, A. K. (2020). Theoretical investigations into magnetorheological finishing of external cylindrical surfaces for improved performance. *Proceedings of the Institution of Mechanical Engineers, Part C: Journal of Mechanical Engineering Science*, *234*(24), 4872-4892.

Singh, S., and Singh, L. (2014). Effect of Magnetic Abrasives in Internal Finishing of Brass Tubes Using MAF Method. *Journal of Academia and Industrial Research*, *2*(12), 689-692.

Sirwal, S. A., and Singh, A. K. (2018). Analysis of the surface roughness for novel magnetorheological finishing of a typical blind hole workpiece. *Proceedings of the Institution of Mechanical Engineers, Part C: Journal of Mechanical Engineering Science*, *233*(5), 1541-1561.

Sirwal, S. A., Singh, A. K., and Paswan, S. K. (2020). Experimental analysis of magnetorheological finishing of blind hole surfaces using permanent magnet designed

tools. *Journal of the Brazilian Society of Mechanical Sciences and Engineering*, *42*(3), 1-23.

Stegmiller, W. K. (2016) Ball Transfer Unit Support Systems. U.S. Patent 9284128.

Taufik, M., and Jain, P. K. (2017). Surface roughness improvement using volumetric error control through adaptive slicing. *International Journal of Rapid Manufacturing*, *6*(4), 279-302.

Tauviqirrahman, M., and Ichsan, B. C. (2019). Influence of roughness on the behavior of three-dimensional journal bearing based on fluid-structure interaction approach. *Journal of Mechanical Science and Technology*, *33*(10), 4783-4790.

Tawakoli, T., Westkaemper, E., and Rabiey, M. (2007). Dry grinding by special conditioning. *The International Journal of Advanced Manufacturing Technology*, *33*(3), 419-424.

Tilger, M., Siebrecht, T., and Biermann, D. (2017). Fundamental Investigations of Honing Processes Related to the Material Removal Mechanisms. *Prof. Dr.-Ing. RH Schmitt Prof. Dr.-Ing. Dipl.-Wirt. Ing. G. Schuh*, 121.

Torrance, A. A. (2002). The effect of grit size and asperity blunting on abrasive wear. *Wear*, *253*, 813–819. https://doi.org/https://doi.org/10.1016/S0043-1648(02)00103-5

Turnbull, R., Rahmani, R., and Rahnejat, H. (2020). The effect of outer ring elastodynamics on vibration and power loss of radial ball bearings. *Proceedings of the Institution of Mechanical Engineers, Part K: Journal of Multi-body Dynamics*, *234*(4), 707-722.

Verma, G. C., Kala, P., & Pandey, P. M. (2017). Experimental investigations into internal magnetic abrasive finishing of pipes. *The international journal of advanced manufacturing technology*, *88*(5-8), 1657-1668.

Walia, R. S., Shan, H. S., and Kumar, P. (2006). Abrasive flow machining with additional centrifugal force applied to the media. *Machining science and technology*, *10*(3), 341-354.

Walter, B., Marschner, S. R., Li, H., and Torrance, K. E. (2007). Microfacet Models for Refraction through Rough Surfaces. *Rendering techniques*, *2007*, 18th.

Wang, Y., & Hu, D. (2005). Study on the inner surface finishing of tubing by magnetic abrasive finishing. *International Journal of Machine Tools and Manufacture*, *45*(1), 43-49.

Wang, J., Chen, W., and Han, F. (2015). Study on the magnetorheological finishing method for the WEDMed pierced die cavity. *The International Journal of Advanced Manufacturing Technology*, *76*(9-12), 1969-1975.

Wang, C. J., Cheung, C. F., Ho, L. T., Liu, M. Y., and Lee, W. B. (2017). A novel multi-jet polishing process and tool for high-efficiency polishing. *International Journal of Machine Tools and Manufacture*, *115*, 60-73.

Wang, Y., and Hu, D. (2005). Study on the inner surface finishing of tubing by magnetic abrasive finishing. *International Journal of Machine Tools and Manufacture*, *45*(1), 43-49.

Yamaguchi, H., and Shinmura, T. (1999). Study of the surface modification resulting from an internal magnetic abrasive finishing process. *Wear*, *225–229*, 246–255.

Yamaguchi, H., Shinmura, T., and Ikeda, R. (2007). Study of internal finishing of austenitic stainless steel capillary tubes by magnetic abrasive finishing. *Journal of Manufacturing Science and Engineering, Transactions of the ASME*, *129*(5), 885–892. https://doi.org/10.1115/1.2738957

Yan, H., Hua, J., and Shivpuri, R. (2007). Flow stress of AISI H13 die steel in hard machining. *Materials and design*, *28*(1), 272-277.

Yan, H., Wu, Y., Li, S., Zhang, L., and Zhang, K. (2020). Research on sound field characteristics of full-ceramic angular contact ball bearing. *Journal of the Brazilian Society of Mechanical Sciences and Engineering*, *42*, 1-16.

Yang, J., and Zhang, T. (2004). The void effect of MEVVA W ion implantation on the tribological properties of H13 steel. *Surface Review and Letters*, *11*(4-5), 363-366.

Yunlong, W., Wenzhong, W., Shengguang, Z., and Ziqiang, Z. (2018). Effects of raceway surface roughness in an angular contact ball bearing. *Mechanism and Machine Theory*, *121*, 198-212.

LIST OF PUBLICATION

SCI Journals:

1. **Aggarwal, A.**, Singh, A. K. Development of grinding wheel type magnetorheological finishing process for blind hole surfaces. *Materials and Manufacturing Processes* 2021, *36*(4): 457−478.
   Status: ***Published Online***
   Publisher: Taylor and Francis
   Impact factor: 4.616.
2. **Aggarwal, A.**, Singh, A. K. Experimental investigation for fine finishing of the tapered mould cavity using a newly developed GWMRF process. *Journal of the Brazilian Society of Mechanical Sciences and Engineering*
   Status: ***Published Online***
   Publisher: Springer
   Impact factor: 2.220.
3. **Aggarwal, A.**, Singh, A. K. Magnetorheological finishing of ball-cup surface using new tool to enhance ball-transfer-unit performance. *Materials and Manufacturing Processes*.
   Status: ***Under Review***
   Publisher: Taylor and Francis
   Impact factor: 4.616.
4. **Aggarwal, A.**, Singh, A. K. Surface roughness investigation for a novel magnetorheological finishing of cylindrical blind hole surfaces using a single magnetic tool. *Journal of Manufacturing Processes.*
   Status: ***Submitted***
   Publisher: Elsevier
   Impact factor: 5.01.
5. **Aggarwal, A.**, Singh, A. K. Experimental investigation for fine finishing of the mould cavity of light cover using the present GWMRF process. *Surface Review and Letters*.
   Status: ***Under Review***
   Publisher: World Scientific Publishing
   Impact factor: 1.152.

International Conference:

Aggarwal, A., Singh, A.K. 2019, Nanofinishing of hemispherical blind hole surface with a newly designed magnetorheological finishing tool, *40th International MATADOR International Conference on Advanced Manufacturing and Design July 8-10, 2019, Hangzhou, China*.

Book Chapter:

Aggarwal, A., Singh, A.K. 2020, A novel magnetorheological grinding process for finishing the internal cylindrical surfaces, *Advances in Unconventional Machining and Composites. Lecture Notes on Multidisciplinary Industrial Engineering. Springer, Singapore.*
https://doi.org/10.1007/978-981-32-9471-4_15